Ultrasound–Assisted Biodiesel Production Using Heterogeneous Catalysts and Mixed Non–Edible Oils Feedstock

A
Thesis
Submitted in
Partial Fulfillment of the
Requirements for the Degree of

DOCTOR OF PHILOSOPHY

Ritesh S. Malani

Center for Energy
Indian Institute of Technology Guwahati
Guwahati – 781 039, Assam, India

April, 2019

Dedicated

to

My Parents

&

My Lovely Wife

Making me be who I am

INDIAN INSTITUTE OF TECHNOLOGY GUWAHATI

CENTER FOR ENERGY

STATEMENT

I do hereby declare that the content embodied in this thesis entitled "**ULTRASOUND–ASSISTED BIODIESEL PRODUCTION USING HETEROGENEOUS CATALYSTS AND MIXED NON–EDIBLE OILS FEEDSTOCK**" is the result of investigations carried out by me at Center for Energy, Indian Institute of Technology Guwahati, Guwahati, India, under the guidance of **Prof. Vijayanand S. Moholkar** and **Prof. Arun Goyal**.

In keeping with the general practice of reporting scientific observations, due acknowledgements have been made wherever the work described is based on the findings of other investigators.

April 2019

Ritesh S. Malani

(Roll No.: 146151011)

INDIAN INSTITUTE OF TECHNOLOGY GUWAHATI

DEPARTMENT OF CHEMICAL ENGINEERING

CERTIFICATE

It is certify that the work contained in the thesis entitled "**ULTRASOUND–ASSISTED BIODIESEL PRODUCTION USING HETEROGENEOUS CATALYSTS AND MIXED NON–EDIBLE OILS FEEDSTOCK**", by **Ritesh S. Malani** (Roll No: 146151011), has been carried out under our supervision and that this work has not been submitted elsewhere for a degree.

Prof. Vijayanand S. Moholkar
Professor
Department of Chemical Engineering
and Head Center for Energy
Indian Institute of Technology, Guwahati
Guwahati – 781 039
Assam, India

Prof. Arun Goyal
Professor
Department of Biosciences and Bioengineering
and Center for Energy
Indian Institute of Technology, Guwahati
Guwahati – 781 039
Assam, India

Date:

Place:

Date:

Place:

CONTENTS

LIST OF TABLES

Chapter 5

Chapter 6

Chapter 7

भारतीय प्रौद्योगिकी संस्थान गुवाहाटी
Indian Institute of Technology Guwahati

LIST OF FIGURES

Chapter 3

Chapter 4

LIST OF SCHEMES

Chapter 1

भारतीय प्रौद्योगिकी संस्थान गुवाहाटी
Indian Institute of Technology Guwahati

CHAPTER 1

INTRODUCTION AND LITERATURE REVIEW

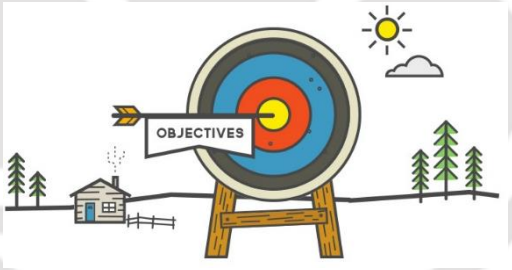

Chapter 1

Introduction and Literature Review

1.1 Global energy and fuel scenario

Energy derived from coal and crude oil in terms of electricity and transportation fuel is one of the primary needs of human civilization and development of society in present scenario. [1] Limited reservoirs of fossil fuels and their uneven distribution make energy utilization through–out the world inappropriate. OPEC (Organization of the Petroleum Exporting Countries) has ~ 75% of world's ascertained oil reservoirs with only 6% of world population. OPEC currently contributes to ~ 50% of oil produced throughout the world [2]. Countries with such high oil reservoirs, consumes more energy per capita as compared to rest of the counties in the world.

As per the report of International Energy Agency (IEA), the global energy demand in 2017 grew by 2.1%, which was more than twice as compared to 2016, and has resulted in enhancement of 1.4% or ~ 450 MT (metric tons) global CO_2 emissions

[3]. 81% of global energy demand has been fulfilled by fossil fuels over last three decades, despite strong growth in renewable energy sources [4]. Asia is the major contributor in global energy demand followed by Africa. China and India together contributed 40% of the increase in Asia's increase in global energy demand, although per capita energy consumption was much below in these region as compared to global average [3].

The average growth of global oil demand was 1.6% in 2017, resulting in 1.5 million barrels per day (mb/d) of oil production. This was much higher than average annual growth rate of 1% over last one decade [3]. Fig. 1.1 shows the average annual growth in oil demand over last three decades. The major contributors for this growth in oil demand were transport sector followed by petrochemical sector. Modern efficient engines showed reduction in average fuel consumption per vehicle but rapid increase in the share of Sport Utility Vehicles (SUVs) and other large vehicle sales, counter the engine energy efficiency [3].

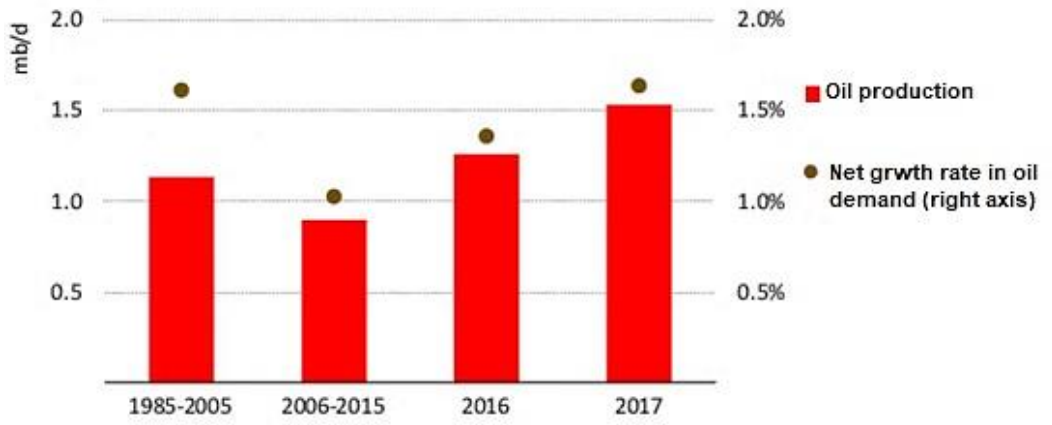

Figure 1.1: Average annual growth in oil demand (Source: [3])

On the other hand, rapid increase in plastic and other petrochemical products promoted petrochemical sector as fastest–growing sector in last few years. Asia becomes the major contributor to global oil demand with ~ 60% of total oil growth [3,6]. China has emerging economy but also the main contributor in oil demand after

India in Asia–pacific region. India has surpassed the oil demand of China and became rising contributor to incremental oil demand [5,7].

Rise in energy related CO_2 emissions in 2017 is a strong indication of climate change and illustrates that present attempts are insufficient to meet goals of 2015 Paris agreement. Fast depletion of oil reservoirs, constantly increasing energy (fuel and electricity) demand, fluctuating prices of crude oil and detrimental exhaust emissions from excess consumption of fossil fuels, intensified the search for alternative energy sources globally.

1.2 Indian energy scenario and biofuel mission

As per the data published by Central Statistics Organisation (Ministry of Statistics and Programme Implementation, Government of India), in India, the production of crude oil was almost constant in last five years (41 – 43 MMT (Million Metric tons) from 2010–11 to 2015–16) with continuously declining production of natural gas (44.3 Mtoe (metric tons oil equivalent) in 2010–11 to 26.3 Mtoe in 2015–16) [8]. India's crude oil import rose to 202.85 MMT in 2015–16 with an annual rise of 7.08%, which not only has created an enormous burden on country's economy but also adversely affected the climate and environment, and has led to global challenges associated with sudden increment in greenhouse gas emissions [9]. To meet the continuous increasing demand for consumption of petroleum products and electricity without contributing excess CO_2 emissions, the energy economics and security policy of Government of India is focused towards generation and utilization of alternate fuels, which are technically efficient, economically viable and environmentally sustainable. Renewable energy from non–conventional sources such as wind, solar (both photovoltaic and thermal), geothermal, hydropower and biomass have a great potential

for generation of clean energy. Central Statistics Organisation (Ministry of Statistics and Programme Implementation, Government of India) estimates the total power generated through renewable energy sources as 11,98,856 MW [8]. Table 1.1 lists all the renewable sources with their estimated potential.

Table 1.1: Source–wise estimated potential of renewable power in India (Source: [8])

Renewable energy source	Estimated power (in MW)	% Distribution
Wind power (both @ 80 m and @100 m)	4,05,023	33.78
Small–hydro power (SHP)	19,749	1.65
Biomass power	17,538	1.46
Bagasse–based co–generation	5,000	0.42
Waste to energy	2,556	0.21
Solar power	7,48,990	62.48
Total	11,98,856	100.00

1.2.1 Indian biofuel mission

Biofuels are exploited as an attractive source of fuel which lowers the CO_2 emission and ultimately improves air quality [10]. Bioethanol and biodiesel have been studied extensively among other biofuels such as biobutanol, biohydrogen, biomethane, etc. due to ease of blending with conventional fuel and compatible with existing engine configuration [11]. Planning Commission, Government of India, proposed 20% biofuel blending target for both bioethanol and biodiesel to be achieved in 12th Five–year plan by the end of 2022 [8].

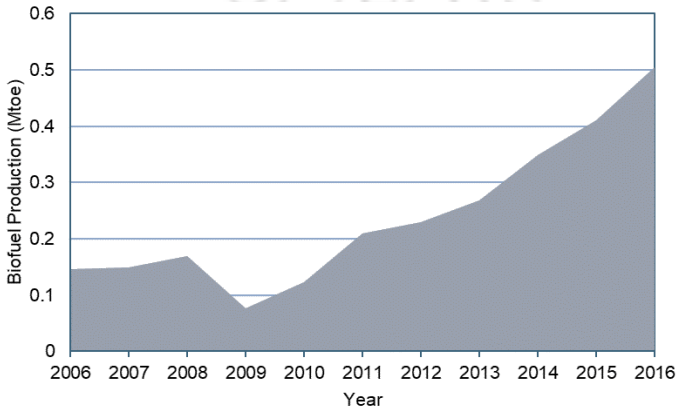

Figure 1.2: Biofuel production in India over last decade (Source: [4])

World's biofuel production has increased from 27.9 Mtoe in 2006 to 82.3 Mtoe in 2016 with an average 14% annual growth rate. During this period, India's biofuel production had risen from 0.15 Mtoe in 2006 to 0.51 Mtoe in 2016 with an average growth rate of 12.7% per annum, contributing to 0.6% of global biofuel production [4], as shown in Fig. 1.2.

Transport sector share among all major energy sectors was the highest. The projected demand for diesel and petrol will rise to 110 MMT (Million Metric tons) and 31.1 MMT, respectively by the year 2021–22 from the current demand of 80.4 MMT and 26.1 MMT in 2017–18 [9]. Thus, biofuels provide a higher degree of national energy security by reducing dependence on imported fossil fuels and help to meet the energy needs of India's massive population.

Planning Commission, Ministry of New and Renewable Energy and Ministry of Petroleum and Natural Gas, Government of India, has been promoting and encouraging production and use of: (a) ethanol derived from sugar molasses and/or second generation biofuels (biomass, agricultural waste etc.) for blending with petrol, and (b) biodiesel derived from non–edible oils, tree borne oil seeds and waste oil for blending with diesel [12]. Recognizing the need of transforming attention in the field of biofuels in terms of emerging international perspectives, technological developments and progressing National scenario, the work related to biofuels had been transferred from Ministry of New and Renewable Energy to Ministry of Petroleum and Natural Gas, Government of India. The new Ministry has working on formulating the National Policy on Biofuels – 2018, which emphasizes on setting up of Biorefineries for 2nd generational ethanol and biodiesel based on crop residues and municipal solid waste (MSW) [12].

1.2.2 India's bioethanol programme

The Government of India is implementing Ethanol Blended Petrol (EBP) Programme under which all the oil marketing companies (OMCs) sell up to 10% ethanol blended petrol. To make it feasible and assure undisturbed supply of ethanol to OMCs, Government had promoted the alternate route for ethanol production from other non–food feedstock's besides molasses, like cellulosic and lingo–cellulosic materials with administered ethanol price. The programme had significantly improved the supply of ethanol from 38 crores litres during 2013–14 to 111 crore litres in 2015–16. For the year 2017–18, Government of India has increased the administered price of ethanol to Rs. 40.85/– per litre from Rs 39/– per litre for the year 2016–17. The current (2018–19) administered price of ethanol is Rs. 52.43/– per litre. This proactive measure in ethanol price led to record high purchase of 139.5 crore litres of ethanol from suppliers to OMCs. On the other hand, oil companies in Public Sector Undertakings (PSUs) are planning to commission of twelve 2nd–generation ethanol producing biorefineries in 11 different states to boost the ethanol production [9].

1.2.3 India's biodiesel programme

The first phase of National Biodiesel Mission was implemented during 2003–2007 by Government of India as a demonstration project. *Jatropha curcas* was identified as the most suitable non–edible oil seed, and was planted over 4,00,000 hector area with support of Ministry of Rural Development, Government of India. In October 2005, the Ministry of Petroleum and Natural Gas announced the policy for biodiesel, for first time, under which oil marketing companies would centrally purchase biodiesel from local manufacturers with a fixed price of Rs. 26.5/– per litre, at twenty purchase centres set up across the country [13].

The second execution phase of National Biodiesel Mission was launched in 2008 for a period of 4–years (2008–12) to produce sufficient biodiesel for 10%–blends by the end of 11th five–year plan. The major impediment for achieving goals of National Biodiesel Mission was the administered price (or minimum support price) of biodiesel. In order to give a boost to biodiesel production, the Government of India, had increased the administered price for biodiesel to Rs. 34/– per litre from Rs. 26.5/– per litre. This price (Rs. 54.65/– per litre) was still much lesser than the actual production cost of biodiesel to attract handsome investment [14].

The Government of India, through vide notification on dated 29th June, 2017, had allowed direct sale of biodiesel (B–100) for blending with high speed diesel (HSD) to all consumers, in accordance with the specified blending limits and the standards specified by the Bureau of Indian Standards (BIS). Prior to this notification the biodiesel blending of 10% was allowed and used only in diesel locomotives of Indian Railways. During the period April– November 2017, biodiesel quantity procured was 43,551 kL (kilolitres) over 34,910 kL procured during the same period in 2016 with an increase of 24% [9].

Despite the potential and promise, the biodiesel program of India has not achieved its goals and targets. There are several hurdles that have contributed to this effect, *viz.* availability of non–edible oil feedstock, lack of fiscal incentives, lack of research & development in commercial technologies and less opportunity for collaborating internationally.

In subsequent sections, a brief description and overview of various techniques for biodiesel production is given with different types of catalysts and feedstocks. In addition to this, a brief review of state–of–the–art research on biodiesel production with use of different heterogeneous catalysts is also presented. On the basis of this review

and analysis of literature, the purpose of the present thesis has been justified, followed by aim, approach and scope (or content) of the thesis.

1.3 Techniques for biodiesel production

Biodiesel basically is a mixture of C_{12} – C_{22} fatty acid monoalkyl esters (FAMEs), and it has several advantages over conventional diesel such as, biodegradable, sulfur–free, sustainable with higher lubricity, flash point etc. [15,16]. It is an alternative to petroleum diesel for reducing emissions of gaseous pollutants such as CO, SO_x, particulate matter and organic compounds. It can be produced from wide range of available feedstocks (more than 350 oil–bearing crops, waste cooking oil, animal fat, algal oil, etc.) making it one of the popular liquid biofuels worldwide [17]. Biodiesel can be produced through different techniques; transesterification is one of the most commonly used technique to produce biodiesel. Other techniques which can be used to produce the biodiesel includes esterification and interesterification [16]. Conventionally, biodiesel was produced using edible oil reacting with short chain primary or secondary monohydric aliphatic alcohols having 1–8 carbon atoms in presence of homogenous base catalyst such as NaOH/ KOH [18]. The non–edible oil/ waste cooking oil or animal fat has higher free fatty acid (FFA) content, which in presence of NaOH/KOH react with methanol to form soap instead of FAME. Thus, to lowers the FFA content of feedstock homogeneous acid catalyst (commonly conc. H_2SO_4) was used [16]. Alternatively, enzyme can also be used to convert the high FFA content feedstock to FAME [18]. The application of homogenous catalyst contaminates the by–product glycerol as well as increases the downstream processing for purification of biodiesel [19]. To overcome these issues extensive research has been done to explore applicability of heterogeneous catalyst for transesterification reaction.

1.3.1 Esterification process

The cost of raw materials (mainly triglycerides) in biodiesel industry contributes to main production cost. However, it is possible to use low cost feedstocks, like non–edible oils, waste cooking oils and animal fats, which could be converted to biodiesel, thus decreasing production costs and devising an environmental friendly biodiesel production process. To utilize the non–edible oils and animal fat as a feedstock for biodiesel production a two–step process was proposed. The first step of the process is aimed at reducing the FFA content in feedstock by esterification with methanol and acid catalyst as shown in Scheme 1.1. Esterification of FFA with low molecular weight alcohols also serves as alternate route to produce biodiesel and avoid saponification, especially when FFA content is higher than 1% (w/w) [20].

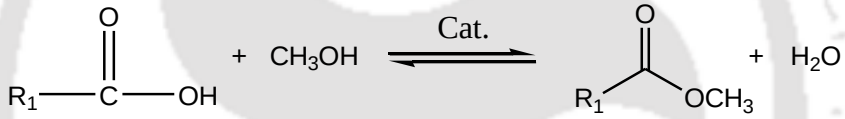

where R_1 – alkyl group of fatty acid chain

Scheme 1.1: Esterification of FFA using methanol

1.3.2 Transesterification process

The most common and favourable method used worldwide for biodiesel production is the transesterification reaction. Basically, the high molecular weight of triglycerides (or oil) have higher viscosities and low volatilities, which results in incomplete burning and blocking of fuel injector when used directly in diesel engine [11]. Transesterification reaction converts the triglyceride molecule into three molecules of esters by reacting with alcohol in presence of catalyst and reduces the viscosity by 90%.

Step–wise reaction

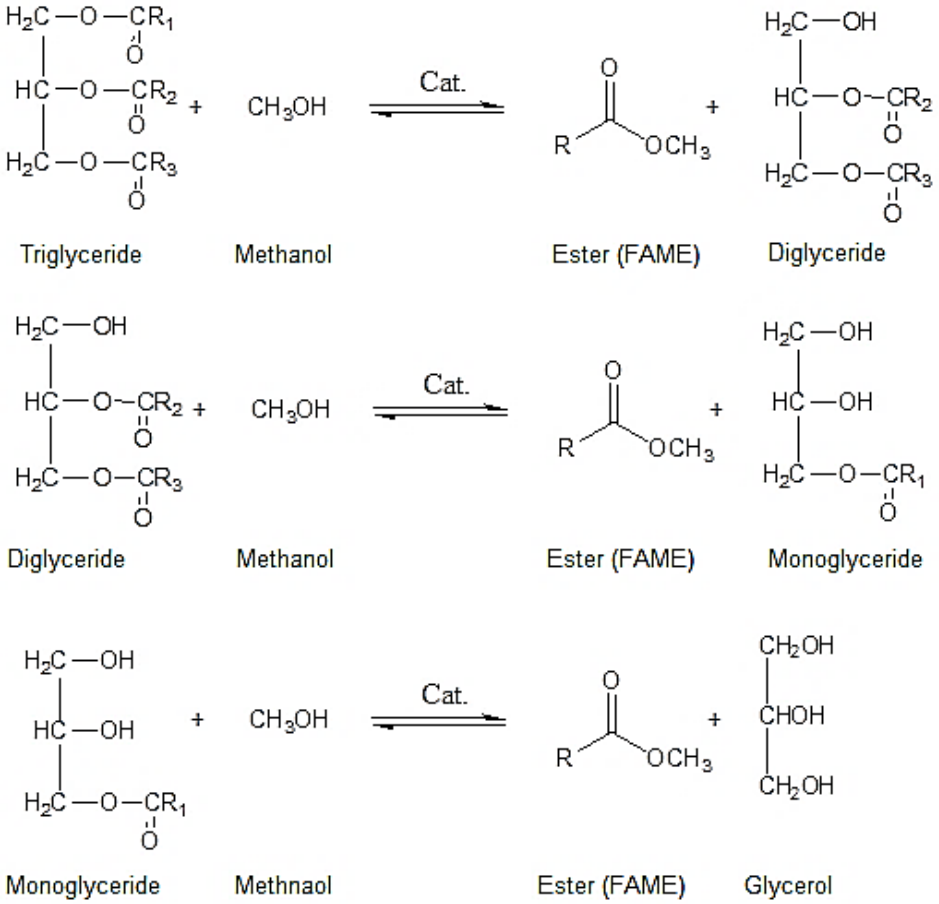

Overall reaction

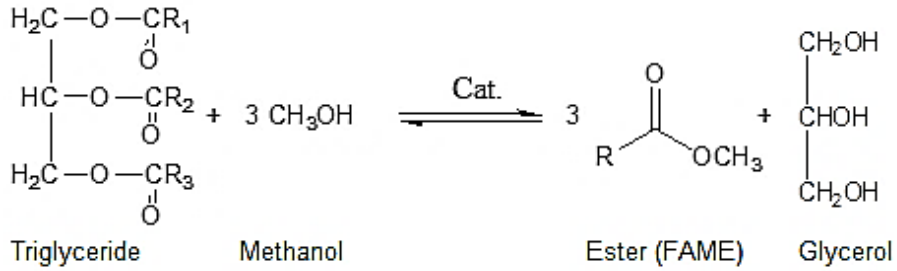

where R_1, R_2 and R_3 – alkyl group of fatty acid chain

Scheme 1.2: Transesterification reaction of triglyceride using methanol.

The transesterification reaction occurs in three steps and it is reversible in nature [18]. Thus, excess alcohol is used to shift the equilibrium on product side. Short chain alcohols used for transesterification reactions are methanol, ethanol, propanol, butanol and amyl alcohol. Methanol is preferred over other alcohols due to its high reactivity in

transesterification reaction and low cost [17]. The reactivity of alcohol in transesterification reaction reduces with increase in number of carbon atoms and chains. The catalyst is used to improve the kinetics of transesterification reaction. The commonly used catalyst for transesterification reaction are alkali, acids and enzymes either in homogeneous or heterogeneous forms. The use of alkali catalyst for transesterification reaction is preferable over acid and enzyme catalyst as kinetics of alkali catalysed transesterification reaction was much higher as compared to acid and enzyme catalysed transesterification reaction [18]. The transesterification reaction occurred in three steps. In step–1, the triglyceride molecule reacts with methanol to form ester and diglyceride molecule, in step–2 the diglyceride molecule reacts with another methanol to form ester and monoglyceride molecule and in step–3, the monoglyceride reacts with another methanol molecule to yield final ester molecule and glycerol as a by–product, as shown in Scheme 1.2.

1.3.3 Interesterification process

One of the major drawbacks of transesterification process is the contamination of by–product glycerol with catalyst (alkali or acid) when used in homogeneous form and alcohol [21]. Thus, making it unsuitable for conventional application in food, cosmetic and pharmaceutical industry and lowers the economy of overall process. Purification of this crude glycerol is cost intensive. Therefore, an alternate route to biodiesel production was developed through interesterification of triglycerides in presence of simple esters such as methyl acetate instead of methanol [22]. The main product of interesterification reaction is biodiesel with by–product as triacetin. Triacetin has higher commercial value than glycerol and it also has several applications including as a blending agent in the fuel. As per current European norms of biodiesel

EN 14214, 10% blending of triacetin is allowed. Casas et al. [23] had investigated the blending of triacetin with biodiesel and found that upto 20% blending of triacetin to biodiesel is acceptable for present IC engines and meets the specified limits of fuel properties.

Step–wise reaction

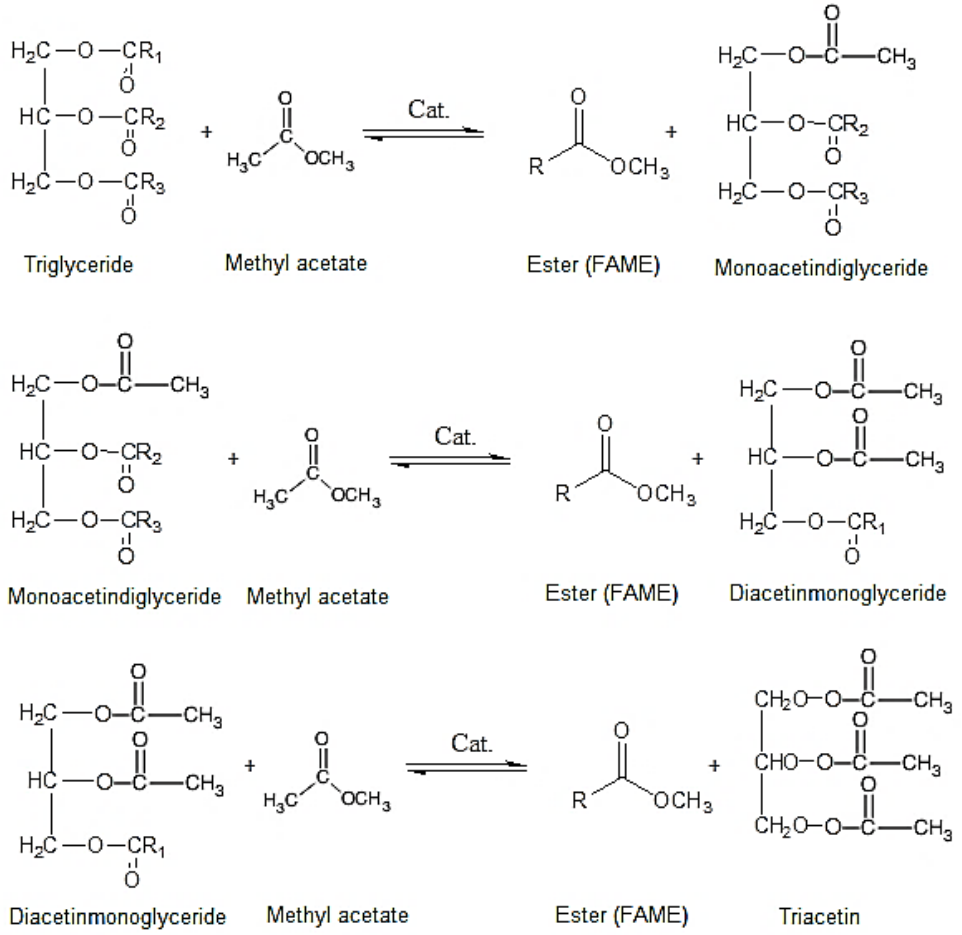

Overall reaction

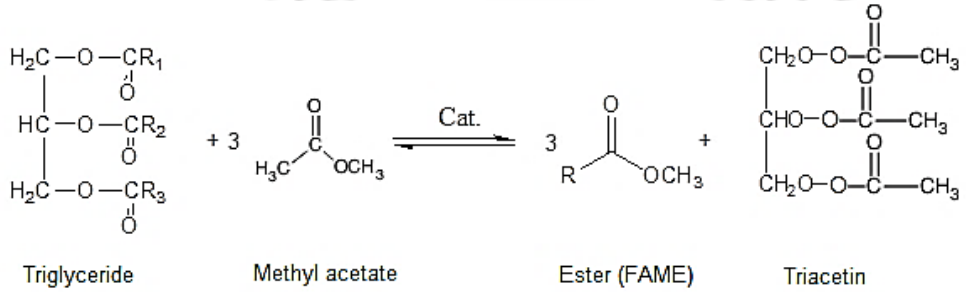

where R_1, R_2 and R_3 – alkyl group of fatty acid chain

Scheme 1.3: Interesterification reaction using methyl acetate

This makes overall interesterification process economically attractive and viable as compared to transesterification process. The interesterification reaction occurs similar to transesterification reaction in three steps as shown in Scheme 1.3.

1.3.4 Non–catalytic transesterification process

The another alternate route for biodiesel production is transesterification of triglycerides over supercritical methanol, ethanol, propanol and butanol [18]. This process doesn't require any catalyst to boost the kinetics of reaction. A non–catalytic route to biodiesel production with supercritical methanol allows a triglyceride feedstock with any FFA content because transesterification of triglycerides and methyl esterification of fatty acids occurs simultaneously at supercritical condition of methanol [24]. Another advantage of non–catalytic transesterification process is the by–product glycerol has minimal contamination and has commercial value [18]. Despite, several advantages, the non–catalytic transesterification process with supercritical methanol/ ethanol has drawback of high operating conditions (temperature > 523 K and pressure > 20 bar) and higher alcohol to oil ratio [18,25]. The co–solvent such as hexane, heptane, propane, etc. may be used to lower the operating condition and methanol: oil ratio [26].

1.4 Catalysts for biodiesel production

As discussed in earlier section 1.3, biodiesel can be synthesized either in absence of catalyst or in presence of homogeneous, heterogeneous (alkali/ acid) or enzymatic catalysts [18,19]. Catalysts usually improve the kinetics of trans–esterification reaction and the product yield as they are able to lower the surface tension

between the two immiscible phases, i.e. triglycerides and alcohol [15]. The classification of different catalysts used for biodiesel production is shown in Fig. 1.3.

Homogeneous catalyst, especially homogeneous alkali catalyst (NaOH/ KOH) are more commonly used for transesterification of feedstock with low FFA content. The presence of FFA and water always produce negative effects on transesterification reaction, since the presence of FFA and water causes soap formation, consumes catalyst and reduces catalyst effectiveness, all of which results in a low conversion of triglyceride to biodiesel [15]. Another major drawback of using homogeneous catalyst is contamination of by–product glycerol, expensive separation of the catalyst from the reaction mixture and generation of large amounts of waste–water during purification of biodiesel.

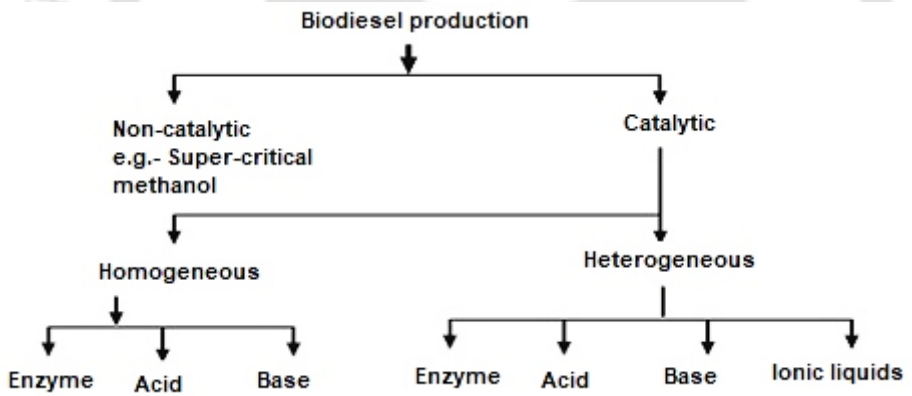

Figure 1.3: Classification of catalysts for biodiesel production.

Biodiesel synthesis by using solid catalysts is therefore a viable environmentally friendly alternative which minimize the consumption of large amounts of water during the purification of biodiesel [19]. Unlike homogeneous catalyst, the heterogeneous catalysts act in a different phase from the reaction mixture. Use of heterogeneous catalyst has the advantage of easy separation from the reaction mixture and recovery as well as reusability of the catalyst, potentially leading to higher efficiencies and lower

production costs [27,28]. Some process parameters for homogeneous and hetero–geneous catalyst are compared in Table 1.2.

Table 1.2: Comparison between homogeneous and heterogeneous catalyst for biodiesel production [27]

Variable	Homogeneous catalyst	Heterogeneous catalyst
Reaction rate and yield	Fast and high conversion	Slow and moderate conversion
Purification of product	Difficult	Easy
Methodology	Batch operation	Continuous operation possible
Presence of FFA and water	Highly sensitive	Low sensitive
Catalyst reusability	Not possible	Possible
Cost	Cheap (but overall process becomes costly)	Potentially cheaper

Extensive research has been carried out in last few decades to develop different catalysts for biodiesel production. A brief discussion on different types of catalysts for biodiesel production is given in following sub–sections.

1.4.1 Alkali or base catalyst for biodiesel production

Due to mild operating conditions and higher reaction yield, homogenous base catalyst (NaOH/ KOH) is most widely used for biodiesel production for feedstocks with very low or negligible content of free fatty acids (typically FFA < 1% w/w). As low as 1 wt% of NaOH or KOH is sufficient to yield around 98% biodiesel from low fatty acid feedstock [29]. As discussed above, the homogeneous base catalyst in presence of FFA and water leads to soap formation. Moreover, fraction of catalyst retained in by–product glycerol act as contaminant and lowers the economy of the overall process [19].

To overcome these hurdles and improve the economics of the large scale transesterification process, the use of heterogeneous catalyst is a feasible solution, which can be easily separated from the reaction mixture for reuse, without contamination of the by–product glycerol. Since the ability of the base to abstract a

proton from the alcohol is directly connected to the base strength, stronger bases are in general more effective to initiate the transesterification of triglycerides in heterogeneous catalyst form [27]. It was reported by Malero et al. [30] that the metal oxide provides sufficient adsorptive sites for alcohol in transesterification reaction and concluded that the high transesterification activity of catalyst might be due to the manifestation of the dissociation of alcohol to RO^- and H^+ on basic sites of metal oxide catalyst surface. Several studies have reported the use of heterogeneous base catalysts synthesized with different methods using silica, zinc oxide, zirconia, zeolites, alumina, aluminosilicates, clays, activated carbon, etc. as supports, and alkali and alkaline earth oxides or their salts (like KOH, KF, KI, KNO_3, K_2CO_3, NaOH, CaO, $Ba(OH)_2$) as functional part [31–41].

1.4.2 Acid catalyst for biodiesel production

The direct application of base catalyst is not possible for non–edible oils feedstock due to their high FFA content, which leads to saponification. Thus, the single step transesterification process is converted in two step process. The first step of the process reduces the FFA content in oil by esterification with methanol and acid catalyst and the second step is conventional transesterification process, in which triglyceride portion of the oil reacts with methanol and base catalyst to form ester and glycerol [18]. Alternatively, the acid catalysts are capable of performing simultaneous esterification and transesterification reaction. The commonly used homogenous acid catalysts are H_2SO_4, HF, H_3PO_4, HCl, and p–toluene sulfonic acid etc. [20, 42, 43]. The major drawbacks of acid catalyst are: (i) their highly corrosive, (ii) hazardous in nature, and (iii) ~ 4000 times slower kinetics as compared to the homogenous base catalyst [44]. Because of the lower activity of the acid catalyst as compared to the base catalyst (both

in homogenous and heterogeneous form), the reactions are generally carried out at higher temperature and pressure [30].

In recent years, a substantial progress has been made on the development of heterogeneous acid catalyst for biodiesel production. Several heterogeneous acid catalysts have been tested in the FFA esterification as well as simultaneous esterification and transesterification reaction, such as sulphated metal oxides, mesoporous silica, modified zeolites, metal organic framework (MOF) structures, ion exchange resins, polymer supported sulphonic groups, carbon–based supports with functionalized acid groups, etc. [44–52]. Therefore, acid heterogeneous catalysts can be considered as an alternative to minimize the environmental damage and reduce the cost of biodiesel production.

1.4.3 Enzymes as a catalyst for biodiesel production

In biological systems, interesterification and transesterification reactions occur naturally. Enzyme catalysed transesterification is another alternate path to produce biodiesel. The most common enzyme used for transesterification reaction is lipase. However, due to the high cost of the enzyme, proper recovery and recycle of the enzyme is essential for the economy of the process [53,54]. Over past few years, lipase from various sources immobilized on different supports has been studied by many researchers. Lipase from *Candida Antarctica* immobilised on mesoporous silica [55], *Candida rugosa* on nanofibrous poly–membrane [56], *Thermomyces lanuginosus* immobilized on microporous polymer [57], *Thermomyces lanuginosus* immobilised on styrene divinylbenzene copolymer [58], *Burkholderia* immobilised on hydrophobic magnetic particles [59], *Candida Antarctica, Thermomyces lanuginosus* and *Rhizomucor miehei* immobilised on epoxy–functionalised silica [60,61], *Aspergillus*

niger immobilised on micro–porous biosilica [62], have been used. Jegannathan et al. [63] and Zhao et al. [64] reviewed many other feasible supports such as calcium alginate beads, anion exchange resin, silica–polymer, acrylic resin and biosilica. for immobilization of lipase. The common aspects of these studies involved optimizing the reaction conditions (solvent, temperature, pH, etc.) in order to establish suitable characteristics for an industrial application. However, the reaction yields as well as the reaction times are still unfavourable compared to the alkali catalysed transesterification systems.

1.4.4 Ionic–liquid as a catalyst for biodiesel production

In recent years, the ionic liquids (ILs) have been also investigated as an alternate to heterogeneous alkali and acid catalyst for biodiesel production [65]. Ionic liquids (ILs) with variety of structures have been considered as green reaction medium due to their negligible volatility, excellent thermal stability and high solubility [66]. Brønsted acid ionic liquid containing an alkane–sulfonic acid group was reported suitable for production of biodiesel from various feedstocks [67].

The ionic liquids exhibit good catalytic activities, especially, 1–(4–sulfonic acid) butylpyridinium hydrogen sulfate was reported to have similar catalytic activity as concentrated sulfuric acid [68]. The ionic liquid catalysts could be recovered and reused after distillation. However, the ionic liquid catalysed transesterification reaction required higher reaction temperature (> 423 K) and longer reaction time as compared to the alkali catalysts [66].

1.5 Feedstocks for biodiesel production

The availability and type of the feedstock is the major contributor to the overall cost of the biodiesel production [69]. The selection of oil for biodiesel production is based on its availability, characteristics and cost [70]. Thus, the feedstock for biodiesel production has been classified under 1st, 2nd and 3rd generation feedstock.

1.5.1 1st generation feedstock for biodiesel production

Transesterification reaction in the beginning (in 1930) were carried out using edible oils, thus edible oils are considered as 1st generation feedstock for biodiesel production. Edible oils (rapeseed and soybean) are commonly used for biodiesel production in Europe and United States of America. Whereas, Philippines and Malaysia are also utilizing edible oils such as coconut oil and palm oil, respectively, for biodiesel production. The edible oils such as soybean, rapeseed, palm, coconut, sunflower and linseed oils, etc. are exploited commercially by some developed countries as raw material for biodiesel production [71].

1.5.2 2nd generation feedstock for biodiesel production

Countries like India, where food security is on priority, edible oils cannot be diverted for fuel production. Non–edible oils have some toxic substances, which restrict their use for human and animal consumption. Thus, non–edible oils with higher free fatty acids are used as feedstock for biodiesel production and considered as 2nd generation feedstock. Non–edible oils such as *Jatropha curcas* (Jatropha), *Ficus elastica* (rubber), *Camelina sativa* L. Crantz (Camelina), *Madhuca indica* (mahua), *Pongamia pinnata* (karanja), *Nicotina tabacum* (tobacco), *Calophyllum inophyllum* (polanga) etc., are explored as raw material for biodiesel production [70, 71].

1.5.3 3rd generation feedstock for biodiesel production

In order to reduce the cost of biodiesel production, micro and macro algae oils have also been used by researchers as a source of feedstock for the production of biodiesel. Therefore, micro and macro algae oils are categorized as 3rd generation of feedstock for biodiesel production. Due to higher biomass production, faster growth and photosynthetic efficiency of microalgae as compared to other energy crops could be a potential source of low cost feedstock for large scale production of biodiesel [69, 70].

The percentage of raw materials utilized for commercial biodiesel production in the world are rapeseed oil (84%), sunflower oil (13%), palm oil (1%), soybean oil and others (2%) which includes 2nd and 3rd generation feedstock [72].

1.6 Ultrasound–assisted intensification for biodiesel production

Application of heterogeneous catalyst for biodiesel production through transesterification reaction makes the reaction mixture a 3–phase heterogeneous system (solid–liquid–liquid), which has high mass transfer constraints. The conventional mixing and heating method includes hot plates (laboratory scale), oil, or sand baths, and water heated jacketed reactors combined with mechanical mixing [73]. This process usually takes longer times to complete the reaction due to lower extent of intermixing of two immiscible phases in each other and uneven heat distribution [19]. Novel mixing and heating techniques like microwave and ultrasound are known to drastically reduce the reaction time while improving the biodiesel yields simultaneously through an effect called “process intensification” [73]. The comparison between conventional transesterification, microwave–assisted transesterification and ultrasound–assisted transesterification method is given below in Table 1.3.

Table 1.3: Comparison between conventional, microwave and ultrasound assisted transesterification methods for biodiesel production [73]

Conventional method (Mechanical agitation)	Microwave–assisted method	Ultrasound–assisted method
Thermal gradient (outside to inside)	Inverse thermal gradient (inside to outside)	Limited thermal gradient due to strong intermixing
Conduction and convection currents	Molecular–level hot spots	Microbubble formation and collapse (compression and rarefaction cycles)
Longer processing and heating time	Very short and instant heating	Relatively very short reaction times, but not as quick as microwaves
Product quality and quantity can be affected	Higher product quality and quantity possible	Higher product quality and quantity possible
High energy consumption	Moderate to low energy consumption	Moderate to low energy consumption
Simple process configuration	Very simple process	Moderate complexity

The present study addresses the ultrasound – assisted process intensification for biodiesel production through transesterification and interesterification process. Thus, in sub–sequent sections basic principles of ultrasound are briefly described.

1.6.1 Basic concepts and principles of ultrasound

Ultrasound essentially refers to the sound waves having frequency beyond the upper limit of human hearing range typically in the range of 20 kHz – 500 MHz. The ultrasound irradiation manifests its physical/chemical effects on reaction system through the process of cavitation [74]. Ultrasound wave passes through an elastic medium as a longitudinal wave, i.e. as a series of alternating compressions and rarefactions, which induces liquid to be displaced parallel to the direction of motion of the wave [75]. The amplitude of displacement of fluid elements depends the pressure amplitude of the ultrasound wave, which in turn depends on the energy of the wave. The frequency (f) and the acoustic amplitude ($P_{A,max}$) are the most important properties that characterize a sound wave. The bulk pressure in the liquid medium undergoes

periodic (usually sinusoidal) variation during propagation of the ultrasound wave. In simple form, the pressure amplitude of the ultrasound wave (P_A) and the bulk pressure in the medium (P_t) at any instance (time, t) for frequency f by the following equation [74]:

$$P_A = P_{A,\max} \sin\left(2\pi ft\right)$$

$$P_t = P_o - P_{A,\max} \sin\left(2\pi ft\right)$$

where, $P_{A,max}$ is the pressure amplitude of the ultrasound wave and P_o is the static pressure in the bulk liquid medium.

Based on the applied frequency, the use of ultrasound can be broadly divided into two categories [74]:

(i) Low intensity, high frequency ultrasound (2 – 500 MHz, 0.1 – 0.5 W/cm^2)

(ii) Power ultrasound with high intensity and low frequency (20 – 900 kHz, >10 W/cm^2)

The first type of ultrasound does not alter the state of the medium, through which it travels and is commonly used for non–destructive evaluation and medical diagnosis. This type of ultrasound cannot be used for reactions. On contrary, power ultrasound uses the energy to create cavitation, which involves the formation, growth and implosive transient collapse of microscopic bubbles in a liquid. Power ultrasound is applied for cleaning purposes, treatment of kidney stones, plastic welding, and for chemical reactions.

Ultrasound waves can be generated in the medium using a transducer, which essentially converts one form of energy (electrical) into another form (mechanical). The piezo–electric crystal under the influence of alternating voltage (or potential) applied across it generates the volume oscillations. These mechanical oscillations can be converted into sound energy, by coupling the piezo–electric element to a fluid medium

such as water [74, 75].

1.6.2 Cavitation

Cavitation is a secondary effect of ultrasound which is the activity of tiny bubbles in the liquid medium. The basic definition of cavitation phenomenon can be given as nucleation, growth and implosive transient collapse of gas or vapour bubbles in the medium driven by pressure variation in the bulk liquid corresponding to ultrasound wave propagation. Transient collapse of cavitation bubbles creates extreme temperatures and pressure on extremely small spatial and temporal scale [76]. This phenomenon also offers high heating and cooling rates, which favours and induces occurrence of various chemical reactions [77]. Occurrence of cavitation phenomenon induced by the propagation of the ultrasound wave as shown in Fig. 1.4, can be explained as follows: In oscillatory motion during propagation of the wave, the fluid elements in the bulk medium are pulled apart from each other resulting in formation of small bubbles from the "*cavitation nuclei*" present in media. These nuclei could be gas pockets trapped in the crevices of the solid boundaries in the reaction system such as reactor wall or surface of sonicator probe. These cavitation nuclei grow into the cavitation bubbles during the rarefaction half cycle of ultrasound due to evaporation of the solvent vapour into the bubble. The bubble undergoes compression in the subsequent compression half cycle of the ultrasound wave. The bubble compression or collapse occurs in almost adiabatic manner with generation of very high temperature and pressure inside the bubble. Temperature > 5000 K and pressure > 1000 atm is generated inside the bubble. During the transient collapse, the gas–vapour mixture inside the bubble undergoes thermal dissociation to generate a wide spectrum of small species – some of which are radical species. This phenomenon known as "*sonochemical*

effect" which generates favourable conditions for occurrence of chemical reaction [74–77].

1.6.3 Types of cavitation

Depending upon the principal which lead to occurrence of cavitation in the medium, various types of cavitation can be categorized as follows [74]:

a. Acoustic cavitation: Acoustic cavitation is caused by the pressure variation in the liquid due to passage of an acoustic wave. It generally occurs in the acoustic frequency range of 20 kHz – 1 MHz.

b. Hydrodynamic cavitation: Hydrodynamic cavitation occurs due to pressure variation in the liquid flow velocity generated by the changing flow geometry. This pressure variation generally occurs at low frequencies (100 Hz – 10 kHz).

c. Optical cavitation: Optical cavitation is a result of local evaporation of liquid due to intense local energy dissipation caused due to sources such as high–intensity laser.

d. Particle cavitation: Particle cavitation is produced by any elementary particle (such as proton) rupturing the liquid.

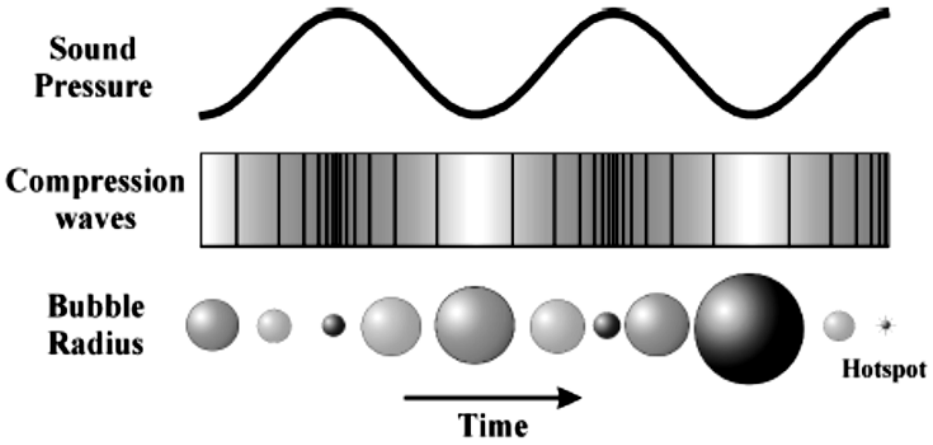

Figure 1.4: Schematic representation of bubble growth and collapse in a liquid irradiated with ultrasound and the resulting hot–spot (adopted from [77])

1.6.4 Physical factors governing cavitation

The phenomenon of cavitation is influenced by many physical factors related to ultrasound itself and the physical properties of the liquid medium, which affects directly the reaction rate and/or yield.

a. Effect of temperature: In most of chemical reactions, increase in temperature increases the rate of reaction, but in case of ultrasound an increase in the bulk liquid reaction temperature results in an overall decrease in the sonochemical effect. It is because, as the reaction temperature increases, the corresponding equilibrium vapour pressure of the system also increases, resulting in greater evaporation of solvent vapour into the bubble during expansion. A fraction of this vapour gets entrapped in the bubble during transient collapse. Due to this vapour, the energy concentration resulting during transient collapse reduces, as the vapour cushions the implosive collapse with addition to increasing the net heat capacity of the bubble contents. The resulting temperature and pressure from the transient collapse of bubbles are reduced, and hence, the extent of production of radicals. Therefore, the highest sonochemical effects are observed at lower temperatures, when the vapour content of bubble is small as possible [74].

b. Effect of ultrasound frequency: The frequency of the ultrasound has a significant effect on the cavitation process, as it governs the nature of bubble dynamics and the intensity of the transient cavitation. Rise in ultrasound frequency reduces the time period of the wave. Thus, larger pressure amplitude is required for the sufficient growth of the bubble so as to undergo a transient collapse. To achieve the similar effect of cavitation at higher frequency, the net power requirement increases largely. As the frequency of the ultrasound wave increases, the period of the wave and the duration of both rarefaction and compression half cycles decrease. For a given pressure amplitude of the ultrasound wave (higher than transient cavitation threshold), expansion of the

bubble reduces with increasing frequency; and hence, the intensity of the subsequent transient collapse as well. Thus, the cavitation effect tends to be lower at higher frequencies. Frequencies in the range of 20–30 kHz are used normally, for sonochemical application corresponding to power ultrasound [74].

c. Effect of acoustic power: It was reported that rate of an ultrasound–assisted reaction shows maxima with input acoustic power. A possible explanation for reduction in reaction rate at high power is the formation of a dense cloud of cavitation bubbles near the probe tip which hinders the transmission of energy from the probe to the fluid [74].

d. Effect of static pressure in the medium: Ambient or static pressure in the medium is an important factor governing the expansion of the cavitation bubble in the rarefaction half cycle of ultrasound. The bubble expands to size higher than its original (or equilibrium) size, only when the instantaneous pressure in the medium falls below the ambient pressure. This means that higher acoustic pressure amplitude (and hence higher energy) is needed for generating cavitation at higher static pressure. In other words, increase in reaction pressure (above static pressure amplitude) eliminates the cavitation phenomena (and converted to stable, small amplitude oscillatory behaviour or set to zero) and maintain only physical effect of ultrasound in the medium i.e. only intense mixing (due to the oscillatory velocity) [74,76].

e. Effect of acoustic intensity or pressure amplitude: Acoustic intensity or acoustic pressure amplitude has a profound effect on the characteristics of cavitation events occurring in the medium. To achieve transient motion of the cavitation bubble which would results in generation of high temperature and pressure during the collapse, would require certain minimum amplitude of the wave, called as “transient cavitation threshold”. The transient cavitation threshold is essentially equal to the static pressure

in the medium. This requires expansion of the bubble to at least twice of its initial size. Below this threshold value, the amplitude of the wave would be too small to cause significant bubble growth. In such cases, the bubble undergoes small amplitude, stable, oscillatory motion, which is not energy intensive [74, 76–77].

f. Effect of nature of cavitation medium: Each solvent has its own properties like viscosity, surface tension, vapour pressure, etc. Thus, the choice of solvent medium is very important factor in case of sonication. These physical properties are of relevance to the nature and intensity of cavitation. The liquid medium with high surface tension, low viscosity and low vapour pressure are conducive for cavitation process [74].

g. Effect of viscosity, surface tension and vapour pressure: Viscosity of the medium is result of the natural cohesive forces active in the liquid. It acts as a break on the radial motion of bubbles. Moreover, it is also responsible for the weakening of the acoustic wave, with loss of the wave energy into the thermal energy. Increase in liquid viscosity diminishes the radial motion of the bubbles, thus limits the maximum size attained during radial motion. The cavitation intensity, as indicated by the temperature and pressure attained during collapse, decreases with increasing viscosity of the liquid [74].

Surface tension indicates the difficulty in creating cavitation in the liquid. An increase in surface tension of the liquid increases the cavitation threshold, i.e. the minimum acoustic pressure amplitude for creation of cavitation in liquid. The intensity of the cavitation bubble collapse increases with increasing surface tension of the medium [76].

The vapour pressure of the bulk liquid medium depends on the temperature of the medium. During ultrasound irradiation, the temperature of the medium increases continuously due to viscous and thermal dissipation of the momentum of the ultrasound

waves. Higher vapour pressure of the liquid medium causes evaporation of the solvent vapor in the bubble. This vapour can cushion the collapse of the bubble in the compression half cycle of the wave and reduce the intensity of the collapse. Some of the vapour can also get entrapped in the bubble which results in generation of chemical and radical species during the collapse [74].

1.6.5 Sonochemical effects of cavitation

The principal chemical effect of cavitation (known popularly as the sonochemical effect) is generation of highly reactive radicals such as $^{\bullet}O$, $^{\bullet}OH$, and $HO_2^{\bullet}$ during transient collapse of the cavitation bubbles. These radicals are mainly produced through the thermal dissociation of the vapour molecules entrapped in the cavitation bubbles at the instance of transient collapse, when the temperature inside the bubble reached extreme. Thus, two factors are mainly responsible for the radical generation by cavitation bubbles, i.e. the composition of the bubble interior (i.e. the number of gas and vapour molecules) and the temperature of the bubble interior reached during collapse. During radial motion, the composition inside the bubble varies continuously due to several phenomena such as gas diffusion, gas rectification, water vapour condensation / evaporation and the chemical reactions. Several authors have addressed the problem of water vapour entrapment in the bubble and its consequences (i.e. chemical reactions, alteration of heat transfer across bubble) with different approaches [78–87].

1.6.6 Physical effects of cavitation

Ultrasound and cavitation render several physical effects on a reaction system. The main manifestation of all of these results is generation of intense micro–convection

and micro–mixing in the reaction system. A brief description of all physical effects of ultrasound and cavitation is given below:

a. Micro–streaming: This is essentially small amplitude oscillatory motion of fluid elements around a mean position, which is induced by propagation of ultrasound wave [74].

b. Microturbulence: The oscillatory motion of fluid induced by volume oscillations of the bubble is called microturbulence. During expansion of the cavitation bubble, the liquid surrounding the bubble is displaced away from bubble interface. In the compression phase, fast contraction of the bubble generates "void" around it, and the liquid is pulled towards the bubble as it fills this void. The velocity of microturbulence, is obviously a function of the amplitude of bubble oscillation. The phenomenon of microturbulence is observed only in the close vicinity of the bubble, and diminishes very rapidly away from it [74–76].

c. Acoustic (or shock) waves: As noted above, the compression of the bubble is mostly adiabatic and the pressure inside the bubble rises rapidly if the bubble contains non–condensable gas such as air. At the point of minimum radius (or maximum compression) during radial motion, the velocity of the bubble wall becomes zero. At this moment, the velocity of the fluid elements converging towards the bubble interface also reduces to zero – almost instantly – which creates rise in pressure (due to conservation of momentum). This generates a high pressure shock wave that propagates through the medium. The bubble may undergo rebounce due to the pressure exerted by the non–condensable gas inside the bubble [74].

d. Microjets: During radial motion driven by ultrasound wave, the initial spherical geometry of the bubble may be disturbed due to non–uniformity of pressure gradients surrounding it. These non–uniform gradients are induced by phase boundaries, either

solid–liquid, gas–liquid or liquid–liquid, due to which the motion of liquid in the vicinity of the cavitation bubble is hindered. Under influence of non–uniform pressure gradient, the bubble undergoes asymmetric radial motion with the portion of bubble exposed to higher pressure collapsing at a faster rate than rest of the bubble. Such asymmetric motion results in formation of a high speed liquid jet. The direction of this jet depends on the type of phase boundary. For a "rigid" boundary such as metal surface, the microjet is directed towards the boundary. For a "free" boundary such as gas–liquid (typically air–water) interface, the microjet is directed away from the boundary. The velocities of these microjets are in the range of 120–150 m/s [74–78].

1.7 Literature on biodiesel production

Several state–of–art reviews focusing different fundamental aspects of biodiesel production have been published in past couple of decades. A brief summary of some of these reviews are discussed herewith to start the literature survey.

Ma and Hanna [88] reviewed the various ways to use vegetable oil as biodiesel in diesel engine. The review also addressed processes of transesterification and its down–stream operations. Gandhi et al. [89] reviewed the lipase–catalysed esterification in anhydrous media, and effect of various process parameters on lipase catalysed esterification. Demirbas [18, 90] reviewed the biodiesel production using catalytic and non–catalytic process (supercritical methanol). In another study, Demirbas [91] summarised different thermal conversion processes for biodiesel production from biomass and vegetable oil. Meher et al. [92] reviewed various technical aspects of biodiesel production such as mode of reaction, molar ratio of alcohol to oil, type of alcohol, type and amount of catalysts, reaction time and temperature and purity of reactants, etc. Marchetti et al. [93] analysed the different possible methods for biodiesel

production and compared their advantages over each other. Basha et al. [94] presented a comprehensive review on biodiesel production, combustion and emission performance of biodiesel in diesel engine.

Banerjee and Chakraborty [95] presented a review on parameter sensitivity in transesterification process from waste cooking oil. Helwani et al. [96] discussed the batch and continuous production of biodiesel using homogenous and heterogeneous catalyst. Fjerbaek et al. [97] presented a review on enzyme catalysed transesterification reaction. The review focussed on critical aspects of the process such as mass transfer limitations, use of solvents and water, and also process considerations and evaluation of industrial scale reactor configurations. In another review, Meng et al. [98] discussed the possibility of biodiesel production from oleaginous microorganisms. Meng et al. [98] reviewed the potential of oleaginous microorganisms like microalgae, bacillus, fungi and yeast for biodiesel production. Jothiramalingam and Wang [99] reviewed the developments in alkali, acid and enzyme heterogeneous catalyst for economical biodiesel production and compare the performance with homogeneous catalyst. Melero et al. [30] reviewed the development of heterogeneous acid catalyst for biodiesel production with using high FFA content feedstock.

Singh and Singh [100] reviewed possible different sources for biodiesel production with their basic characterization. Leung et al. [101] reviewed the various catalysed transesterification process and different approaches for reducing free fatty acids in the raw oil that can be adopted in the industry. Mata et al. [102] overviewed the current status of microalgae use for biodiesel production, including their cultivation, harvesting, and processing. The microalgae species mostly used for biodiesel production are analysed with their advantages over other available biodiesel feedstocks. Tan et al. [103] reviewed the new techniques for immobilization of lipase with higher

activity and stability for biodiesel production. Math et al. [104] explored various possibilities of biodiesel production using waste frying oil from different sources. Knothe [105] exclusively reviewed biodiesel as a renewable fuel and compared with mineral diesel. Various aspects such as production cost, energy balance, fuel properties and environmental effects with respect to exhaust emissions have been discussed judiciously.

Koh and Ghazi [106] reviewed the different approaches and techniques used to generate biodiesel from non–edible *Jatropha curcas* oil. Chen et al. [107] and Ahmad et al. [108] studied the cultivation, production and harvesting of microalgae for sustainable biodiesel production. Chen et al. [107] explored the different aspects of photo–bioreactor design to improve the microalgae yield. Balat [109] also explored the production of biodiesel from different non–edible oilseed crops. Chouhan and Sarma [32] explored the modern heterogeneous catalyst for biodiesel production. The main focused of the review was on the recent invention and use of the heterogeneous acid, base and biocatalysts for biodiesel production and their suitability for industrial application. Boney et al. [110] evaluated the performance of calcium oxide as heterogeneous catalyst in biodiesel production using different feedstocks.

Kiss and Bildea [111] critically analysed the biodiesel production using integrated reactive separation technologies. The review provided a detailed overview of novel reactive separation technologies used in biodiesel production: reactive distillation/ absorption/ extraction and membrane reactors. Abbaszaadeh et al. [112] have reviewed different catalytic and non–catalytic techniques for biodiesel production. Borges and Díaz [20] reviewed developments in bi–functional (acid–base character) heterogeneous catalyst which can catalyse both esterification and transesterification reaction. Boro et al. [113] reviewed the possibility of solid oxide derived from waste

shells as heterogeneous catalyst for biodiesel production. Giakoumis et al. [17] reviewed the exhaust emissions of diesel engine operated with biodiesel fuel blends under different operating conditions. Halim et al. [114] summarised various techniques for efficient oil extraction from microalgae for biodiesel production. Atabani et al. [115] comprehensively reviewed the biodiesel as an alternate energy source from its economy and feasibility point of view. Yusuf et al. [116] reviewed the biodiesel production using heterogeneous catalyst and design the system via process simulation and optimization with the persistent challenges facing this process for commercial application. Santori et al. [117] have analysed economics of industrial biodiesel production. Atadashi et al. [118, 119] reviewed the effects of water and catalyst on transesterification process with identification of means of improvement of the catalysts performance.

Silitonga et al. [120] reviewed biodiesel production from *Jatropha curcas* using different homogeneous acid and alkaline catalysts. Su and Guo [15] reviewed the potential and recent development of solid acid catalyst in biodiesel production. Baskar and Aiswarya [121] evaluated the trends in catalytic production of biodiesel using various edible and non–edible feedstocks. Recently, Knothe and Razon [122] published a review on biodiesel as an alternate fuel, discussing increasing biodiesel need and socio–economic issue related with the production and use of biodiesel.

1.7.1 Ultrasound–assisted biodiesel production

Extensive research has been carried out on biodiesel synthesis and over 2000 papers have been published during last two decades. These reports have focused on different aspects of biodiesel production such as feedstocks selection, catalysts synthesis and its application, production techniques and performance of biodiesel. A detailed review of all these reports is not practically possible and also inappropriate

with respect to theme of present work. The main objective of this work was to investigate the heterogeneously catalysed biodiesel production using mixed non–edible oil feedstock and its intensification through application of ultrasound. Thus, according to theme of present work, the review of literature in the area of heterogeneously catalysed transesterification process has been given. The focus of this section remains at heterogeneous catalysts (alkali, acid or enzyme) and intensification of the process with application of ultrasound. Few state–of–art reviews focussing on sonication as a tool for process intensification of biodiesel synthesis have been published, and are discussed below.

Lam et al. [123] published a comprehensive review on homogeneous, heterogeneous and enzymatic catalyst for biodiesel production. The review also discussed various methods to intensify the transesterification reaction and lower heterogeneity of the system through application of co–solvent method, oscillatory flow reactor system, microwave mixing and ultrasound assisted system. Ramachandran et al. [71] reviewed the developments in the heterogeneously catalysed biodiesel production in presence of ultrasound irradiation. The review concludes that ultrasonic energy emulsifies the reactants to reduce the catalyst requirement, methanol–oil ratio, reaction time and reaction temperature, as compared to conventional mechanically agitated system. Lerin et al. [124] overviewed the ultrasound–assisted enzymatic esterification and transesterification reactions for biodiesel production. The review also explored several other enzyme catalysed reactions such as alcoholysis and glycerolysis for production of biodiesel and glycerides (mono and di). The review suggests sono–chemical reactors advantages and application for biodiesel production at large scale process. Islam et al. [125] had compared various advancements in catalytic and non–catalytic reactions for biodiesel production with application of ultrasound in process

intensification. The review published by Lourinho and Brito [126] analysed the novel developments in biodiesel production in terms of feedstock selection and process intensification. They discussed different operational aspects of process intensification technologies such as ultrasound irradiation, microwave heating, use of co–solvents and membrane reactors for economical biodiesel production.

Ho et al. [127] summarized the advances in ultrasound–assisted transesterification reaction. They critically appraised the status of current technology on application of ultrasound energy in conjunction with heterogeneous catalysts for biodiesel production. They also analysed the existing pilot scale ultrasound–assisted biodiesel production and suggested techno–economic feasible solutions for future developments. Chuah et al. [128] discussed issues of cleaner intensification technologies in biodiesel production. They discussed application of hydrodynamic cavitation for biodiesel production at large scale level, over ultrasonic cavitation and conventional mechanical agitation. Gude and Martinez-Guerra [73] assessed the process intensification in sustainable biodiesel production using green chemistry approach. They compared the reaction efficiency between the conventional mechanical agitation, microwave and ultrasound enhanced biodiesel synthesis. A combination of microwave and ultrasound assisted intensification of transesterification reaction was analysed based on reaction mass efficiency, mass productivity, atomic efficiency and environmental E–factor. They also compared the working principles of conventional mechanical agitation, microwave heating and ultrasound irradiation. Non–catalytic transesterification reaction with effect of addition of various co–solvents have also been discussed for greener and sustainable biodiesel production.

1.7.2 Alkali catalysed transesterification reaction

Moghzi and Soleimannejad [129] synthesized new nano–sized barium coordination polymer using ultrasound and studied its application as a heterogeneous catalyst for biodiesel production. A full conversion of soybean oil (> 99%) to biodiesel was accomplished in 150 min, with 6% (w/w) synthesized catalyst loading, 12:1 alcohol molar ratio, at 338 K and ultrasonic frequency of 37 kHz. Korkut and Bayramoglu [130] studied the ultrasound assisted biodiesel production from canola oil in presence of CaO, calcined dolomite and calcium diglyceroxide (CaD G) as catalyst. CaO–catalysed transesterification reaction resulted in maximum biodiesel yield of 99.4% in 150 min with 5.35% (w/w) catalyst loading, 7.48:1 alcohol molar ratio and ultrasonic power of 40 W at 333 K.

Varghese et al. [131] studied the ultrasound–assisted biodiesel production from waste cooking oil using heterogeneous ZnO nano–catalyst. The transesterification reaction yielded 96% conversion of waste cooking oil to biodiesel in 15 min reaction with 1.5% (w/w) catalyst loading, 6:1 alcohol molar ratio at 333 K in presence of ultrasonic frequency of 32 kHz. Yadav et al. [132] studied the optimization of biodiesel production from Karabi oil using CaO as heterogeneous catalyst in presence of ultrasound. The transesterification reaction resulted in 94.1% conversion of Karabi oil to biodiesel in 120 min reaction with 5% (w/w) catalyst loading, 12:1 alcohol molar ratio and ultrasonic power of 50 W at 333 K. Karthikeyan et al. [133] reported ultrasound–assisted production of biodiesel from waste cooking oil using $MgMoO_4$ – supported TiO_2 as a heterogeneous catalyst. The catalyst was prepared by wet impregnation method followed by calcination at 883 K for 4 h. Transesterification reaction gave 97% biodiesel yield from waste cooking oil in 30 min reaction with 0.5% (w/w) catalyst loading, 9:1 alcohol molar ratio at 338 K.

Jookjantra and Wongwuttanasatian [134] studied the optimization of biodiesel production from refined palm oil with heterogeneous CaO catalyst using pulse ultrasonic waves under a vacuum condition. The transesterification reaction gives 95% conversion of palm oil to biodiesel in 37 min with 8% (w/w) CaO catalyst, 9:1 alcohol molar ratio at 323 K under vacuum. An ultrasound irradiation (28 kHz and 200 W in the 6/2 pulse mode) was applied in transesterification reaction. Vaz et al. [135] reported ultrasound–assisted transesterification of soybean oil with methanol and sodium zirconate supported in polyvinyl alcohol as catalyst. The biodiesel yield of 80% was achieved in an ultrasonic bath (25 kHz and 360 W) in 8 h reaction with 3% (w/w) catalyst loading, 6:1 alcohol molar ratio at 328 K. Singhasiri and Tantemsapya [136] prepared the catalyst from waste egg and cockle shell and evaluate its application in biodiesel production from food processing waste oil. The maximum biodiesel yields obtained using egg and cockle shells as catalysts were 94.7% and 94.4% for alcohol molar ratios of 9.3:1 and 8.5:1, catalyst loading (egg and cockle shell catalyst) of 3.8% and 3.5%, and reaction period of 47 and 44 min, respectively. Sonication was applied using an ultrasonic processor (frequency 30 kHz and rated power of 200 W). Poosumas et al. [137] studied the role of ultrasonic irradiation on transesterification of palm oil using calcium oxide as a solid base catalyst. The biodiesel yield of ~80% was achieved at the end of 1 h reaction with 2% (w/w) catalyst loading, 9:1 alcohol molar ratio at 333 K. The process was carried out in packed bed reactor, with heterogeneous catalysts packed into screened mesh baskets inside the rectangular shape reactor (2.5 × 2.5 × 30 cm^3). The outside wall of the reactor was attached by 16 transducers (4 per each side, with two different frequencies 20 and 50 kHz and total power of 800 W). The reactants were fed to the reactor using a peristaltic pump with a feed flow rate of 55 mL/min through a 6 mm diameter silicone tube with a residence time of 4 min.

Table 1.4: Heterogeneously base catalysed biodiesel synthesis using ultrasound

Oil (source)	Catalyst	Molar ratio (Methanol/ oil)	Catalyst loading (w/w)	Reaction temperature (K)	Time (min)	Ultrasonic frequency/power (kHz/W)	% FAME (yield)	Reference
Canola oil	Dolomite	9:1	5%	333	90	20/45	97.4	[138]
Waste cooking oil	Hydrotalcite	15:1	0.08 g/g oil	330	60	20/11	76.45	[139]
Waste cooking oil	Coal fly ash	10.71:1	4.97%	333	1.41	20/108	95.57	[140]
Kusum oil	$Ba(OH)_2$	9:1	3%	323	80	20/250	96.8	[141]
Karanja oil	$Ba(OH)_2$	9:1	5%	303	60	30/100	83.87	[142]
Palm oil	SrO/Al_2O_3	9.2:1	1.6%	333	30.2	20/200	80.2	[143]
Waste cooking oil	Calcium diglyceroxide	9:1	1%	333	30	22/120	93.5	[144]
Crude palm oil	Fly ash on CaO	12:1	4%	318	30	20/700	97.04	[145]
Jatropha oil	$Na_2SiO_3@Fe_3O_4/C$	7:1	5%	328	80	25/36	94.7	[146]
Sesame oil	$Ba(OH)_2$	6.69:1	1.79%	305	40.3	20/1200	98.6	[147]
Soybean oil	$KF/\gamma–Al_2O_3$	12:1	2%	323	40	20/45	95	[148]
Waste cooking oil	$Ba(OH)_2$	6:1	0.75%	333	2	25/200	83.5	[149]
Palm oil	Ostrich eggshell–derived CaO	9:1	8%	333	60	20/120	92.7	[150]
Milk thistle oil	TiO_2 doped with $C_4H_4O_6HK$	16:1	5%	333	30	40/250	90.1	[37]
Waste cooking oil	Smoke deposited nano MgO	5:1	1.5%	328	45	24/200	98.7	[151]
Jatropha oil	CaO	11:1	5.5%	337	60	35/35	96	[152]
Soybean oil	CaO	10.1:1	6%	335	60	35/35	90	[153]

1.7.3 Acid catalysed esterification and transesterification reaction

Peña–Rodríguez et al. [154] synthesised cobalt (II) 3D metal–organic framework acid catalyst and studied its application in the ultrasonic–assisted transesterification process of *Erythrina mexicana* oil. The catalyst cobalt (II) metal–organic framework MOF (1), was synthesized by the hydrothermal reaction of $Co(NO_3)_2{\cdot}6H_2O$, 1,2–di–(4–pyridyl)–ethylene (L1) and 5–Nitroisophthalic acid (L2) in water at 433 K. The maximum 80% fatty acid methyl ester yield was obtained using prepared catalyst after 12 h reaction at 333 K. Sonication was applied using an ultrasonic processor of 40 kHz frequency. Dehghani and Haghighi [155] prepared sulfated zirconia nano–catalyst supported on MCM–41 by ultrasound–assisted impregnation/hydrothermal hybrid method and studied its application in ultrasound–assisted transesterification of sunflower oil. The nano–catalyst prepared by sonication for 30 min showed very narrow particle size distribution. More than 50% of nano–catalyst particles were in the range of 1–30 nm. Biodiesel conversion of 96.9% was achieved in 30 min with methanol/oil molar ratio of 9:1 and 5% (w/w) catalyst loading at 333 K under sonication with total power output of 90 W. Yu et al. [156] synthesised the coal–based solid acid catalysts through incomplete carbonization followed by sulfonation and investigate the activity of prepared catalyst in esterification of oleic acid with methanol. Experiments results showed 91.4% esterification was obtained in 1 h reaction under the optimized process conditions, viz. power = 270 W, catalyst dosage = 6% (w/w), methanol to oleic acid molar ratio = 10:1 and reaction temperature = 340 K; as compared to 87.9% conversion without ultrasonic irradiation under same operating conditions.

Table 1.5: Heterogeneously acid catalysed esterification and transesterification reaction using ultrasound

Oil (source)	Catalyst	Reaction	Molar ratio (Methanol/ oil)	Catalyst loading (w/w)	Reaction temperature (K)	Time (min)	Ultrasound frequency/power (kHz/W)	Yield (%)	Reference
Pistacia khinjuk seed oil	Sulphated tin oxide impregnated with silicon dioxide	Transesterification	13:1	3.5%	338	50	20 kHz	88	[157]
Oleic acid	PTA@MIL–53 (Fe) (hetero–polyacid on Fe(III)–based MOF)	Esterification	16:1	100 mg	333	15	37/50	96	[158]
Sunflower oil	Sono–sulfated zirconia on MCM–41	Transesterification	9:1	5%	333	30	20/90	96.9	[159]
Waste fish oil	Sulfonated activated carbon	Esterification	14.85:1	11.4%	328	60	20/296	56	[160]
Waste cooking oil	Sulfonated carbon catalyst from cyclodextrin	Transesterification	16:1	11.5%	390	8.8	25 kHz	90.8	[161, 162]
Palm fatty acid distillate	Sulfonated cellulose	Transesterification	6:1	3%	333	180	20/120	81.2	[163]
Waste cooking oil	Tri–potassium phosphate	Transesterification	6:1	3%	323	90	22/375	92	[164]
Crude Jatropha oil	carbon–supported heteropoly acid	Transesterification	20:1	4%	323	60	20/400	87.33	[165]
Crude Jatropha oil	Cesium doped heteropoly acid	Transesterification	25:1	3%	327	34	20/400	90.5	[166]

1.7.4 Enzyme catalysed esterification and transesterification reaction

The transesterification of waste frying oil and soybean oil by combi–lipases reactions in presence of ultrasound was studied by Poppe et al. [167]. Different immobilized lipases CALB, TLL, and RML were investigated as biocatalysts for biodiesel production. Maximum 90% and 70% biodiesel yields obtained from soybean oil and waste cooking oil, respectively at the end of 18 h using enzyme mixtures as catalyst, with 9:1 ethanol to oil molar ratio at 298 K using ultrasound bath. Santin et al. [168] studied the ultrasound–assisted enzymatic biodiesel production using macauba and soybean oil as feedstock. Soybean oil yield 88%, whereas macauba fruit oil yield 75.2% fatty acid ethyl ester in 120 min of reaction carried out using 20% (w/w) enzyme loading, 1:3 molar ratio of oil to ethanol and 40 W ultrasound power at 343 K. Bhangu et al. [169] studied the production of biodiesel from canola oil and methanol catalysed by lipase from *Candida rugosa* under different ultrasonic experimental conditions. Application of ultrasound decreased the transesterification reaction time from 22–24 h to 1.5 h using ultrasonic horn with an applied power of 40 W, methanol to oil molar ratio of 5:1 and enzyme concentration of 0.23% (w/w) and resulted in 99% yield. Gharat and Rathod [170] studied ultrasound assisted enzyme catalysed transesterification of waste cooking oil with dimethyl carbonate using Novozym 435. FAME conversion using conventional stirring, ultrasound alone and ultrasound with conventional stirring was analysed and found to be 38.69%, 57.68% and 86.61%, respectively at the end of 4 h reaction. The optimum process conditions were dimethyl carbonate to oil molar ratio – 6:1, enzyme loading 10% and reaction temperature 343 K. Ultrasound bath with operating frequency of 25 kHz and a maximum rated power output of 200 W was used.

Table 1.6: Immobilized enzyme catalysed esterification and transesterification reaction using ultrasound techniques

Oil (source)	Enzyme	Support	Molar ratio (alcohol/ oil)	Enzyme loading (w/w)	Reaction temperature (K)	Time (min)	Ultrasonic frequency/power (kHz/W)	Yield (%)	Reference
Waste lard	Lipase B from *Candida antarctica*	Commercially immobilized	4:1	6%	323	20	20/500	96.8	[171]
Waste tallow	Lipase B from *Candida antarctica*	Commercially immobilized	4:1	6%	323	20	20/500	85.6	[172]
Sunflower oil	Lipase from *T. lanuginosu*	Immobilized on silica granules)	3:1	3%	313	240	40/120	96	[173]
Macauba coconut oil	Lipase B from *Candida antarctica*	Immobilized on macroporous anionic resin	9:1	20%	338	30	40/132	70	[174]
Soybean oil	Lipase B from *Candida antarctica*	Immobilized on macroporous anionic resin	3:1	20%	343	60	40/132	78	[175]
Waste cooking oil	Lipase from *T. lanuginose*	Mesoporous silica/ iron oxide magnetic core–shell nanoparticles	4.34:1	43.6%	303	360	40/150	91	[176]
Soybean oil	Lipase from *Rhizomucor miehei*	Immobilized on macroporous anion exchange resin	3:1	5%	338	240	100 W	90	[177]
Jatropha curcas oil	Lipase from *E. aerogenes*	Activated silica	4:1	5%	298	30	24/200	84.5	[178]
Soybean oil	Lipase B from *Candida antarctica*	Immobilized on polyacrylic resin	6:1	6%	313	240	40/500	96	[179]

1.7.5 Interesterification reaction

Limited literature is available on biodiesel synthesis through ultrasound–assisted interesterification process. Only one article has been published on use of immobilized enzyme and only two articles have been published on use of homogeneous alkali catalyst in ultrasound–assisted interesterification biodiesel production.

Subhedar and Gogate [180] studied ultrasound assisted interesterification of waste cooking oil using immobilized lipase from *Thermomyces lanuginosus* (Lipozyme TLIM) as a catalyst. The optimum conditions for the conventional system (without ultrasound) were found as the reactant molar ratio of 1:12 (oil: methyl acetate), enzyme loading of 6% (w/v), temperature of 313 K and reaction time of 24 h yields 90.1% biodiesel. Whereas, optimum conditions for ultrasound assisted system were found as the oil to methyl acetate molar ratio of 1:9, enzyme loading of 3% (w/v), and reaction time of 3 h resulting in biodiesel yield of 96.1%. Maddikeri et al. [181] studied biodiesel synthesis through interesterification of waste cooking oil using hydrodynamic cavitation reactors and KOH as catalyst. Maximum 90% biodiesel yield from WCO was obtained at oil to methyl acetate molar ratio of 1:12 and catalyst loading of 1.0% using slit venturi at the inlet pressure of 3 bar. Maddikeri et al. [22] in another study studied the ultrasound–assisted interesterification of waste cooking oil using KOH as catalyst. Ultrasonic horn (22 kHz and rated power of 750 W) was used as a source of ultrasound. Maximum 90% biodiesel yield was achieved using sonochemical reactors in 30 min at optimised process conditions as – molar ratio (oil to methyl acetate) of 1:12, catalyst concentration of 1.0% and temperature of 313 K. It has been observed that rate constant increases with an increase in temperature and the activation energy is found to be 56.97 kJ/mol.

1.8 Aim and Scope of present research

The literature review presented in the previous sections gives an overview of research and development on biodiesel production with different feedstocks and employing different techniques. Large number of reports on biodiesel production have been published using various feedstocks, catalysts and synthesis techniques. However, the focus of the research has been on the results and not the rationale, viz. the exact mechanism of the process that govern the kinetics and yield of biodiesel. Thus, there is significant knowledge gap in biodiesel production techniques using various processes and catalyst. This makes the scale–up of the process to industrial scale rather difficult. At present the production cost of biodiesel is higher than petroleum derived diesel. The large–scale production of biodiesel is hampered by its unattractive production economics. Two factors that influence feasibility and viability of the biodiesel process are cost of feedstock and sufficient availability of feedstock throughout the year. The possible solution to the first issue is use of non–edible oil feedstock (such as Neem, Karanja, Kusum, Jatropha, Rubber, Cassava, etc.), which are far cheaper than the edible oils. The solution to second issue is feedstock flexibility or possibility of use of mixed feedstock for the process, as sufficient oil of single species or type may not be available in required quantities. As far as use of non–edible oils as a feedstock concerned, it has a high potential for future prospective. However, due to their high free fatty acid (FFA) content, conventional alkali catalysed transesterification is not feasible. This necessitates the two–step process, first acid catalysed esterification to convert the FFA, separation of the oil phase, followed by transesterification with alkali catalyst. Another problem with acid catalysed biodiesel process is its extremely slow kinetics, which can put limit to the production rate. For the second problem, use of heterogeneous catalyst is the potential solution. Heterogeneous catalysts can drastically reduce the

contamination of glycerol that will help in improving the quality of glycerol and also the sale price. However, the bottleneck in application of heterogeneous catalyst is slow kinetics of the transesterification reaction due to the three–phasic heterogeneity nature of the reaction system (liquid–liquid–solid). The mass transfer limitations bring down the kinetics drastically, which is again a hurdle for effective scale–up of the process with use of heterogeneous catalyst.

In the present thesis research, an attempt has been made to address these issues. The ultrasound technique as a means of intensification of the process will be applied. Several biodiesel synthesis processes with mixture of non–edible oils feedstock and different heterogeneous catalysts have been studied from mechanistic viewpoint. The dynamics of the reaction system has been analysed on the basis of kinetic model. This approach will help in getting the physical insights into the process and deduce the exact nature of interaction or links between mass transfer and kinetics of transesterification/ interesterification reaction. Such physical insights can form crucial guidelines for effective scale–up of the process.

The specific objectives of the present investigations are as follows:

1. Synthesis and characterization of heterogeneous catalysts for biodiesel production
2. Use of mixture of different non–edible oils as a feedstock for single and two step biodiesel production.
3. Use of ultrasound as a tool to intensify biodiesel production.
4. Optimization of biodiesel production processes using statistical optimization tool.
5. Investigations of heterogeneously catalysed transesterification/ interesterification process through kinetic modelling.

The thesis comprises of 7 chapters (including the present one) and the contents of the each of these chapters are briefly outlined below:

Chapter 1 gives the literature review of various aspects biodiesel synthesis. In addition, an introduction to basic principles of ultrasound and cavitation is also given, which could be useful for readers not much conversant with this subject.

Chapter 2 presents studies in mechanistic analysis of ultrasound–assisted biodiesel synthesis with Cu_2O catalyst and mixed oil feedstock using continuous (packed bed) and batch (slurry) reactors. This chapter essentially demonstrates the feasibility of heterogeneous catalyst for transesterification with ultrasonic techniques in packed bed system. Mixed non–edible oil has been used as a feedstock for biodiesel production. The process has been analysed using Eley–Rideal based kinetic model to link mass transfer limitation with reaction kinetics.

Chapter 3 presents studies in physical insight into ultrasound–assisted biodiesel production using heterogeneous base catalyst and mixed non–edible oils. Synthesis of heterogeneous base catalyst, KI impregnated on ZnO and its application in biodiesel production using blended feedstock has been presented in this chapter. Additionally, the effect of non–edible oils in their blends has also disused. The process has been analysed using Eley–Rideal based kinetic model as developed in Chapter 2.

Chapter 4 presents the studies in ultrasound intensified biodiesel production from mixed non–edible oil feedstock using heterogeneous acid catalyst supported on rubber de–oiled cake. The synthesis and characterization of two different carbon based catalyst has been evaluated. The superior catalyst has been selected for biodiesel production using non–edible oil mixed feedstock, in batch process. The process has been analysed using a modified Eley–Rideal based kinetic model that considers FAME as adsorbed product on catalyst – instead of intermediates of di– and mono–glycerides.

In Chapter 5, the studies on ultrasound–assisted enzymatic biodiesel production using blended non–edible oils feedstock have been presented. The commercially immobilized lipase has been employed for biodiesel production using mixture of non–edible oil. The process was analysed for kinetic and thermodynamic analysis.

In Chapter 6, the glycerol free biodiesel production through ultrasound–assisted interesterification of mixed non–edible oil feedstock has been studied. This chapter essentially demonstrates the feasibility of heterogeneous Cu_2O catalyst for ultrasound–assisted interesterification. The process has been analysed using LHHW based kinetic model to link mass transfer limitation with reaction kinetics.

Chapter 7 presents summary and overview of the various individual studies presented in the preceding chapters and collective interpretations. Based on the results of the chapters, some suggestions for future work have also been given.

References

[1] Moholkar, V.S., Choudhary, H.A., Singh, S., Khanna, S., Ranjan, A., Chakma, S., Bhasarkar S. Physical and Chemical Mechanisms of Ultrasound in Biofuel Synthesis, in Fang, Z., Smith, R.L. Jr., Qi, X. (Eds). Biofuels and Biorefineries Vol.4 – Production of Biofuels and Chemicals with Ultrasound, Springer, Dordrecht, 2015, 35–86.

[2] A report on "World Energy Resources Oil 2016", from World Energy Resources, available online at https://www.worldenergy.org/wp–content/ uploads/2017/03/ WEResources_Oil_2016.pdf (Access on 16th June 2018).

[3] A report on "Global Energy & CO2 Status Report 2017" from International Energy Agency available online at https://www.iea.org/publications /freepublications/ publication/GECO2017.pdf (Access on 10th July 2018).

[4] A report on "Statistical Review of World Energy June 2017" from "BP Statistical Review" available online at https://www.bp.com /content/dam/bp/en/corporate/pdf/energy–economics/statistical–review–2017/ bp–statistical–review–of–world–energy–2017–full–report.pdf (Access on 25th June 2018).

[5] A report on "Global Economic Prospects 2018" from "A World Bank Group" available online at https://openknowledge.worldbank.org/bitstream/handle/ 10986/.../9781464812576.pdf (Access on 10th July 2018)

[6] A report on "OPEC Monthly Oil Market Report – November 2016" available online at https://www.opec.org/opec_web/static_files_project/media/ downloads/publications/ MOMR%20November%202016.pdf (Access on 13th July 2018)

[7] A report on "IEA: OIL 2017 – Analysis and Forecasts to 2022" available online at https://www.iea.org/publications/freepublications/publication/Market_Report_Series_Oil2017.pdf (Access on 18th July 2018).

[8] A report on "Energy Statics" from "Central Statistics Office Ministry of Statistics and Programme Implementation, Government of India" available online at http:// www.mospi.nic.in/sites/default/files/publication_reports/ Energy_Statistics_2017r.pdf.pdf (Access on 21st July 2018)

[9] An "Annual Report 2017–18" from "Ministry of Petroleum and Natural Gas, Government of India" available online at http://petroleum.nic.in /sites/default/files/ APR_E_1718.pdf (Access on 18th July 2018).

[10] Knothe, G., 2001. Historical perspectives on vegetable oil–based diesel fuels. Inform, 12(11), 1103–1107.

[11] Knothe, G. and Razon, L.F., 2017. Biodiesel fuels. Progress in Energy and Combustion Science, 58, 36–59.

[12] An "Annual Report 2017–18" from "Ministry of New and Renewable Energy, Government of India" available online at https://mnre.gov.in/file–manager/annual–report/2017–2018/EN/index.html (Access on 18th July 2018).

[13] A report on "Development of Biofuels" from "Planning Commission, Government of India" available online at http://planningcommission.nic.in /reports/genrep/ cmtt_bio.pdf (Access on 21st July 2018)

[14] A report on "India Biofuels Annual 2017" from "GAIN (Global Agricultural Information Network), USDA Foreign Agricultural Service, Washington DC, USA," available online at https://gain.fas.usda.gov/Recent%20GAIN%20 Publications/Biofuels%20Annual_New%20Delhi_India_6–27–2017.pdf (Access on 25th July 2018).

[15] Su, F. and Guo, Y., 2014. Advancements in solid acid catalysts for biodiesel production. Green Chemistry, 16(6), 2934–2957.

[16] M. Mittelbach and C. Remschmidt, Biodiesel, the comprehensive handbook, Boersedruck Ges.m.b.H, Vienna, Graz, Austria, 2nd edn, 2004.

[17] Giakoumis, E.G., Rakopoulos, C.D., Dimaratos, A.M. and Rakopoulos, D.C., 2012. Exhaust emissions of diesel engines operating under transient conditions with biodiesel fuel blends. Progress in Energy and Combustion Science, 38(5),691–715.

[18] Demirbas, A., 2005. Biodiesel production from vegetable oils via catalytic and non–catalytic supercritical methanol transesterification methods. Progress in Energy and Combustion Science, 31(5–6), 466–487.

[19] Aransiola, E.F., Ojumu, T.V., Oyekola, O.O., Madzimbamuto, T.F. and Ikhu–Omoregbe, D.I.O., 2014. A review of current technology for biodiesel production: State of the art. Biomass and Bioenergy, 61, 276–297.

[20] Borges, M.E. and Díaz, L., 2012. Recent developments on heterogeneous catalysts for biodiesel production by oil esterification and transesterification reactions: a review. Renewable and Sustainable Energy Reviews, 16(5), 2839–2849.

[21] Casas, A., Ramos, M.J. and Perez, A., 2011. New trends in biodiesel production: Chemical interesterification of sunflower oil with methyl acetate. Biomass and Bioenergy, 35(5), 1702–1709.

[22] Maddikeri, G.L., Pandit, A.B. and Gogate, P.R., 2013. Ultrasound assisted interesterification of waste cooking oil and methyl acetate for biodiesel and triacetin production. Fuel Processing Technology, 116, pp.241–249.

[23] Casas, A., Ruiz, J.R., Ramos, M.J. and Pérez, A., 2010. Effects of triacetin on biodiesel quality. Energy & Fuels, 24(8), 4481–4489.

[24] Van Kasteren, J.M.N. and Nisworo, A.P., 2007. A process model to estimate the cost of industrial scale biodiesel production from waste cooking oil by supercritical transesterification. Resources, Conservation and Recycling, 50(4), 442–458.

[25] Marulanda, V.F., Anitescu, G. and Tavlarides, L.L., 2009. Biodiesel fuels through a continuous flow process of chicken fat supercritical transesterification. Energy & Fuels, 24(1), 253–260.

[26] Maçaira, J., Santana, A., Recasens, F. and Larrayoz, M.A., 2011. Biodiesel production using supercritical methanol/carbon dioxide mixtures in a continuous reactor. Fuel, 90(6), 2280–2288.

[27] Abbaszaadeh, A., Ghobadian, B., Omidkhah, M.R. and Najafi, G., 2012. Current biodiesel production technologies: a comparative review. Energy Conversion and Management, 63, 138–148.

[28] Vyas, A.P., Verma, J.L. and Subrahmanyam, N., 2010. A review on FAME production processes. Fuel, 89(1), 1–9.

[29] Drapcho, C.M., Nhuan, N.P. and Walker, T.H., 2008. Biofuels engineering process technology. New York: McGraw–Hill.

[30] Melero, J.A., Iglesias, J. and Morales, G., 2009. Heterogeneous acid catalysts for biodiesel production: current status and future challenges. Green Chemistry, 11(9), 1285–1308.

[31] Xie, W. and Huang, X., 2006. Synthesis of biodiesel from soybean oil using heterogeneous KF/ZnO catalyst. Catalysis Letters, 107(1–2), 53–59.

[32] Chouhan, A.S. and Sarma, A.K., 2011. Modern heterogeneous catalysts for biodiesel production: A comprehensive review. Renewable and Sustainable Energy Reviews, 15(9), 4378–4399.

[33] Vyas, A.P., Subrahmanyam, N. and Patel, P.A., 2009. Production of biodiesel through transesterification of Jatropha oil using KNO_3/Al_2O_3 solid catalyst. Fuel, 88(4), pp.625–628.

[34] Lukić, I., Krstić, J., Glišić, S., Jovanović, D. and Skala, D., 2010. Biodiesel synthesis using K_2CO_3/Al–O–Si aerogel catalysts. Journal of the Serbian Chemical Society, 75(6), 789–801.

[35] Baroutian, S., Aroua, M.K., Raman, A.A.A. and Sulaiman, N.M.N., 2010. Potassium hydroxide catalyst supported on palm shell activated carbon for transesterification of palm oil. Fuel Processing Technology, 91(11), 1378–1385.

[36] Soetaredjo, F.E., Ayucitra, A., Ismadji, S. and Maukar, A.L., 2011. KOH/bentonite catalysts for transesterification of palm oil to biodiesel. Applied Clay Science, 53(2), 341–346.

[37] Takase, M., Zhang, M., Feng, W., Chen, Y., Zhao, T., Cobbina, S.J., Yang, L. and Wu, X., 2014. Application of zirconia modified with KOH as heterogeneous solid base catalyst to new non–edible oil for biodiesel. Energy Conversion and Management, 80, 117–125.

[38] Dai, Y.M., Chen, K.T., Wang, P.H. and Chen, C.C., 2016. Solid–base catalysts for biodiesel production by using silica in agricultural wastes and lithium carbonate. Advanced Powder Technology, 27(6), 2432–2438.

[39] Liu, H., shuang Guo, H., jing Wang, X., zhong Jiang, J., Lin, H., Han, S. and peng Pei, S., 2016. Mixed and ground KBr–impregnated calcined snail shell and

kaolin as solid base catalysts for biodiesel production. Renewable Energy, 93, 648–657.

[40] Yadav, M., Singh, V. and Sharma, Y.C., 2017. Methyl transesterification of waste cooking oil using a laboratory synthesized reusable heterogeneous base catalyst: Process optimization and homogeneity study of catalyst. Energy Conversion and Management, 148, 1438–1452.

[41] Alba–Rubio, A.C., Santamaría–González, J., Mérida–Robles, J.M., Moreno–Tost, R., Martín–Alonso, D., Jiménez–López, A. and Maireles–Torres, P., 2010. Heterogeneous transesterification processes by using CaO supported on zinc oxide as basic catalysts. Catalysis Today, 149(3–4), 281–287.

[42] Srilatha, K., Lingaiah, N., Devi, B.P., Prasad, R.B.N., Venkateswar, S. and Prasad, P.S., 2009. Esterification of free fatty acids for biodiesel production over heteropoly tungstate supported on niobia catalysts. Applied Catalysis A: General, 365(1), 28–33.

[43] SathyaSelvabala, V., Varathachary, T.K., Selvaraj, D.K., Ponnusamy, V. and Subramanian, S., 2010. Removal of free fatty acid in Azadirachta indica (Neem) seed oil using phosphoric acid modified mordenite for biodiesel production. Bioresource Technology, 101(15), 5897–5902.

[44] Zabeti, M., Daud, W.M.A.W. and Aroua, M.K., 2009. Activity of solid catalysts for biodiesel production: a review. Fuel Processing Technology, 90(6),770–777.

[45] Lam, E. and Luong, J.H., 2014. Carbon materials as catalyst supports and catalysts in the transformation of biomass to fuels and chemicals. ACS Catalysis, 4(10), 3393–3410.

[46] Toda, M., Takagaki, A., Okamura, M., Kondo, J.N., Hayashi, S., Domen, K. and Hara, M., 2005. Green chemistry: biodiesel made with sugar catalyst. Nature, 438(7065), 178.

[47] Stellwagen, D.R., van der Klis, F., van Es, D.S., de Jong, K.P. and Bitter, J.H., 2013. Functionalized carbon nanofibers as solid-acid catalysts for transesterification. ChemSusChem, 6(9), 1668–1672.

[48] Hara, M., 2009. Environmentally benign production of biodiesel using heterogeneous catalysts. ChemSusChem: Chemistry & Sustainability Energy & Materials, 2(2), 129–135.

[49] Wang, H., Covarrubias, J., Prock, H., Wu, X., Wang, D. and Bossmann, S.H., 2015. Acid–functionalized magnetic nanoparticle as heterogeneous catalysts for biodiesel synthesis. The Journal of Physical Chemistry C, 119(46), 26020–26028.

[50] Melero, J.A., Bautista, L.F., Morales, G., Iglesias, J. and Briones, D., 2008. Biodiesel production with heterogeneous sulfonic acid–functionalized mesostructured catalysts. Energy & Fuels, 23(1), 539–547.

[51] Xie, W., Wang, H. and Li, H., 2011. Silica–supported tin oxides as heterogeneous acid catalysts for transesterification of soybean oil with methanol. Industrial & Engineering Chemistry Research, 51(1), 225–231.

[52] Liu, H., Chen, J., Chen, L., Xu, Y., Guo, X. and Fang, D., 2016. Carbon nanotube–based solid sulfonic acids as catalysts for production of fatty acid methyl ester via transesterification and esterification. ACS Sustainable Chemistry & Engineering, 4(6), 3140–3150.

[53] Bajaj, A., Lohan, P., Jha, P.N. and Mehrotra, R., 2010. Biodiesel production through lipase catalyzed transesterification: an overview. Journal of Molecular Catalysis B: Enzymatic, 62(1), 9–14.

[54] Amini, Z., Ilham, Z., Ong, H.C., Mazaheri, H. and Chen, W.H., 2017. State of the art and prospective of lipase–catalyzed transesterification reaction for biodiesel production. Energy Conversion and Management, 141, 339–353.

[55] Blanco, R.M., Terreros, P., Fernández–Pérez, M., Otero, C. and Dıaz–González, G., 2004. Functionalization of mesoporous silica for lipase immobilization: characterization of the support and the catalysts. Journal of Molecular Catalysis B: Enzymatic, 30(2), 83–93.

[56] Ye, P., Xu, Z.K., Wu, J., Innocent, C. and Seta, P., 2006. Nanofibrous poly (acrylonitrile–co–maleic acid) membranes functionalized with gelatin and chitosan for lipase immobilization. Biomaterials, 27(22), 4169–4176.

[57] Dizge, N., Aydiner, C., Imer, D.Y., Bayramoglu, M., Tanriseven, A. and Keskinler, B., 2009. Biodiesel production from sunflower, soybean, and waste cooking oils by transesterification using lipase immobilized onto a novel microporous polymer. Bioresource Technology, 100(6), 1983–1991.

[58] Aybastıer, Ö. and Demir, C., 2010. Optimization of immobilization conditions of Thermomyces lanuginosus lipase on styrene–divinylbenzene copolymer using response surface methodology. Journal of Molecular Catalysis B: Enzymatic, 63(3–4), 170–178.

[59] Liu, C.H., Huang, C.C., Wang, Y.W., Lee, D.J. and Chang, J.S., 2012. Biodiesel production by enzymatic transesterification catalyzed by Burkholderia lipase immobilized on hydrophobic magnetic particles. Applied Energy, 100, 41–46.

[60] Babaki, M., Yousefi, M., Habibi, Z., Brask, J. and Mohammadi, M., 2015. Preparation of highly reusable biocatalysts by immobilization of lipases on epoxy–functionalized silica for production of biodiesel from canola oil. Biochemical Engineering Journal, 101, 23–31.

[61] Babaki, M., Yousefi, M., Habibi, Z., Mohammadi, M. and Brask, J., 2015. Effect of water, organic solvent and adsorbent contents on production of biodiesel fuel from canola oil catalyzed by various lipases immobilized on epoxy–functionalized silica as low cost biocatalyst. Journal of Molecular Catalysis B: Enzymatic, 120, 93–99.

[62] Bayramoglu, G., Akbulut, A., Ozalp, V.C. and Arica, M.Y., 2015. Immobilized lipase on micro–porous biosilica for enzymatic transesterification of algal oil. Chemical Engineering Research and Design, 95, 12–21.

[63] Jegannathan, K.R., Abang, S., Poncelet, D., Chan, E.S. and Ravindra, P., 2008. Production of biodiesel using immobilized lipase—a critical review. Critical Reviews in Biotechnology, 28(4), 253–264.

[64] Zhao, X., Qi, F., Yuan, C., Du, W. and Liu, D., 2015. Lipase–catalyzed process for biodiesel production: enzyme immobilization, process simulation and optimization. Renewable and Sustainable Energy Reviews, 44, 182–197.

[65] Guo, W., Li, H., Ji, G. and Zhang, G., 2012. Ultrasound–assisted production of biodiesel from soybean oil using Brønsted acidic ionic liquid as catalyst. Bioresource Technology, 125, 332–334.

[66] Lapis, A.A., de Oliveira, L.F., Neto, B.A. and Dupont, J., 2008. Ionic liquid supported acid/base-catalyzed production of biodiesel. ChemSusChem: Chemistry & Sustainability Energy & Materials, 1(8-9), 759–762.

[67] Liang, X., Gong, G., Wu, H. and Yang, J., 2009. Highly efficient procedure for the synthesis of biodiesel from soybean oil using chloroaluminate ionic liquid as catalyst. Fuel, 88(4), 613–616.

[68] Han, M., Yi, W., Wu, Q., Liu, Y., Hong, Y. and Wang, D., 2009. Preparation of biodiesel from waste oils catalyzed by a Brønsted acidic ionic liquid. Bioresource Technology, 100(7), 2308–2310.

[69] Nurfitri, I., Maniam, G.P., Hindryawati, N., Yusoff, M.M. and Ganesan, S., 2013. Potential of feedstock and catalysts from waste in biodiesel preparation: a review. Energy conversion and Management, 74, 395–402.

[70] Ng, J.H., Ng, H.K. and Gan, S., 2010. Recent trends in policies, socioeconomy and future directions of the biodiesel industry. Clean Technologies and Environmental Policy, 12(3), 213–238.

[71] Ramachandran, K., Suganya, T., Gandhi, N.N. and Renganathan, S., 2013. Recent developments for biodiesel production by ultrasonic assist transesterification using different heterogeneous catalyst: a review. Renewable and Sustainable Energy Reviews, 22, 410–418.

[72] Sohpal, V.K., Singh, A. and Dey, A., 2011. Fuzzy modeling to evaluate the effect of temperature on batch transesterification of Jatropha curcas for biodiesel production. Bulletin of Chemical Reaction Engineering & Catalysis, 6(1), 31–38.

[73] Gude, V.G. and Martinez–Guerra, E., 2017. Green chemistry with process intensification for sustainable biodiesel production. Environmental Chemistry Letters, 1–15.

[74] Shah, Y.T., Pandit, A.B. Moholkar, V.S., 1999. Cavitation reaction engineering. Plenum Press, New York.

[75] Mason, T.J., Lorimer, J.P., 2002. Applied sonochemistry: The uses of power ultrasound in chemistry and processing. Wiley–VCH, Coventry.

[76] Leighton, T.G., 1994. The acoustic bubble. Academic Press, San Diego.

[77] Suslick, K.S., 1990. Sonochemistry. Science, 247(4949), 1439–1445.

[78] Kamath, V., Prosperetti, A. and Egolfopoulos, F.N., 1993. A theoretical study of sonoluminescence. The Journal of the Acoustical Society of America, 94(1), 248–260.

[79] Naidu, D.P., Rajan, R., Kumar, R., Gandhi, K.S., Arakeri, V.H. and Chandrasekaran, S., 1994. Modelling of a batch sonochemical reactor. Chemical Engineering Science, 49(6), 877–888.

[80] Sochard, S., Wilhelm, A.M. and Delmas, H., 1997. Modelling of free radicals production in a collapsing gas–vapour bubble. Ultrasonics Sonochemistry, 4(2), 77–84.

[81] Yasui, K., 1997. Chemical reactions in a sonoluminescing bubble. Journal of the Physical Society of Japan, 66(9), 2911–2920.

[82] Gong, C. and Hart, D.P., 1998. Ultrasound induced cavitation and sonochemical yields. The Journal of the Acoustical Society of America, 104(5), 2675–2682.

[83] Colussi, A.J. and Hoffmann, M.R., 1999. Vapor supersaturation in collapsing bubbles. Relevance to the mechanisms of sonochemistry and sonoluminescence. The Journal of Physical Chemistry A, 103(51), 11336–11339.

[84] Colussi, A.J., Weavers, L.K. and Hoffmann, M.R., 1998. Chemical bubble dynamics and quantitative sonochemistry. The Journal of Physical Chemistry A, 102(35), 6927–6934.

[85] Moss, W.C., Young, D.A., Harte, J.A., Levatin, J.L., Rozsnyai, B.F., Zimmerman, G.B. and Zimmerman, I.H., 1999. Computed optical emissions from a sonoluminescing bubble. Physical Review E, 59(3), 2986–2992.

[86] Storey, B.D. and Szeri, A.J., 2000, July. Water vapour, sonoluminescence and sonochemistry. In Proceedings of the Royal Society of London A: Mathematical, Physical and Engineering Sciences Vol. 456, No. 1999, 1685–1709.

[87] Toegel, R., Gompf, B., Pecha, R. and Lohse, D., 2000. Does water vapor prevent upscaling sonoluminescence? Physical Review Letters, 85(15), 3165–3168.

[88] Ma, F. and Hanna, M.A., 1999. Biodiesel production: a review. Bioresource Technology, 70(1), 1–15.

[89] Gandhi, N.N., Patil, N.S., Sawant, S.B., Joshi, J.B., Wangikar, P.P. and Mukesh, D., 2000. Lipase–catalyzed esterification. Catalysis Reviews, 42(4), 439–480.

[90] Demirbas, A., 2006. Biodiesel production via non–catalytic SCF method and biodiesel fuel characteristics. Energy conversion and Management, 47(15–16), 2271–2282.

[91] Demirbas, A., 2007. Progress and recent trends in biofuels. Progress in Energy and Combustion Science, 33(1), 1–18.

[92] Meher, L.C., Sagar, D.V. and Naik, S.N., 2006. Technical aspects of biodiesel production by transesterification—a review. Renewable and Sustainable Energy Reviews, 10(3), 248–268.

[93] Marchetti, J.M., Miguel, V.U. and Errazu, A.F., 2007. Possible methods for biodiesel production. Renewable and Sustainable Energy Reviews, 11(6), 1300–1311.

[94] Basha, S.A., Gopal, K.R. and Jebaraj, S., 2009. A review on biodiesel production, combustion, emissions and performance. Renewable and Sustainable Energy Reviews, 13(6–7), 1628–1634.

[95] Banerjee, A. and Chakraborty, R., 2009. Parametric sensitivity in transesterification of waste cooking oil for biodiesel production—a review. Resources, Conservation and Recycling, 53(9), 490–497.

[96] Helwani, Z., Othman, M.R., Aziz, N., Fernando, W.J.N. and Kim, J., 2009. Technologies for production of biodiesel focusing on green catalytic techniques: a review. Fuel Processing Technology, 90(12), 1502–1514.

[97] Fjerbaek, L., Christensen, K.V. and Norddahl, B., 2009. A review of the current state of biodiesel production using enzymatic transesterification. Biotechnology and Bioengineering, 102(5), 1298–1315.

[98] Meng, X., Yang, J., Xu, X., Zhang, L., Nie, Q. and Xian, M., 2009. Biodiesel production from oleaginous microorganisms. Renewable Energy, 34(1), 1–5.

[99] Jothiramalingam, R. and Wang, M.K., 2009. Review of recent developments in solid acid, base, and enzyme catalysts (heterogeneous) for biodiesel production via transesterification. Industrial & Engineering Chemistry Research, 48(13), 6162–6172.

[100] Singh, S.P. and Singh, D., 2010. Biodiesel production through the use of different sources and characterization of oils and their esters as the substitute of diesel: a review. Renewable and Sustainable Energy Reviews, 14(1), 200–216.

[101] Leung, D.Y., Wu, X. and Leung, M.K.H., 2010. A review on biodiesel production using catalyzed transesterification. Applied Energy, 87(4), 1083–1095.

[102] Mata, T.M., Martins, A.A. and Caetano, N.S., 2010. Microalgae for biodiesel production and other applications: a review. Renewable and Sustainable Energy Reviews, 14(1), 217–232.

[103] Tan, T., Lu, J., Nie, K., Deng, L. and Wang, F., 2010. Biodiesel production with immobilized lipase: a review. Biotechnology Advances, 28(5), 628–634.

[104] Math, M.C., Kumar, S.P. and Chetty, S.V., 2010. Technologies for biodiesel production from used cooking oil—A review. Energy for Sustainable Development, 14(4), 339–345.

[105] Knothe, G., 2010. Biodiesel and renewable diesel: a comparison. Progress in Energy and Combustion Science, 36(3), 364–373.

[106] Koh, M.Y. and Ghazi, T.I.M., 2011. A review of biodiesel production from Jatropha curcas L. oil. Renewable and Sustainable Energy Reviews, 15(5), 2240–2251.

[107] Chen, C.Y., Yeh, K.L., Aisyah, R., Lee, D.J. and Chang, J.S., 2011. Cultivation, photobioreactor design and harvesting of microalgae for biodiesel production: a critical review. Bioresource Technology, 102(1), 71–81.

[108] Ahmad, A.L., Yasin, N.M., Derek, C.J.C. and Lim, J.K., 2011. Microalgae as a sustainable energy source for biodiesel production: a review. Renewable and Sustainable Energy Reviews, 15(1), 584–593.

[109] Balat, M., 2011. Potential alternatives to edible oils for biodiesel production–A review of current work. Energy Conversion and Management, 52(2), pp.1479–1492.

[110] Boey, P.L., Maniam, G.P. and Hamid, S.A., 2011. Performance of calcium oxide as a heterogeneous catalyst in biodiesel production: a review. Chemical Engineering Journal, 168(1), 15–22.

[111] Kiss, A.A. and Bildea, C.S., 2012. A review of biodiesel production by integrated reactive separation technologies. Journal of Chemical Technology & Biotechnology, 87(7), 861–879.

[112] Abbaszaadeh, A., Ghobadian, B., Omidkhah, M.R. and Najafi, G., 2012. Current biodiesel production technologies: a comparative review. Energy Conversion and Management, 63, 138–148.

[113] Boro, J., Deka, D. and Thakur, A.J., 2012. A review on solid oxide derived from waste shells as catalyst for biodiesel production. Renewable and Sustainable Energy Reviews, 16(1), 904–910.

[114] Halim, R., Danquah, M.K. and Webley, P.A., 2012. Extraction of oil from microalgae for biodiesel production: a review. Biotechnology Advances, 30(3), 709–732.

[115] Atabani, A.E., Silitonga, A.S., Badruddin, I.A., Mahlia, T.M.I., Masjuki, H.H. and Mekhilef, S., 2012. A comprehensive review on biodiesel as an alternative energy resource and its characteristics. Renewable and Sustainable Energy Reviews, 16(4), 2070–2093.

[116] Yusuf, N.N., Kamarudin, S.K. and Yaakob, Z., 2012. Overview on the production of biodiesel from Jatropha curcas L. by using heterogenous catalysts. Biofuels, Bioproducts and Biorefining, 6(3), 319–334.

[117] Santori, G., Di Nicola, G., Moglie, M. and Polonara, F., 2012. A review analyzing the industrial biodiesel production practice starting from vegetable oil refining. Applied Energy, 92, 109–132.

[118] Atadashi, I.M., Aroua, M.K., Aziz, A.A. and Sulaiman, N.M.N., 2012. The effects of water on biodiesel production and refining technologies: A review. Renewable and Sustainable Energy Reviews, 16(5), 3456–3470.

[119] Atadashi, I.M., Aroua, M.K., Aziz, A.A. and Sulaiman, N.M.N., 2013. The effects of catalysts in biodiesel production: A review. Journal of Industrial and Engineering Chemistry, 19(1), 14–26.

[120] Silitonga, A.S., Masjuki, H.H., Mahlia, T.M.I., Ong, H.C., Atabani, A.E. and Chong, W.T., 2013. A global comparative review of biodiesel production from jatropha curcas using different homogeneous acid and alkaline catalysts: Study of physical and chemical properties. Renewable and Sustainable Energy Reviews, 24, 514–533.

[121] Baskar, G. and Aiswarya, R., 2016. Trends in catalytic production of biodiesel from various feedstocks. Renewable and Sustainable Energy Reviews, 57, 496–504.

[122] Knothe, G. and Razon, L.F., 2017. Biodiesel fuels. Progress in Energy and Combustion Science, 58, 36–59.

[123] Lam, M.K., Lee, K.T. and Mohamed, A.R., 2010. Homogeneous, heterogeneous and enzymatic catalysis for transesterification of high free fatty acid oil (waste cooking oil) to biodiesel: a review. Biotechnology Advances, 28(4), 500–518.

[124] Lerin, L.A., Loss, R.A., Remonatto, D., Zenevicz, M.C., Balen, M., Netto, V.O., Ninow, J.L., Trentin, C.M., Oliveira, J.V. and de Oliveira, D., 2014. A review on lipase–catalyzed reactions in ultrasound–assisted systems. Bioprocess and Biosystems Engineering, 37(12), 2381–2394.

[125] Islam, A., Taufiq–Yap, Y.H., Chan, E.S., Moniruzzaman, M., Islam, S. and Nabi, M.N., 2014. Advances in solid–catalytic and non–catalytic technologies for biodiesel production. Energy Conversion and Management, 88, 1200–1218.

[126] Lourinho, G. and Brito, P., 2015. Advanced biodiesel production technologies: novel developments. Reviews in Environmental Science and Bio/Technology, 14(2), 287–316.

[127] Ho, W.W.S., Ng, H.K. and Gan, S., 2016. Advances in ultrasound–assisted transesterification for biodiesel production. Applied Thermal Engineering, 100, 553–563.

[128] Chuah, L.F., Klemeš, J.J., Yusup, S., Bokhari, A. and Akbar, M.M., 2017. A review of cleaner intensification technologies in biodiesel production. Journal of Cleaner Production, 146, 181–193.

[129] Moghzi, F. and Soleimannejad, J., 2018. Sonochemical synthesis of a new nano–sized barium coordination polymer and its application as a heterogeneous catalyst towards sono–synthesis of biodiesel. Ultrasonics Sonochemistry, 42, 193–200.

[130] Korkut, I. and Bayramoglu, M., 2018. Selection of catalyst and reaction conditions for ultrasound assisted biodiesel production from canola oil. Renewable Energy, 116, 543–551.

[131] Varghese, R., Henry, J.P. and Irudayaraj, J., 2018. U ltrasonication-assisted transesterification for biodiesel production by using heterogeneous ZnO nanocatalyst. Environmental Progress & Sustainable Energy, 37(3), 1176–1182.

[132] Yadav, A.K., Khan, M.E., Pal, A. and Singh, B., 2018. Ultrasonic–assisted optimization of biodiesel production from Karabi oil using heterogeneous catalyst. Biofuels, 9(1), 101–112.

[133] Karthikeyan, M., Renganathan, S. and Baskar, G., 2017. Production of biodiesel from waste cooking oil using $MgMoO_4$–supported TiO_2 as a heterogeneous

catalyst. Energy Sources, Part A: Recovery, Utilization, and Environmental Effects, 39(21), 2053–2059.

[134] Jookjantra, K. and Wongwuttanasatian, T., 2017. Optimisation of biodiesel production from refined palm oil with heterogeneous CaO catalyst using pulse ultrasonic waves under a vacuum condition. Energy Conversion and Management, 154, 1–10.

[135] Vaz, L.M., Martins, M.I., Coutinho Filho, U., Cardoso, V.L. and Reis, M.H., 2017. Ultrasound-assisted transesterification reactions for biodiesel production with sodium zirconate supported in polyvinyl alcohol as catalyst. Environmental Progress & Sustainable Energy, 36(4), 1262–1267.

[136] Singhasiri, T. and Tantemsapya, N., 2016. The utilization of waste egg and cockle shell as catalysts for biodiesel production from food processing waste oil using stirring and ultrasonic agitation. Energy Sources, Part A: Recovery, Utilization, and Environmental Effects, 38(21), 3125–3131.

[137] Poosumas, J., Ngaosuwan, K., Quitain, A.T. and Assabumrungrat, S., 2016. Role of ultrasonic irradiation on transesterification of palm oil using calcium oxide as a solid base catalyst. Energy Conversion and Management, 120, 62–70.

[138] Korkut, I. and Bayramoglu, M., 2016. Ultrasound assisted biodiesel production in presence of dolomite catalyst. Fuel, 180, 624–629.

[139] Anuar, M.R. and Abdullah, A.Z., 2016. Ultrasound–assisted biodiesel production from waste cooking oil using hydrotalcite prepared by combustion method as catalyst. Applied Catalysis A: General, 514, 214–223.

[140] Xiang, Y., Wang, L. and Jiao, Y., 2016. Ultrasound strengthened biodiesel production from waste cooking oil using modified coal fly ash as catalyst. Journal of Environmental Chemical Engineering, 4(1), 818–824.

[141] Sarve, A.N., Varma, M.N. and Sonawane, S.S., 2016. Ultrasound assisted two–stage biodiesel synthesis from non–edible Schleichera triguga oil using heterogeneous catalyst: Kinetics and thermodynamic analysis. Ultrasonics Sonochemistry, 29, 288–298.

[142] Saha, R. and Goud, V.V., 2015. Ultrasound assisted transesterification of high free fatty acids karanja oil using heterogeneous base catalysts. Biomass Conversion and Biorefinery, 5(2), 195–207.

[143] Mootabadi, H. and Abdullah, A.Z., 2015. Response Surface Methodology for Simulation of Ultrasonic–assisted Biodiesel Production Catalyzed by SrO/Al_2O_3 Catalyst. Energy Sources, Part A: Recovery, Utilization, and Environmental Effects, 37(16), 1747–1755.

[144] Gupta, A.R., Yadav, S.V. and Rathod, V.K., 2015. Enhancement in biodiesel production using waste cooking oil and calcium diglyceroxide as a heterogeneous catalyst in presence of ultrasound. Fuel, 158, 800–806.

[145] Ho, W.W.S., Ng, H.K., Gan, S. and Chan, W.L., 2015. Ultrasound-assisted transesterification of refined and crude palm oils using heterogeneous palm oil mill fly ash supported calcium oxide catalyst. Energy Science & Engineering, 3(3), 257–269.

[146] Zhang, F., Fang, Z. and Wang, Y.T., 2015. Biodiesel production directly from oils with high acid value by magnetic Na_2SiO_3@ Fe_3O_4/C catalyst and ultrasound. Fuel, 150, 370–377.

[147] Sarve, Antaram, Shriram S. Sonawane, and Mahesh N. Varma. 2015 "Ultrasound assisted biodiesel production from sesame (Sesamum indicum L.) oil using barium hydroxide as a heterogeneous catalyst: comparative assessment of prediction abilities between response surface methodology (RSM) and artificial neural network (ANN)." Ultrasonics Sonochemistry, 26, 218–228.

[148] Shahraki, H., Entezari, M.H. and Goharshadi, E.K., 2015. Sono–synthesis of biodiesel from soybean oil by KF/γ–Al_2O_3 as a nano–solid–base catalyst. Ultrasonics Sonochemistry, 23, 266–274.

[149] Martinez–Guerra, E. and Gude, V.G., 2014. Transesterification of used vegetable oil catalyzed by barium oxide under simultaneous microwave and ultrasound irradiations. Energy Conversion and Management, 88, 633–640.

[150] Chen, G., Shan, R., Shi, J. and Yan, B., 2014. Ultrasonic–assisted production of biodiesel from transesterification of palm oil over ostrich eggshell–derived CaO catalysts. Bioresource Technology, 171, 428–432.

[151] Sivakumar, P., Sankaranarayanan, S. and Renganathan, S., 2013. Studies on sono–chemical biodiesel production using smoke deposited nano MgO catalyst. Bulletin of Chemical Reaction Engineering & Catalysis, 8(2), 89–96.

[152] Choudhury, H.A., Goswami, P.P., Malani, R.S. and Moholkar, V.S., 2014. Ultrasonic biodiesel synthesis from crude Jatropha curcas oil with heterogeneous base catalyst: mechanistic insight and statistical optimization. Ultrasonics Sonochemistry, 21(3), 1050–1064.

[153] Choudhury, H.A., Chakma, S. and Moholkar, V.S., 2014. Mechanistic insight into sonochemical biodiesel synthesis using heterogeneous base catalyst. Ultrasonics Sonochemistry, 21(1), 169–181.

[154] Peña–Rodríguez, R., Márquez–López, E., Guerrero, A., Chiñas, L.E., Hernández–González, D.F. and Rivera, J.M., 2018. Hydrothermal synthesis of cobalt (II) 3D metal–organic framework acid catalyst applied in the transesterification process of vegetable oil. Materials Letters, 217, 117–119.

[155] Dehghani, S. and Haghighi, M., 2017. Sono–sulfated zirconia nanocatalyst supported on MCM–41 for biodiesel production from sunflower oil: influence of ultrasound irradiation power on catalytic properties and performance. Ultrasonics Sonochemistry, 35, 142–151.

[156] Yu, H., Niu, S., Lu, C., Li, J. and Yang, Y., 2017. Sulfonated coal–based solid acid catalyst synthesis and esterification intensification under ultrasound irradiation. Fuel, 208, 101–110.

[157] Asif, S., Ahmad, M., Bokhari, A., Chuah, L.F., Klemeš, J.J., Akbar, M.M., Sultana, S. and Yusup, S., 2017. Methyl ester synthesis of Pistacia khinjuk seed oil by ultrasonic–assisted cavitation system. Industrial Crops and Products, 108, 336–347.

[158] Nikseresht, A., Daniyali, A., Ali–Mohammadi, M., Afzalinia, A. and Mirzaie, A., 2017. Ultrasound–assisted biodiesel production by a novel composite of Fe (III)–based MOF and phosphotangestic acid as efficient and reusable catalyst. Ultrasonics Sonochemistry, 37, pp.203–207.

[159] Dehghani, S. and Haghighi, M., 2017. Sono–sulfated zirconia nanocatalyst supported on MCM–41 for biodiesel production from sunflower oil: influence of ultrasound irradiation power on catalytic properties and performance. Ultrasonics Sonochemistry, 35, 142–151.

[160] Hajamini, Z., Sobati, M.A., Shahhosseini, S. and Ghobadian, B., 2016. Waste fish oil (WFO) esterification catalyzed by sulfonated activated carbon under ultrasound irradiation. Applied Thermal Engineering, 94, 141–150.

[161] Maneechakr, P., Samerjit, J., Uppakarnrod, S. and Karnjanakom, S., 2015. Experimental design and kinetic study of ultrasonic assisted transesterification of waste cooking oil over sulfonated carbon catalyst derived from cyclodextrin. Journal of Industrial and Engineering Chemistry, 32, 128–136.

[162] Maneechakr, P., Samerjit, J. and Karnjanakom, S., 2015. Ultrasonic–assisted biodiesel production from waste cooking oil over novel sulfonic functionalized carbon spheres derived from cyclodextrin via one–step: a way to produce biodiesel at short reaction time. RSC Advances, 5(68), 55252–55261.

[163] Gaikwad, N.D. and Gogate, P.R., 2015. Synthesis and application of carbon based heterogeneous catalysts for ultrasound assisted biodiesel production. Green Processing and Synthesis, 4(1), 17–30.

[164] Pukale, D.D., Maddikeri, G.L., Gogate, P.R., Pandit, A.B. and Pratap, A.P., 2015. Ultrasound assisted transesterification of waste cooking oil using heterogeneous solid catalyst. Ultrasonics Sonochemistry, 22, 278–286.

[165] Badday, A.S., Abdullah, A.Z. and Lee, K.T., 2014. Transesterification of crude Jatropha oil by activated carbon–supported heteropolyacid catalyst in an ultrasound–assisted reactor system. Renewable Energy, 62, 10–17.

[166] Badday, A.S., Abdullah, A.Z. and Lee, K.T., 2013. Ultrasound–assisted transesterification of crude Jatropha oil using cesium doped heteropolyacid catalyst: Interactions between process variables. Energy, 60, 283–291.

[167] Poppe, J.K., Matte, C.R., Fernandez–Lafuente, R., Rodrigues, R.C. and Ayub, M.A.Z., 2018. Transesterification of waste frying oil and soybean oil by combi–

lipases under ultrasound–assisted reactions. Applied Biochemistry and Biotechnology, 1–14.

[168] Santin, C.M., Michelin, S., Scherer, R.P., Valério, A., di Luccio, M., Oliveira, D. and Oliveira, J.V., 2017. Comparison of macauba and soybean oils as substrates for the enzymatic biodiesel production in ultrasound–assisted system. Ultrasonics Sonochemistry, 35, 525–528.

[169] Bhangu, S.K., Gupta, S. and Ashokkumar, M., 2017. Ultrasonic enhancement of lipase–catalysed transesterification for biodiesel synthesis. Ultrasonics Sonochemistry, 34, pp.305–309.

[170] Gharat, N. and Rathod, V.K., 2013. Ultrasound assisted enzyme catalyzed transesterification of waste cooking oil with dimethyl carbonate. Ultrasonics Sonochemistry, 20(3), 900–905.

[171] Adewale, P., Dumont, M.J. and Ngadi, M., 2016. Enzyme–catalyzed synthesis and kinetics of ultrasonic assisted methanolysis of waste lard for biodiesel production. Chemical Engineering Journal, 284, 158–165.

[172] Adewale, P., Dumont, M.J. and Ngadi, M., 2015. Enzyme–catalyzed synthesis and kinetics of ultrasonic–assisted biodiesel production from waste tallow. Ultrasonics Sonochemistry, 27, 1–9.

[173] Subhedar, P.B., Botelho, C., Ribeiro, A., Castro, R., Pereira, M.A., Gogate, P.R. and Cavaco–Paulo, A., 2015. Ultrasound intensification suppresses the need of methanol excess during the biodiesel production with Lipozyme TL–IM. Ultrasonics Sonochemistry, 27, 530–535.

[174] Michelin, S., Penha, F.M., Sychoski, M.M., Scherer, R.P., Treichel, H., Valério, A., Di Luccio, M., de Oliveira, D. and Oliveira, J.V., 2015. Kinetics of

ultrasound–assisted enzymatic biodiesel production from Macauba coconut oil. Renewable Energy, 76, 388–393.

[175] Trentin, C.M., Popiolki, A.S., Batistella, L., Dalla Rosa, C., Treichel, H., de Oliveira, D. and Oliveira, J.V., 2015. Enzyme–catalyzed production of biodiesel by ultrasound–assisted ethanolysis of soybean oil in solvent–free system. Bioprocess and Biosystems Engineering, 38(3), 437–448.

[176] Karimi, M., Keyhani, A., Akram, A., Rahman, M., Jenkins, B. and Stroeve, P., 2013. Hybrid response surface methodology–genetic algorithm optimization of ultrasound–assisted transesterification of waste oil catalysed by immobilized lipase on mesoporous silica/iron oxide magnetic core–shell nanoparticles. Environmental Technology, 34(13–14), 2201–2211.

[177] Batistella, L., Lerin, L.A., Brugnerotto, P., Danielli, A.J., Trentin, C.M., Popiolski, A., Treichel, H., Oliveira, J.V. and de Oliveira, D., 2012. Ultrasound–assisted lipase–catalyzed transesterification of soybean oil in organic solvent system. Ultrasonics Sonochemistry, 19(3), 452–458.

[178] Kumar, G., Kumar, D., Johari, R. and Singh, C.P., 2011. Enzymatic transesterification of Jatropha curcas oil assisted by ultrasonication. Ultrasonics Sonochemistry, 18(5), 923–927.

[179] Yu, D., Tian, L., Wu, H., Wang, S., Wang, Y., Ma, D. and Fang, X., 2010. Ultrasonic irradiation with vibration for biodiesel production from soybean oil by Novozym 435. Process Biochemistry, 45(4), 519–525.

[180] Subhedar, P.B. and Gogate, P.R., 2016. Ultrasound assisted intensification of biodiesel production using enzymatic interesterification. Ultrasonics Sonochemistry, 29, 67–75.

[181] Maddikeri, G.L., Gogate, P.R. and Pandit, A.B., 2014. Intensified synthesis of biodiesel using hydrodynamic cavitation reactors based on the interesterification of waste cooking oil. Fuel, 137, 285–292.

CHAPTER 2

MECHANISTIC ANALYSIS OF ULTRASOUND–ASSISTED BIODIESEL SYNTHESIS WITH Cu_2O CATALYST AND MIXED OIL FEEDSTOCK USING CONTINUOUS (PACKED BED) AND BATCH (SLURRY) REACTORS

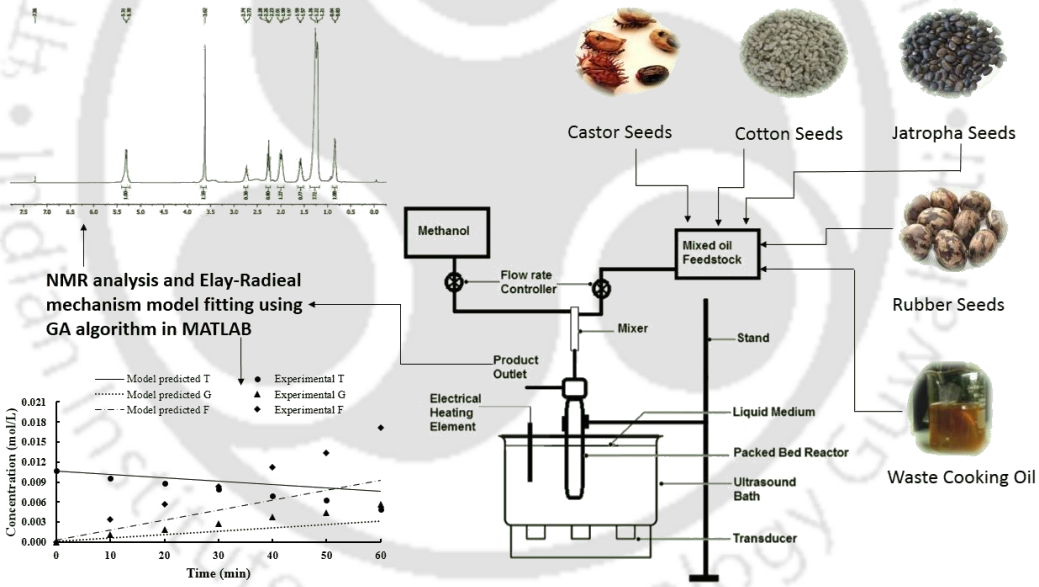

Chapter 2

Mechanistic analysis of ultrasound–assisted biodiesel synthesis with Cu_2O catalyst and mixed oil feedstock using continuous (packed bed) and batch (slurry) reactors

2.1 Introduction

In chapter 1, the overview on Indian and Global energy scenario was presented, which clearly reveals that renewable alternative fuel is urgent need of hour in perspective of environmental concern and continuous increasing energy requirement. Biodiesel and bioethanol had shown potential as alternate transportation fuel. In previous chapter, the various aspects of biodiesel production as an alternate transportation fuel was analysed in terms of feedstock, catalyst and process. The large–scale production of biodiesel is hampered by unattractive economy [1]. Two factors that influence feasibility and viability of the biodiesel process are cost of feedstock and sufficient availability of feedstock all through the year. Possible solution to the first issue is use of non–edible oil feedstock (such as *Neem, Karanja, Kususm, Jatropha, Rubber, Cassava, Mahua,* etc.), which are far cheaper than the edible oils [2]. The solution to second issue is feedstock flexibility or possibility of use of mixed feedstock

for the process, as sufficient oil of single species or type may not be available in required quantities. Another approach to improve the economy of biodiesel production, is simplifying the downstream process and recover the high quality of by-product glycerol. One feasible solution to minimize the contamination of glycerol and reducing the steps in downstream processing, use of heterogeneous catalyst for biodiesel production. However, the transesterification reaction system with heterogeneous solid catalyst suffers drawback of slow kinetics due to mass transfer limitations of three phase (liquid–liquid–solid) reaction system [3]. Possible solutions to enhance the mass transfer, and hence, the reaction kinetics are: intense agitation or stirring, application of high pressure and temperature, use of a co–solvent [4], etc. Recently, ultrasound irradiation or sonication has been attempted as a means of intensification of kinetics of transesterification. The previous studies have employed alkali or alkaline earth metal oxides like CaO, $Ba(OH)_2$, basic zeolites as the catalyst for transesterification [5-8]. Most of these studies have been conducted in batch mode with mechanical shaking of reaction mixture. Biodiesel synthesis in continuous process using packed bed solid base catalyst has also been reported by few authors, and a summary of this literature in this area is given in Table 2.1.

The present study has addressed the matter of biodiesel production using new solid catalyst of cuprous oxide and mixed feedstock of five non–edible oils, viz. cotton seed oil, castor oil, jatropha oil, rubber seed oil and waste cooking oil. The approach adopted in this study is two–fold, viz. (1) statistical optimization of the transesterification process in a continuous packed bed reactor with Cu_2O catalyst, coupled with sonication (or ultrasound irradiation), and (2) kinetic and mechanistic analysis of transesterification process using mathematical model based on Eley–Rideal mechanism.

Table 2.1: Summary of literature on biodiesel synthesis with heterogeneous solid catalyst in packed bed reactor configuration

Transesterification system	Experimental parameters/ Conditions	Major Results	Reference
Soybean oil, canola oil and sunflower oil and methanol Catalyst: shell–core $Ca(C_3H_7O_3)_2/CaCO_3$ solid–base catalyst	Temperature: 333 K; Residence time: 168 min; Molar ratio (MeOH/Soybean oil): 6– 36. Reactor: length = 26 cm, inner diameter = 1.71 cm	Optimum conditions: residence time = 168 min, molar ratio = 30, Temperature = 333 K, FAME yield = 95%, Activation energy = 42 kJ/mol Catalyst reuse for 5 cycles. Water in the oil can deactivate the catalyst.	[9]
Sunflower oil and methanol Catalyst: calcium oxide particles 1–2 mm in diameter	Temperature: 353 – 413 K; Flow rate: Oil= 4.1 –7.7 mL/min; Methanol= 1 – 4 mL/min; Packing height: 5, 10 and 12.5 cm. Trickle bed reactor, Countercurrent flow of oil droplets and vaporized methanol	Significant effect of oil residence time in the reactor on FAME yield. FAME yield = 98% for temperature = 373 K, methanol flow rate = 3.8 mL/min, oil flow rate = 4.1 mL/min.	[10]
Soybean oil and methanol Catalyst: $K/\gamma–Al_2O_3$ catalyst	Temperature: 303 – 333 K; Molar ratio (MeOH/Oil): 6–24; RPM: 150–1500; Catalyst packing: 3.00, 7.05, and 10.6% (w/w)	Methanol–to oil molar ratio = 24, reaction temperature = 333 K, void space in packed bed column = 0.638 cm^3/cm^3, rotational speed = 900–1500 rpm. Loss of catalyst activity due to leaching of potassium species and blockage of catalyst pores.	[11]
Palm oil and methanol Catalyst: Microporous TiO_2/Al_2O_3 membrane packed with KOH catalyst supported on palm shell activated carbon.	Temperature: 323 – 343 K; Mass of catalyst per unit volume of reactor = 37.50 to 250.00 mg/cm^3 Cross flow circulation velocity = 0.179 to 0.212 cm/s	Highest conversion of palm oil to biodiesel at 343 K, catalyst per unit volume of the reactor = 157.04 g, cross flow circulation velocity = 0.21 cm/s	[12]
Acidified oil and methanol Catalyst: NKC–9 cation–exchange resin	Temperature: 298 – 338 K; Packing Height: 11 – 44 cm; Mass ratio (MeOH/Oil): 0.35:1 – 1.25:1; Flow rate: 0.82 to 2.32 ml/min. Reactor: internal diameter = 25 mm, height = 450 mm	Optimum conditions: FFA conversion = 98% in 500 h of continuous esterification. Methanol/oleic acid mass ratio = 2.8:1, catalyst bed height = 44.0 cm, feed flow rate = 0.62 ml/min, reaction temperature = 338 K. Loss of sulfonic acid groups from NKC–9 resin into the production is very less during continuous esterification.	[13]
Waste frying oil and methanol Catalyst: KOH catalyst supported on *Jatropha curcas* fruit shell (JS) activated carbon	Temperature: 323 –343 K; Residence Time: 1–3 h; Molar ratio (MeOH/Oil): 10–20; Catalyst bed height=150–300 mm	FAME yield = 86.7%, residence time = 2 h, temperature = 333 K, methanol/oil molar ratio = 16, catalyst bed height = 250 mm. No significant catalyst activity loss for 5 cycles of use.	[14]
Jatropha curcus oil and methanol Catalyst: solid acid heterogeneous catalyst	Temperature: 453 – 513 K; Residence time: 5–80 min; Molar ratio (MeOH/Oil): 6–40, statistical optimization of reaction conditions	FAME yield = 89% for temperature = 473 K, molar ratio = 1:38, reaction time = 60 min	[15]

Table 2.1 (continued……)

Transesterification system	Experimental parameters/ Conditions	Major Results	Reference
Rapeseed oil and methanol Catalyst: Ca/Al composite oxide–based alkaline catalysts	Molar ratio (MeOH/Oil): 3:1; Oil flow rate: 0.6 mL/min. Reactor: Countercurrent trickle bed reactors and it modification (inner diameter = 2.5 cm, height = 30 cm, catalyst loadings = 113.6 and 73.8 g)	Modified trickle bed reactor: FAME yield = 94.5%, oil flow rate = 0.6 mL/min, catalyst bed volume = 91 mL Coupling of transesterification reaction and methanol separation in modified reactor gives greater operational stability.	[16]
Soybean oil and methanol Catalyst: $Ca(C_3H_7O_3)_2$/CaO solid–base catalyst	Temperature: 313 – 333 K; Molar ratio (MeOH/Oil): 5–20; Residence time: 23–123 min; catalyst columns rotation: 200, 500 and 800 rpm. Catalyst packed in 4 static perforated columns attached to rotor.	Biodiesel yield = 96.75% for residence time = 123 min, molar ratio = 20:1, rotational speed = 200 rpm, temperature = 333 K. Stirring packed–bed reactor overcomes mass transfer limitations. Activation energy = 46.2 kJ/mol	[17]
Soybean oil/ Macauba oil and methyl aceate	Temperature: 573 – 673 K Pressure: 20 MPa Residence time: 45 min Mass ratio (Oil/MA): 1:2 to 1:5	Soybean oil: Ester yield = 44% at 623 K. Oil/methyl acetate mass ratio = 1:5, Decomposition = 48% Macauba oil: Ester yield = 83% at 598 K. Oil/methyl acetate mass ratio = 1:5, Decomposition = 17%. Better performance of macauba oil attributed to higher free fatty acid content.	[18]
Sunflower oil, waste frying oil and methanol. Catalyst: Pumice exchanged with potassium	Temperature: 323 – 333 K; Flow rate (reactant): 15 ml/min; bed porosity: 0.74; Reaction time : 15 min – 2 h	FAME yield = 99.5%, methanol/ oil molar ratio = 20:1, temperature = 328 K, packing height = 8.2 cm, reaction time = 2 h. For waste oil higher molar ratio of 28:1 required.	[19]
Waste cooking oil and methanol Catalyst: agglomerated Zr–SBA–15/bentonite catalyst (1.5 mm particles, 28 g loading)	Temperature: 423 – 483 K; Pressure: 70 bar; Residence time: 30 min; Molar ratio (MeOH/WCO): 50:1 Packed bed: length= 120 cm, diameter= 0.9 cm	Catalyst performance attributed due to the presence of active acid sites in the Zr–SBA–15 material. Optimum parameters: Residence time = 30 min (LHSV = $2h^{-1}$), molar ratio = 50:1, Temperature = 483 K, steady state FAME yield = 95%. Catalytic activity preserved for over 260 h of continuous operation.	[20]

For this purpose, the experiments have been conducted in batch mode using slurry reactor coupled with sonication. The experimental data has been fitted to kinetic model to obtain the values of kinetic parameters. An additional objective of this study is to gain mechanistic insight into the process intensification (in terms of enhancement of reaction kinetics) induced by ultrasound. Hence, the experiments in batch mode have been conducted using mechanical agitation as well, and the kinetic parameters for sonication and mechanical agitation have been compared. This analysis has assisted in discriminating between the roles of mass transfer and reaction kinetics, and has provided insight into the physical mechanism of ultrasound–assisted transesterification process, as explained in the subsequent sections.

2.2 Material and Methods

2.2.1 Materials

Following chemicals have been used in the experiments: Methanol (AR grade, 99%, Merck, India), sulphuric acid (98% conc., Merck, India), Cu_2O (AR grade, 92%, Himedia, India). Anhydrous methanol was prepared by distillation.

Crude *Jatropa curcas* oil and crude castor oil were procured from local farmers. Waste cooking oil was collected from a restaurant on institute campus. Crude cotton seed oil was a gift from M/s. Govind Krupa Oil Industry (Amravati, Maharashtra, India). Rubber seeds were purchased from local farmers, and oil was extracted from the seeds using Soxhlet extraction method with *n*–hexane as solvent. Approx. 100 g of dried fine crushed powder (particle size 1–2 mm) of rubber seeds was placed in a thimble covered with blotting paper, and 1.25 L *n*–hexane was used for oil–extraction. The heating rate was manually controlled so as to complete one extraction cycle in 60–75 min. Each batch of rubber seed powder was subjected to 9 cycles of extraction.

Extracted oil was recovered using a rotary vacuum evaporator (Make: Buchi; Model: Rotavapor R–300) for removal (and subsequent recycle) of solvent. Net average oil yield per batch of extraction was 40.7 g (44.24 mL) per 100 g seeds. This yield is comparable with the results reported by Reshad et al. [2].

Waste cooking oil was collected from a restaurant on the Institute campus of IIT Guwahati. The waste cooking oil was pre–treated prior to use for biodiesel production by heating up to 453 K and cooling to room temperature. This procedure was carried out twice followed by filtration. The pre–treatment was aimed at removal of moisture and other suspended impurities in waste cooking oil. Viscosities of oil samples were measured by using rheometer (Make: M/s Thermo Electron, Germany; Model: Rheostress RS 1) at 313 K. Acid value (AV) and saponification value (SV) of all the oils were analysed using titration method (standard procedure for determination of acid value and saponification value is given in Annexure A) and the average molecular weight of oil was determined by using the following expression [21]:

$$\text{Average molecular weight} = 56.1 \times 3 \times 1000/(SV - AV)$$

The basic properties of all individual oils are given in Annexure B. The feedstock for transesterification was prepared by blending different oils as follows: Jatropha oil (15% v/v), castor oil (25% v/v), rubber seed oil (20% v/v), cotton seed oil (25% v/v), and waste cooking oil (15% v/v). The blended feedstock has density 0.93 g/mL, acid value 8.78 mg KOH/g, saponification value 193.72 mg KOH/g, viscosity of 32.28 mPa-s (at 313K) and average molecular weight 910.04 g/mol.

2.2.2 Catalyst preparation and characterization

The fine powder of Cu_2O catalyst, as received from supplier, was initially dried in hot air oven at 393 K for 3 h to remove moisture. Dried or de–moisturized catalyst

was cooled to ambient temperature, and was characterized using X–ray diffraction (XRD) (Bruker, Model: D8 Advance) for identification of different phases in the catalyst. The surface area of the catalyst was determined using surface area and pore size analyzer (Quanta chrome, Model: Autosorb–IQ MP) and Field–emission scanning electron microscopy (FE–SEM, Zeiss, Model: Sigma). Due to fine size, direct packing of catalyst in reactor bed was not possible, as voidage of such bed would be too small to have proper flow of methanol/oil mixture. As a solution to this issue, the catalyst was used in supported form as follows: glass beads (diameter 3–5 mm, Himedia, India) were used as the catalyst support. These beads were coated with a film of Cu_2O particles. For firm adherence of the Cu_2O powder onto the surface of the glass beads, glutaraldehyde was employed as a surface binding agent. Cu_2O–coated glass beads were dried in hot air oven at 393 K for 3 h, and were used for making up the packed catalyst bed after cooling.

2.2.3 Experimental setup and protocol

Experiments in the present study were carried out in three parts: (1) reduction in the free fatty acid (FFA) content of the mixed oil feedstock by preliminary esterification, (2) transesterification of mixed oil feedstock in continuous packed bed reactor and optimization of process variables using statistical design of experiments (DoE), and (3) determination of kinetic and Arrhenius parameters of transesterification reaction of mixed oil feedstock in batch slurry reactors. The experimental details for preliminary esterification is described in supplementary material provided with this manuscript. However, the experimental protocol and experimental set-up for packed bed reactor and batch slurry reactor described below:

Transesterification in continuous packed bed reactor using statistical DoE Experimental set–up: Transesterification reactions were carried out in an ultrasound bath (Elma Transonic T–460 type, Germany, capacity: 2 L, frequency: 35 kHz, power: 35 W). A schematic of the experimental setup for trans–esterification reaction is given in Fig. 2.1 (A). 2/3rd of bath volume was filled with distilled water, which acted as medium for transmission of ultrasound. The fixed bed of catalyst was made using a cylindrical column made of borosilicate glass (total volume = 135 mL, height = 18, internal diameter = 3 cm) fitted with a cap which had central tube (internal diameter = 4 mm, height = 20 cm) that extended till the bottom of the column. The schematics of the packed bed reactor (cylindrical column and cap) have been shown in Fig. 2.1 (B).

The outer end of this tube was used for injection of the reaction mixture into packed catalyst bed. The exit port for the reaction mixture was also located on the cap adjacent to the injection port. The catalyst was packed in the annular space between the injection tube and the column. As noted earlier, the catalyst was in the form of glass beads coated with film of Cu_2O particles. At the bottom of the catalyst bed, a small layer of silica particles (height = 3 cm) was provided, which is fixed for all set of experiments. This layer was meant for adsorptive removal of residual moisture in the reaction mixture before it is contacted with the Cu_2O catalyst. This configuration essentially generated an upward flow of the reaction mixture through the catalyst bed. Sonication of the catalyst bed and the reaction mixture in it was achieved by immersing the cylindrical column in the ultrasound bath, as shown in Fig. 2.1 (A). By filling the annular space between column and tube to different heights using catalyst beads, the quantity of the catalyst in the bed was varied. The position of the cylinder holding packed bed of catalyst was kept same carefully in all experiments, since the intensity/ pressure amplitude of the ultrasound wave field shows significant spatial variation [22].

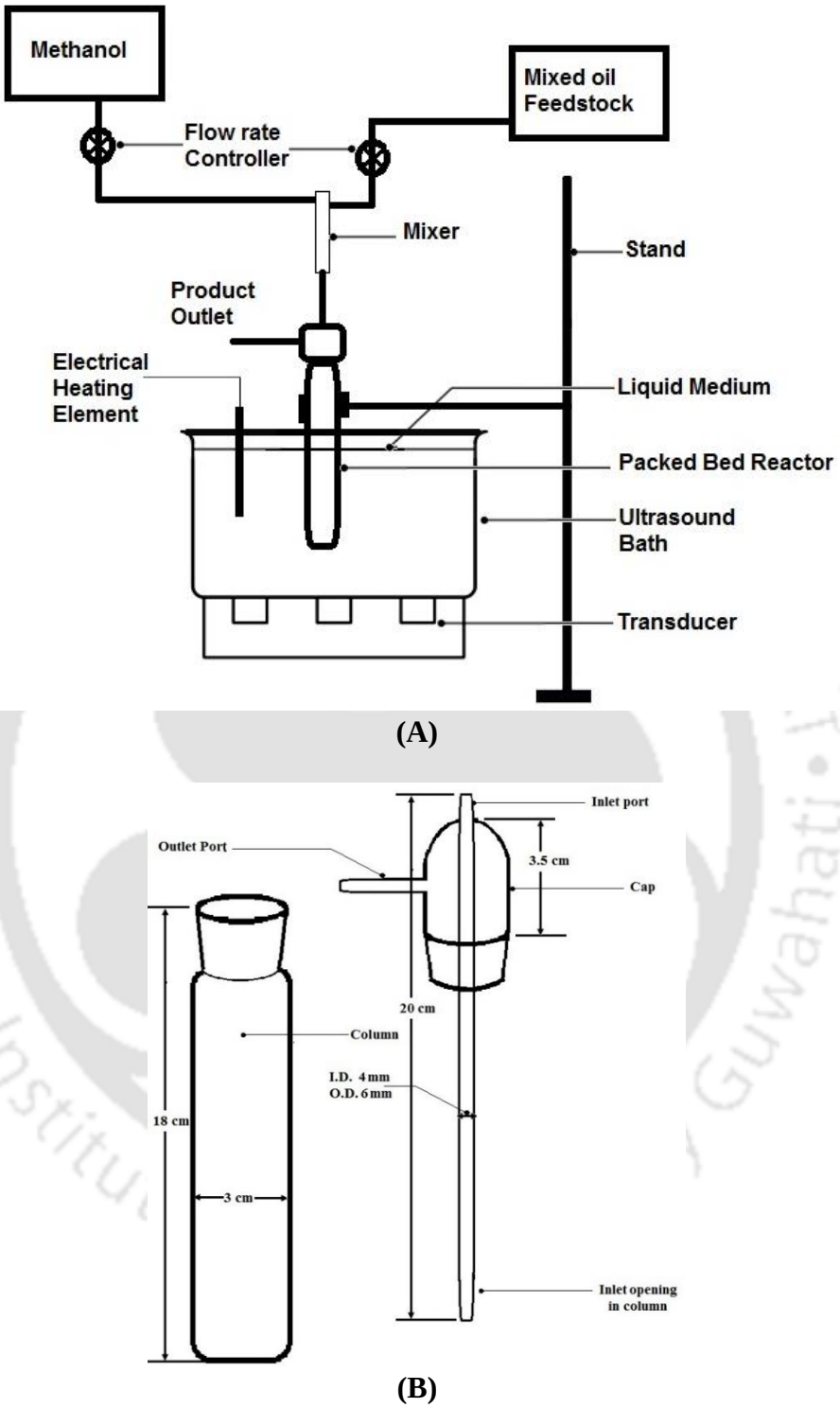

Figure 2.1: Experimental setup for ultrasound-assisted biodiesel synthesis in packed bed catalytic reactor. (A) Schematic of the complete assembly comprising reactor, ultrasound bath and feed/outlet system for reaction mixture. (B) Schematic (with dimensions) of the glass column and cap used for making the packed catalyst bed.

The temperature of water in the ultrasound bath was maintained at desired level using an immersed heating element coupled with temperature indicator and controller. The mixture of oil and methanol for injection into the catalyst bed was prepared by mixing controlled flows of methanol and oil from separate reservoirs. Gravity driven flow of both oil and methanol from the reservoirs was controlled using roller clamp (or flow regulator) of intravenous (IV) injection set. The flows of oil and methanol were mixed using a Y–connector prior to admission in the injection port, as shown in the schematic in Fig. 2.1 (A).

The individual flows of oil and methanol generated through roller clamp were calibrated prior to experiments. The out–coming reaction mixture from the packed bed reactor was collected in conical flask. The reaction mixture was filtered and glycerol was separated using centrifuge, followed by water washing to remove unreacted methanol. The product was then stored under refrigerated condition for subsequent analysis, i.e. estimation of triglyceride conversion.

Statistical Design of Experiments (DoE): Box–Behnken statistical design of experiments (DoE) has been used to devise the transesterification experiments comprising 4 factors and 3 levels. This design had 27 individual sets of experiments with permutation–combination of experimental parameters. Oil feedstock with reduced FFA–content (as obtained from esterification) has been used for transesterification. The following experimental parameters (or independent variables) have been chosen for optimization: catalyst packing height (C), temperature (T), residence time (R) and alcohol to oil molar ratio (M). The exact experimental design, formulated using Minitab 16 trial version software, indicating range and levels of the independent variables or parameters in each experimental set is shown in Table 2.2 (A) and (B). The response variable, i.e. %triglyceride conversion, has been fitted to a quadratic model for

correlating response variable to the independent (or optimization) parameters given as:

$$Y = \beta_o + \sum_{i=1}^{4} \beta_i x_i + \sum_{i=1}^{4} \beta_{ii} x_i^2 + \sum_{i=1}^{3} \sum_{j=i+1}^{4} \beta_{ij} x_i x_j$$

Table 2.2 (A): Experimental range and level of independent variables

Independent variables (or Factors)	Symbol coded	Levels of factors Coded value (Actual value)		
Catalyst packing height (mm)	C	–1 (15)	0 (30)	+1 (45)
Reaction temperature (K)	T	–1 (328)	0 (333)	+1 (338)
Alcohol to oil molar ratio	M	–1 (4:1)	0 (8:1)	+1 (12:1)
Residence time (min)	R	–1 (30)	0 (45)	+1 (60)

2.2.4 Transesterification in slurry batch reactor

The kinetic parameters of the transesterification process have been determined at optimized process conditions of transesterification process obtained from statistical optimization of packed bed experiments. As the kinetic analysis requires time profiles of the reactants, the experiments have been carried out in batch mode (slurry reactors). In order to get an insight into the effect of sonication on the Cu_2O catalysed transesterification process, experiments have been conducted in two categories, viz. (1) control (using mechanical shaking), and (2) test (using sonication). The control experiments have been conducted at 400 rpm using a magnetic stirrer and water bath to control temperature of reaction mixture. Determination of the Arrhenius parameters requires kinetic constants at different temperatures. Therefore, batch experiments with sonication have been conducted at two other temperatures than optimum. The Arrhenius analysis in this study has been conducted in two parts, viz. (1) the overall transesterification process, and (2) individual reaction steps of triglyceride conversion to FAME and glycerol.

Table 2.2 (B): Box–Behnken experimental design matrix

Packing height (mm)	Molar ratio	Residence time (min)	Temperature (K)	Oil volume (mL)	Methanol volume (mL)	Total flow rate (mL/min)	Oil flow rate (mL/min)	Methanol flow rate (mL/min)	Triglyceride conversion (Expt, %)	Triglyceride conversion (Model, %)
30	8	45	338	75.21	24.79	2.22	1.67	0.55	57.85±1.48	59.54
30	12	30	328	66.91	33.09	3.33	2.23	1.10	43.30±1.27	42.70
15	8	45	333	75.21	24.79	2.22	1.67	0.55	35.40±1.56	35.60
45	8	30	328	75.21	24.79	3.33	2.51	0.83	34.10±1.84	34.74
30	4	30	338	85.85	14.15	3.33	2.86	0.47	26.70±1.27	27.25
45	8	45	333	75.21	24.79	2.22	1.67	0.55	59.80±1.41	57.80
30	12	15	333	66.91	33.09	6.67	4.46	2.21	53.40±1.70	54.26
30	8	15	328	75.21	24.79	6.67	5.01	1.65	35.40±2.12	34.96
45	8	15	333	75.21	24.79	6.67	5.01	1.65	47.60±2.40	46.35
15	8	15	333	75.21	24.79	6.67	5.01	1.65	37.95±2.76	38.90
15	8	30	338	75.21	24.79	3.33	2.51	0.83	41.25±2.05	40.41
45	4	30	333	85.85	14.15	3.33	2.86	0.47	30.20±2.40	32.86
30	4	45	333	85.85	14.15	2.22	1.91	0.31	23.45±1.63	22.39
30	8	30	333	75.21	24.79	3.33	2.51	0.83	83.85±2.19	82.97
30	8	15	338	75.21	24.79	6.67	5.01	1.65	44.30±1.56	45.01
45	12	30	333	66.91	33.09	3.33	2.23	1.10	72.80±1.41	74.59
30	8	30	333	75.21	24.79	3.33	2.51	0.83	84.60±0.99	82.97
30	8	45	328	75.21	24.79	2.22	1.67	0.55	28.05±1.91	28.59
30	4	30	328	85.85	14.15	3.33	2.86	0.47	24.95±1.20	24.17
30	8	30	333	75.21	24.79	3.33	2.51	0.83	80.45±1.77	82.97
30	12	30	338	66.91	33.09	3.33	2.23	1.10	80.90±2.83	80.62
15	12	30	333	66.91	33.09	3.33	2.23	1.10	55.40±2.12	53.99
30	4	15	333	85.85	14.15	6.67	5.72	0.94	30.20±2.12	29.36
30	12	45	333	66.91	33.09	2.22	1.49	0.74	68.75±2.76	69.39
15	4	30	333	85.85	14.15	3.33	2.86	0.47	24.35±3.18	23.81
45	8	30	338	75.21	24.79	3.33	2.51	0.83	70.90±2.26	69.06
15	8	30	328	75.21	24.79	3.33	2.51	0.83	32.10±1.84	33.74

For the first part, the time profiles of triglyceride conversion have been fitted to pseudo–1st order kinetic model. This model fits the following expression to the time profile of triglyceride conversion: $\ln(1-X) = -kt$, where k is the pseudo–1st order kinetic constant of the overall transesterification process. The time profile of triglyceride conversion (X vs. t) is determined from the NMR analysis. The kinetic constant k is essentially the slope of plot of $-\ln(1-X)$ versus t. For the second part, the time profiles of consumption of the two reactants, viz. triglyceride and methanol, and formation of the two products, viz. FAME and glycerol, have been fitted to kinetic model for transesterification process based on Eley–Rideal mechanism. This model has been explained in greater detail in the next section. The ^{1}H NMR analysis used in the present study gives the time profile of gross conversion of the triglycerides. The time profiles of methanol, FAME and glycerol have been calculated using stoichiometry. These profiles have been fitted to the kinetic expressions of Eley–rideal model using Runge–Kutta 4th order ODE solver coupled with Genetic Algorithm. Arrhenius analysis (based on Arrhenius kinetic expression: $k = A\exp(-E_a/RT)$) is done using plots of ln k versus $1/T$. For Arrhenius analysis, test experiments have been performed at 3 different temperatures (including the optimum temperature). The time profiles of reactants and products obtained from these experiments have been fitted to Eley–Rideal kinetic model to obtain the kinetic constants of the reaction steps of transesterification process. The activation energy of these reaction steps has been determined using these kinetic constants.

Analytical method: The gross conversion of triglycerides in mixed oil to biodiesel has been determined using ^{1}H Nuclear Magnetic Resonance (NMR) technique (600 MHz Bruker) with $CDCl_3$ (Merck, India) as a solvent and TMS (tetramethylsilane) as internal standard [23]. The following equation [24,25] has been used for calculating gross molar

conversion of triglycerides in oil: $X = (2 \times A_{ME}) \times 100 / (3 \times A_{\alpha-CH_2})$, where, A_{ME} = integration value of the protons of the methyl esters (the strong singlet peak at 3.6 ppm), $A_{\alpha-CH_2}$ = integration value of the methylene protons at 2.3 ppm.

2.3 Kinetic model based on Eley–Rideal mechanism

Transesterification reaction with heterogeneous solid catalyst is essentially a surface reaction. These reactions involve adsorption of at least one or more reactants on the active site on the surface of catalyst. Several mechanisms have been proposed to explain the kinetics of surface reactions. In the present study, we have used the Eley–Rideal mechanism for developing kinetic expressions for transesterification. In this mechanism, only one of the reactants is assumed to adsorb on the catalyst surface, and the others react directly with adsorbed reactant from bulk phase. The product forms on the catalyst surface in adsorbed form, and later it desorbs from the active site making it available for further reaction. In the present context, we have assumed that excess reactant methanol preferentially adsorbs onto the active catalyst sites, and the other reactant triglyceride reacts with it from bulk phase to form diglyceride, which occupies the site and an ester (FAME) molecule, which is released into bulk. Subsequently, the diglyceride also desorbs from catalyst surface – making it available for adsorption of next methanol molecule. It then reacts with the adsorbed methanol to yield monoglyceride in adsorbed form and an ester (FAME) molecule, which is released into bulk. The transesterification process comprises of three components, viz. adsorption, reaction and desorption. The final product glycerol also forms in adsorbed form and is later desorbed from catalyst surface. Biodiesel or FAME formation thus occurs through three reaction steps that are preceded and succeeded by mass transfer steps of adsorption and desorption, respectively. The overall transesterification reaction is

written as:

$$T + 3CH_3OH \rightleftarrows 3F + G$$

where, T – triglyceride, F – fatty acid methyl ester (or biodiesel) and G – glycerol.

As per Eley–Rideal mechanism, different steps in the transesterification process and the corresponding rate expressions are given in Table 2.3, assuming only the forward reaction. The Eley–Rideal mechanism treats each of the above steps as rate–determining step. The catalyst surface is assumed to be homogeneous without any contamination or inert species.

Derivation of the rate expression for each species involves mass balance, i.e. generation and consumption in bulk phase. For the surface–species (or adsorbed species), assumption of quasi–steady state is made in that the rate of generation is assumed to be same as consumption, and the concentration of these species remains constant with respect to time [26].

Table 2.3: The steps and corresponding kinetic expressions in Eley-Rideal (ER) mechanism of transesterification using a solid heterogeneous catalyst

Step in the mechanism	Chemical equation	Rate expression
1. Methanol adsorption	$* + CH_3OH \rightleftarrows CH_3OH^*$	$r_1 = -k_1 [*]_f [CH_3OH]$
2. Transesterification reactions	$CH_3OH^* + T \rightleftarrows D^* + F$	$r_2 = -k_2 [T][CH_3OH^*]$
	$CH_3OH^* + D \rightleftarrows M^* + F$	$r_3 = -k_3 [D][CH_3OH^*]$
	$CH_3OH^* + M \rightleftarrows G^* + F$	$r_4 = -k_4 [M][CH_3OH^*]$
3. Desorption of adsorbed species	$D^* \rightleftarrows D + *$	$r_5 = -k_5 [D^*]$
	$M^* \rightleftarrows M + *$	$r_6 = -k_6 [M^*]$
	$G^* \rightleftarrows G + *$	$r_7 = -k_7 [G^*]$

Symbols: * - free catalyst active site, T – triglyceride, D – diglyceride, M – monoglyceride, G – glycerol, F – fatty acid methyl ester (biodiesel)

***Derivations of rate expressions*:** Mass balance for each of the species (either in bulk phase or in adsorbed form – denoted by superscript of *) is given as follows:

$$\frac{d[CH_3OH]}{dt} = -r_1$$

$$\frac{d[CH_3OH^*]}{dt} = r_1 - (r_2 + r_3 + r_4)$$

$$\frac{d[T]}{dt} = -r_2$$

$$\frac{d[D]}{dt} = -r_3 + r_5$$

$$\frac{d[D^*]}{dt} = r_2 - r_5$$

$$\frac{d[M]}{dt} = -r_4 + r_6$$

$$\frac{d[M^*]}{dt} = r_3 - r_6$$

$$\frac{d[G]}{dt} = r_7$$

$$\frac{d[G^*]}{dt} = r_4 - r_7$$

$$\frac{d[F]}{dt} = r_2 + r_3 + r_4$$

Rate of consumption of the initial reactant triglyceride is given by:

$$\frac{d[T]}{dt} = -r_2 = -k_2[CH_3OH^*][T]$$

Mass balance for [CH_3OH^*] can be written as:

$$\frac{d[CH_3OH^*]}{dt} = r_1 - (r_2 + r_3 + r_4)$$

As per quasi–steady state assumption, the rate of formation of surface species (or adsorbed species) is equal to its consumption, and hence:

$$\frac{d\left[CH_3OH^*\right]}{dt} = r_1 - (r_2 + r_3 + r_4) = 0$$

Substituting rate expressions for r_1, r_2, r_3, and r_4 gives:

$$k_1[*]_f[CH_3OH] = k_2[T]\left[CH_3OH^*\right] + k_3[D]\left[CH_3OH^*\right] + k_4[M]\left[CH_3OH^*\right]$$

$$\frac{k_1[*]_f[CH_3OH]}{\left[CH_3OH^*\right]} = k_2[T] + k_3[D] + k_4[M]$$

$$\frac{[*]_f}{\left[CH_3OH^*\right]} = \frac{k_2[T] + k_3[D] + k_4[M]}{k_1[CH_3OH]} \quad \text{(A)}$$

As per the site balance, the sum of fractions of free and occupied sites is unity. Thus, $[*]_o + [*]_f = 1$, where $[*]_o$ = fraction of occupied sites and $[*]_f$ = fraction of free sites.

Mass balance for occupied sites gives:

$$[*]_o = \left[CH_3OH^*\right] + \left[D^*\right] + \left[M^*\right] + \left[G^*\right]$$

$$\frac{[*]_o}{\left[CH_3OH^*\right]} = 1 + \frac{\left[D^*\right]}{\left[CH_3OH^*\right]} + \frac{\left[M^*\right]}{\left[CH_3OH^*\right]} + \frac{\left[G^*\right]}{\left[CH_3OH^*\right]} \quad \text{(B)}$$

Adding equations A and B and using overall site balance: $[*]_o + [*]_f = 1$

$$\frac{1}{\left[CH_3OH^*\right]} = 1 + \frac{\left[D^*\right]}{\left[CH_3OH^*\right]} + \frac{\left[M^*\right]}{\left[CH_3OH^*\right]} + \frac{\left[G^*\right]}{\left[CH_3OH^*\right]} + \frac{k_2[T] + k_3[D] + k_4[M]}{k_1[CH_3OH]}$$

In the above expression, we need to convert adsorbed species concentrations in terms of their bulk concentrations. The mass balance for the adsorbed species [D^*] using quasi–steady state assumption gives:

$$\frac{d\left[D^*\right]}{dt} = r_2 - r_5 = k_2[T]\left[CH_3OH^*\right] - k_5\left[D^*\right] = 0$$

$$\frac{[D^*]}{[CH_3OH^*]} = \frac{k_2[T]}{k_5}$$

Similarly, the mass balances for adsorbed species [M*] and [G*] yield:

$$\frac{[M^*]}{[CH_3OH^*]} = \frac{k_3[D]}{k_6}$$

$$\frac{[G^*]}{[CH_3OH^*]} = \frac{k_4[M]}{k_7}$$

Substitution of the above expressions in the mass balance for adsorbed methanol gives:

$$[CH_3OH^*] = \frac{1}{1+\frac{k_2[T]}{k_5}+\frac{k_3[D]}{k_6}+\frac{k_4[M]}{k_7}+\frac{k_2[T]+k_3[D]+k_4[M]}{k_1[CH_3OH]}}$$

Substituting for [CH_3OH^*] in the mass balance for triglyceride gives:

$$r_T = \frac{d[T]}{dt} = -\frac{k_2[T]}{1+\frac{k_2[T]}{k_5}+\frac{k_3[D]}{k_6}+\frac{k_4[M]}{k_7}+\frac{k_2[T]+k_3[D]+k_4[M]}{k_1[CH_3OH]}}$$

Similar mass balances for diglyceride and monoglyceride yield following expressions:

$$r_D = \frac{d[D]}{dt} = -\frac{k_3[D]-k_2[T]}{1+\frac{k_2[T]}{k_5}+\frac{k_3[D]}{k_6}+\frac{k_4[M]}{k_7}+\frac{k_2[T]+k_3[D]+k_4[M]}{k_1[CH_3OH]}}$$

$$r_M = \frac{d[M]}{dt} = -\frac{k_4[M]-k_3[D]}{1+\frac{k_2[T]}{k_5}+\frac{k_3[D]}{k_6}+\frac{k_4[M]}{k_7}+\frac{k_2[T]+k_3[D]+k_4[M]}{k_1[CH_3OH]}}$$

Mass balance for methanol gives following rate expression:

$$r_{CH_3OH} = \frac{d[CH_3OH]}{dt} = -\frac{k_2[T]+k_3[D]+k_4[M]}{1+\frac{k_2[T]}{k_5}+\frac{k_3[D]}{k_6}+\frac{k_4[M]}{k_7}+\frac{k_2[T]+k_3[D]+k_4[M]}{k_1[CH_3OH]}}$$

Mass balances for the products of transesterification, viz. glycerol and fatty acid methyl ester (FAME or biodiesel) yield following rate expressions:

$$r_G = \frac{d[G]}{dt} = \frac{k_4[M]}{1+\frac{k_2[T]}{k_5}+\frac{k_3[D]}{k_6}+\frac{k_4[M]}{k_7}+\frac{k_2[T]+k_3[D]+k_4[M]}{k_1[CH_3OH]}}$$

$$r_F = \frac{d[F]}{dt} = \frac{(k_2[T]+k_3[D]+k_4[M])}{1+\frac{k_2[T]}{k_5}+\frac{k_3[D]}{k_6}+\frac{k_4[M]}{k_7}+\frac{k_2[T]+k_3[D]+k_4[M]}{k_1[CH_3OH]}}$$

Fitting of experimental data to kinetic model and optimization: The system of four simultaneous ordinary differential equations, i.e. rate expressions for triglyceride, methanol, FAME and glycerol, have been solved using Runge–Kutta 4th order method in MATLAB (ODE solver), as IVP (initial value problem). This subroutine was coupled to Genetic Algorithm (GA) solver. The four differential equations contained 7 kinetic parameters, viz. k_1, k_2, k_3, k_4, k_5, k_6 and k_7, for which upper and lower bounds were specified on the basis of the results of Kapil et al. [26]. The GA solver randomly chooses the values of the model parameters within the bound to generate numerical solutions of the time profiles of triglyceride, methanol, glycerol and FAME. This solution is compared with the experimental profiles of these components on the basis of root mean square (RMS) error between experimental and simulated profiles. The objective function (Obj) for optimization is defined as [27]: $Obj = \min\left(\sum_{i=1}^{n} er_i\right)$, where n is the number of experimental data points for concentrations of the four species. The error (er) is defined as:

$$er_i = \left[\left(T_i^{\exp} - T_i^{\text{model}}\right)^2 + \left(CH_3OH_i^{\exp} - CH_3OH_i^{\text{model}}\right)^2 + \left(F_i^{\exp} - F_i^{\text{model}}\right)^2 + \left(G_i^{\exp} - G_i^{\text{model}}\right)^2\right]^{1/2}$$

Coupled numerical solution from ODE solver and GA the set of values of the seven model parameters (k_1 to k_7) for which the objective function is minimum.

2.4 Results and Discussion

2.4.1 Characterization of catalyst

***XRD analysis*:** Cuprous oxide (Cu_2O) catalyst has been examined to identify existence of different phases prior to transesterification. The X–ray diffractogram of cuprous oxide is shown in Fig. 2.2.

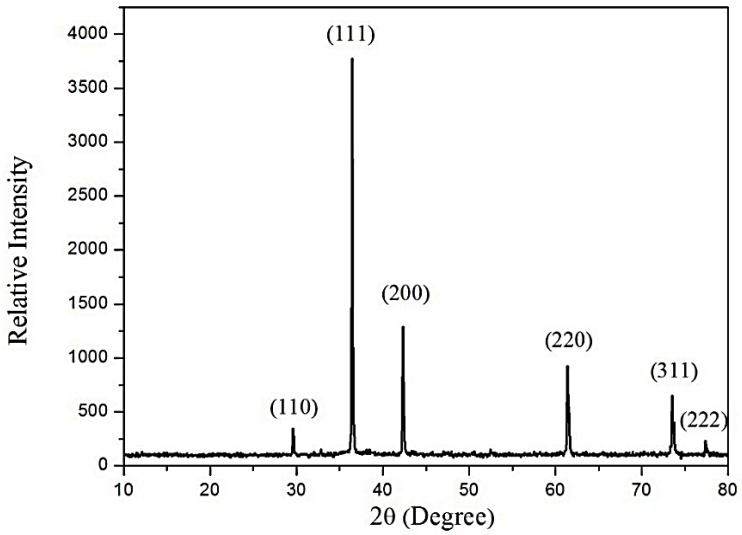

Figure 2.2: X-ray diffractogram of Cu_2O catalyst

The diffractogram of Cu_2O shows peaks corresponding to ⟨1 1 0⟩, ⟨1 1 1⟩, ⟨2 0 0⟩, ⟨2 2 0⟩, ⟨3 1 1⟩ and ⟨2 2 2⟩ planes that represent cubic FCC structure as per standard JCPDS 05–0667 [28].

Pore size and surface area analysis: Dried cuprous oxide (Cu_2O) has been analyzed for pore size distribution and surface area using nitrogen adsorption and desorption isotherm. The average pore diameter of Cu_2O was found to be 15.05 nm. The BET surface area and total pore volume of Cu_2O was 2.939 m^2/g and 0.007 cm^3/g, respectively.

FE–SEM analysis: The FE–SEM micrograph of dried Cu_2O particles shown in Fig. 2.3 confirms the cubic morphology in the size range of 0.2–2 μm. Existence of central pores in some of the Cu_2O particles is also visible in the micrograph.

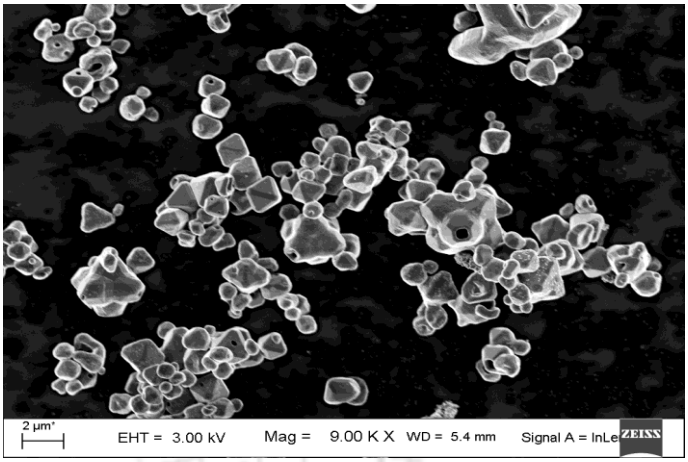

Figure 2.3: FE–SEM micrograph of Cu_2O catalyst

2.4.2 Transesterification experiments (Box–Behnken statistical DoE)

Preliminary esterification: Preliminary esterification of the mixed feedstock results in 88.27% reduction in the acid value of the feedstock. This result is similar to earlier studies of Choudhury et al. [3,23]. The mixed oil feedstocks used for experiments in packed bed and slurry reactor have acid value 1.03 mg KOH/ g oil, which is within acceptable limits for transesterification with base catalyst.

***Optimization of transesterification parameters using RSM*:** The results of Box–Behnken statistical experimental design are given in Table 3 (B) that lists the experimental and predicted values of response variable (i.e. triglyceride conversion) in 27 experimental sets. In each set, experiments have been conducted in duplicate to assess reproducibility of the results, and the standard deviation in these experimental results is also shown with average triglyceride conversion. Fitting of the experimental results to the quadratic model (equation 2) using coded values for the experimental parameters yields following expression:

$$Y = 82.967 + 2.038R + 7.413C + 17.975M + 10.975T - 20.385R^2 - 17.923C^2 - 18.729M^2 - 20.554T^2 + 3.687R \times C + 5.525R \times M + 5.225R \times T + 2.888C \times M + 6.912C \times T + 8.713M \times T$$

A close match between model–predicted and experimental values of triglyceride conversion in Table 2.2 (B) indicates that model fits well to experimental data. This is also corroborated by values of regression coefficients, viz. R^2 = 0.9957; R^2 (predicted) = 0.9783; R^2 (adjusted) = 0.9907.

Table 2.4: Statistical analysis of experimental results

(A) Estimated regression coefficients for % triglyceride conversion

Term	Coefficients	*t*–stat	*p*–value
Constant (β)	82.967	73.057	0.000
Residence Time (*R*)	2.038	3.588	0.004
Catalyst Packing Height *(C)*	7.413	13.054	0.002
Molar ratio (*M*)	17.975	31.656	0.000
Temperature (*T*)	10.975	18.052	0.000
Residence Time× Residence Time (R^2)	–20.385	–23.934	0.000
Catalyst Packing Height×Catalyst Packing Height (C^2)	–17.923	–21.043	0.016
Molar ratio × Molar ratio (M^2)	–18.729	–21.990	0.000
Temperature × Temperature (T^2)	–20.554	–24.132	0.000
Residence Time× Catalyst Packing Height *(RC)*	3.687	3.749	0.003
Residence Time× Molar Ratio *(RM)*	5.525	5.618	0.000
Residence Time× Temperature *(RT)*	5.225	5.313	0.000
Catalyst Packing Height× Molar ratio (*CM*)	2.888	2.936	0.012
Catalyst Packing Height×Temperature *(CT)*	6.912	7.029	0.000
Molar ratio ×Temperature (*MT*)	8.713	8.859	0.004

(B) Analysis of variance (ANOVA) for transesterification reaction

Source	Degrees of freedom	F–value	*p*–value
Regression	14	197.80	0.000
Linear	4	377.82	0.000
Square	4	261.90	0.000
Interaction	6	35.06	0.000
Residual Error	12	—	—
Lack–of–Fit	10	0.75	0.694
Pure Error	2	—	—
Total	26	—	—

R^2 = 99.57%; R^2 (pred) = 97.83%; R^2 (adj) = 99.07%

The linear, square and interaction coefficients of the quadratic model along with their *p*– and *t*–values are listed in Table 2.4 (A). Large (absolute) *t*–stat value and *p*–value < 0.05 indicates significance of the coefficient and the corresponding

optimization parameter. Relative *F*–values of linear, interaction and quadratic expression indicate the significance of the individual effect of corresponding optimization variable and the magnitude of interaction among them. The ANOVA (analysis of variance) of the fitted model is described in Table 2.4 (B). Although *p*–values of all coefficients are < 0.05 as per ANOVA results in Table 2.4 (B), the absolute *t*– stat values of interaction coefficients are relatively lower than the linear or quadratic coefficients, which indicates relatively independent effect of these parameters on response variable. The relative *F*–values of linear, square and interaction coefficients also corroborate this conclusion. The *F*– value of linear coefficients (377.82) is an order of magnitude higher than *F*– value of the interaction coefficients (35.06). Finally, the Lack–of–Fit *F*– value of 0.75 and *p*–value of 0.694 implies that Lack–of–Fit is not significant as compared to pure error or the model was significant.

The contour plots depicted in Fig. 2.4, shows the influence of two process variables on transesterification yield, keeping other two variables at its centre point. The innermost contours of contour plots predict the optimum transesterification yield representing the interaction of process variables. The contour plots between catalyst packing height *vs* molar ratio, residence time *vs* molar ratio, residence time *vs* catalyst packing height and residence time *vs* temperature are circular in nature predicting low interaction between them. Whereas, contour plots between molar ratio *vs* temperature and catalyst packing height *vs* temperature are elliptical in nature predicting higher interacting between these two process variables.

Quadratic model has been used to determine the combination or set of values of optimization parameters corresponding to maximum triglyceride conversion as follows: residence time = 33.48 min; catalyst packing height = 35.61 mm; molar ratio (alcohol/oil) = 10.62; temperature = 335.5 K; triglyceride conversion = 92.95%

(predicted). A confirmation experiment has been performed at the optimum conditions predicted by the model. The triglyceride conversion in the confirmation experiment is 89.95 ± 0.78%, which confirms validity of the statistical experimental design, as the experimental triglyceride conversion matches closely with the triglyceride conversion predicted by the model.

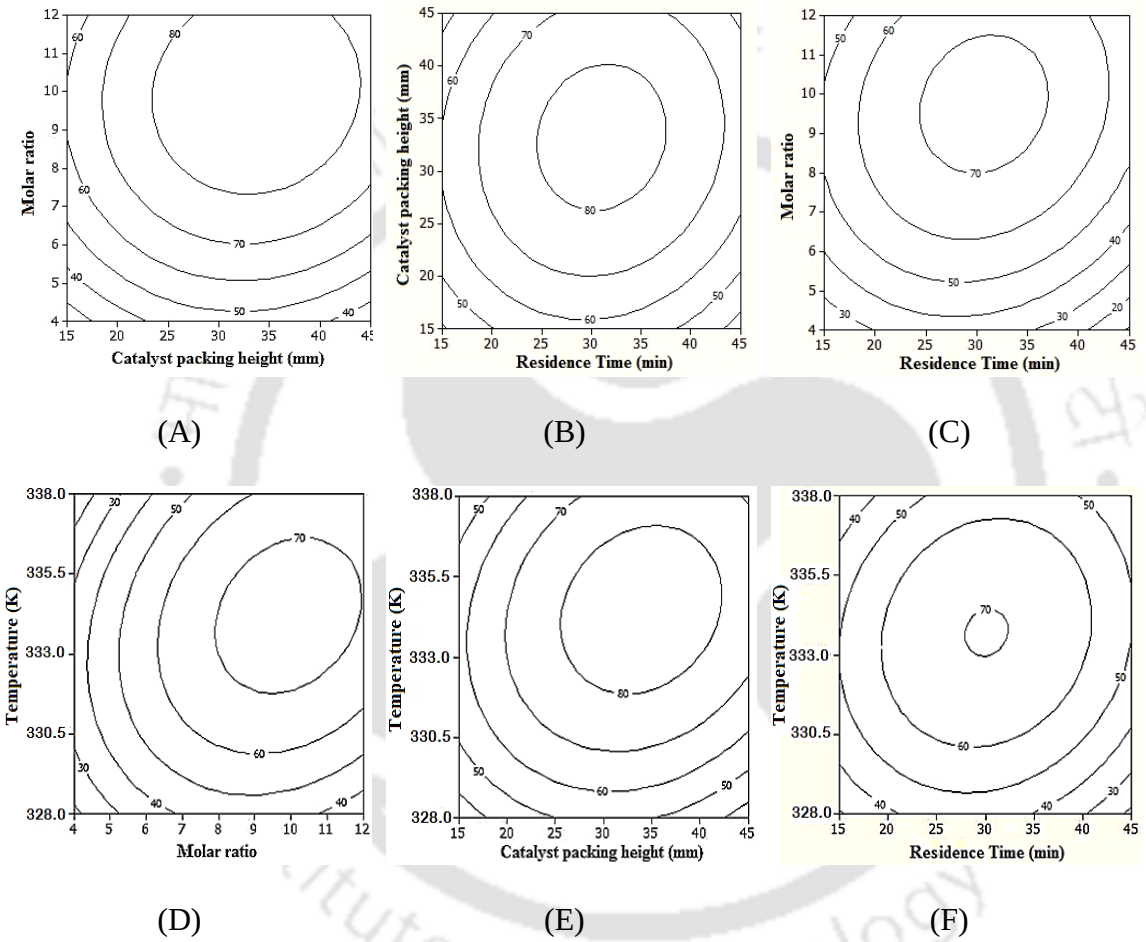

Figure 2.4: Contour plots depicting interactions among parameters for statistical optimization of transesterification process in packed bed reactor. (A) Catalyst packing height *vs* Molar ratio; (B) Residence time *vs* Catalyst packing height; (C) Residence time *vs* Molar ratio; (D) Molar ratio *vs* Temperature; (E) Catalyst packing height *vs* Temperature and (F) Residence time *vs* Temperature.

2.4.3 Kinetic and Arrhenius analysis of transesterification reaction

For determination of the kinetic parameters of transesterification process using Eley–Rideal model, experiments have been conducted in the batch mode in slurry

reactor at the optimum conditions predicted by the statistical experimental design using packed bed reactor. These conditions are: molar ratio = 10.6, temperature = 335.5 K, catalyst = 7.25% (w/w) oil (corresponding to packed bed height of 35.61 mm, with steady–state hold–up of 100 mL oil/methanol mixture). Greater details of the calculations of catalyst concentration at steady–state operation of packed bed reactor are provided in Annexure C.

The reactions in batch mode have been conducted in 25 mL two–neck round bottom flask (15 mL reaction mixture) fitted with reflux condenser. For control reactions, the mechanical agitation of reaction mixture at 400 rpm was provided using magnetic stirrer (Tarson–spinot digital model MC–02). In case of test reaction, the reaction flask was immersed in ultrasound bath at the same location as the packed bed reactor. The reaction mixture composition in batch experiments (as per the optimum conditions stated above) was as follows: mixed oil feedstock = 10.46 mL, methanol = 4.54 mL, catalyst = 0.76 g. The reaction was conducted for 1 h and samples from reaction mixture were withdrawn at the successive interval of 10 min and analysed using ^{1}H NMR to determine the gross conversion of the triglyceride.

Fig. 2.5 A and B shows the representative ^{1}H NMR spectra of organic layers of transesterification product, which contain FAME and unreacted triglycerides in oil feedstock for reactions conducted with sonication at optimum conditions in packed bed and slurry reactor.

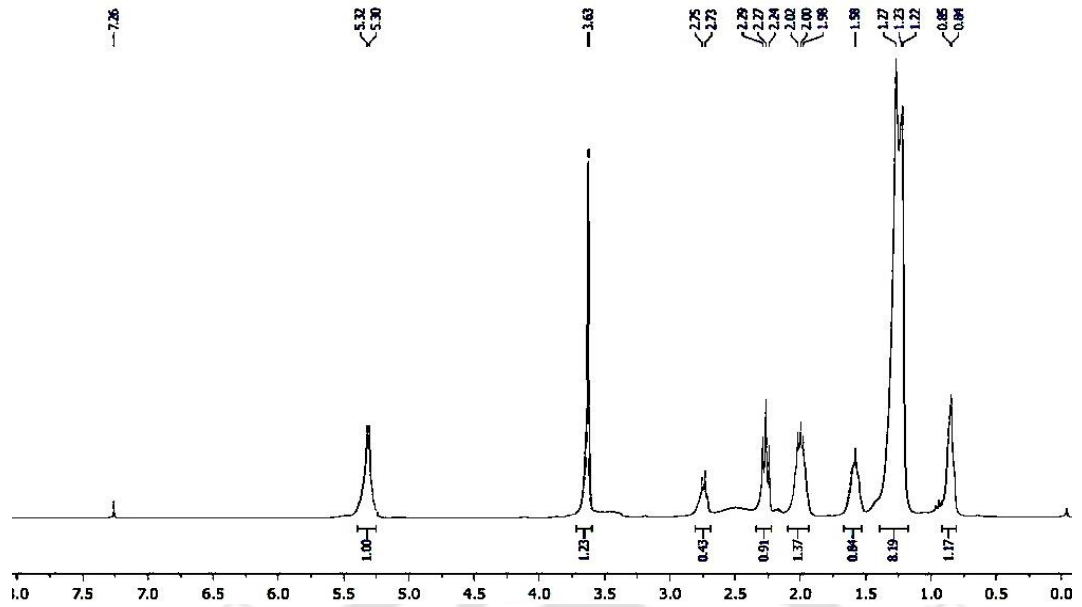

(A)

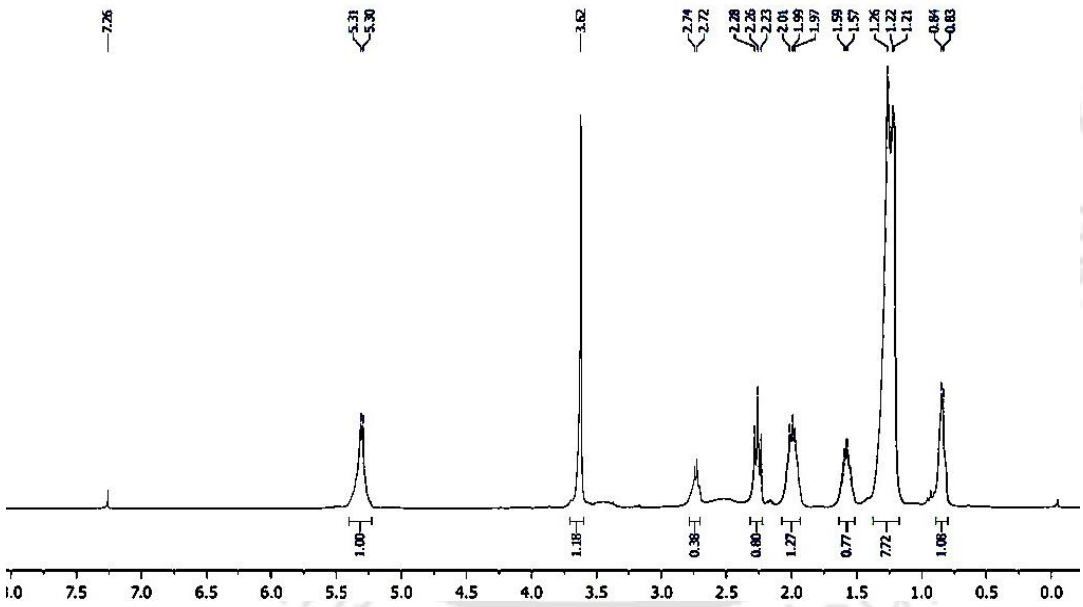

(B)

Figure 2.5: ^{1}H NMR spectra of organic layer of the product of transesterification reaction conducted at optimum conditions with sonication. (A) packed bed reactor (B) slurry batch reactor

The results of fitting of kinetic model to experimental profiles of triglyceride, glycerol and FAME are shown in Fig. 2.6 (A) and (B), for control and test experiments, respectively. It could be inferred from Fig. 2.6 that experimental and model predicted

profiles of reactants and product shows reasonable match. The kinetic rate constants (i.e. model parameters) for the control and test experiment have been listed in Table 2.5. It could be inferred from Table 2.5 that all kinetic constants except k_1 shows almost 2-fold enhancement, as mechanical agitation is replaced with sonication. The rate constant for methanol adsorption (k_1), however, shows moderate reduction with sonication. Moreover, the value of k_1 is 2 to 3 order of magnitude smaller than all other kinetic constants. Thus, methanol adsorption on catalyst essentially becomes the rate limiting step of transesterification process. This is attributed to high temperature of the transesterification process (335.5 K), which is close to the boiling point of methanol. Adsorption, being as exothermic process, is not favoured at high temperature.

Table 2.5: Kinetic rate constants for different steps of transesterification process in batch mode at 335.5 K

Rate constants (s^{-1})	Control experiment (with mechanical shaking)	Test experiment (with sonication)
k_1	1.32×10^{-4}	1.04×10^{-4}
k_2	1.24×10^{-2}	5.84×10^{-2}
k_3	2.11×10^{-2}	4.10×10^{-2}
k_4	5.97×10^{-1}	9.88×10^{-1}
k_5	3.55×10^{-2}	7.26×10^{-2}
k_6	1.45×10^{-1}	1.01×10^{-1}
k_7	1.58×10^{-2}	2.82×10^{-2}
Cumulative error	8.01×10^{-2}	2.61×10^{-1}

Moreover, it is also noteworthy that intense turbulence generated by ultrasound/ cavitation is not able to overcome the adverse thermal effect on adsorption. In fact, the micro–turbulence generated by ultrasound/ cavitation creates hindrance to adsorption of methanol, which is manifested in reduction in value of k_1, in test experiments. The probable cause leading to this effect is generation of discrete and intermittent shock waves by transient cavitation bubbles [29]. Random motion of the catalyst particles in these shock waves can cause desorption of the adsorbed molecules, as demonstrated in

our previous work [30,31]. This conjecture is further supported by rise in kinetic constants of k_5, k_6, k_7, in test experiments (with sonication) which corresponds to desorption of the intermediates (di– and mono–glyceride) and final by-product (glycerol) of the transesterification process from catalyst surface.

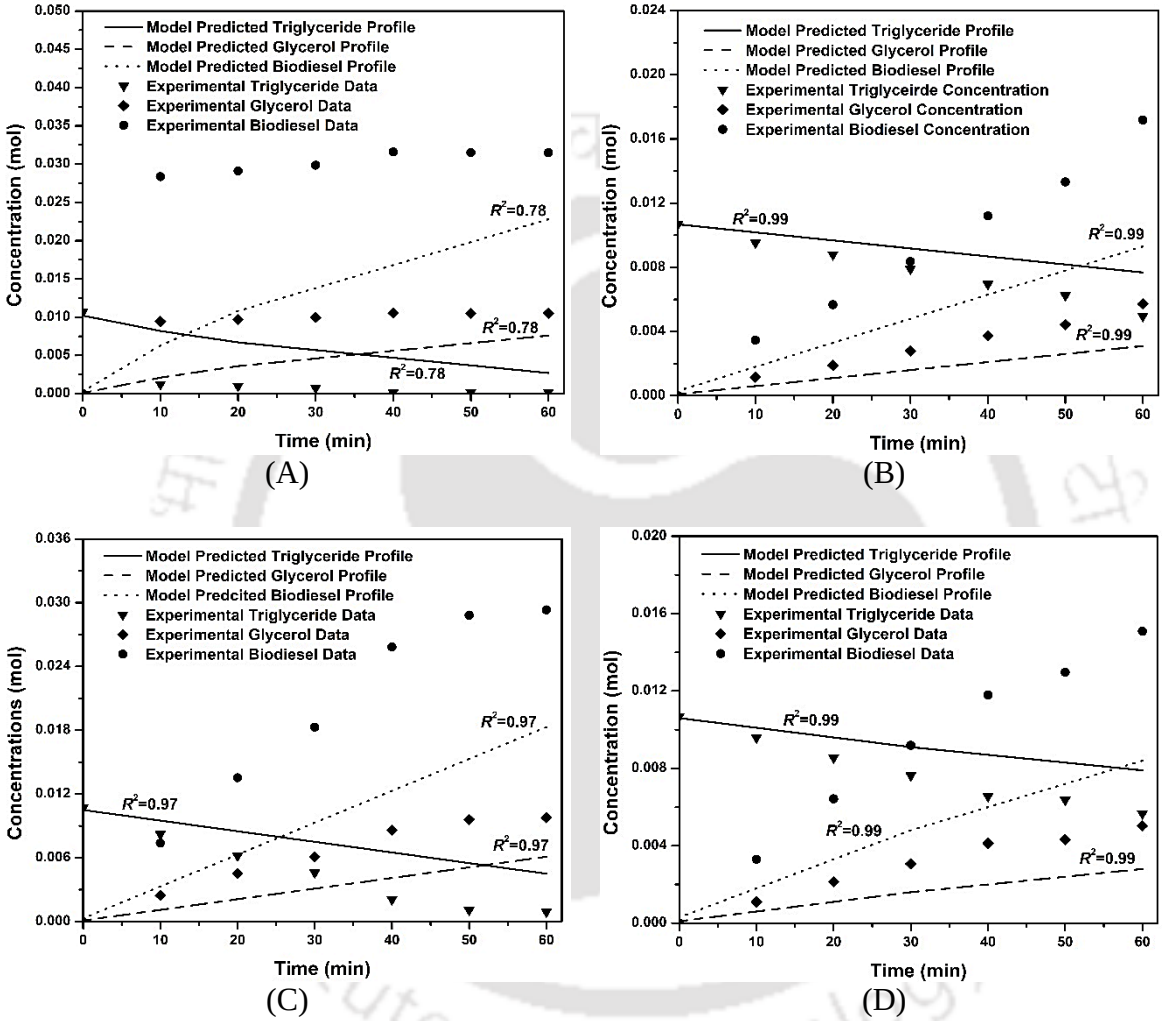

Figure 2.6: Experimental and simulated profiles (using Eley-Rideal kinetic model) of triglyceride (T), glycerol (G) and FAME (or biodiesel, F) in transesterification process in slurry reactor (batch) mode under different conditions. (A) transesterification with mechanical shaking at 335.5 K; (B) transesterification with sonication at 335.5 K; (C) transesterification with sonication at 325.5 K; (D) transesterification with sonication at 315.5 K.

As noted earlier, for determination of Arrhenius parameters of activation energy, experiments have been conducted at two more temperatures (in addition to the optimum temperature of 335.5 K), viz. 315.5 K and 325.5 K. The time profiles of

reactants and products have been fitted to Eley–Rideal kinetic model to obtain the kinetic constants of three reaction steps (r_2, r_3, r_4) in the transesterification process, which have been listed in Table 2.6. The model predicted and experimental profiles of the reactant and products for batch transesterification at 325.5 K and 315.5 K have been depicted in Figs. 2.6 (C) and (D). The kinetic constants of the overall transesterification process at the three temperatures of 315.5, 325.5 and 335.5 K have also been determined using pseudo–1st order kinetic model and listed in Table 2.6.

Table 2.6: Arrhenius analysis of transesterification process: kinetic rate constants (s^{-1}) and activation energies (kJ/mol) for the three steps and overall reaction of transesterification

Transesterification reaction	315.5 K	325.5 K	335.5 K	Activation energy	R^2
Step 1 (rate expression = r_2, kinetic constant = k_2)	3.85×10^{-2}	4.38×10^{-2}	5.84×10^{-2}	18.21	0.95
Step 2 (rate expression = r_3, kinetic constant = k_3)	2.98×10^{-2}	3.32×10^{-2}	4.10×10^{-2}	13.97	0.96
Step 3 (rate expression = r_4, kinetic constant = k_4)	8.08×10^{-1}	8.74×10^{-1}	9.88×10^{-1}	8.80	0.98
Overall transesterification reaction (k)	1.09×10^{-2}	4.04×10^{-2}	8.41×10^{-2}	90.14	0.98

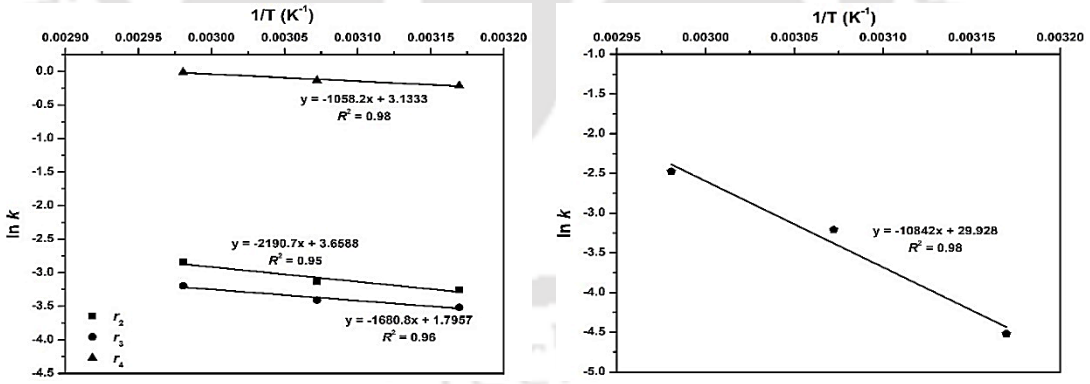

(A) (B)

Figure 2.7: Arrhenius plots for transesterification process using Cu_2O catalyst in slurry reactor configuration (A) individual reaction steps of transesterification process and (B) overall transesterification reaction

The Arrhenius plots (ln k vs 1/T) for the three reaction steps of transesterification process and the overall transesterification process have been shown in Fig. 2.7 (A) and (B). The activation energies determined from these plots and are

listed in Table 2.6. The activation energies for three reaction steps show the trend: $r_2 > r_3 > r_4$. This essentially means that the activation energies reduce with successive transesterification of triglyceride to di– and mono–glycerides. Moreover, the activation energy of all three reaction steps is significantly smaller than the overall activation energy. The sum total of the activation energies of all three reaction steps (40.98 kJ/mol) is less than half of the activation energy of 90.14 kJ/mol for overall process. A possible explanation for these results can be given as follows:

1. The extent of emulsification between methanol and oil phase, and the overall mass transfer resistance of the system depends on interfacial tension between oil and methanol. Successive transformation of triglyceride to di– and mono– glyceride results in reduction of the interfacial tension and rise in miscibility of the phases, as demonstrated by Bhoi et al. (2014). This essentially results in reduction in mass transfer barriers and also activation energy.

2. The smallest value of kinetic constant k_1 indicates low adsorption of methanol on catalytic sites. Thus, it is the rate determining step in the process. The reaction kinetics varies proportionally with temperature and this effect is further augmented by sonication. The adsorption of methanol on catalytic sites has to precede the commencement of the transesterification process. Thus, the overall transesterification essentially remains a mass transfer controlled process, even in presence of sonication. This facet is also reflected in the values of the activation energy, in that the sum total of the activation energies of all three reaction steps is less than half of the activation energy for the overall transesterification process. These results reveal an important mechanistic facet of ultrasound–assisted transesterification process with solid Cu_2O catalyst in that contribution of sonication towards intensification of process is more in

terms of boosting of the reaction kinetics than the adsorptive mass transfer, which is offset due to high reaction temperature.

2.5 Conclusion

The present study has explored the mechanistic features of the ultrasound–assisted biodiesel synthesis using Cu_2O catalyst and mixed feedstock of various non–edible oils. The process of transesterification has been optimized on the basis of statistical design of experiments (DoE) using a continuous packed bed reactor subjected to external sonication using an ultrasound bath. For determination of the kinetic parameters, batch experiments have been performed using slurry reactor (also subjected to external sonication) at the optimum conditions predicted by the statistical experimental design. The time profiles of reactants and products have been fitted to the kinetic model based on Eley–Rideal mechanism. The activation energies of the three reaction steps of successive triglyceride conversion in the transesterification process, and the overall transesterification process have been determined. The results of this study have revealed interesting facets of the Cu_2O catalysed transesterification process. The limiting step in the transesterification process, as per Eley–Rideal kinetic model, is revealed to be methanol adsorption onto the catalyst sites. The kinetic constants of the reaction step in Eley–Rideal mechanism shows enhancement with sonication. This is essentially attributed to generation of strong micro–turbulence in the reaction system by ultrasound and cavitation. However, the kinetic constant for adsorption of methanol shows reduction with sonication due to intermittent nature of the shock waves contributing to micro–turbulence. Interestingly, the sum total of the activation energies of the three reaction steps in the transesterification process is less than half of the activation energy of the overall process. This essentially indicates strong influence of

mass transfer on the overall process, even in presence of sonication. The mechanistic facets of Cu_2O–catalysed transesterification process in this study will give useful inputs for further research.

References

[1] Aransiola, E.F., Ojumu, T.V., Oyekola, O.O., Madzimbamuto, T.F. and Ikhu-Omoregbe, D.I.O., 2014. A review of current technology for biodiesel production: State of the art. Biomass and Bioenergy, 61, 276-297.

[2] Reshad, A.S., Tiwari, P. and Goud, V.V., 2015. Extraction of oil from rubber seeds for biodiesel application: Optimization of parameters. Fuel, 150, 636-644.

[3] Choudhury, H.A., Goswami, P.P., Malani, R.S. and Moholkar, V.S., 2014. Ultrasonic biodiesel synthesis from crude Jatropha curcas oil with heterogeneous base catalyst: mechanistic insight and statistical optimization. Ultrasonics Sonochemistry, 21(3), 1050-1064.

[4] Boocock, D.G., Konar, S.K., Mao, V. and Sidi, H., 1996. Fast one-phase oil-rich processes for the preparation of vegetable oil methyl esters. Biomass and Bioenergy, 11(1), 43-50.

[5] Lukić, I., Krstić, J., Jovanović, D. and Skala, D., 2009. Alumina/silica supported K_2CO_3 as a catalyst for biodiesel synthesis from sunflower oil. Bioresource Technology, 100(20), 4690-4696.

[6] Zabeti, M., Daud, W.M.A.W. and Aroua, M.K., 2009. Activity of solid catalysts for biodiesel production: a review. Fuel Processing Technology, 90(6),770-777.

[7] Takase, M., Zhang, M., Feng, W., Chen, Y., Zhao, T., Cobbina, S.J., Yang, L. and Wu, X., 2014. Application of zirconia modified with KOH as heterogeneous solid base catalyst to new non-edible oil for biodiesel. Energy Conversion and Management, 80, 117-125.

[8] Alonso, D.M., Mariscal, R., Granados, M.L., Maireles–Torres, P., 2009. Biodiesel preparation using Li/CaO catalysts: activation process and homogeneous contribution. Catalysis Today, 143, 167–171.

[9] Hsieh, L.S., Kumar, U., Wu, J.C., 2010. Continuous production of biodiesel in a packed–bed reactor using shell–core structural $Ca(C_3H_7O_3)_2/CaCO_3$ catalyst. Chemical Engineering Journal, 158(2), 250–256.

[10] Son, S.M., Kusakabe, K., 2011. Transesterification of sunflower oil in a countercurrent trickle–bed reactor packed with a CaO catalyst. Chemical Engineering and Processing: Process Intensification, 50(7), 650–654.

[11] Chen, Y.H., Huang, Y.H., Lin, R.H., Shang, N.C., Chang, C.Y., Chang, C.C., Chiang, P.C., Hu, C.Y., 2011. Biodiesel production in a rotating packed bed using $K/\gamma–Al_2O_3$ solid catalyst. Journal of Taiwan Institute of Chemical Engineering, 42, 937–944.

[12] Baroutian, S., Aroua, M.K., Raman, A.A.A., Sulaiman, N.M., 2011. A packed bed membrane reactor for production of biodiesel using activated carbon supported catalyst. Bioresource Technology, 102(2), 1095–1102.

[13] Feng, Y., Zhang, A., Li, J., He, B., 2011. A continuous process for biodiesel production in a fixed bed reactor packed with cation–exchange resin as heterogeneous catalyst. Bioresource Technology, 102(3), 3607–3609.

[14] Buasri, A., Chaiyut, N., Loryuenyong, V., Rodklum, C., Chaikwan, T., Kumphan, N., 2012. Continuous process for biodiesel production in packed bed reactor from waste frying oil using potassium hydroxide supported on Jatropha curcas fruit shell as solid catalyst. Applied Sciences, 2, 641–653.

[15] Sakthivel, S., Halder, S., Gupta, P.D., 2013. Optimisation of process variables for production of biodiesel in packed bed reactor using response surface methodology. International Journal of Ambient Energy, 34(2), 83–91.

[16] Meng, Y.L., Tian, S.J., Li, S.F., Wang, B.Y., Zhang, M.H., 2013. Transesterification of rapeseed oil for biodiesel production in trickle–bed

reactors packed with heterogeneous Ca/Al composite oxide–based alkaline catalyst. Bioresource Technology, 136, 730–734.

[17] Li, Z.H., Lin, P.H., Wu, J.C., Huang, Y.T., Lin, K.S., Wu, K.C.W., 2013. A stirring packed–bed reactor to enhance the esterification–transesterification in biodiesel production by lowering mass–transfer resistance. Chemical Engineering Journal, 234, 9–15.

[18] Doná, G., Cardozo–Filho, L., Silva, C., Castilhos, F., 2013. Biodiesel production using supercritical methyl acetate in a tubular packed bed reactor. Fuel Processing Technology, 106, 605–610.

[19] Borges, M.E., Díaz, L., 2013. Catalytic packed–bed reactor configuration for biodiesel production using waste oil as feedstock. Bioenergy Research., 6(1), 222–228.

[20] Melero, J.A., Bautista, L.F., Iglesias, J., Morales, G., Sánchez–Vazquez, R., 2014. Production of biodiesel from waste cooking oil in a continuous packed bed reactor with an agglomerated Zr–SBA–15/bentonite catalyst. Applied Catalysis B: Environmental, 145, 197–204.

[21] Deng, X., Fang, Z., Liu, Y.H., 2010. Ultrasonic transesterification of Jatropha curcas L. oil to biodiesel by a two–step process. Energy Conversion and Management, 51(12), 2802–2807.

[22] Moholkar, V.S., Sable, S.P., Pandit, A.B., 2000. Mapping the cavitation intensity in an ultrasonic bath using the acoustic emission. AIChE Journal, 46(4), 684–694.

[23] Choudhury, H.A., Malani, R.S., Moholkar, V.S., 2013. Acid catalyzed biodiesel synthesis from Jatropha oil: mechanistic aspects of ultrasonic intensification. Chemical Engineering Journal, 231, 262–272.

[24] Gelbard, G., Bres, O., Vargas, R.M., Vielfaure, F., Schuchardt, U.F., 1995. ^{1}H nuclear magnetic resonance determination of the yield of the transesterification of rapeseed oil with methanol. Journal of American Oil Chemists' Society., 72(10), 1239–1241.

[25] Knothe, G., 2001. Analytical methods used in the production and fuel quality assessment of biodiesel. Transactions of the ASAE, 44(2), 193-200.

[26] Kapil, A., Wilson, K., Lee, A.F., Sadhukhan, J., 2011. Kinetic modeling studies of heterogeneously catalyzed biodiesel synthesis reactions. Industrial & Engineering Chemistry Research, 50(9), 4818–4830.

[27] Singh, S., Sarma, S., Agarwal, M., Goyal, A., Moholkar, V.S., 2015. Ultrasound enhanced ethanol production from Parthenium hysterophorus: a mechanistic investigation. Bioresource Technology, 188, 287–294.

[28] Meghana, S., Kabra, P., Chakraborty, S., Padmavathy, N., 2015. Understanding the pathway of antibacterial activity of copper oxide nanoparticles. RSC Advances, 5(16), 12293–12299.

[29] Shah, Y.T., Pandit, A.B., Moholkar, V.S., 1999. Cavitation Reaction Engineering, Plenum Press, New York.

[30] Midathana, V.R., Moholkar, V.S., 2009. Mechanistic studies in ultrasound–assisted adsorption for removal of aromatic pollutants. Industrial & Engineering Chemistry Research, 48(15), 7368–7377.

[31] Chakma, S., Moholkar, V.S., 2011. Mechanistic features of ultrasonic desorption of aromatic pollutants. Chemical Engineering Journal, 175, 356–367.

[32] Bhoi, R., Sen, N., Singh, K.K., Mahajani, S.M., Shenoy, K.T., Rao, H., Ghosh, S.K., 2014. Transesterification of sunflower oil in microreactors. International Journal of Chemical Reactor Engineering, 12(1), 47–62.

Chapter 3

Ultrasound-Assisted Biodiesel Production Using Heterogeneous Base Catalyst and Mixed Non-Edible Oils

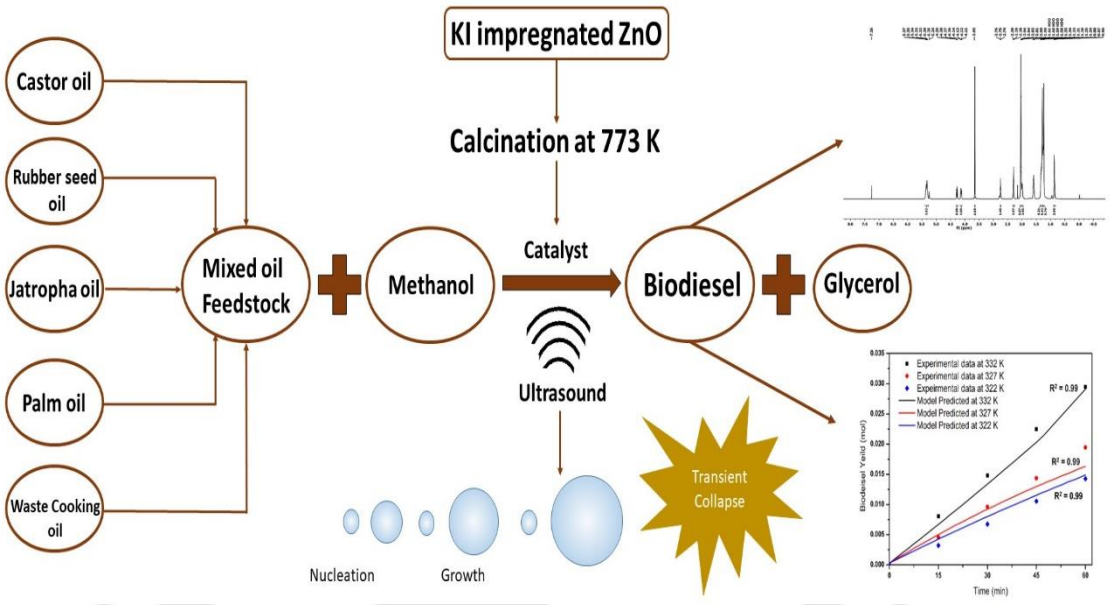

Chapter 3

Ultrasound–Assisted Biodiesel Production Using Heterogeneous Base Catalyst and Mixed Non–Edible Oils

3.1 Introduction

The previous chapter studied the ultrasound–assisted biodiesel production from mixed non–edible oil feedstock and Cu_2O catalyst in packed bed and batch–slurry reactors. Several other studies have been also reported, which uses heterogeneous base catalysts for biodiesel production, synthesized with different methods and materials using silica, zinc oxide, zirconia, zeolites, alumina, aluminosilicates, clays, activated carbon, etc. as supports, and alkali and alkaline earth oxides or their salts (like KOH, KF, KI, KNO_3, K_2CO_3, NaOH, CaO, $Ba(OH)_2$) as functional part [1–13]. ZnO is one of the supports which is stable, non–corrosive, economical and available easily. It is amphoteric in nature, which means it can be transformed into a basic as well as an acidic catalyst by reacting with different promoters such as alkaline earth metals/alkali or sulphates [14]. Reaction systems with heterogeneous catalyst suffer from slower kinetics due to strong mass transfer limitation in 3–phase (solid–liquid–liquid) reaction

mixture. The mass transfer barrier could be overcome using intense mixing, increasing temperature or pressure, application of co–solvents etc. [15] In the present study, the ultrasound irradiation or sonication was applied for boosting the reaction kinetics. Ultrasound and transient cavitation (which is nucleation, growth and implosive collapse of gas/vapour bubble driven by pressure variation induced by ultrasound) have distinct physical and chemical effects on reaction system [16,17]. The physical effect of sonication involves generation of strong micro–convection in the system, while the chemical effect involves generation of highly reactive radicals during transient collapse of the gas/vapour bubbles [17].

A major problem for large–scale production of biodiesel is availability of feedstock. Countries like India, edible oils with high price cannot used as feedstock for economic biodiesel production. However, non–edible oils such as Rubber, Neem, Karanja, Jatropha, Cassava, Castor etc. can be utilized as alternate low–cost feedstock [18]. Availability of a single non–edible feedstock throughout the year is another challenge for viable large scale production of biodiesel. As a possible solution to this issue, in present study, a blend of different non–edible oils was used as feedstock for transesterification reaction using an in–house synthesized heterogeneous base catalyst [19]. This study has dual approach, viz. (1) optimization of transesterification process using statistical methods, and (2) mechanistic investigation of the process with kinetic and Arrhenius analysis through mathematical model based on Eley–Rideal mechanism.

3.2 Material and methods

3.2.1 Materials and chemicals

Zinc oxide (> 99%, AR Grade) used as support material and potassium iodide (> 99%, AR Grade) used as a source of potassium were procured from Himedia Ltd.,

India. Methanol (99%, ACS grade) and sulfuric acid (conc. 98%, AR grade) were procured from Merck, India. Methanol was distilled to get anhydrous methanol.

Different non–edible oils (such as Jatropha, Castor, Rubber) and Waste cooking oil were collected as stated in chapter 2, section 2.2. Crude palm oil was procured from local market of Guwahati. The basic physical properties of the oils are given in Annexure B.

3.2.2 KI impregnated ZnO catalyst synthesis and characterization

Catalyst preparation: Wet impregnation method was used to synthesis the catalyst. Briefly, 25 g of ZnO was mixed with 75 mL of 35 % (w/w) KI solution in beaker under constant mixing (Tarson–spinot, Model MC–02) at 150 rpm and heating at 373 K for 3 h. The semi–solid impregnate was dried overnight in oven at 383 K, followed by calcination in muffle furnace at 773 K for 3 h with temperature rise of 10 K/min. The calcined catalyst was cooled and stored in vacuum desiccator for further characterization.

***Characterization of catalyst*:** Pristine ZnO and synthesized KI/ZnO catalyst were characterized by X–ray diffraction (XRD) analysis by using a Philips equipment (Model: X'Pert Pro MPD) 2θ range = 10°–80°, step size = 0.01º, scanning speed = 5º min^{-1} and compared with standard JCPDS data files to identify different phases. The surface elemental compositions of the pristine ZnO and synthesized catalyst were measured by X–ray photoelectron spectroscopy (XPS, Auger Electron Spectroscopy (AES) Module, Model: PHI 5000 Versa Probe II, FEI Inc.). Surface morphologies of ZnO and KI/ZnO were analysed by field emission scanning electron microscopy (FE–SEM, Zeiss, Model: Sigma). The surface area of support ZnO and KI impregnated ZnO catalyst were determined by using N_2 adsorption–desorption isotherms, using surface

area and pore analyzer (Make: Quanta chrome, Model: Autosorb–IQ MP). Prior to measurements, the samples were degassed at 423 K for 3 h in vacuum. The specific surface area of the samples was calculated from the adsorption data using Brunauer–Emmett–Teller (BET) method. The Barrett–Joyner–Halenda (BJH) model was used to determine the pore size distribution from adsorption isotherms. The presence of basic sites (K_2O) on the catalyst surface was determined using Flame photometric study using Flame Photometer (Make: Systronics; Model: 128). 0.25 g catalyst was mixed with 40 mL of 0.05 M HCl and digested at 353 K for 1 h using hot plate (Remi, 2 MLH). The solution was filtered using Whatman 40 filter paper followed by dilution using deionised water to total volume 200 mL. Standard (10 ppm) sample was prepared using KCl (AR Grade, Himedia, India) for calibration of Flame Photometer [20,21].

3.2.3 Preliminary esterification process

All non–edible oils used in present study have high acid values (i.e. AV > 2 mg KOH/g) that restricts direct transesterification with base catalyst. Therefore, the oils were initially subjected to esterification process to reduce the free fatty acid content. Esterification experiments were carried out with conc. H_2SO_4 [22]. The esterification reaction was carried out for 1 h, at alcohol/oil molar ratio of 15:1 with catalyst concentration of 5% (w/w) at 338 K in a 2–neck round bottom flask (250 mL) fixed with a reflux condenser using mechanical agitation at 400 rpm (Tarson–Spinot, Model MC–02). After completion of reaction, the mixture was separated in two phases (organic and aqueous) using a separating funnel. The traces of acids and methanol were removed from the organic layer with hot water wash. The traces of moisture from the organic layer were removed by passing it over activated silica (230–400 mesh, Merck, India) and Whatmann 40 filter paper. The filtrate was stored in clean and air–tight

containers. The acid values of esterified oils were determined using titration method.

3.2.4 Transesterification process

Transesterification experiments were performed in two stages aimed at: (1) optimization of the composition of feedstock, and (2) optimization of process parameters. In the first part, optimization of feedstock composition was done using mixture pseudo–component design with Minitab 16 software (trail version). The limits (volume fraction) selected for different oils were as follows Jatropha oil (0.05; 0.5), Castor oil (0.05; 0.5), Rubber seed oil (0.05; 0.5), Waste cooking oil (0.2; 0.65) and Palm oil (0.2; 0.65). A total 36 experimental sets were obtained for different feedstock compositions. Transesterification reaction of these feedstocks was carried out using following parameters: catalyst loading = 3% w/w, molar ratio = 9:1, and reaction temperature = 333 K. The feedstock compositions and the corresponding transesterification yields in 36 experimental sets are listed in Table 3.1.

In second part, process optimization was done for the optimum feedstock composition using Box–Behnken statistical design coupled with response surface methodology (RSM). Three process parameters, viz. catalyst loading, molar ratio and reaction temperature were selected for optimization of transesterification yield. The Box–Behnken statistical design consisted of 15 experimental sets with different combinations of individual parameters (further details of levels and combination of parameters in each experimental set are given in Table 3.2 (A) and (B)).

All transesterification experiments (in both stages of feedstock optimization and process optimization) were carried out for 1 h in batch mode using ultrasound bath (Make: Elma Transsonic, Germany, Model: T–460, total capacity: 2 L, power: 35 W, frequency: 35 kHz). The ultrasound bath was filled by distilled water up to 2/3rd of total

volume, which worked as the medium for transmission of ultrasound. Transesterification experiments were performed in 25 mL two neck round bottom borosilicate flask with a batch size of 15 mL. A coiled condenser was fitted to round bottom flask for refluxing of methanol. Circulation water bath (Jeio Tech, Lab Companion RW 0525G) was used to control the reaction temperature.

Table 3.1: Experimental sets for feed optimization experiments

Sr. No.	Volumetric ratio of oils					Average % Conversion
	Castor	Jatropha	Rubber	Waste cooking	Palm	
1	0.05	0.05	0.275	0.2	0.425	43.18 ± 0.28
2	0.275	0.05	0.05	0.425	0.2	15.89 ± 0.52
3	0.05	0.05	0.05	0.65	0.2	20.18 ± 0.35
4	0.05	0.275	0.05	0.2	0.425	22.18 ± 0.44
5	0.2	0.2	0.2	0.2	0.2	26.08 ± 0.41
6	0.2	0.05	0.2	0.2	0.35	38.17 ± 1.09
7	0.095	0.32	0.095	0.245	0.245	20.73 ± 0.62
8	0.1625	0.05	0.1625	0.3125	0.3125	30.89 ± 0.75
9	0.05	0.2	0.05	0.35	0.35	27.31 ± 0.82
10	0.05	0.05	0.05	0.2	0.65	43.17 ± 0.78
11	0.05	0.05	0.5	0.2	0.2	46.18 ± 0.51
12	0.095	0.095	0.095	0.47	0.245	26.17 ± 0.54
13	0.05	0.5	0.05	0.2	0.2	21.76 ± 0.83
14	0.1625	0.1625	0.1625	0.3125	0.2	26.02 ± 0.33
15	0.1625	0.1625	0.05	0.3125	0.3125	27.53 ± 0.51
16	0.05	0.2	0.2	0.2	0.35	28.68 ± 0.57
17	0.2	0.05	0.05	0.35	0.35	27.14 ± 0.95
18	0.275	0.05	0.275	0.2	0.2	30.11 ± 0.35
19	0.05	0.275	0.275	0.2	0.2	22.16 ± 0.27
20	0.2	0.05	0.2	0.35	0.2	26.38 ± 0.83
21	0.32	0.095	0.095	0.245	0.245	19.92 ± 0.52
22	0.095	0.095	0.32	0.245	0.245	36.28 ± 0.86
23	0.05	0.05	0.05	0.425	0.425	33.28 ± 0.72
24	0.2	0.2	0.05	0.2	0.35	27.76 ± 1.46
25	0.275	0.05	0.05	0.2	0.425	30.83 ± 0.92
26	0.275	0.275	0.05	0.2	0.2	17.98 ± 0.83
27	0.05	0.275	0.05	0.425	0.2	26.91 ± 1.13
28	0.1625	0.1625	0.1625	0.2	0.3125	29.89 ± 1.20
29	0.05	0.05	0.275	0.425	0.2	32.27 ± 1.29
30	0.05	0.2	0.2	0.35	0.2	24.18 ± 1.00
31	0.2	0.2	0.05	0.35	0.2	19.94 ± 0.41
32	0.05	0.05	0.2	0.35	0.35	36.11 ± 1.39
33	0.05	0.1625	0.1625	0.3125	0.3125	27.19 ± 0.83
34	0.14	0.14	0.14	0.29	0.29	26.15 ± 0.37
35	0.5	0.05	0.05	0.2	0.2	8.18 ± 0.55
36	0.095	0.095	0.095	0.245	0.47	35.16 ± 0.38

The power (or pressure amplitude) of ultrasound varies point to point in bath, hence the position of reaction flask was cautiously maintained same in all experiments [23]. The pressure amplitude and energy dissipation of the ultrasound wave in the bath was characterized using calorimetry study as described in earlier papers [22,24,25]. The acoustic pressure amplitude generated in the bath was calculated as 150 kPa. The results of calorimetric study show that the actual power transferred to bath was 18.6 W with an energy density of 9.3 W/L, from the theoretical supplied power of 35 W.

All experiments were performed in duplicate to confirm the reproducibility.

Table 3.2 (A): Experimental range and level of independent variables

Variables	Symbol	Level of factors coded values (Actual values)		
Catalyst loading (wt% oil)	C	–1 (3)	0 (6)	+1 (9)
Temperature (K)	T	–1 (318)	0 (328)	+1 (338)
Alcohol : oil molar ratio (M)	M	–1 (5:1)	0 (10:1)	+1 (15:1)

Table 3.2 (B): Experimental design matrix for Box–Behnken statistical design with triglyceride conversion

Sr. No.	Catalyst Loading (% w/w)	Molar Ratio	Temperature (K)	Experimental % Conversion	Model Predicted % Conversion
1	3	10	318	28.78 ± 1.13	28.44
2	6	10	328	86.78 ± 2.14	86.34
3	9	15	328	71.98 ± 0.99	72.00
4	9	10	338	73.98 ± 0.57	74.33
5	3	5	328	37.69 ± 0.95	37.67
6	6	10	328	86.02 ± 0.83	86.34
7	3	15	328	41.28 ± 0.79	41.73
8	6	15	318	40.82 ± 0.58	40.72
9	9	5	328	41.79 ± 1.41	41.35
10	6	15	338	71.28 ± 0.89	70.92
11	6	5	318	24.28 ± 0.55	24.65
12	6	5	338	52.18 ± 0.51	52.28
13	9	10	318	27.18 ± 0.41	27.26
14	3	10	338	39.28 ± 0.72	39.20
15	6	10	328	86.22 ± 0.72	86.34

Reusability of catalyst: The catalyst was also tested for reusability. The catalyst was recovered after transesterification reaction, by centrifuging the reaction mixture at 6000***g*** for 15 min at 298 K. The recovered catalyst was washed three times using 5 mL of *n*–hexane solvent to remove any impurity from the catalyst surface viz., oil, methanol or glycerol. Catalyst was then dried in oven at 383 K for 1 h followed by calcination at 773 K for 3 h. The regenerated catalyst was used for transesterification process at optimized process conditions. The transesterification experiments were repeated with recycled catalyst till the biodiesel yield reduced to half of fresh catalyst. The regenerated recycled catalyst was analysed for BET, FE–SEM and basicity determination using Flame photometric analysis after the 5th (final) cycle.

3.2.5 Kinetic and Arrhenius analysis

To study the mechanistic aspects of ultrasound–induced intensification of transesterification reaction, the experiments were performed in two categories, viz. (1) control (using mechanical agitation), and (2) test (using sonication). Mechanical agitation in control experiments was provided at 400 rpm using magnetic stirrer (Tarson–spinot, Model MC–02).

The time profiles of reactants and products were determined by withdrawing 500 µL samples of reaction mixture at intervals of 15, 30, 45 and 60 min and analysing them for triglyceride conversion by ^{1}H NMR. To determine the Arrhenius parameters (such as activation energy and frequency factor), kinetic constants of transesterification were obtained by conducting transesterification reaction at temperatures of 327 and 322 K, in addition to the optimum temperature predicted through Box–Behnken method.

The Arrhenius analysis was carried out with two approaches, viz. (1) the overall transesterification process and (2) individual reaction steps of triglyceride conversion

to FAME and glycerol. In first approach, time profiles of overall triglyceride conversion were fitted to pseudo first order kinetic model to determine overall kinetic constant. The pseudo first order kinetic expression is: $\ln(1-X) = -kt$, where *k* is the pseudo first order kinetic constant and *X* is the conversion of limiting reactant.

In the second part, the time profiles of two reactants (triglyceride and methanol) and two products (fatty acid methyl ester (FAME) and glycerol) were fitted to Eley–Rideal kinetic model for transesterification process, as described and derived in previous chapter (section 2.3). The time profiles of methanol, FAME and glycerol were obtained stoichiometrically using the overall triglyceride conversion. All 4 profiles were fitted to kinetic expressions of Eley–Rideal model using 4th order Runge–Kutta ordinary differential equation solver coupled with Genetic Algorithm. Finally, Arrhenius parameters (using kinetic expression: $k = A\exp(-E_a/RT)$) were obtained by plotting ln *k* versus 1/*T*.

Analytical method: The gross conversion of triglycerides to biodiesel was determined by ^{1}H NMR (Nuclear Magnetic Resonance) spectroscopy (Bruker Advance III HD Ascend 600 MHz) using TMS (tetramethylsilane) as internal standard and $CDCl_3$ (Merck, India) as a solvent [22]. Following equation was used for calculating gross molar conversion of triglycerides to biodiesel [26,27]: $X = (2\times A_{ME})\times 100 / (3\times A_{\alpha-CH_2})$, where, A_{ME} = integration value of methyl esters protons, the strong singlet peak at 3.6 ppm, $A_{\alpha-CH_2}$ = integration value of methylene protons at 2.3 ppm.

3.3 Results and discussion

3.3.1 Characterization of catalyst

***XRD analysis*:** Pristine ZnO and KI/ZnO catalyst were characterised by X–Ray

Diffraction to identify the different phases. The X–ray diffractograms of pristine ZnO and KI/ZnO catalyst are shown in Fig. 3.1. Diffractogram of ZnO shows the different peaks at 2θ = 31.8° ⟨1 0 0⟩; 34.4° ⟨0 0 2⟩; 36.2° ⟨1 0 1⟩; 47.5° ⟨1 0 2⟩; 56.6° ⟨1 0 1⟩; 62.8° ⟨1 0 3⟩; 66.3° ⟨1 1 2⟩; 67.8° ⟨1 1 2⟩ and 69.1° ⟨1 1 2⟩ (as per standard JCPDS file no. 36–1451). The diffractogram of KI impregnated ZnO shows the additional peaks at 2θ = 24.3°, 29.4°, 41.8°, and 77° which confirmed the presence of K_2O phase (as per JCPDS file no. 77–2176). K_2O phase on catalyst surface, acts as active sites for the transesterification reaction and imparts basicity to the catalyst [1, 19].

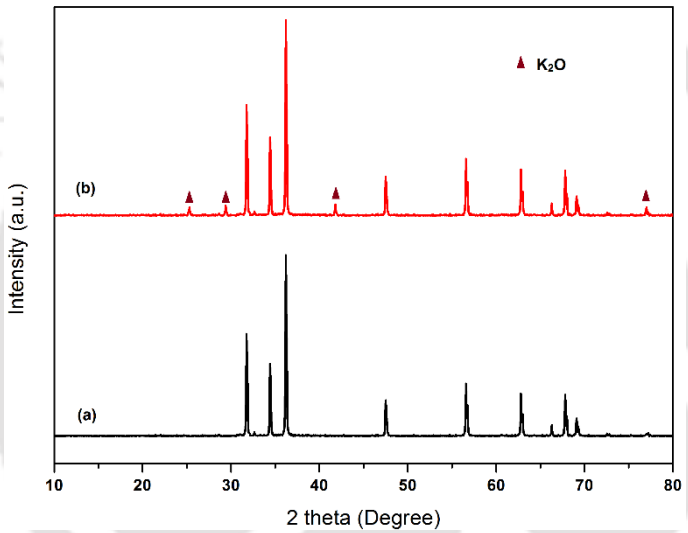

Figure 3.1: X–ray diffractogram of (a) ZnO and (b) KI impregnated ZnO catalyst

XPS analysis: The XPS spectrum of KI/ZnO is shown in Fig. 3.2, which confirmed the presence of Zn, O and K on the catalyst surface. The two peaks corresponding to binding energies 291.55 eV and 295.15 eV in K 2p spectrum correlates with the presence of potassium in +1 state. The two high intense peaks at 1022.35 eV and 1048.25 eV in Zn 2p spectrum attributed to the presence of elemental Zn in +2 state. The binding energy of O 1s for KI/ZnO catalyst in present study was found to be 533.90 eV, which exactly matches with the reported values by Yadav et al. [12]. However,

Yadav et al. [12] have also reported binding energy of O 1s in pristine ZnO as 532.94 eV. Higher binding energy of O 1s in catalyst, as compared to O 1s in pure ZnO could be attributed to distortion of ZnO lattice due to introduction of K ions.

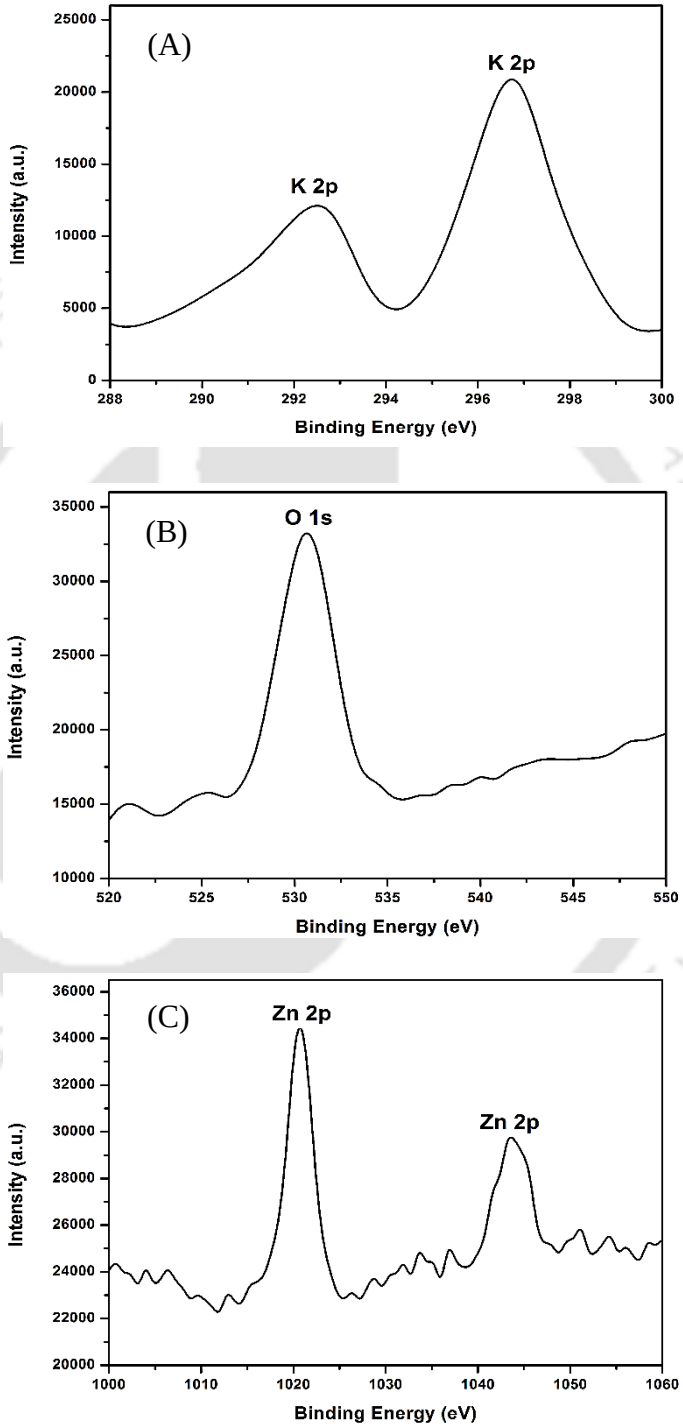

Figure 3.2: XPS spectra of (a) Potassium; (b) Oxygen and (c) Zinc molecule in KI/ZnO catalyst

FE–SEM analysis: Fig. 3.3 shows the FE–SEM micrographs of support ZnO and KI/ZnO catalyst particles. FE–SEM micrograph of pristine ZnO material shows the heterogeneous cylindrical shaped particles in size range 100 to 500 nm. On the other hand, KI impregnated ZnO catalyst micrograph shows larger particles with heterogeneity in shape and size as compared to pristine ZnO. The size of KI/ZnO catalyst particles ranges from 300 to 700 nm with agglomeration of particles. The agglomerated particles are in the range 1–2 µm.

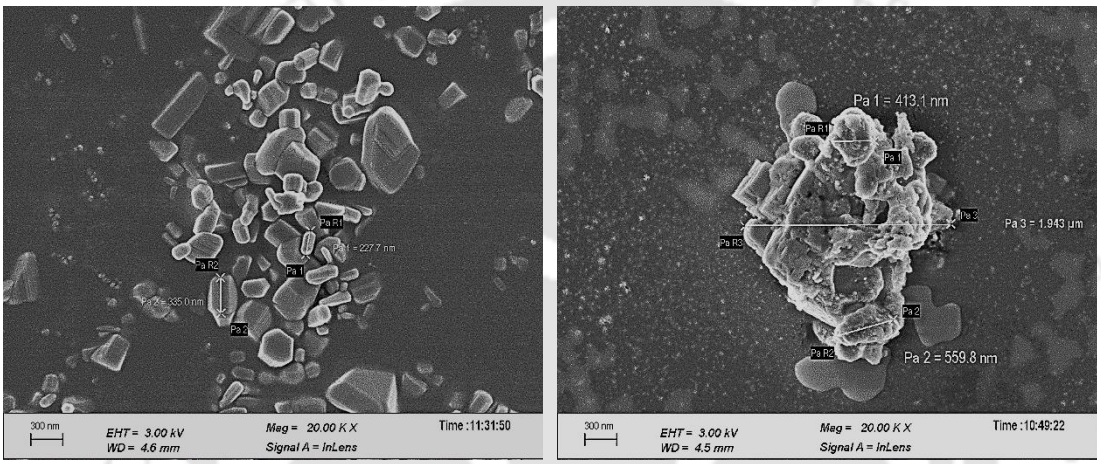

(a) **(b)**

Figure 3.3: FE–SEM micrographs of (a) ZnO particle and (b) KI/ZnO catalyst particles

Surface area and pore size analysis: Nitrogen adsorption–desorption isotherms for pure ZnO and KI/ZnO catalyst are shown in Fig. 3. Pure ZnO and synthesized ZnO catalyst follow type II isotherm, which predicts the non–porous structure of material. The average pore diameter of pure ZnO and KI impregnated ZnO were 1.87 nm and 2.12 nm, respectively. The BET surface areas of pure ZnO and KI impregnated ZnO were 6.327 m^2/g and 3.853 m^2/g, respectively. The sharp reduction in surface area of synthesized catalyst was mainly due to covering and agglomeration of KI over ZnO fine pores.

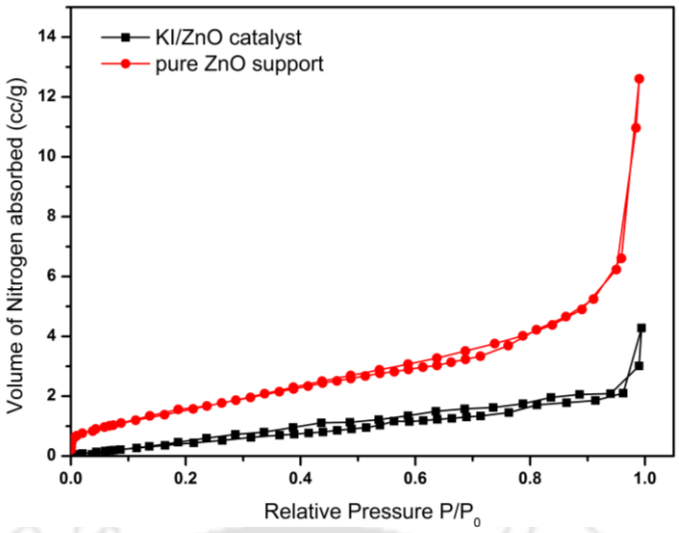

Figure 3.4: N_2 adsorption–desorption isotherm for ZnO and KI/ZnO catalyst

Flame photometric analysis: The basicity of synthesized catalyst was determined using flame photometer. The results showed that the synthesized KI impregnated ZnO catalyst had 195.65 mg K/g catalyst.

3.3.2 Preliminary esterification experiments

Esterification of all non–edible oils with homogeneous acid catalyst, resulted in average 80–90% reduction of acid value. These results are in line with reported studies of Choudhury et al. [22]. The reduction in acid values and viscosities of different oils after esterification are listed in Annexure B. It can be noted from Annexure B, that the highest reduction in acid values occurs in Jatropha and Rubber seed oil, but final values achieved are still not within the limits and thus restricts the use of either (Jatropha or Rubber seed) oil for biodiesel production with base catalyst in individual form. The least reduction in acid value occurs in Castor oil, this may be due to its high viscosity, which restricts the uniform mixing of oil, methanol and acid catalyst.

3.3.3 Transesterification experiments

Feedstock optimization: The pseudo–component mixture design with 36 experimental sets and corresponding triglyceride conversion with standard deviation is shown in Table 3.1. In feedstock optimization the esterified oils are blended in different volumetric propositions. From Table 3.1, it can be seen that, no single oil feedstock has significant dominance in blends. The highest conversion of triglyceride was obtained with experimental set 11, followed by set 1 and set 10. Some major observations from these experiments are as follows:

1. As the volume of Castor oil increases above 20% in the mixed feedstock, the transesterification yield reduces significantly. The decrease in transesterification yield attributed to high viscosity of castor oil, which increases the overall feedstock viscosity. This is manifested in terms of mass transfer limitations between oil and methanol phase. This result also suggests that in order to enhance the transesterification yield, volume fraction of castor oil in mixed feedstock should be kept minimum (< 0.1 v/v).

2. Blending of Jatropha oil at moderate to higher volumetric ratio (> 0.275 v/v) has adverse impact on transesterification yield. Reduction in transesterification yield is mainly due to its high acid value even after esterification reaction. Thus low to moderate (< 0.275 v/v) fraction of Jatropha oil to should be blended to enhance the transesterification yield.

3. Waste cooking oil in mixed oil feedstock shows mixed response on transesterification yield. In some experimental sets, moderate or higher volume fraction of waste cooking oil shows good transesterification yield, while in other experimental sets it resulted in lower transesterification yields. This mixed reaction depends on the volume fractions of other oils especially volume fraction of Castor, Jatropha and Palm oil. Hence, the moderate volume fraction (0.1 to 0.25 v/v) of waste cooking oil is

favourable for higher yield of transesterification reaction.

4. Blending of Rubber seed oil to mixed oil feedstock improved the yield of transesterification reaction. This could be attributed to its relatively low viscosity, which helps in mixing of other oils and methanol with each other. The highest yield of transesterification was obtained at 50% volume of rubber seed oil in feedstock blend.

5. Addition of Palm oil to mixture feedstock showed effect as that of waste cooking oil, i.e. for some experimental sets with higher volume fraction of palm oil, enhanced the transesterification yield and for some experimental sets, it reduced the yield. Palm oil has second highest viscosity after Castor oil among all oils used in feedstock. On the other hand, the acid value of esterified palm oil is low (0.95 mg KOH/g), which helps promoting the transesterification reaction. However, for volume fraction of palm oil > 0.2, overall viscosity of feedstock increases leading to lower mass transfer between oil and methanol. Therefore, moderate volume fraction (0.1 to 0.2 v/v) of Palm oil in blended feedstock results higher transesterification yield.

On the basis of above observations and experimental results, the optimum volume fractions of different oils in mixed oil feedstock were selected as experimental set 11. The experimental set 1 and 10 are also good alternatives for large scale transesterification process in case of non–availability of any oil feedstock.

Process optimization: After initial screening of different oil mixtures for transesterification reaction, an attempt was made to maximize the yield of transesterification reaction by varying the operating parameters such as alcohol: oil molar ratio, operating temperature of reaction and addition of catalyst to reaction mixture. The process optimization was done using Box–Behnken statistical design coupled with response surface methodology. Statistical optimization helps in understanding the interaction between two operating parameters.

The experimental transesterification yield and the model predicted yield for 15 experimental sets of Box–Behnken statistical design are tabulated in Table 3.2B. The experimental yield consisted of the average of two runs and corresponding standard deviation, as the experiment for each set was carried out in duplicate to validate reproducibility of results. A quadratic equation was fitted to the experimental data using coded values of process parameters as follows:

$$Y = 86.34 + 8.49C + 8.68M + 14.46T - 21.50C^2 - 16.66M^2 - 22.54T^2 + 6.65C \times M + 9.08T \times C + 0.64M \times T$$

From Table 3.2 (B), the experimental results showed a close match with model–predicted values of triglyceride conversion, indicating that the model prediction matches well to the experimental results. This statement is also strengthened by the regression coefficients values, viz. R^2 = 0.9998; R^2 (predicted) = 0.9979; R^2 (adjusted) =0.9995. The ANOVA (analysis of variance) of the fitted model predicted various coefficients of the quadratic model such as linear, square and interaction coefficients. *p*– and *t*– values of these coefficients are listed in Table 3.3. From ANOVA predicted coefficients, large (absolute) *t*–stat value and *p*–value < 0.05 indicated the consequence of the coefficient and thus, corresponding process parameter. *F*–values related to coefficients of linear, interaction and quadratic variables, indicated the importance of the individual effect of corresponding optimization variable and the magnitude of interaction between them. From ANOVA results the *p*–values of all coefficients are < 0.05, which indicates all the process parameters have significant impact on process optimization. Based on *p*–values of interactions, the interaction between catalyst loading and reaction temperature is most significant followed by the interaction between molar ratio and catalyst, while the temperature and molar ratio showed the least interaction. The *F*–value and *p*–value of Lack–of–Fit were 2.01 and 0.351 respectively, which denotes that Lack–of–Fit is not significant with compared to pure

error or in other way, the model is significant.

Table 3.3: Statistical analysis of experimental results

(A) Estimated regression coefficients for triglyceride conversion %

Term	Coefficients	SE coeff	*t*–stat	*p*–value
Constant (β)	86.34	0.288	299.75	0
Catalyst (C)	8.49	0.1764	48.12	0.002
Molar ratio (M)	8.68	0.1764	49.2	0
Temperature (T)	14.46	0.1764	81.96	0
Catalyst × Catalyst (C^2)	–21.5	0.2596	–82.79	0.008
Molar ratio × Molar ratio (M^2)	–16.66	0.2596	–64.17	0
Temperature × Temperature (T^2)	–22.54	0.2596	–86.82	0
Molar ratio × Catalyst (MC)	6.65	0.2495	26.66	0.006
Temperature × Catalyst (TC)	9.08	0.2495	36.4	0
Temperature × Molar ratio (TM)	0.64	0.2495	2.57	0.01

(B) Analysis of variance (ANOVA) for transesterification reaction

Source	Degrees of freedom	Sq SS	F–value	*p*–value
Regression	9	7367	3288.56	0
Linear	3	2850.85	3817.78	0
Square	3	4008.2	5367.67	0
Interaction	3	507.95	680.23	0
Residual Error	5	1.24	–	–
Lack–of–Fit	3	0.93	2.01	0.35
Pure Error	2	0.31	–	–
Regression	14	7368.24	–	–

R^2 = 99.98%; R^2 (pred) = 99.79%; R^2 (adj) = 99.95%

The response surface plots for the quadratic model are shown in Fig. 3.5, which indicated the interaction between two process parameters on transesterification yield, with retaining the third parameter at its centre point. The surface plots are graphical presentations of quadratic equation. The top (dark) colour region displays to the maximum transesterification yield. The surface plots indicated the strong interaction between the parameters as same predicted by ANOVA analysis.

The optimum set of parameters predicted by the quadratic model was: catalyst loading = 7% (w/w); molar ratio (alcohol/oil) = 11.68:1; temperature = 332 K. The validation experiment was performed at optimum set of parameters. Triglyceride

conversion in the validation experiment was 92.35 ± 1.08%, which is very close to the triglyceride conversion of 92.03% predicted by the model.

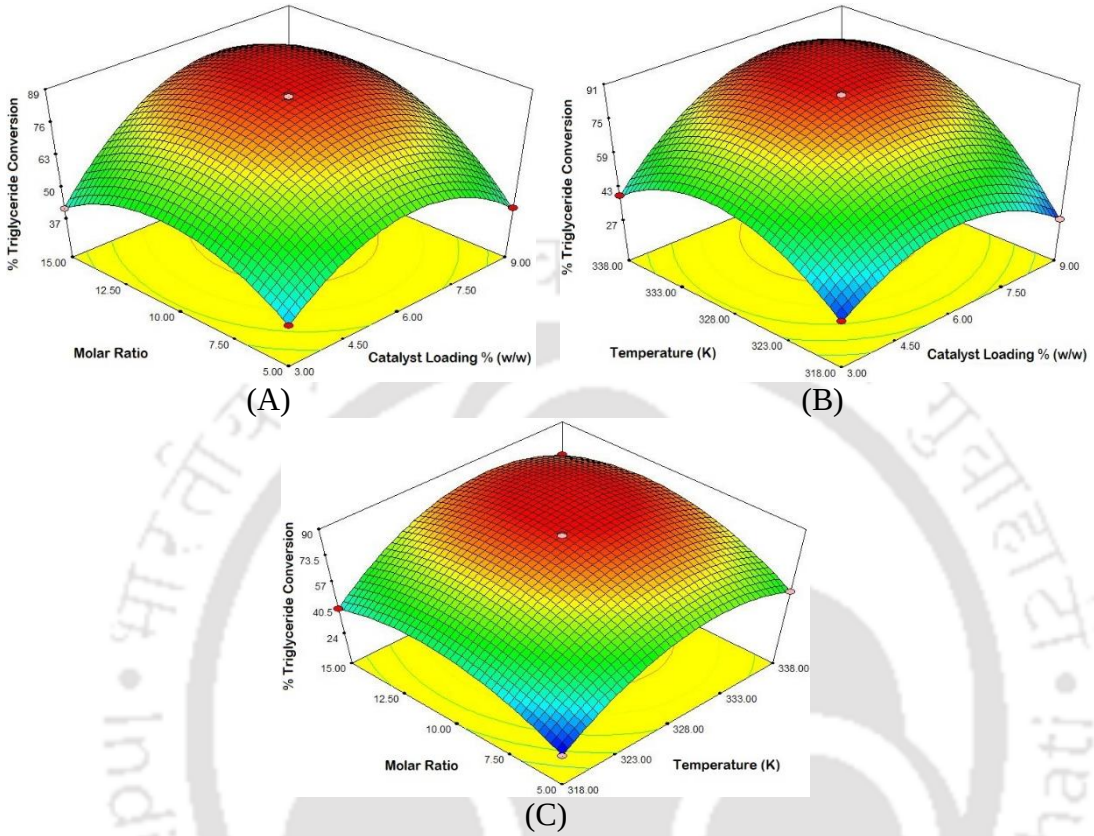

Figure 3.5: Contour plots depicting interactions among parameters for statistical optimization of transesterification process (A) molar ratio *vs* catalyst loading; (B) temperature *vs* catalyst loading and (C) molar ratio *vs* temperature

3.3.4 Kinetic modelling and Arrhenius analysis

Batch experiments were conducted at optimum conditions obtained from Box–Behnken statistical optimization design to determine the kinetic parameters or rate constants. Fig. 3.6 shows the representative ^{1}H NMR spectrum of triglyceride conversion in test experiment conducted at optimized conditions. The kinetic rate constants were determined using pseudo first order kinetics (overall process) and Eley–Rideal model (individual reaction steps) for both control and test conditions and are summarised in Table 3.5.

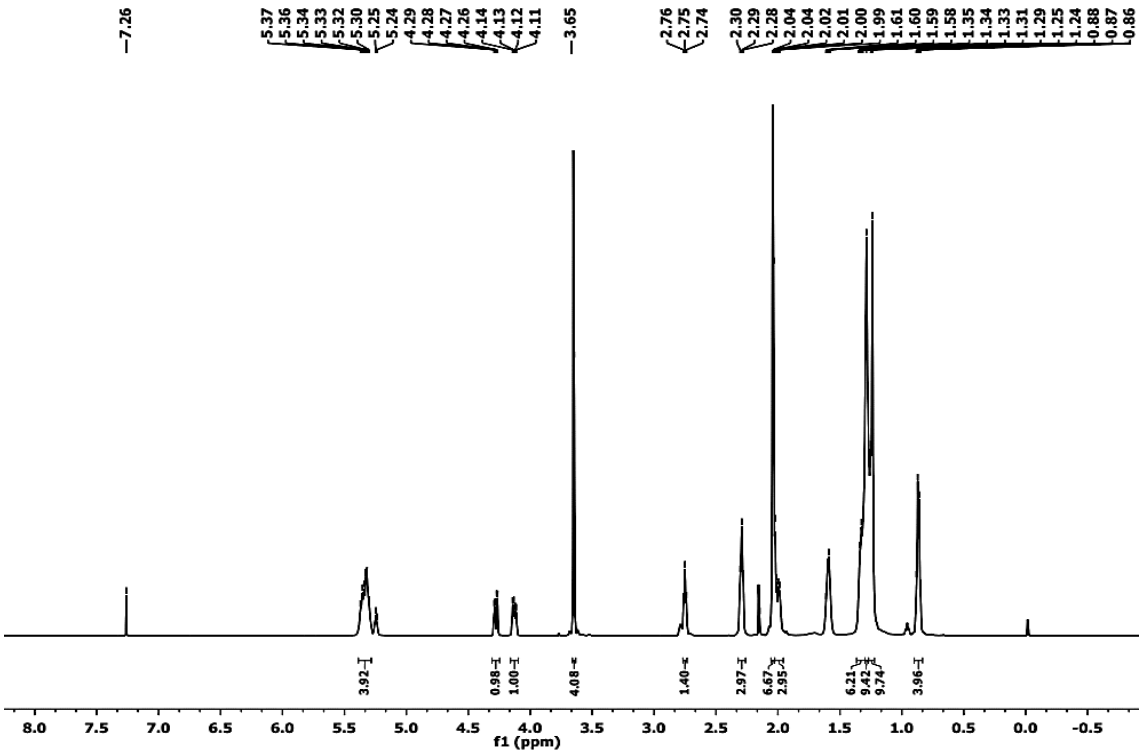

Figure 3.6: ^{1}H NMR spectra of mixed oil transesterification reaction at optimum conditions in presence of ultrasound

Table 3.5: Kinetic rate constants (min^{-1}) for different steps of transesterification process at 332 K

Rate constants (min^{-1})	Control experiment (with mechanical agitation)	Test experiment (with sonication)
k_1	7.19×10^{-3}	4.42×10^{-3}
k_2	4.36×10^{-2}	5.60×10^{-2}
k_3	4.92×10^{-2}	6.24×10^{-2}
k_4	5.26×10^{-2}	7.38×10^{-2}
k_5	6.64×10^{-2}	8.17×10^{-2}
k_6	8.48×10^{-2}	1.02×10^{-1}
k_7	2.42×10^{-1}	2.78×10^{-1}
Cumulative error	2.85×10^{-2}	4.05×10^{-2}

The experimental profiles of FAME or biodiesel yield were fitted to Eley–Rideal model as shown in Fig. 3.7. As mentioned earlier, for Activation energy (E_a) determination, the transesterification reaction (both test and control) were conducted at two different temperatures (other than optimum temperature) 327 and 322 K with same molar ratio (11.68:1) and catalyst loading (7% w/w).

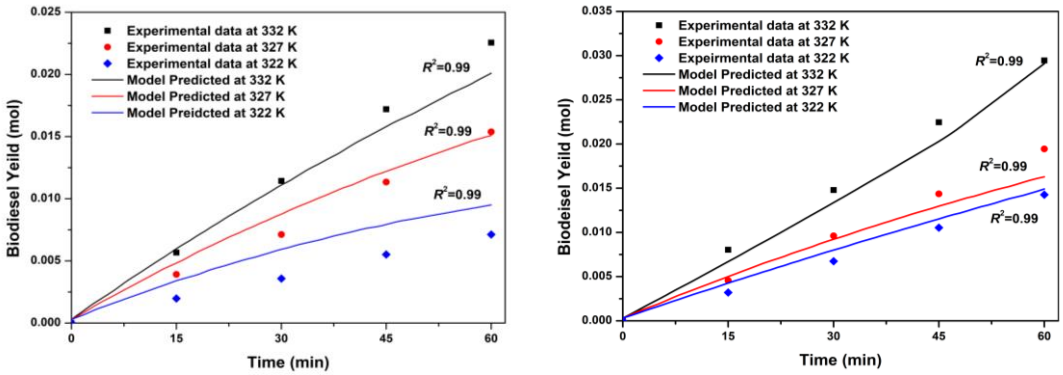

(A) **(B)**

Figure 3.7: Fitting of experimental and model predicted data for biodiesel yield (A) with mechanical agitation and (B) with ultrasound treatment

Table 3.6: Kinetic rate constants (min^{-1}) and activation energies (kJ/mol) for the three reaction steps and overall transesterification reaction

(A) With mechanical agitation

Transesterification reaction (MA)	332 K	327 K	322 K	E_a (kJ/mol)	R^2
Step 1 (rate expression = r_2, kinetic constant = k_2)	4.36×10^{-2}	3.86×10^{-2}	3.14×10^{-2}	29.09	0.98
Step 2 (rate expression = r_3, kinetic constant = k_3)	4.92×10^{-2}	4.25×10^{-2}	3.85×10^{-2}	21.80	0.99
Step 3 (rate expression = r_4, kinetic constant = k_4)	5.26×10^{-2}	4.79×10^{-2}	4.50×10^{-2}	13.80	0.98
Overall transesterification reaction (k)	1.97×10^{-2}	1.07×10^{-2}	4.30×10^{-3}	135.40	0.99

(B) With ultrasound system

Transesterification reaction (US)	332 K	327 K	322 K	E_a (kJ/mol)	R^2
Step 1 (rate expression = r_2, kinetic constant = k_2)	5.60×10^{-2}	4.85×10^{-2}	4.35×10^{-2}	22.40	0.99
Step 2 (rate expression = r_3, kinetic constant = k_3)	6.24×10^{-2}	5.59×10^{-2}	5.28×10^{-2}	14.81	0.96
Step 3 (rate expression = r_4, kinetic constant = k_4)	7.38×10^{-2}	6.90×10^{-2}	6.64×10^{-2}	9.42	0.97
Overall transesterification reaction (k)	3.91×10^{-2}	1.51×10^{-2}	9.70×10^{-3}	123.65	0.95

For calculating the activation energy of overall transesterification process, the kinetic constants determined at three reaction temperatures were used, whereas kinetic constants of three individual reaction steps were used for determining the activation

energy of these steps. All rate constants are tabulated in Tables 3.6 (A) and (B). Activation energies calculated using Arrhenius plots (ln *k* vs 1/T, shown in Fig. 3.8) are also listed in Tables 3.6 (A) and (B).

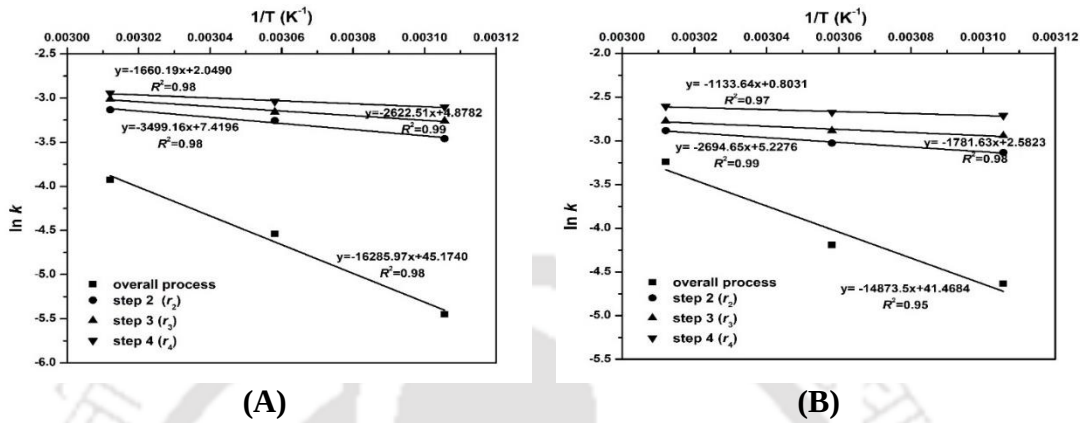

(A) **(B)**

Figure 3.8: Arrhenius plots of individual reaction steps and overall transesterification process (A) with mechanical agitation; (B) with ultrasound

The kinetic and Arrhenius analyses showed some interesting trends and revealed facts of transesterification reaction and the role of ultrasound in transesterification reaction. These findings are as follows:

- The simulated FAME or biodiesel yield profile was compared with the experimental data. A good match between the simulated results and experimental data could be seen from Fig. 3.7, which validated the selected kinetic model.
- It could be seen from Table 3.5, that the rate constants k_2 – k_7 showed 25–50% enhancement, as mechanical agitation is replaced by ultrasound, while the rate constant k_1 shows ~ 50% reduction when mechanical agitation is replaced by ultrasound.
- Among all the rate constants the value of k_1 is ~ 10–100 times smaller than other rate constants, which indicated that the adsorption of methanol on the catalyst surface is the slowest or rate limiting step in transesterification process.

- The sum of activation energies of three individual reaction steps (r_2, r_3, r_4) was significantly smaller than the activation energy of overall transesterification process in both test and control conditions. For the test experiments, the total activation energy for three reactions steps was 46.63 kJ/mol, with overall activation energy of transesterification was 123.65 kJ/mol. While for the control experiments, the total activation energy for three reactions steps was 64.69 kJ/mol, with overall activation energy of transesterification was 135.40 kJ/mol.
- The activation energies of three individual reaction steps showed the trend: $r_2 > r_3 > r_4$, for both the test and control conditions, which means that successive transformation of tri–, di– and mono– glycerides to biodiesel requires less activation energy.
- A marginal reduction (~ 9%) in overall activation energy of transesterification process was observed with application of ultrasound, which is in concurrence with observation of Choudhury et al [28]. But, the reduction in activation energies of three individual reaction steps is remarkable (~ 30%), when mechanical agitation was replaced with ultrasound as listed in Table 3.6.

Plausible explanations to these trends, which may help in identifying the mechanistic role of ultrasound in transesterification reaction, are as follows:

1. The lowest value of methanol adsorption rate constant (k_1) results in less adsorption of methanol on catalyst active sites/surface. The probable reason is high reaction temperature, which is close to boiling point of methanol, and does not favour adsorption process. The rate of adsorption of methanol in test experiments is further reduced, due to the shock waves generated by transient cavitation that cause desorption of adsorbed species [29,30]. These phenomena are essentially manifested in terms of reduction in value of k_1. Moreover, this speculation can also

be proven from the increase in the values of kinetic rate constants k_5, k_6, and k_7, in test experiments when compared to the control experiments. The desorption rate of intermediates and by–product glycerol enhanced significantly in the test experiments in presence of sonication.

2. The enhancement in rate constants of individual reaction steps with application of sonication could be attributed to intense mixing between the two phases (oil and methanol). The micro–convection generated by sonication causes fine emulsification of the phases and reduction in the interfacial tension and consequently, the activation energies.
3. The reduction in activation energies of three individual reaction steps (i.e. $r_2 > r_3 > r_4$) is again a mass transfer effect. Successive conversion of triglyceride to diglyceride, results in lower interfacial tension and enhanced mixing with methanol phase. Similarly, this effect is more prominent with conversion of diglyceride to monoglcyeride. This effect was also demonstrated by Bhoi et al. [31]. Thus, the activation energies of the individual reaction steps decreased from r_2 to r_4.
4. The marginal reduction in activation energy of overall transesterification process in presence of sonication demonstrates influence of mass transfer in transesterification reaction with heterogeneous catalyst. This result is further corroborated by comparing the difference between the sum of activation energies of three individual reaction steps and the overall activation energy in both control and test experiments. For mechanically agitated system, the overall activation energy was 135.40 kJ/mol, whereas for ultrasound–assisted system the overall activation energy was 123.65 kJ/mol. However, the sum of activation energies for three reactions steps in control and test experiments were 64.69 and 46.63 kJ/mol, respectively. The discrepancy between the overall activation energy and sum of activation energies of three

reaction steps is attributed to mass transfer limitation of the process. Notably, this discrepancy is higher for ultrasound–assisted experiments, which demonstrates greater control of mass transfer limitation on the transesterification reaction.

3.3.5 Reusability of the catalyst

The KI/ZnO catalyst was also tested for reusability. The activity of the catalyst was analysed on the basis of triglyceride conversion in successive reaction cycles as compared with fresh catalyst. The results of these experiments are given in Fig. 3.9. It could be inferred from Fig. 3.9 that KI/ZnO catalyst retained ~ 50% of its initial activity after 5 successive reaction cycles.

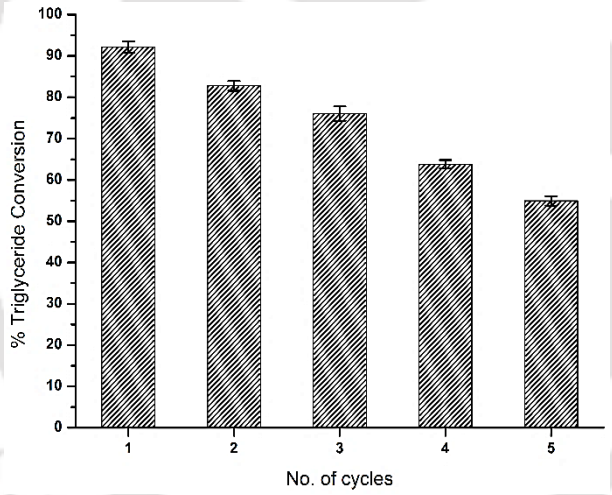

Figure 3.9: Performance of KI/ZnO catalyst in the reusability study

The reused/ recycled catalyst (after 5th cycle) was analysed for BET and FE–SEM analysis to determine changes in surface morphology. The BET surface area of reused catalyst was found to be 2.426 m^2/g, lower as compared to fresh catalyst. The FE–SEM micrograph of recycled catalyst as shown in Fig. 3.10 shows that the catalyst had morphology similar to pure KI/ZnO catalyst with higher agglomeration of particles. The recycled catalyst was also tested for Flame photometric analysis. The results indicated that recycled catalyst had 127.68 mg K/g catalyst after 5 cycles of reuse. The

reduction in potassium from catalyst was the major reason for loss of catalytic activity of catalyst. A probable cause of loss of catalyst activity is presence of impurities (triglyceride or glycerol) on catalyst surface that block the active sites [12].

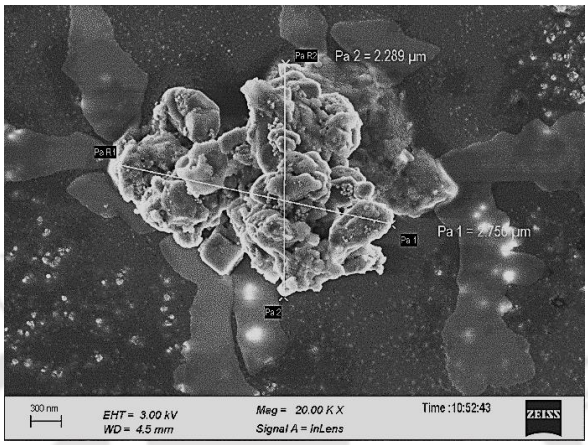

Figure 3.10: FE–SEM micrographs of recycled catalyst after 5th cycle

3.4 Conclusion

The present study has demonstrated feasibility of mixed non–edible oil feedstock for biodiesel synthesis with heterogeneous base catalyst. This process could be intensified with application of ultrasound. Activation energy of the transesterification showed significant reduction with application of ultrasound with concurrent rise in kinetics. However, the kinetic analysis of the transesterification process using Eley–Rideal model has revealed strong mass transfer influence on the process even with application of sonication. Methanol adsorption on the solid catalyst has been revealed to be the rate limiting step of overall process. Moreover, the synthesized KI/ZnO catalyst after regeneration was reusable up to 5 cycles.

References

[1] Xie, W. and Huang, X., 2006. Synthesis of biodiesel from soybean oil using heterogeneous KF/ZnO catalyst. Catalysis Letters, 107(1–2), 53–59.

[2] Chouhan, A.S. and Sarma, A.K., 2011. Modern heterogeneous catalysts for biodiesel production: A comprehensive review. Renewable and Sustainable Energy Reviews, 15(9), 4378–4399.

[3] Vyas, A.P., Subrahmanyam, N. and Patel, P.A., 2009. Production of biodiesel through transesterification of Jatropha oil using KNO_3/Al_2O_3 solid catalyst. Fuel, 88(4), 625–628.

[4] Lukić, I., Krstić, J., Glišić, S., Jovanović, D. and Skala, D., 2010. Biodiesel synthesis using K_2CO_3/Al–O–Si aerogel catalysts. Journal of the Serbian Chemical Society, 75(6), 789–801.

[5] Baroutian, S., Aroua, M.K., Raman, A.A.A. and Sulaiman, N.M.N., 2010. Potassium hydroxide catalyst supported on palm shell activated carbon for transesterification of palm oil. Fuel Processing Technology, 91(11), 1378–1385.

[6] Soetaredjo, F.E., Ayucitra, A., Ismadji, S. and Maukar, A.L., 2011. KOH/bentonite catalysts for transesterification of palm oil to biodiesel. Applied Clay Science, 53(2), 341–346.

[7] Wang, J.X., Chen, K.T., Wu, J.S., Wang, P.H., Huang, S.T. and Chen, C.C., 2012. Production of biodiesel through transesterification of soybean oil using lithium orthosilicate solid catalyst. Fuel processing technology, 104, 167–173.

[8] Takase, M., Zhang, M., Feng, W., Chen, Y., Zhao, T., Cobbina, S.J., Yang, L. and Wu, X., 2014. Application of zirconia modified with KOH as heterogeneous

solid base catalyst to new non–edible oil for biodiesel. Energy Conversion and Management, 80, 117–125.

[9] Tao, G., Hua, Z., Gao, Z., Zhu, Y., Chen, Y., Shu, Z., Zhang, L. and Shi, J., 2013. KF–loaded mesoporous Mg–Fe bi–metal oxides: high performance transesterification catalysts for biodiesel production. Chemical Communications, 49(73), 8006–8008.

[10] Dai, Y.M., Chen, K.T., Wang, P.H. and Chen, C.C., 2016. Solid–base catalysts for biodiesel production by using silica in agricultural wastes and lithium carbonate. Advanced Powder Technology, 27(6), 2432–2438.

[11] Liu, H., shuang Guo, H., jing Wang, X., zhong Jiang, J., Lin, H., Han, S. and peng Pei, S., 2016. Mixed and ground KBr–impregnated calcined snail shell and kaolin as solid base catalysts for biodiesel production. Renewable Energy, 93, 648–657.

[12] Yadav, M., Singh, V. and Sharma, Y.C., 2017. Methyl transesterification of waste cooking oil using a laboratory synthesized reusable heterogeneous base catalyst: Process optimization and homogeneity study of catalyst. Energy Conversion and Management, 148, 1438–1452.

[13] Albuquerque, M.C., Jiménez–Urbistondo, I., Santamaría–González, J., Mérida–Robles, J.M., Moreno–Tost, R., Rodríguez–Castellón, E., Jiménez–López, A., Azevedo, D.C., Cavalcante Jr, C.L. and Maireles–Torres, P., 2008. CaO supported on mesoporous silicas as basic catalysts for transesterification reactions. Applied Catalysis A: General, 334(1–2), 35–43.

[14] Alba–Rubio, A.C., Santamaría–González, J., Mérida–Robles, J.M., Moreno–Tost, R., Martín–Alonso, D., Jiménez–López, A. and Maireles–Torres, P., 2010.

Heterogeneous transesterification processes by using CaO supported on zinc oxide as basic catalysts. Catalysis Today, 149(3–4), 281–287.

[15] Luu, P.D., Takenaka, N., Van Luu, B., Pham, L.N., Imamura, K. and Maeda, Y., 2014. Co–solvent method produce biodiesel form waste cooking oil with small pilot plant. Energy Procedia, 61, 2822–2832.

[16] Ranjan, A., Singh, S., Malani, R.S. and Moholkar, V.S., 2016. Ultrasound–assisted bioalcohol synthesis: review and analysis. RSC Advances, 6(70), 65541–65562.

[17] Malani, R. S., Goyal, A. and Moholkar, V. S. Ultrasound–Assisted Biodiesel Synthesis: A Mechanistic Insight, in: Agrawal, A. K., Agarwal, R. A., Gupta, T. and Gurjar, B. R. (Eds.), Biofuels, Springer, Singapore, 2017, pp. 103–135.

[18] Reshad, A.S., Tiwari, P. and Goud, V.V., 2015. Extraction of oil from rubber seeds for biodiesel application: Optimization of parameters. Fuel, 150, 636–644.

[19] Xie, W. and Li, H., 2006. Alumina–supported potassium iodide as a heterogeneous catalyst for biodiesel production from soybean oil. Journal of Molecular Catalysis A: Chemical, 255(1–2), 1–9.

[20] Cooper, J.A., 1963. The flame photometric determination of potassium in geological materials used for potassium argon dating. Geochimica et Cosmochimica Acta, 27(5), 525–546.

[21] DOTD Designation 531–11, Available online at http://wwwsp.dotd.la.gov/Inside_LaDOTD/Divisions/Engineering/Materials_Lab/TPM_Vol_II_Part_V/tr_531–11.pdf (Access on 11–06–18).

[22] Choudhury, H.A., Malani, R.S., Moholkar, V.S., 2013. Acid catalyzed biodiesel

synthesis from Jatropha oil: mechanistic aspects of ultrasonic intensification. Chemical Engineering Journal, 231, 262–272.

[23] Moholkar, V.S., Sable, S.P., Pandit, A.B., 2000. Mapping the cavitation intensity in an ultrasonic bath using the acoustic emission. AIChE Journal, 46(4), 684–694.

[24] Chakma, S. and Moholkar, V.S., 2011. Mechanistic features of ultrasonic desorption of aromatic pollutants. Chemical Engineering Journal, 175, 356–367.

[25] Choudhury, H.A., Chakma, S. and Moholkar, V.S., 2014. Mechanistic insight into sonochemical biodiesel synthesis using heterogeneous base catalyst. Ultrasonics Sonochemistry, 21(1), 169–181.

[26] Gelbard, G., Bres, O., Vargas, R.M., Vielfaure, F., Schuchardt, U.F., 1995. ^{1}H nuclear magnetic resonance determination of the yield of the transesterification of rapeseed oil with methanol. Journal of American Oil Chemists' Society., 72(10), 1239–1241.

[27] Knothe, G., 2001. Analytical methods used in the production and fuel quality assessment of biodiesel. Transactions of the ASAE, 44(2), 193–200.

[28] Choudhury, H.A., Goswami, P.P., Malani, R.S. and Moholkar, V.S., 2014. Ultrasonic biodiesel synthesis from crude Jatropha curcas oil with heterogeneous base catalyst: mechanistic insight and statistical optimization. Ultrasonics Sonochemistry, 21(3), 1050–1064.

[29] Midathana, V.R., Moholkar, V.S., 2009. Mechanistic studies in ultrasound–assisted adsorption for removal of aromatic pollutants. Industrial & Engineering Chemistry Research, 48(15), 7368–7377.

[30] Chakma, S., Moholkar, V.S., 2011. Mechanistic features of ultrasonic desorption of aromatic pollutants. Chemical Engineering Journal, 175, 356–

367.

[31] Bhoi, R., Singh, D. and Mahajani, S., 2017. Investigation of mass transfer limitations in simultaneous esterification and transesterification of triglycerides using a heterogeneous catalyst. Reaction Chemistry & Engineering, 2(5), 740–753.

CHAPTER 4

ULTRASOUND INTENSIFIED BIODIESEL PRODUCTION FROM MIXED NON-EDIBLE OIL FEEDSTOCK USING HETEROGENEOUS ACID CATALYST SUPPORTED ON RUBBER DE-OILED CAKE

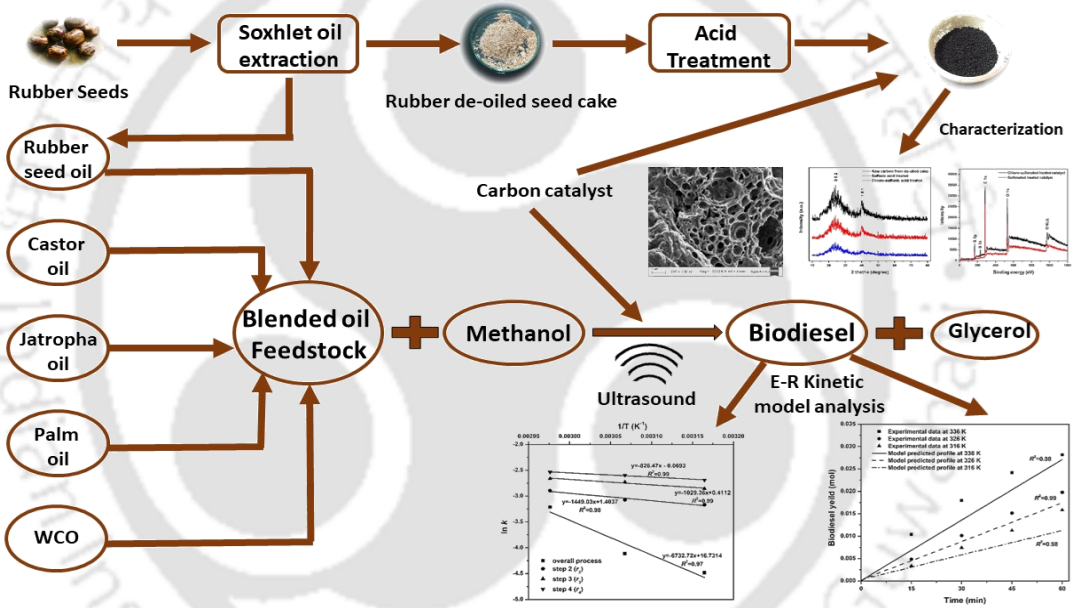

Chapter 4

Ultrasound Intensified Biodiesel Production from Mixed Non–Edible Oil Feedstock Using Heterogeneous Acid Catalyst Supported on Rubber De–oiled Cake

4.1 Introduction

Preceding chapter deals with in–lab synthesised KI impregnated ZnO catalysed ultrasound–assisted biodiesel production using mixed non–edible oil feedstock. The process was carried out two stages of separate esterification and transesterification of esterified oils mixed in optimum volumetric ratios. Use of non–edible or waste cooking oil is a feasible alternative as compared to costlier edible oils for viable and economic production of biodiesel at commercial scale [1–3]. The non–edible oils have high free fatty acid (FFA) content along with water traces that restrict direct application of base catalyst. The acid catalysts (H_2SO_4) have higher tolerance towards FFA content and water traces, but suffer from slower kinetics and low yields [3–5]. On the other hand, use of homogenous acid catalyst makes overall process uneconomical with major drawbacks of corrosion of reactors, contamination of by–product glycerol and requirement of excess water for purification of biodiesel [2,6].

In last decade, substantial progress has been made on development of heterogeneous acid catalyst for biodiesel production [6–10]. Heterogeneous acid catalysts overcome the major demerit of corrosion of reaction vessels. Moreover, they can be separated easily from the reaction mixture resulting in a simple downstream process with minimum contamination of glycerol. These catalysts also retain substantial activity during recycle. Heterogeneous catalysts also offer flexibility of operating transesterification process in continuous mode using fixed bed reactors [11,12]. Thus, with the use of heterogeneous acid catalyst, which promotes esterification and transesterification reaction simultaneously (as shown in scheme 1 and 2), the economical production of biodiesel at large scale can be achieved by using non–edible oil feedstocks [6,8]. Heterogeneous acid catalysts have much slower reaction kinetics (as compared to homogeneous catalysts) due to 3–phase heterogeneity of reaction system. In recent years, several studies have dealt with this issue using different techniques, which enhance the intermixing of two phases as well as the contact of reactant with catalyst [8,13,14].

Several heterogeneous acid catalysts have been synthesized and investigated in recent years for reduction of FFA content as well as for parallel esterification and transesterification reaction [2,11]. These catalysts include sulphated metal oxides, mesoporous silica, modified zeolites, metal organic framework (MOF) structures, ion exchange resins, polymer supported sulphonic groups, carbon–based supports with functionalized acid groups, etc. [15–28]. Among these different catalysts, carbon–based catalysts are best choice for sustainable and economical production of biodiesel, as many of other catalysts are prepared from expensive materials, while, carbon is abundantly available and is inexpensive [6,11,15,24,27,28]. In the present study, the rubber de–oiled cake obtained after oil extraction from rubber seeds was used as a

support for catalyst preparation.

Numerous studies have been conducted on sustainable production of biodiesel using different non–edible oils, such as Karanja, Cassava, Castor, Jatropha, Kusum, Mahua, Neem, Rubber seeds, etc. [4]. Availability of single non–edible oil feedstock at large scale through the year is difficult. These non–edible oil crops can be grown on low–fertile lands without disturbing the regular crops. Hence, present study investigated the mixture of non–edible oils as a feedstock for producing biodiesel, which adds to economic viability and sustainability of biodiesel production process. Process optimization was done using statistical techniques. The slower kinetics due to three–phase heterogeneity was tackled with the application the ultrasound irradiation or sonication [12,29]. Ultrasound or sonication helps in intense mixing of two phases resulting in enhanced kinetics [30,31]. This intense mixing is a result of micro–conventions generated during the transient collapse of gas/vapour bubbles, known as cavitation phenomenon [31–33]. Enhancement in the yield of transesterification process by application of ultrasound was determined by comparing with yield using mechanical agitation. The mathematical model established on Eley–Rideal kinetic mechanism with some modifications (that considers FAME as adsorbed product on catalyst – instead of intermediates of di– and mono–glycerides) was used to get physical insight into the enhancement induced by sonication.

4.2 Material and methods

4.2.1 Materials and chemicals

Sulfuric acid (98% conc., AR grade) and Methanol (99%, ACS grade) were procured from Merck, India. Chloro–sulfonic acid (99%, AR grade) was procured from

Sigma Aldrich, Germany. Anhydrous methanol was obtained using distillation of methanol.

Different non–edible oils (such as Jatropha, Castor, Rubber and Waste cooking oil) were collected as stated in chapter 2, section 2.2. Crude palm oil was procured from local market of Guwahati. The basic physical properties of the oils are given in Annexure B. The oils were blended to prepare mixed feedstock for transesterification with following composition: Jatropha = 0.15 (v/v); Castor = 0.1 (v/v); Rubber = 0.3 (v/v); Palm = 0.2 (v/v) and Waste cooking oil = 0.25 (v/v).

The density and viscosity was measured using density bottle and rheometer (Make: M/s Thermo Electron, Germany; Model: Rheostress RS 1), respectively. The acid and saponification value of oil sample was analysed using titration method and average molecular weight was calculated using following expression [34]:

$$\text{Average molecular weight} = 56.1\times 3\times 1000/(SV - AV)$$

The blended feedstock had acid value of 12.42 mg KOH/ g, saponification value = 202.93 mg KOH/ g, density = 0.921 g/mL, viscosity = 28.95 mPa–s (at 313 K) and average molecular weight = 883.4 g/mol.

4.2.2 Acid catalyst preparation and characterization

Catalyst preparation: The rubber de–oiled seed cake after oil extraction from Soxhlet extraction unit was dried in oven at 383 K for 3 h to eliminate the traces of solvent. The dried de–oiled cake was grounded into fine powder. Two types of catalysts were prepared through direct sulfonation using two acids (1) Sulfuric acid and (2) Chloro–sulfonic acid. Powder of de–oiled cake was mixed with acid in the ratio of 1:2 (i.e. 1 g of powder and 2 mL of conc. acid) thoroughly for 30 min. The catalyst was calcined at 573 K for 5 h in a muffle furnace with a temperature ramp of 10 K min^{-1}. The catalyst

was further cooled and kept in a desiccator and characterized using different analytical facilities.

Catalyst characterization: Both sulfonated (prepared with sulfuric acid) and chloro–sulfonated (prepared using chloro–sulfonic acid) catalysts were characterized by X–ray diffraction (XRD, Bruker, Model: D8 Advance) for 2θ range of 10–80° with scanning speed – 5^{o} min^{-1} and step size – 0.01^{o}. The elemental compositions of both catalysts were determined by X–ray photoelectron spectroscopy (XPS, Auger Electron Spectroscopy (AES) Module, Model: PHI 5000 Versa Probe II, FEI Inc.). External morphologies of sulfonated and chloro–sulfonated catalysts were examined by Field Emission Scanning Electron Microscopy (FE–SEM, Zeiss, Model: Sigma). The elemental mapping distribution and composition was measured using Energy–dispersive X–ray spectroscopy (EDX) in FE–SEM. The surface area of both catalysts was evaluated by a surface area and pore size analyzer (Quanta chrome, Model: Autosorb–IQ MP) using nitrogen adsorption–desorption isotherms. Preceding to nitrogen adsorption–desorption isotherms, degassing of catalyst samples was done at 383 K for 6 h in vacuum. The surface area and the pore size distribution was obtained from adsorption data using Brunauer–Emmett–Teller (BET) and Barrett–Joyner–Halenda (BJH) model, respectively. Total acidic site concentration which consists of carboxylic and sulfonic groups on the catalyst surface was measured using back titration method [35]. Catalyst sample (~ 0.l g) was mixed with 60 mL of 8 mM NaOH solution with continued stirring for 1 h. The solution was neutralized against the 8 mM HCl solution using phenolphthalein as an indicator. The titration was performed in triplicate to confirm the results of both catalysts.

4.2.3 Experimental protocol for transesterification

The transesterification experiments were performed in two categories, viz. (1) single–step process – optimization of reaction parameters using central composite design (CCD), and (2) Two–step process – to identify role of sonication in enhancement of transesterification reaction. The two–step transesterification process was conducted in two separate stages of esterification followed by transesterification. The esterification reaction was accomplished using H_2SO_4 catalyst and mechanical agitation, whereas the transesterification reaction was carried out using as–synthesized heterogeneous acid catalyst in presence of ultrasound. Moreover, the role of ultrasound in process intensification was investigated by performing the experiments with mechanical agitation in both the categories under similar optimized conditions. The experimental setup and protocol is described below.

The transesterification experiments with ultrasound (single–step and two–step) were conducted in batch mode in an ultrasound bath (Make: Elma Transonic, Germany, Model: T–460, Total volume: 2 L, frequency: 35 kHz and power input: 35 W). Distilled water was used as medium for ultrasound wave transmission. Transesterification reaction was conducted in a two neck round bottom flask of 25 mL. The total reaction mixture volume for each experiment was 15 mL. A coiled condenser was used for refluxing methanol. The reaction temperature was controlled using circulating water bath (Make: Jeio Tech, Lab Companion, Korea; Model: RW 0525G). The pressure amplitude of ultrasound irradiation differs from point to point in sonication bath, thus the position of round bottom flask was maintained same in all experiments [36].

The experiments with mechanical agitation (400 rpm) were carried out using a magnetic stirrer (Tarson–spinot, Model MC–02) in a simple water bath. Other experimental parameters (i.e. time, reaction volume and conditions) were same as in

ultrasound–assisted experiments. All experiments were carried out in duplicate to check the reproducibility of the results.

Process optimization: Process optimization of single–step transesterification reaction was done using statistical experimental design – CCD design using Minitab 16 software (trial version). The statistical experimental design was used to optimize the yield of transesterification process comprising 3 factors with 3 levels. The operating parameters such as, reaction time, catalyst dosages, oil to alcohol molar ratio, reaction temperature, mode of mixing, etc. have direct impact on the transesterification yield. Among these parameters, catalyst loading (% w/w), alcohol/ oil molar ratio and reaction temperature were chosen as optimization variables. Sonication was applied for mixing of the reaction mixture. The single–step reaction was conducted for 3 h and the levels of process variables were selected on the basis of preliminary experiments. The statistical design comprised of 20 experimental sets with combination of different process variables, details of which are shown in Table 4.1 (A) and (B).

Two–step transesterification process: (1) Esterification experiments: For two–step transesterification process, the esterification step was performed by using homogeneous acid catalyst, aimed at reducing the FFA content of the blended feedstock. The experimental procedure used for esterification was same as described by Choudhury et al. [37]. This involved the use of the alcohol to oil molar ratio of 15:1, with 5% w/w of catalyst concentration and temperature of 338 K. The esterification reaction (total reaction volume 150 mL) was carried out in 250 mL two necked borosilicate round bottom flask fitted with a reflux condenser. Mechanical agitation of reaction mixture was provided at 400 rpm using a magnetic stirrer (Tarson–spinot, model: MC–02). Reaction was conducted for 1 h followed by separation of reaction mixture into two phases (viz. organic or oil and aqueous or methanol) using separating funnel. Further,

the organic phase was washed 3 times to remove traces of unreacted acid. Later, the organic phase was stored in clean air–tight container after eliminating the moisture by passing it through the activated silica (granules, desiccant ~ 0.2–1 mm, Merck, India) and Whatmann 40 filter paper (with particle retention size of 8 μm). The acid value of final organic phase was determined by using the titration method.

(2) Transesterification experiments: Mixed vegetable oil with reduced FFA content was used as feedstock for transesterification reaction. Operating conditions for transesterification were same as the optimum conditions resulted from CCD statistical design for single–step transesterification. The reaction period was reduced to 1 h (instead of 3 h as in previous case).

Table 4.1 (A): CCD statistical experimental design range and level of independent parameters

Variables	Symbol	Level of factors coded values (actual values)		
Catalyst loading (% w/w oil)	C	–1 (4)	0 (7)	+1 (10)
Alcohol: oil molar ratio	M	–1 (7:1)	0 (14:1)	+1 (21:1)
Temperature (K)	T	–1 (328)	0 (333)	+1 (338)

Table 4.1 (B): Experimental sets of CCD design with experimental and model predicted triglyceride conversion

Sr. No.	Catalyst Loading (% w/w)	Molar ratio	Temperature (K)	% Triglyceride conversion (Experimental)	% Triglyceride conversion (Model predicted)
1	4	7	338	42.23 ± 0.79	41.11
2	7	14	328	60.98 ± 1.11	59.51
3	7	7	333	66.87 ± 0.89	69.99
4	4	21	328	18.12 ± 1.37	19.29
5	7	14	333	84.80 ± 1.33	84.43
6	10	14	333	78.89 ± 0.88	76.83
7	10	21	328	31.20 ± 1.08	31.91
8	7	14	333	82.46 ± 0.79	84.43
9	4	7	328	18.34 ± 1.57	16.46
10	7	21	333	64.89 ± 0.69	63.42
11	7	14	338	80.93 ± 1.08	84.05
12	10	7	328	23.76 ± 0.88	25.23
13	7	14	333	85.30 ± 1.42	84.43
14	7	14	333	86.20 ± 0.87	84.43
15	10	7	338	73.90 ± 1.32	72.32
16	7	14	333	86.20 ± 1.57	84.43
17	4	14	333	51.20 ± 0.69	54.91
18	4	21	338	23.18 ± 0.42	21.30
19	7	14	333	84.92 ± 0.67	84.43
20	10	21	338	54.89 ± 2.04	56.36

Reusability of catalyst: The chloro–sulfonated catalyst was tested for reusability. The catalyst recovered at the end of transesterification reaction (both case, single–step and two–step process) was separated from the reaction mixture by centrifuging it at 6000g for 15 min at 298 K. The separated catalyst was washed 3 times with 5 mL solvent (n–hexane) to remove impurities, viz. oil, glycerol or methanol, from the catalyst surface. Further, the catalyst was dried in oven at 393 K for 2 h and used in the next cycle. The procedure was repeated for 3 cycles and the activity of the catalyst was determined on the basis of biodiesel yield. The catalyst reused after 3 cycles was analysed for acid site density calculation and surface morphology was monitored through FE–SEM analysis.

4.2.4 Kinetic and Arrhenius analysis

The kinetic and Arrhenius analysis were performed in two parts, viz. (1) Overall transesterification process, and (2) Eley–Rideal (E–R) mechanism based individual reaction steps. To study, the kinetic analysis of transesterification reaction, the extent of conversion/ formation of reactant/ product with respect to time is necessary. 500 µL aliquots of reaction mixture were withdrawn at uniform intervals (30 min interval for single–step process and 15 min interval in each of two–step process) from reaction mixture (15 mL) and analysed by ^{1}H NMR to determine triglyceride conversion. For Arrhenius analysis, the kinetic rate constants at various temperatures were required. Thus, the experiments were performed at two altered temperatures (other than optimized temperature) at same process parameters.

For the first part, i.e. kinetic analysis of overall transesterification reaction, pseudo–1st order kinetic model was used, and kinetic rate constants were determined by the 1st order kinetic expression: $\ln(1-X) = -kt$, where k – 1st order rate constant, X – fraction of reactant consumed or product formed at any time t. The value of k at

different temperatures was determined using slope of the plot between $-\ln(1-X)$ and *t*. The activation energy was calculated from the Arrhenius equation: $k = A\exp(-E_a / RT)$, using the plot between ln *k* and 1/T, the slope gives the activation energy.

For second part i.e. kinetic analysis of individual reaction steps, Eley–Rideal mechanism based model was used, and the kinetic rate of each individual reaction was obtained by solving the final rate expression. This model is explained briefly in next section. To obtain the kinetic rate constants based on Eley–Rideal model, the time profiles of two reactants (triglyceride and methanol) and two products (biodiesel and glycerol) were fitted to kinetic expressions using Range–Kutta 4th order ordinary differential equation solver coupled with Genetic Algorithm in MATLAB R 2016b. NMR analysis gave the triglyceride conversion profile with respect to time. The stoichiometry of transesterification reaction was used to calculate the time profiles of methanol, fatty acid methyl ester (FAME) and glycerol. After calculating all the kinetic rate constants of individual steps at different temperatures the activation energies of reaction steps were calculated using Arrhenius equation.

Analytical method: The overall triglyceride conversion to biodiesel was determined by ^{1}H NMR (Nuclear Magnetic Resonance) spectroscopy (Bruker, 600 MHz). The samples were dissolved in $CDCl_3$ solvent (Merck, India) and TMS (tetramethylsilane) was used as internal standard. Gross conversion of triglyceride to fatty acid methyl ester was calculated using the following expression [38,39]: $X = (2\times A_{ME})\times 100 \big/ (3\times A_{\alpha-CH_2})$, where, A_{ME} – integration value of protons of the methyl esters (the singlet peak at 3.6 ppm), $A_{\alpha-CH_2}$ – integration value of methylene protons (peak at 2.3 ppm).

4.3 Eley–Rideal based kinetic model (FAME as adsorbed product)

Heterogeneously catalysed reactions are ultimately surface reactions, which involves the adsorption of reactants (one or more) on the active sites of the catalyst surface followed by the chemical reaction. Few mechanisms were proposed to kinetically model such reactions. In present study, the Eley–Rideal mechanism was used to examine the heterogeneously acid catalysed transesterification reaction. The basic steps involved in Eley–Rideal mechanism is one of the reactant is supposed to adsorb on the catalyst active site and it reacts with other reactant directly from the bulk reaction medium. The resultant product will be formed on the active site of catalyst in adsorbed state, which is later desorbed into the bulk medium, making the active site free for continuation of the reaction.

Transesterification reaction is a reversible reaction, and to shift the equilibrium towards product side, one of the reactants is taken in excess. In present context, methanol was taken in excess, and due to hydrophilic nature of catalyst surface, methanol preferably gets adsorbed on the active sites of catalyst surface. The other reactant, i.e. triglyceride, will react with the adsorbed methanol from bulk medium. The conversion of triglyceride occurs in three steps via successive conversion of triglyceride to diglyceride, monoglyceride and glycerol with formation of FAME or biodiesel molecule in each step. Thus, during each step, the adsorbed methanol molecule will react with tri–, di– and mono–glyceride from bulk medium and form the FAME or biodiesel on the active site of catalyst in adsorbed form. The adsorbed FAME molecule later gets desorbed to bulk medium.

The individual reaction steps based on this mechanism along with their forward rate expressions are given in Table 4.2. The assumptions in this model are as follows: 1. Each step in Eley–Rideal mechanism is considered as rate limiting step; 2. The

surface of catalyst is expected to have uniform distribution of active sites without any contamination/ inert species; 3. Quasi–steady state condition holds true for adsorbed species i.e. the rate of production of adsorbed species is same as that of rate of its utilization; 4. The number of active sites i.e. adsorbed sites and free sites, remains same with respect to time [40].

Table 4.2: Elementary reaction steps with corresponding forward kinetic rate expressions based on Eley–Rideal (ER) mechanism

Step in the mechanism	Chemical equation	Rate expression
1. Methanol adsorption	$* + CH_3OH \rightleftarrows CH_3OH^*$	$r_1 = -k_1 [*]_f [CH_3OH]$
2. Transesterification reactions	$CH_3OH^* + T \rightleftarrows F^* + D$	$r_2 = -k_2 [T][CH_3OH^*]$
	$CH_3OH^* + D \rightleftarrows F^* + M$	$r_3 = -k_3 [D][CH_3OH^*]$
	$CH_3OH^* + M \rightleftarrows F^* + G$	$r_4 = -k_4 [M][CH_3OH^*]$
3. Desorption of adsorbed species	$F^* \rightleftarrows F + *$	$r_5 = -k_5 [F^*]$

Symbols: * – free catalyst active site, T – triglyceride, D – diglyceride, M – monoglyceride, G – glycerol, F – fatty acid methyl ester (biodiesel)

Derivation of final rate (kinetic) expressions: Species mass balance for each species is as given below

$$\frac{d[CH_3OH]}{dt} = -r_1$$

$$\frac{d[CH_3OH^*]}{dt} = r_1 - (r_2 + r_3 + r_4)$$ (superscript of * denotes the adsorbed form)

$$\frac{d[T]}{dt} = -r_2$$

$$\frac{d[D]}{dt} = r_2 - r_3$$

$$\frac{d[M]}{dt} = r_3 - r_4$$

$$\frac{d[G]}{dt} = r_4$$

$$\frac{d\left[F^*\right]}{dt} = r_2 + r_3 + r_4 - r_5$$

$$\frac{d\left[F\right]}{dt} = r_5$$

Triglyceride consumption rate is given by:

$$\frac{d\left[T\right]}{dt} = -r_2 = -k_2\left[CH_3OH^*\right][T]$$

[CH_3OH^*] mass balance can be obtained as:

$$\frac{d\left[CH_3OH^*\right]}{dt} = r_1 - (r_2 + r_3 + r_4)$$

As per the condition of quasi–steady state, rate of generation of absorbed species on surface is equivalent to rate of its utilization, and thus:

$$\frac{d\left[CH_3OH^*\right]}{dt} = r_1 - (r_2 + r_3 + r_4) = 0$$

Substituting rate expressions for r_1, r_2, r_3, and r_4 gives:

$$k_1\left[*\right]_f\left[CH_3OH\right] = k_2\left[T\right]\left[CH_3OH^*\right] + k_3\left[D\right]\left[CH_3OH^*\right] + k_4\left[M\right]\left[CH_3OH^*\right]$$

$$\frac{k_1\left[*\right]_f\left[CH_3OH\right]}{\left[CH_3OH^*\right]} = k_2\left[T\right] + k_3\left[D\right] + k_4\left[M\right]$$

$$\frac{\left[*\right]_f}{\left[CH_3OH^*\right]} = \frac{k_2\left[T\right] + k_3\left[D\right] + k_4\left[M\right]}{k_1\left[CH_3OH\right]} \qquad \text{(A)}$$

According to site balance, the sum of free and occupied sites fraction should be 1.

Hence,

$\left[*\right]_o + \left[*\right]_f = 1$, where $\left[*\right]_o$ – occupied sites fraction and $\left[*\right]_f$ – free sites fraction.

Occupied sites mass balance results in:

$$\left[*\right]_o = \left[CH_3OH^*\right] + \left[F^*\right]$$

$$\frac{[*]_o}{[CH_3OH^*]} = 1 + \frac{[F^*]}{[CH_3OH^*]}$$

Mass balance for [*F**] can be obtained as:

$$\frac{d[F^*]}{dt} = r_2 + r_3 + r_4 - r_5$$

Applying quasi–steady state condition:

$$\frac{d[F^*]}{dt} = r_2 + r_3 + r_4 - r_5 = 0$$

Substituting rate expressions for r_2, r_3, r_4, and r_5 gives:

$$k_5[F^*] = k_2[T][CH_3OH^*] + k_3[D][CH_3OH^*] + k_4[M][CH_3OH^*]$$

$$\frac{[F^*]}{[CH_3OH^*]} = \frac{k_2[T] + k_3[D] + k_4[M]}{k_5}$$

$$\frac{[*]_o}{[CH_3OH^*]} = 1 + \frac{k_2[T] + k_3[D] + k_4[M]}{k_5} \quad \text{(B)}$$

Adding equations, A and B and overall site balance: $[*]_o + [*]_f = 1$

$$\frac{1}{[CH_3OH^*]} = 1 + \frac{k_2[T] + k_3[D] + k_4[M]}{k_5} + \frac{k_2[T] + k_3[D] + k_4[M]}{k_1[CH_3OH]}$$

$$[CH_3OH^*] = \frac{1}{1 + \frac{k_2[T] + k_3[D] + k_4[M]}{k_5} + \frac{k_2[T] + k_3[D] + k_4[M]}{k_1[CH_3OH]}} \quad \text{(C)}$$

Substituting for [CH_3OH^*] in the triglyceride mass balance gives:

$$r_T = \frac{d[T]}{dt} = -\frac{k_2[T]}{1 + \frac{k_2[T] + k_3[D] + k_4[M]}{k_5} + \frac{k_2[T] + k_3[D] + k_4[M]}{k_1[CH_3OH]}}$$

Similarly, the diglyceride and monoglyceride mass balances yields the following expressions:

$$r_D = \frac{d[D]}{dt} = -\frac{k_3[D] - k_2[T]}{1 + \frac{k_2[T] + k_3[D] + k_4[M]}{k_5} + \frac{k_2[T] + k_3[D] + k_4[M]}{k_1[CH_3OH]}}$$

$$r_M = \frac{d[M]}{dt} = -\frac{k_4[M] - k_3[D]}{1 + \frac{k_2[T] + k_3[D] + k_4[M]}{k_5} + \frac{k_2[T] + k_3[D] + k_4[M]}{k_1[CH_3OH]}}$$

Methanol mass balance gives following expression:

$$r_{CH_3OH} = \frac{d[CH_3OH]}{dt} = -\frac{k_2[T] + k_3[D] + k_4[M]}{1 + \frac{k_2[T] + k_3[D] + k_4[M]}{k_5} + \frac{k_2[T] + k_3[D] + k_4[M]}{k_1[CH_3OH]}}$$

Mass balances of glycerol and biodiesel or FAME yields the following expressions:

$$r_G = \frac{d[G]}{dt} = \frac{k_4[M]}{1 + \frac{k_2[T] + k_3[D] + k_4[M]}{k_5} + \frac{k_2[T] + k_3[D] + k_4[M]}{k_1[CH_3OH]}}$$

$$r_F = \frac{d[F]}{dt} = \frac{k_2[T] + k_3[D] + k_4[M]}{1 + \frac{k_2[T] + k_3[D] + k_4[M]}{k_5} + \frac{k_2[T] + k_3[D] + k_4[M]}{k_1[CH_3OH]}}$$

Fitting of experimental data to E–R kinetic model: The kinetic rate constants were determined by solving the four ordinary differential equations (ODE), i.e. rate expressions for reactants (triglyceride and methanol) and products (biodiesel and glycerol), simultaneously using 4th order Runge–Kutta method paired with Genetic Algorithm (GA) solver in MATLAB R 2016b as IVP (initial value problem). Five kinetic parameters, viz. k_1, k_2, k_3, k_4 and k_5 in four differential equations were determined, by specifying the upper and lower bounds based on previous results (chapter 2 and 3). The GA solver provided kinetic rate constants (within specified bounds) with minimization of the objective function (Obj). The values of kinetic rate constants (k_1 – k_5) were used to generate theoretical profiles of biodiesel yield. This

model–predicted profile is compared with the experimental data. The objective function (Obj) for minimizing root mean square (RMS) error is expressed as: $Obj = \min\left(\sum_{i=1}^{n} er_i\right)$, where n – the number of data points of experimental concentrations of four species. The error function (er) is described as:

$$er_i = \left[\left(T_i^{\exp} - T_i^{\text{model}}\right)^2 + \left(CH_3OH_i^{\exp} - CH_3OH_i^{\text{model}}\right)^2 + \left(F_i^{\exp} - F_i^{\text{model}}\right)^2 + \left(G_i^{\exp} - G_i^{\text{model}}\right)^2\right]^{1/2}$$

4.4 Results and discussion

4.4.1 Characterization of catalyst

XRD analysis: The raw carbon from de–oiled cake and synthesised catalyst (de–oiled cake treated with sulfuric acid as well as chloro–sulfonic acid) were examined for identification of different phases by X–ray diffraction. The XRD patterns of all three samples are shown in Fig. 4.1. Raw carbon and both prepared catalyst samples showed the characteristic peaks at 2θ = 20º–30º ⟨0 0 2⟩ with varying intensities. This peak was the characteristic nature of amorphous carbon with unsystematically oriented polycyclic aromatic carbon sheets present in sample. The higher intensity of ⟨0 0 2⟩ peak predicts more chemically activated carbon [24].

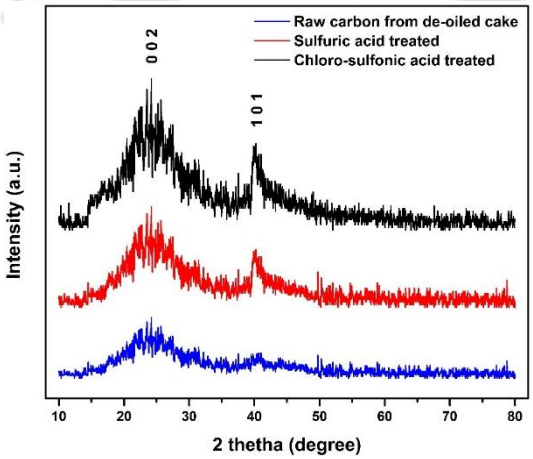

Figure 4.1: X–ray diffractogram of raw carbon, sulfonated and chloro–sulfonated catalyst

The other low intensity peak at $2\theta = 39^{o}–43^{o}$ ⟨1 0 0⟩ represents graphitic structure observed in both sulfonated and chloro–sulfonated catalysts. Moreover, the intensities of both peaks were relatively smaller in sulfonated catalyst as compared to chloro–sulfonated catalyst. This indicated higher activated (amorphous) sulfonated carbon with predominant graphitic structure [11,24,25,35].

XPS analysis: The broad XPS spectrum of sulfonated catalyst and chloro–sulfonated catalyst between the binding energies of 0 to 1200 eV is shown in Fig. 4.2 (A). The XPS spectrum of both catalysts confirmed the presence of oxygen, carbon and sulfur on the surface.

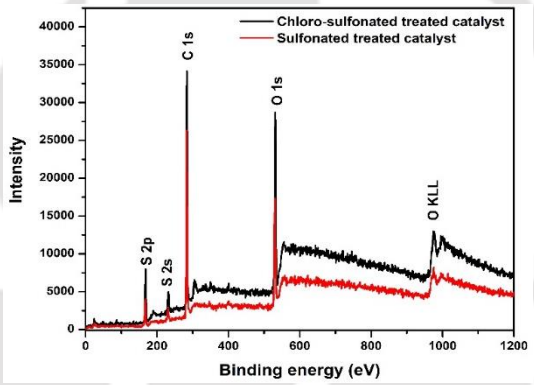

(A)

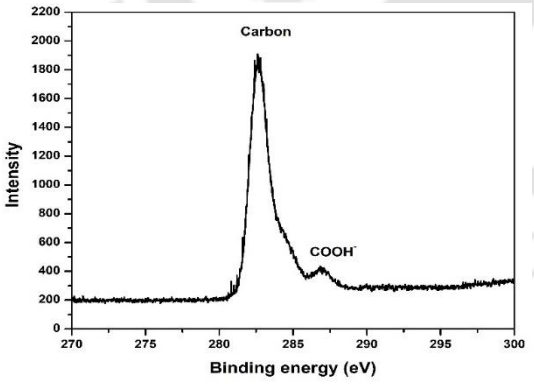

(B)

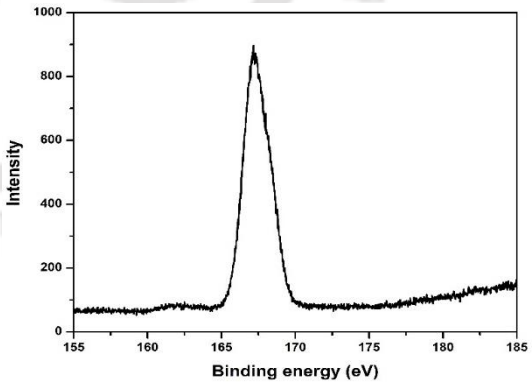

(C)

Figure 4.2: XPS scan spectrum (A) sulfonated and chloro–sulfonated catalyst; (B) Narrow scan in C 1s region for chloro–sulfonated catalyst and (C) Narrow scan in S 2p region for chloro–sulfonated catalyst

The narrow XPS scans for C 1s region (binding energy 270–300 eV) and S 2p region (binding energy 155–185 eV) for chloro–sulfonated catalyst are also shown in Figs. 4.2 (B) and (C), respectively. The peak corresponding to binding energy 168 eV is characteristic of S ($2p_{1/2}$) in sulfonated materials and validates the existence of ¯SO3H group on catalyst surface. The two distinguishing peaks identified at binding energy of 283 eV (the large one) and 286.8 eV (the small one) in narrow C 1s scan (shown in Fig. 4.2 (B)), correspond to elemental carbon from support material and to carboxylic acid on catalyst's surface formed due to carboxylation side reaction, respectively. These results are similar to those reported earlier [2,11,24,41]. Presence of chlorine was not confirmed by the XPS analysis of chloro–sulfonated catalyst, which indicates the absence of chlorine or chlorine is present below detectable limits.

FE–SEM and EDX analysis: FE–SEM micrographs of sulfonated and chloro–sulfonated catalysts are shown in Fig. 4.3. These micrographs showed the catalysts surface as highly porous and irregular in shape. The chloro–sulfonated catalyst has greater and large number of pores as compared to the sulfonated catalyst. This probably due to the disappearance of chlorine as Cl_2 gas during the calcination at 573 K, resulting in larger and bigger porous structure for chloro–sulfonated catalyst.

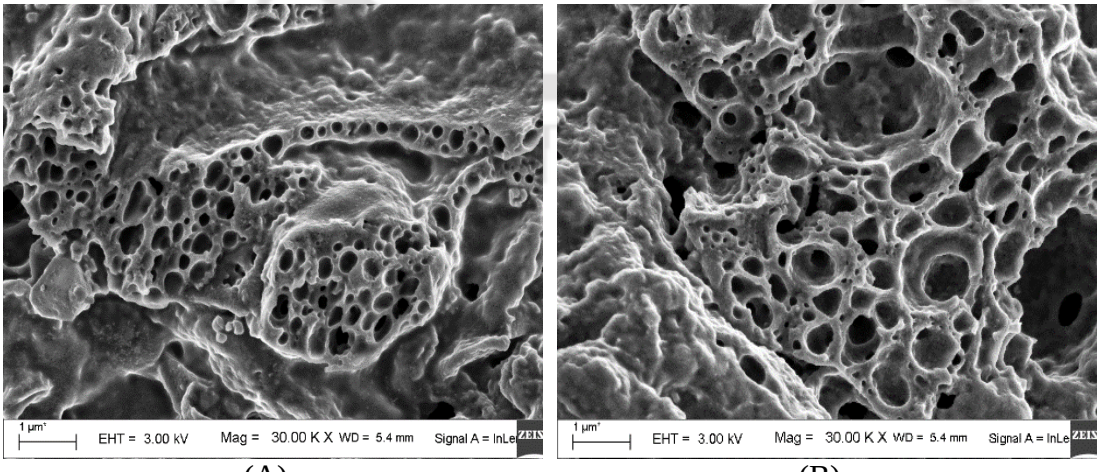

(A) (B)

Figure 4.3: FE–SEM image of synthesized carbon catalyst (A) sulfuric acid treated and (B) chloro–sulfonic acid treated

Energy–dispersive X–ray spectroscopy (EDX) for both catalyst was also carried out by FE–SEM to analyse the elemental distribution present at the catalyst surface as shown in Fig. 4.4. The EDX data as depicted in Table 4.3 shows that chloro–sulfonated catalyst has higher elemental sulfur composition than sulfonated catalyst and traces of chlorine. The values of elemental sulfur composition on catalyst surface were slightly higher than the values reported in literature by Galhardo et al. [2], Dehkhoda et al. [24] and Lou et al. [41] for similar type of catalyst. This may be perhaps due to excess sulfonation of carbon support due to high strength of the acid.

Table 4.3: Elemental analysis of synthesized heterogeneous acid catalyst from rubber de–oiled seed cake

Sample	C	O	S	Cl	Total acid density (mmol/g)
Sulfonated catalyst	59.0	36.9	4.1	Nil	2.92
Chloro–sulfonated catalyst	58.4	36.1	5.4	0.1	3.76

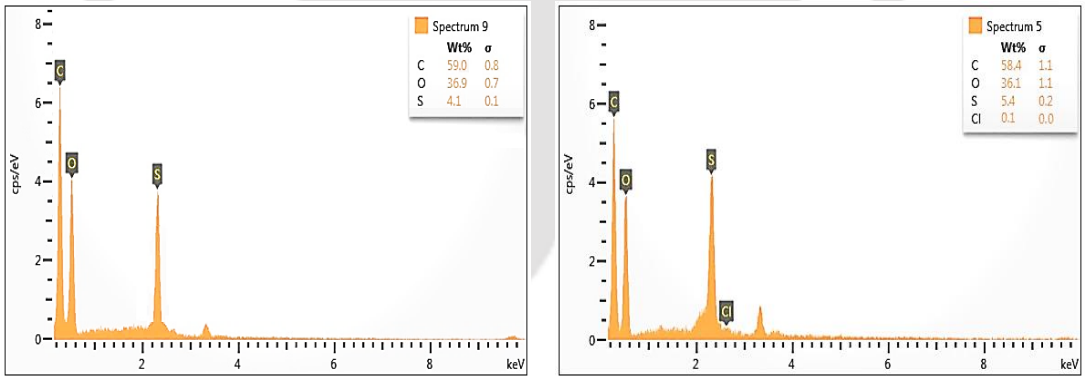

(A) (B)

Figure 4.4: EDX spectrum of synthesized carbon catalyst (A) sulfuric acid treated and (B) chloro–sulfonic acid treated

Surface area and pore size analysis: N_2 adsorption–desorption isotherm obtained for both catalysts as shown in Fig. 4.5, predicted the combination of type I and IV isotherms representing the characteristic of mesoporous and microporous material. The BET surface area of sulfonated and chloro–sulfonated catalyst was found to be 10.208 m^2/g and 16.187 m^2/g, respectively. The average pore diameter and total pore volume of

sulfonated catalyst was found to be 3.21 nm and 0.09 cc/g, respectively, whereas for chloro–sulfonated catalyst average pore diameter and total pore volume of sulfonated catalyst was 8.16 nm and 0.13 cc/g, respectively. These results of surface area, average pore diameter and pore volume are similar to the results reported by Dehkhoda et al. [24], but lower as compared with the reported results of Lui et al. [25].

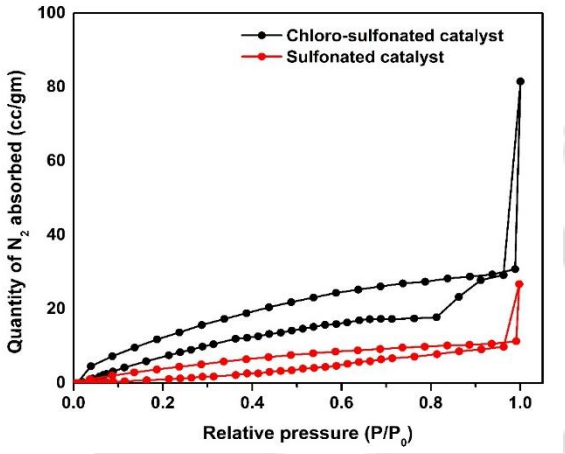

Figure 4.5: Nitrogen adsorption–desorption isotherm of synthesized acid catalyst

Total acidity: The total acidic site concentration was calculated from back titration method as described earlier. The results showed that the sulfonated catalyst has the total acidic site density of 2.92 mmol/g, whereas chloro–sulfonated catalyst have total acidic site density of 3.76 mmol/g. For chloro–sulfonated catalyst, the total acidic site density obtained was slightly higher as compared to sulfonated catalyst, but the values are analogous to those reported by Konwar et al. [11,35] and Luo et al. [41]. This is perhaps due to the existence of two–functional groups in chloro–sulfonic acid resulting in higher acidic strength than sulfuric acid.

The above characterization of both heterogeneous acid catalysts showed excellent surface properties required for transesterification of non–edible oil. Chloro–sulfonated catalyst showed better surface properties and morphology as compared to sulfonated catalyst. Thus, chloro–sulfonated catalyst was selected for transesterification

process for producing biodiesel from mixed non–edible oil feedstock.

4.4.2 Process optimization of single–step transesterification process

After initial assessment of heterogeneous acid catalyst, the single–step transesterification process was optimized using CCD design in presence of ultrasound. The experimental transesterification conversion at the end of 3 h reaction and the model predicted yield, for 20 experimental sets are tabulated in Table 4.1 (B). In each set, experiment was performed in duplicate to evaluate the validity of the results. The values presented in Table 4.1 (B) are average of two experimental runs with standard deviation. Fitting of the experimental results with variables in coded values to quadratic model, gave the following equation:

$$Y = 84.43 + 10.96C - 3.28M + 12.27T - 18.56C^2 - 17.72M^2 - 12.65T^2 + 0.96C \times M + 5.61T \times C - 5.66M \times T$$

where, Y is the transesterification yield which is the maximized by varying the process variables.

The close match of experimental results with model predicted data of triglyceride conversion as seen from Table 4.1 (B), indicated the suitability of selected model and process variables. The values of regression coefficients, *viz.* R^2 = 0.9943; R^2 (predicted) = 0.9733; R^2 (adjusted) = 0.9891, also corroborated the above statement. ANOVA (Analysis of variance) results estimate different coefficients such as linear, square and interaction of the fitted quadratic model. The values of this coefficient with p– and t– values are tabulated as Table 4.4. The p–value < 0.05, predicts the parameter or coefficient to be significant. The absolute t–stat values of linear or quadratic coefficients are relatively higher than the interaction coefficients, which predicts the comparatively independent influence of these process parameters on transesterification yield. The same conclusion was also obtained from F–values of linear, interaction and

quadratic coefficients, which examine the magnitude of interaction and corresponding individual influence on transesterification yield. The p–value and F–value of Lack–of–Fit were 0.431 and 6.41, respectively, conveys that the Lack–of–Fit is irrelevant as compared with pure error or in other words, the selected model is prominent.

Table 4.4: Statistical analysis of experimental results

(A) Estimated regression coefficients for % triglyceride conversion

Term	Coefficients	SE coeff	*t*–stat	*p*–value
Constant (β)	84.43	0.91	92.73	0.017
Catalyst (C)	10.96	0.84	13.08	0.000
Molar ratio (M)	–3.28	0.84	–3.92	0.003
Temperature (T)	12.27	0.84	14.65	0.008
Catalyst × Catalyst (C^2)	–18.56	1.60	–11.62	0.000
Molar ratio × Molar ratio (M^2)	–17.73	1.60	–11.10	0.001
Temperature × Temperature (T^2)	–12.65	1.60	–7.92	0.001
Molar ratio × Catalyst (MC)	0.96	0.94	1.03	0.018
Temperature × Catalyst (TC)	5.61	0.94	5.99	0.000
Temperature × Molar ratio (TM)	–5.66	0.94	–6.04	0.000

R^2 = 99.43%; R^2 (pred) = 97.30%; R^2 (adj) = 98.91%

(B) Analysis of variance (ANOVA) for transesterification reaction

Source	Degrees of freedom	Sq SS	F–value	*p*–value
Regression	9	12150.8	192.45	0.008
Linear	3	2814.5	133.73	0.017
Square	3	8820.8	419.12	0.009
Interaction	3	515.5	24.49	0.028
Residual Error	10	70.2	—	—
Lack–of–Fit	5	60.7	6.41	0.431
Pure Error	5	9.5	—	—
Regression	19	12220.9	—	—

The contour plots depicted in Fig. 4.6, shows the influence between any two process variable, keeping the third variable at its centre point, on the triglyceride conversion. The contour plots which represents the quadratic model predicts the optimum transesterification yield by the innermost contours. The interaction of catalyst loading with temperature and molar ratio with temperature can be assessed from Fig 4.6 (A) and (B), respectively. Similarly, the interaction of catalyst loading and molar ratio on transesterification yield can be reviewed from Fig. 4.6 (C). The contour plots

of catalyst loading *vs* temperature, and temperature *vs* molar ratio are elliptical, which predict good interaction between the variables, whereas contour plot of catalyst loading *vs* molar ratio is circular indicating relatively lower interaction.

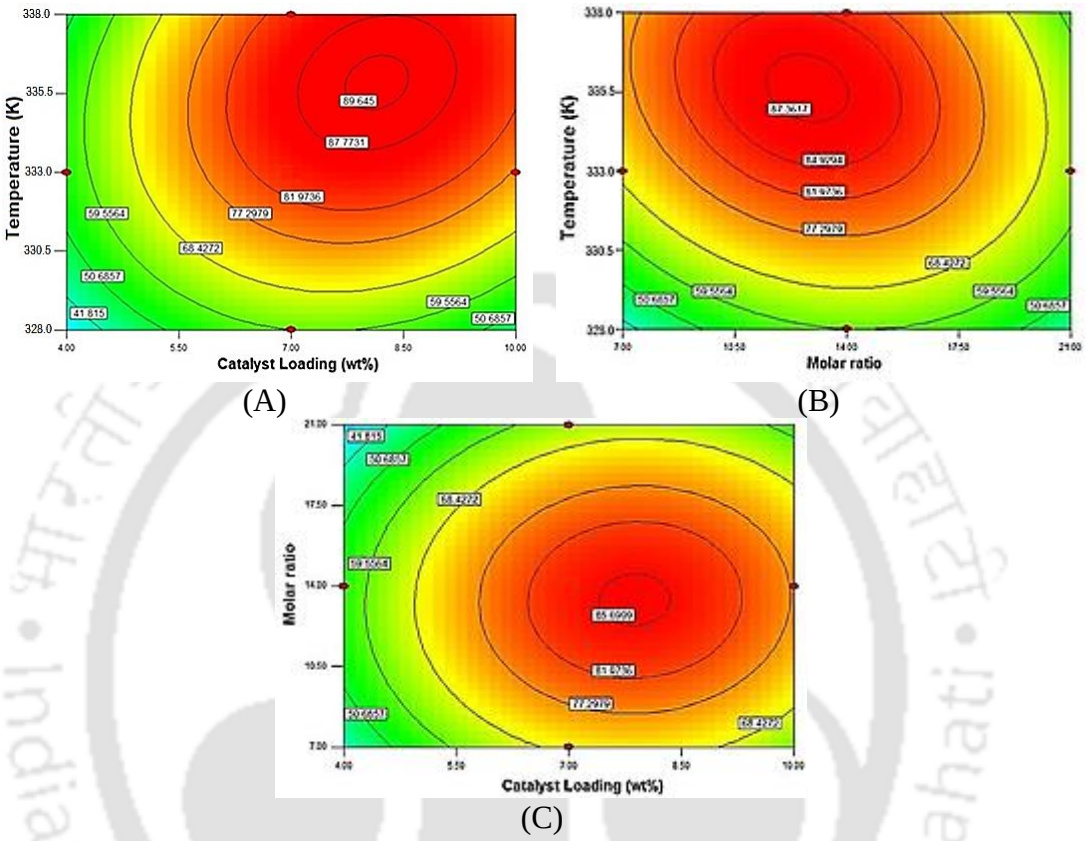

Figure 4.6: Contour plots depicting interaction between the process parameters in single–step transesterification process (A) catalyst loading *vs* temperature; (B) molar ratio *vs* temperature and (C) catalyst loading *vs* molar ratio

It could be inferred from contour plots (Fig. 4.6) that maximum yield can be achieved for catalyst loading = 7–9% (w/w), temperature = 335 – 337 K and alcohol to oil molar ratio = 11–15:1. Lower catalyst amount results in lesser active sites for methanol adsorption to initiate the reaction. On the other hand, when excess catalyst amount was loaded, the part of catalyst may transfer in oil phase (through convections generated from sonication). The oil adheres the catalyst molecule completely, resulting in deactivating the catalyst [42]. Optimum reaction temperature range of 335 – 337 K

is close to boiling point of methanol, and this is indicative of intrinsically slow kinetics of the reaction system. The optimum molar ratio was also higher than homogeneous system, this is essentially due to mass transfer limitation in three–phase heterogeneous system, requiring high interfacial surface area for maximum yield. Viscosity of oil is much higher than methanol, thus the convention/ turbulence generated from cavitation is much higher in methanol as compared to oil. At lower molar ratio, dispersion of oil in methanol may not be uniform resulting in lower interfacial area and lower yield. On the other hand, excess molar ratio also reduces the yield of transesterification reaction. The plausible reason is larger diffusional resistance for triglyceride molecules to reach catalyst surface [37,42]. Hence moderate molar ratio resulted in higher triglyceride conversion.

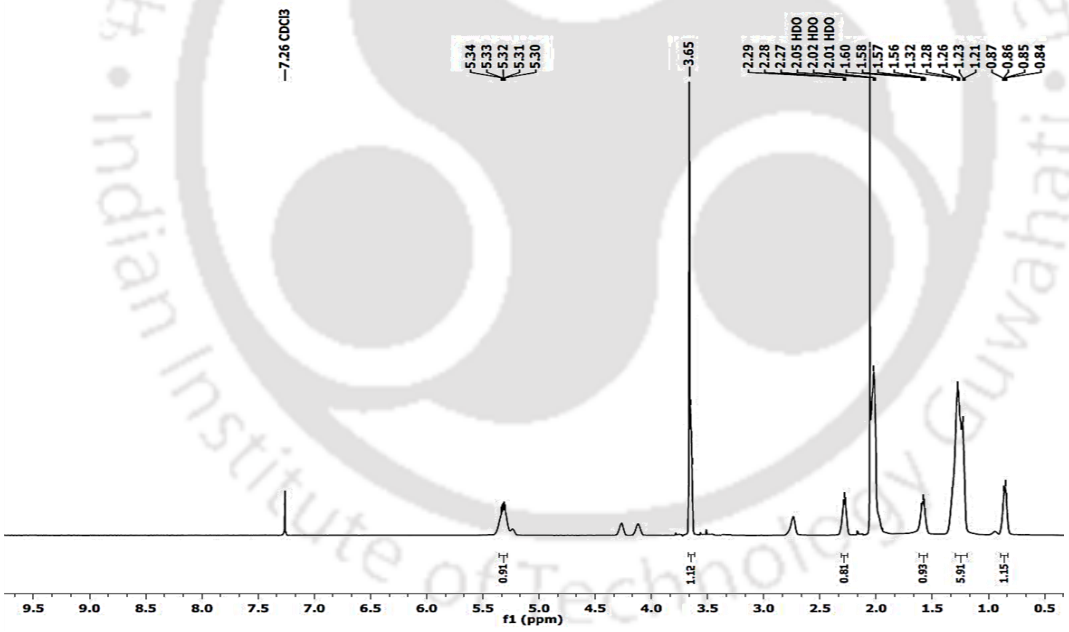

Figure 4.7: ^{1}H NMR spectrum of single–step transesterification reaction with mixed non–edible oil at optimum conditions

The quadratic model predicts the optimum transesterification yield of 90.56% at the end of 3 h reaction with set of operating parameters, the values of process variables are as follows: molar ratio = 12.8:1; catalyst loading = 8.18% (w/w) and reaction temperature = 336 K. The validation experiments performed at optimized

operating conditions results in 91.2 ± 1.08% with 3 h of transesterification reaction. ^{1}H NMR for triglyceride conversion at the end of 3 h is as shown in Fig. 4.7. The ^{1}H NMR spectra showed different characteristic peaks. A singlet peak for methyl ester protons is observed at 3.6 ppm, whereas triplet peak is observed for α–carbonyl methylene protons. The presence of olefinic hydrogens can be identified from the peaks at 5.33 ppm. The different peaks between 2.0 to 2.8 correspond to different unsaturated and polyunsaturated carbons [43]. The triglyceride conversion obtained in validation experiment was relatively similar to that of predicted yield, displayed the validity of the statistical model of experiment.

4.4.3 Two–step transesterification process

Esterification experiments: The primary step of two–step transesterification process resulted in 82.29% reduction of acid value of the feedstock. This reduction in acid value is similar to our previous study of Choudhury et al. [12]. The reduced (final) acid value of the blended non–edible oil feedstock was 2.20 mg KOH/ g. The viscosity of esterified oil was 14.7 mPa–s (at 313 K). This reduced acid value feedstock was further used for transesterification reaction by employing the optimized conditions by CCD design.

Transesterification experiments: Two–step transesterification reaction was carried out for 1 h and at the end of the reaction, samples of reaction mixture were analysed for triglyceride conversion. The reaction yield was superior as compared to single–step process. Two–step process resulted in 93.7±1.47% triglyceride conversion in 1 h. Thus, separate esterification and transesterification process resulted in enhanced triglyceride conversion in reduced time as compared to single–step process. The plausible explanation to this advancement in transesterification yield is removal of water formed

during the esterification reaction that deactivates the acid catalyst [42].

4.4.4 Kinetic modelling and Arrhenius analysis

The kinetic and Arrhenius analysis of transesterification process (single–step and two–step) was performed at optimum conditions obtained from statistical experimental design. The experiments were performed as described in section 4.2.4. To distinguish the role of ultrasound in intensification of transesterification (single–step and two–step), experiments were also conducted with mechanical agitation without altering the process parameters, viz. catalyst loading, batch size, reaction temperature, reaction time and molar ratio. The experiments conducted in presence of ultrasound were termed as "test", whereas experiments carried out using mechanical agitation were termed as "control". The overall triglyceride conversion profile for single–step and two–step transesterification process at optimum conditions in test and control conditions are shown in Fig. 4.8.

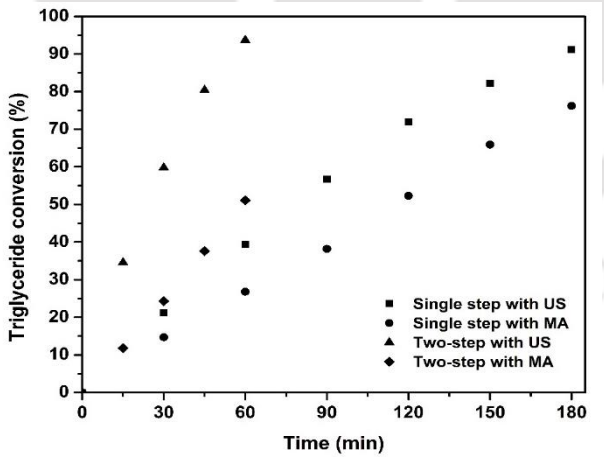

Figure 4.8: Triglyceride conversion profile at optimum process conditions in different reaction categories

Single–step transesterification process at optimized parameters resulted in 78.2 ± 0.89% and 91.2 ± 1.08% triglyceride conversion at the end of 3 h reaction in control

and test conditions, respectively. However, the two–step transesterification process gave 51.1 ± 1.04% and 93.7± 1.47% of triglyceride conversion in 1 h reaction in control and test conditions, respectively.

As mentioned earlier the kinetic analysis was performed in two categories: (1) overall process, and (2) E–R kinetic model based individual reaction steps. The kinetic rate constants for single–step and two–step process in test and control conditions are listed in Table 4.5. The experimental data was fitted to Eley–Rideal model to predict theoretical profiles shown in Fig. 4.9.

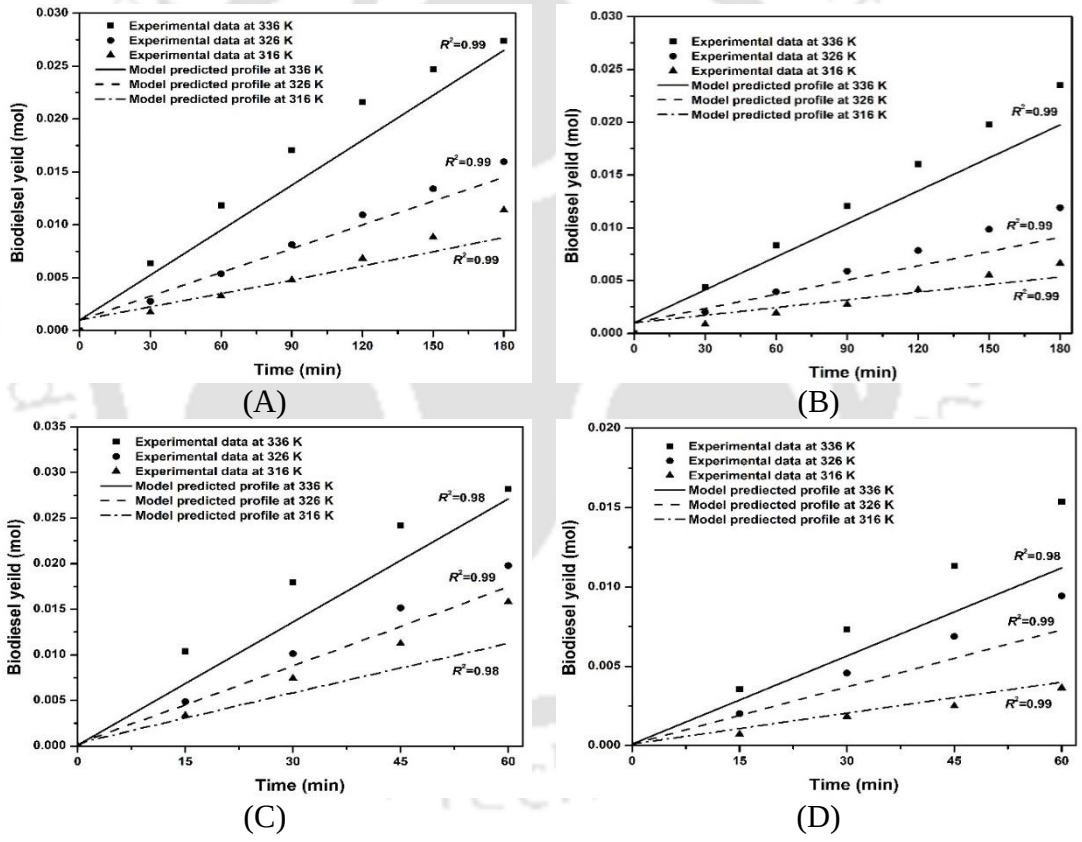

Figure 4.9: Eley–Rideal model predicted profile fitting of biodiesel yield to experimental data (A) single step process with ultrasound; (B) single step process with mechanical agitation; (C) second step (in two–step) process with ultrasound and (D) second step (in two–step) process with mechanical agitation

A reasonable match between experimental data and simulated profiles could be seen in Fig. 4.9, validating the selection of kinetic model for analysis of the

transesterification process. For determination of activation energy, the experiments were conducted at 316 K and 326 K without changing molar ratio and catalyst loading in all categories. These experimental data also fitted to kinetic models (pseudo–first order and E–R kinetic model) to evaluate kinetic rate constants.

Table 4.5: Kinetic rate constants (min^{-1}) for single– and two–step transesterification processes at 336 K

Rate constants (min^{-1})	Single–step process		Two–step process	
	Control experiment (with MA)	Test experiment (with US)	Control experiment (with MA)	Test experiment (with US)
k_1	6.31×10^{-3}	4.80×10^{-3}	7.90×10^{-3}	6.70×10^{-3}
k_2	8.02×10^{-3}	8.53×10^{-3}	3.12×10^{-2}	5.54×10^{-2}
k_3	1.04×10^{-2}	1.12×10^{-2}	3.80×10^{-2}	6.98×10^{-2}
k_4	1.37×10^{-2}	1.46×10^{-2}	4.76×10^{-2}	7.94×10^{-2}
k_5	8.22×10^{-2}	9.99×10^{-2}	9.20×10^{-2}	9.99×10^{-2}
Cumulative error	1.48×10^{-2}	1.46×10^{-2}	1.18×10^{-2}	2.67×10^{-2}

MA – Mechanical Agitation; US – Ultrasound

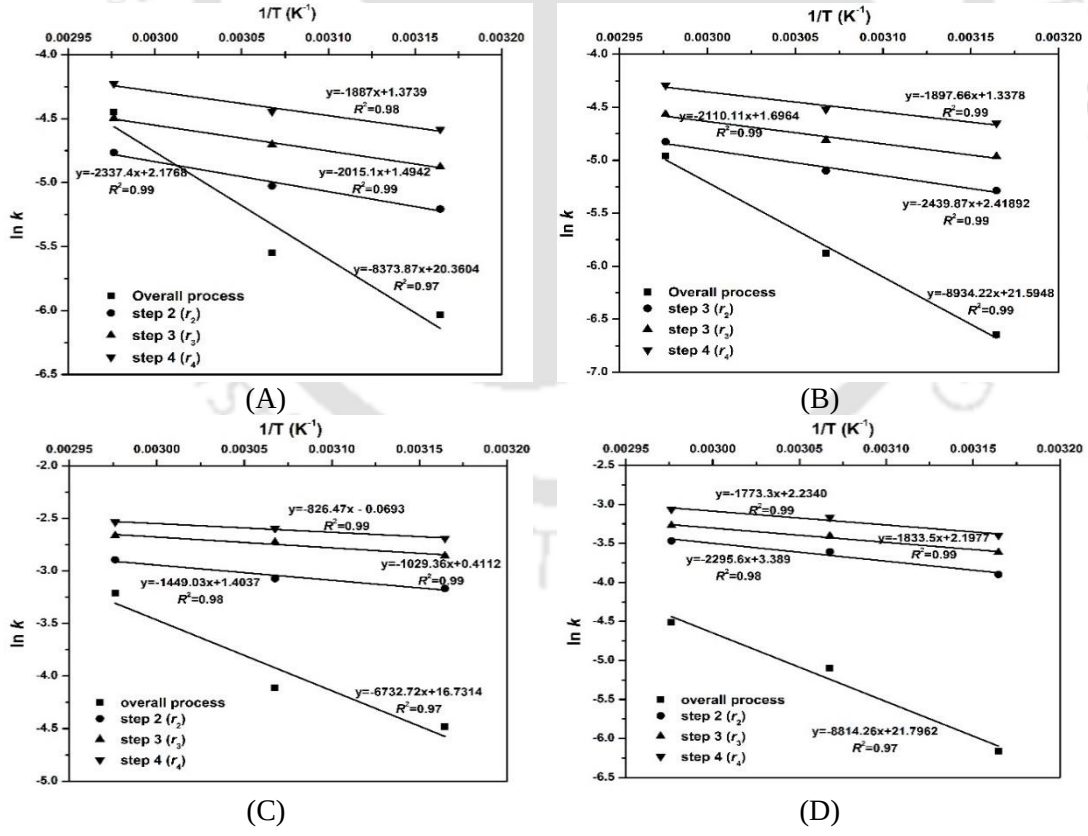

Figure 4.10: Arrhenius plot for overall transesterification process and three reaction steps (A) single step process with ultrasound; (B) single step process with mechanical agitation; (C) second step (in two–step) process with ultrasound and (D) second step (in two–step) process with mechanical agitation.

Table 4.6: Arrhenius analysis of single– and two–step transesterification process: kinetic rate constants (min^{-1}) and activation energies (kJ/mol) for three individual reaction steps and overall process

(A) Single–step transesterification process with ultrasound system

Transesterification reaction (US)	336 K	326 K	316 K	Activation energy (kJ/mol)	R^2
Step 1 (rate expression = r_2, kinetic constant = k_2)	8.53×10^{-3}	6.57×10^{-3}	5.49×10^{-3}	19.43	0.98
Step 2 (rate expression = r_3, kinetic constant = k_3)	1.12×10^{-2}	9.08×10^{-3}	7.63×10^{-3}	16.75	0.99
Step 3 (rate expression = r_4, kinetic constant = k_4)	1.46×10^{-2}	1.18×10^{-2}	1.02×10^{-2}	15.69	0.98
Overall transesterification reaction (k)	1.17×10^{-2}	3.90×10^{-3}	2.40×10^{-3}	69.62	0.95

(B) Single–step transesterification process with mechanical agitation

Transesterification reaction (MA)	336 K	326 K	316 K	Activation energy (kJ/mol)	R^2
Step 1 (rate expression = r_2, kinetic constant = k_2)	8.02×10^{-3}	6.10×10^{-3}	5.06×10^{-3}	20.29	0.98
Step 2 (rate expression = r_3, kinetic constant = k_3)	1.04×10^{-2}	8.14×10^{-3}	6.98×10^{-3}	17.54	0.98
Step 3 (rate expression = r_4, kinetic constant = k_4)	1.37×10^{-2}	1.09×10^{-2}	9.56×10^{-3}	15.78	0.97
Overall transesterification reaction (k)	7.30×10^{-3}	2.60×10^{-3}	1.30×10^{-3}	75.98	0.98

(C) Two–step transesterification process with ultrasound system

Transesterification reaction (US)	336 K	326 K	316 K	Activation energy (kJ/mol)	R^2
Step 1 (rate expression = r_2, kinetic constant = k_2)	5.54×10^{-2}	4.63×10^{-2}	4.21×10^{-2}	12.05	0.96
Step 2 (rate expression = r_3, kinetic constant = k_3)	6.98×10^{-2}	6.55×10^{-2}	5.75×10^{-2}	8.55	0.97
Step 3 (rate expression = r_4, kinetic constant = k_4)	7.94×10^{-2}	7.46×10^{-2}	6.79×10^{-2}	6.87	0.99
Overall transesterification reaction (k)	4.04×10^{-2}	1.64×10^{-2}	1.13×10^{-2}	55.98	0.94

(D) Two–step transesterification process with mechanical agitation

Transesterification reaction (MA)	336 K	326 K	316 K	Activation energy (kJ/mol)	R^2
Step 1 (rate expression = r_2, kinetic constant = k_2)	3.12×10^{-2}	2.71×10^{-2}	2.03×10^{-2}	19.09	0.97
Step 2 (rate expression = r_3, kinetic constant = k_3)	3.80×10^{-2}	3.32×10^{-2}	2.69×10^{-2}	15.24	0.99
Step 3 (rate expression = r_4, kinetic constant = k_4)	4.67×10^{-2}	4.21×10^{-2}	3.35×10^{-2}	14.74	0.96
Overall transesterification reaction (k)	1.10×10^{-2}	6.01×10^{-3}	2.10×10^{-3}	73.28	0.98

Arrhenius plot used to determine activation energies are shown in Fig. 4.10. The obtained rate constants and corresponding activation energies calculated from Fig. 4.10 are listed in Table 4.6.

The kinetic and Arrhenius analysis revealed interesting aspects of heterogeneous acid catalysed transesterification process and the advantage of ultrasound in process intensification. The major findings of the analyse are as follows:

i. From Table 4.5, among all cases (test and control with single–step and two–step process) the rate constants of methanol adsorption i.e. k_1 was lowest (~ 0.5–10 times lower than k_2, k_3, k_4 and k_5), indicating the mass transfer limitation in heterogeneous acid catalysed transesterification reaction.

ii. The values of rate constants k_2, k_3, k_4 and k_5 (depicted in Table 4.5) showed enhancement when control condition (mechanical agitation) was replaced by test condition (ultrasound). The enhancement was marginal in single–step process, but significant in two–step process.

iii. A notable enhancement was observed in the rate constants k_2, k_3, k_4 and k_5 when single–step process was converted to two–step process. The enhancement of rate constants in control condition (single–step vs two–step of mechanical agitation) was ~ 2.5 – 3×, whereas the enhancement with test condition (single–step vs two–step of ultrasound) was ~ 4.5–5.5×.

iv. The activation energy of overall transesterification process in test and control experiments showed a lower (~ 8%) difference in single–step process, which rises to ~ 23% in two–step transesterification process. The activation energies of control experiments were higher than that of test experiments in both single–step and two–step process.

v. As analysed from Fig. 4.10 (or Table 4.6), the reduction in activation energy of

overall transesterification process with mechanical agitation was negligible (from 75.98 kJ/mol to 73.28 kJ/mol) when single–step process was converted in two–step process, but in case of ultrasound system, this value reduces to ~ 20% from 69.62 kJ/mol to 55.98 kJ/mol, signifies the suitability of ultrasound in two–step process over single–step process.

vi. As seen from Fig. 4.10 (or Table 4.6), the summation of activation energies of three reaction steps (r_2, r_3 and r_4) was considerably smaller than overall activation energies in all the cases. For single–step process, in test condition the summation of activation energies of three individual reaction steps was 51.87 kJ/mol which was ~ 74% of the overall 69.62 kJ/mol of activation energy; while in control condition it was 53.6 kJ/mol (~ 71%) of the overall 75.98 kJ/mol of activation energy. In two–step process, with test condition the summation of activation energies of three individual reaction steps was 27.47 kJ/mol which was nearly half of the overall activation energy (55.98 kJ/mol). In control experiments, the sum of activation energies of 3 steps was 49.07 kJ/mol, which was ~ 67% of overall activation energy (73.28 kJ/mol).

vii. The activation energies of reaction steps r_2, r_3 and r_4 showed the trend: $r_2 > r_3 > r_4$, in all cases, which indicated reduced mass transfer limitation between the phases with successive transformation of triglyceride to diglyceride and monoglyceride [44].

An attempt was made to provide probable justification to above examined observations, which helped in finding the role of ultrasound in process intensification of heterogeneous acid catalysed transesterification process.

1. The lowest value of rate constant k_1 (methanol adsorption step, as observed from Table 4.5) in all cases indicated the rate limiting step in transesterification process. The probable reason for low value of k_1 was the reaction temperature, which was close to boiling point of the methanol. The adsorption occurred at lower temperature and the

desorption process was favoured at higher temperature. At the same time, application of ultrasound supported the desorption process through the intermittent acoustic waves generated through transient collapse of cavitation bubbles. Rapid random motion of catalyst particles induced by these waves causes collisions between particles, and promotes desorption, as demonstrated in our earlier work [45,46]. Therefore, reduction in values of k_1 was observed in test experiments as compared to control experiments. Moreover, higher values of k_5 (rate constant for desorption of FAME from active sites) in test experiments as compared to control experiments in both single–step and two–step process also corroborate this conjecture.

2. The marginal decrease in the overall activation energy of single–step transesterification process in test experiment when compared with the control experiment was attributed to intrinsic kinetics of the esterification reaction. Simultaneous esterification and transesterification with acid catalyst resulted in formation of water as by–product of esterification of free fatty acids. The presence of water in medium can shield the proton of acid catalyst [42]. At the same time the water molecules will compete with methanol for active sites. These effects are relatively independent of the chemical and physical effects of ultrasound. Thus, the overall kinetics of single–step transesterification process remains slow in both test and control experiments. On the other hand, when transesterification process was conducted in two–step process i.e. separate esterification and transesterification. The water formed during esterification was removed and the reversible nature of transesterification reaction was diminished. This resulted in improved kinetics and desirable yield with reduced time and this can be corroborated by the reduction in activation energy of two–step transesterification process (55.98 kJ/mol) from single–step transesterification process (69.62 kJ/mol) in test experiments. The related change in control experiments

was very small.

3. In two–step transesterification process, the change in overall activation energy in test condition was significant as compared with the control condition. The possible reason for this change is the three–phase heterogeneity of the reaction system and the mass transfer barrier in the system. The application of ultrasound irradiation resulted in intense mixing through cavitation phenomenon. The micro–turbulence and micro–jets generated during transient collapse of bubbles resulted in higher intermixing of oil and methanol in each other, through formation of fine emulsion. The emulsion reduces the mass transfer barrier between methanol and oil phase and enhances the interfacial area between two phases [43]. This enhancement helped in achieving higher conversion with reduction in reaction time (from 3 h to 1 h) and improved kinetics. Mechanical agitation mixes the two phases at macro–level but could not achieve the micro–mixing (fine emulsion) as in ultrasound–assisted system. This observation is also supported by the reduction in overall activation energy from 73.28 kJ/mol to 55.98 kJ/mol in test condition.

4. In mechanically agitated system, the overall activation energies of single–step and two–step processes remained almost the same. It may be probably due to the dominance of intrinsic kinetics of esterification reaction in single–step process and mass transfer limitation in two–step transesterification process [42]. At the same time, the kinetic rate constants showed significant enhancement, resulting in similar extent of triglyceride conversion in half reaction time.

5. The sum of the activation energies of three individual reaction steps, helped in understanding the nature of transesterification reaction. In single–step heterogeneous acid catalysed transesterification process with test and control condition, 70–74% of overall activation energy was used by reaction kinetics and only 26–30% of overall

activation energy was utilized to overcome the mass transfer limitation. Thus, the dominance of reaction kinetics over the mass transfer limitation was prominent in single–step transesterification process even with application of ultrasound.

6. In case of two–step transesterification process, the effects of reaction kinetics and the mass transfer barrier were of mixed type. In control experiments, 2/3rd of overall activation energy was utilized by reaction kinetics and 1/3rd (24.21 kJ/mol) of overall activation energy was used to overcome the mass transfer barrier. This ratio predicts the slower kinetics of heterogeneous acid catalysed transesterification, which required most of the overall activation energy. While in test experiments, ~ 50% of overall activation energy was utilized by reaction kinetics and equal amount ~ 50% (28.51 kJ/mol) of energy was consumed to overcome the mass transfer limitation. The fraction utilized to overcome mass transfer barrier looks slightly higher when compared to two–step process with control condition, but the actual amount of energy was nearly same. The application of ultrasound in two–step transesterification reaction boosted the kinetic rate constants remarkably (as seen from Table 4.6 (C) and (D)), with enhanced intermixing and reduction in surface tension between oil and methanol. Overall, the activation energy of reaction kinetics (sum of activation energy of three reaction steps) was reduced drastically as compared to control experiments (from 49.07 to 27.47 kJ/mol) but consumed somewhat higher energy (~ 4.5 kJ/mol) to overcome the mass transfer limitation.

4.4.5 Reusability of the catalyst

The chloro–sulfonated catalyst was also tested for its reusability. Fig. 4.11 shows successive triglyceride conversion with recycled catalyst. The reduction in catalytic activity of the catalyst was prominent in single–step process as compared to

two–step transesterification process. The probable reason behind this additional loss of activity is water which is formed during esterification reaction. The reduction of acidic active sites of catalyst in successive cycles is mainly due to partial blocking of active sites and pores by impurities (bigger molecules of reactants or products), which might get adsorbed irreversibly [35].

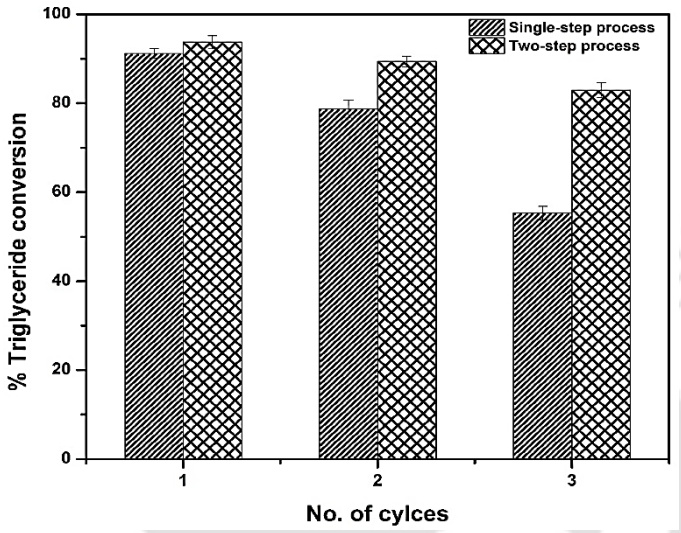

Figure 4.11: Performance of chloro–sulfonated catalyst in reusability study

The FE–SEM micrograph shown in Fig. 4.12 of recycled catalyst after three cycles showed the reduction in porous surface structure of the catalyst. The reduction may be due to chemisorption of impurities. The total acid density results showed sharp reduction from 3.76 to 2.29 mmol/g for single–step transesterification process, confirming excess loss in SO_3H active sites. Similarly, the total acid density of catalyst in two–step process reduced from 3.76 to 3.27 mmol/g. Results of reusability study showed ~ 40% activity loss of chloro–sulfonated catalyst in single–step process, while only ~ 10% loss was seen in two–step process.

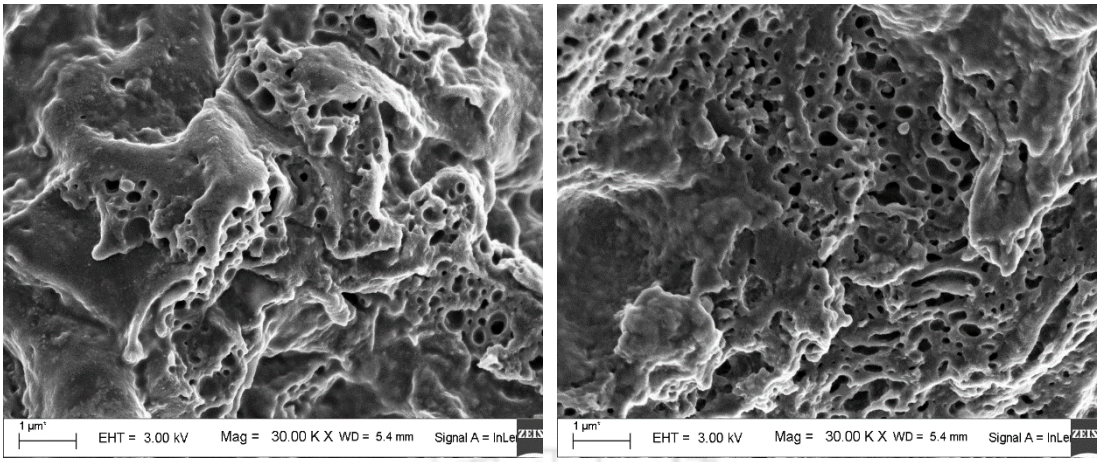

(A) (B)

Figure 4.12: FE–SEM image of recycled chloro–sulfonic acid catalyst after 3 cycles (A) single–step transesterification process and (B) two–step transesterification process

4.5 Conclusion

The application of waste rubber seed cake as solid heterogeneous acid catalyst for biodiesel synthesis was explored. As–synthesized catalyst is readily cheap, renewable with high acidic strength and mesoporous morphology. This study has also investigated application of this catalyst for biodiesel synthesis in single–step and two–step transesterification process, with application of sonication for intensification of reaction kinetics. A significant reduction in activation energy and reaction time is achieved when single–step process converted to two–step process. Kinetic analysis based on Eley–Rideal model has exposed the precise physical mechanism of transesterification process, where the intensification can be achieved with application of ultrasound. Additionally, the chloro–sulfonated catalyst reported in present study could be effectively recycled.

References

[1] Luque, R., Lovett, J.C., Datta, B., Clancy, J., Campelo, J.M. and Romero, A.A., 2010. Biodiesel as feasible petrol fuel replacement: a multidisciplinary overview. Energy & Environmental Science, 3(11), 1706–1721.

[2] Galhardo, T.S., Simone, N., Gonçalves, M., Figueiredo, F.C., Mandelli, D. and Carvalho, W.A., 2013. Preparation of sulfonated carbons from rice husk and their application in catalytic conversion of glycerol. ACS Sustainable Chemistry & Engineering, 1(11), 1381–1389.

[3] Lotero, E., Liu, Y., Lopez, D.E., Suwannakarn, K., Bruce, D.A. and Goodwin, J.G., 2005. Synthesis of biodiesel via acid catalysis. Industrial & Engineering Chemistry Research, 44(14), 5353–5363.

[4] Jothiramalingam, R. and Wang, M.K., 2009. Review of recent developments in solid acid, base, and enzyme catalysts (heterogeneous) for biodiesel production via transesterification. Industrial & Engineering Chemistry Research, 48(13), 6162–6172.

[5] Lestari, S., Mäki-Arvela, P., Beltramini, J., Lu, G.M. and Murzin, D.Y., 2009. Transforming triglycerides and fatty acids into biofuels. ChemSusChem: Chemistry & Sustainability Energy & Materials, 2(12), 1109–1119.

[6] Trombettoni, V., Lanari, D., Prinsen, P., Luque, R., Marrocchi, A. and Vaccaro, L., 2018. Recent advances in sulfonated resin catalysts for efficient biodiesel and bio–derived additives production. Progress in Energy and Combustion Science, 65, 136–162.

[7] Helwani, Z., Othman, M.R., Aziz, N., Kim, J. and Fernando, W.J.N., 2009. Solid heterogeneous catalysts for transesterification of triglycerides with methanol: a review. Applied Catalysis A: General, 363(1–2), 1–10.

[8] Zabeti, M., Daud, W.M.A.W. and Aroua, M.K., 2009. Activity of solid catalysts

for biodiesel production: a review. Fuel Processing Technology, 90(6), 770–777.

[9] Balakrishnan, M., Batra, V.S., Hargreaves, J.S.J. and Pulford, I.D., 2011. Waste materials–catalytic opportunities: an overview of the application of large scale waste materials as resources for catalytic applications. Green Chemistry, 13(1), 16–24.

[10] Melero, J.A., Iglesias, J. and Morales, G., 2009. Heterogeneous acid catalysts for biodiesel production: current status and future challenges. Green Chemistry, 11(9), 1285–1308.

[11] Konwar, L.J., Mäki–Arvela, P., Salminen, E., Kumar, N., Thakur, A.J., Mikkola, J.P. and Deka, D., 2015. Towards carbon efficient biorefining: multifunctional mesoporous solid acids obtained from biodiesel production wastes for biomass conversion. Applied Catalysis B: Environmental, 176, 20–35.

[12] Alcantara, R., Amores, J., Canoira, L.T., Fidalgo, E., Franco, M.J. and Navarro, A., 2000. Catalytic production of biodiesel from soy–bean oil, used frying oil and tallow. Biomass and Bioenergy, 18(6), 515–527.

[13] Kiss, A.A., Dimian, A.C. and Rothenberg, G., 2006. Solid Acid Catalysts for Biodiesel Production–-Towards Sustainable Energy. Advanced Synthesis & Catalysis, 348(1-2), 75–81.

[14] Su, F. and Guo, Y., 2014. Advancements in solid acid catalysts for biodiesel production. Green Chemistry, 16(6), 2934–2957.

[15] Lam, E. and Luong, J.H., 2014. Carbon materials as catalyst supports and catalysts in the transformation of biomass to fuels and chemicals. ACS catalysis, 4(10), 3393–3410.

[16] Toda, M., Takagaki, A., Okamura, M., Kondo, J.N., Hayashi, S., Domen, K. and Hara, M., 2005. Green chemistry: biodiesel made with sugar catalyst. Nature, 438(7065), 178.

[17] Stellwagen, D.R., van der Klis, F., van Es, D.S., de Jong, K.P. and Bitter, J.H., 2013. Functionalized carbon nanofibers as solid-acid catalysts for transesterification. ChemSusChem, 6(9), 1668–1672.

[18] Chang, B., Fu, J., Tian, Y. and Dong, X., 2013. Multifunctionalized ordered mesoporous carbon as an efficient and stable solid acid catalyst for biodiesel preparation. The Journal of Physical Chemistry C, 117(12), 6252–6258.

[19] Hara, M., 2009. Environmentally benign production of biodiesel using heterogeneous catalysts. ChemSusChem: Chemistry & Sustainability Energy & Materials, 2(2), 129–135.

[20] Wang, H., Covarrubias, J., Prock, H., Wu, X., Wang, D. and Bossmann, S.H., 2015. Acid–functionalized magnetic nanoparticle as heterogeneous catalysts for biodiesel synthesis. The Journal of Physical Chemistry C, 119(46), 26020–26028.

[21] Melero, J.A., Bautista, L.F., Morales, G., Iglesias, J. and Briones, D., 2008. Biodiesel production with heterogeneous sulfonic acid–functionalized mesostructured catalysts. Energy & Fuels, 23(1), 539–547.

[22] Xie, W., Wang, H. and Li, H., 2011. Silica–supported tin oxides as heterogeneous acid catalysts for transesterification of soybean oil with methanol. Industrial & Engineering Chemistry Research, 51(1), 225–231.

[23] Lien, Y.S., Hsieh, L.S. and Wu, J.C., 2010. Biodiesel synthesis by simultaneous esterification and transesterification using oleophilic acid catalyst. Industrial & Engineering Chemistry Research, 49(5), 2118–2121.

[24] Dehkhoda, A.M., West, A.H. and Ellis, N., 2010. Biochar based solid acid catalyst for biodiesel production. Applied Catalysis A: General, 382(2), 197–204.

[25] Liu, H., Chen, J., Chen, L., Xu, Y., Guo, X. and Fang, D., 2016. Carbon nanotube–based solid sulfonic acids as catalysts for production of fatty acid methyl

ester via transesterification and esterification. ACS Sustainable Chemistry & Engineering, 4(6), 3140–3150.

[26] Zong, M.H., Duan, Z.Q., Lou, W.Y., Smith, T.J. and Wu, H., 2007. Preparation of a sugar catalyst and its use for highly efficient production of biodiesel. Green Chemistry, 9(5), 434–437.

[27] Prabhavathi Devi, B.L., Gangadhar, K.N., Sai Prasad, P.S., Jagannadh, B. and Prasad, R.B., 2009. A glycerol-based carbon catalyst for the preparation of biodiesel. ChemSusChem: Chemistry & Sustainability Energy & Materials, 2(7), 617–620.

[28] Arancon, R.A., Barros Jr, H.R., Balu, A.M., Vargas, C. and Luque, R., 2011. Valorisation of corncob residues to functionalised porous carbonaceous materials for the simultaneous esterification/transesterification of waste oils. Green Chemistry, 13(11), 3162–3167.

[29] Malani, R. S., Goyal, A. and Moholkar, V. S. Ultrasound–Assisted Biodiesel Synthesis: A Mechanistic Insight, in: Agrawal, A. K., Agarwal, R. A., Gupta, T. and Gurjar, B. R. (Eds.), Biofuels, Springer, Singapore, 2017, pp. 103–135.

[30] Ranjan, A., Singh, S., Malani, R.S. and Moholkar, V.S., 2016. Ultrasound–assisted bioalcohol synthesis: review and analysis. RSC Advances, 6(70), 65541–65562.

[31] Shah, Y.T., Pandit, A.B., Moholkar, V.S., 1999. Cavitation Reaction Engineering, Plenum Press, New York.

[32] Goswami, P.P., Choudhury, H.A., Chakma, S. and Moholkar, V.S., 2013. Sonochemical synthesis and characterization of manganese ferrite nanoparticles. Industrial & Engineering Chemistry Research, 52(50), 17848–17855.

[33] Choudhury, H.A., Choudhary, A., Sivakumar, M. and Moholkar, V.S., 2013. Mechanistic investigation of the sonochemical synthesis of zinc ferrite. Ultrasonics

sonochemistry, 20(1), 294–302.

[34] Deng, X., Fang, Z. and Liu, Y.H., 2010. Ultrasonic transesterification of Jatropha curcas L. oil to biodiesel by a two–step process. Energy Conversion and Management, 51(12), 2802–2807.

[35] Konwar, L.J., Das, R., Thakur, A.J., Salminen, E., Mäki–Arvela, P., Kumar, N., Mikkola, J.P. and Deka, D., 2014. Biodiesel production from acid oils using sulfonated carbon catalyst derived from oil–cake waste. Journal of Molecular Catalysis A: Chemical, 388, 167–176.

[36] Moholkar, V.S., Sable, S.P. and Pandit, A.B., 2000. Mapping the cavitation intensity in an ultrasonic bath using the acoustic emission. AIChE journal, 46(4), 684–694.

[37] Choudhury, H.A., Malani, R.S. and Moholkar, V.S., 2013. Acid catalyzed biodiesel synthesis from Jatropha oil: mechanistic aspects of ultrasonic intensification. Chemical engineering journal, 231, 262–272.

[38] Gelbard, G., Bres, O., Vargas, R.M., Vielfaure, F. and Schuchardt, U.F., 1995. ^{1}H nuclear magnetic resonance determination of the yield of the transesterification of rapeseed oil with methanol. Journal of the American Oil Chemists' Society, 72(10), 1239–1241.

[39] Knothe, G., 2001. Analytical methods used in the production and fuel quality assessment of biodiesel. Transactions of the ASAE, 44(2), 193–200.

[40] Kapil, A., Wilson, K., Lee, A.F. and Sadhukhan, J., 2011. Kinetic modeling studies of heterogeneously catalyzed biodiesel synthesis reactions. Industrial & Engineering Chemistry Research, 50(9), 4818–4830.

[41] Lou, W.Y., Guo, Q., Chen, W.J., Zong, M.H., Wu, H. and Smith, T.J., 2012. A highly active bagasse-derived solid acid catalyst with properties suitable for production

of biodiesel. ChemSusChem, 5(8), 1533–1541.

[42] Choudhury, H.A., Srivastava, P. and Moholkar, V.S., 2014. Single-step ultrasonic synthesis of biodiesel from crude Jatropha curcas oil. AIChE Journal, 60(5), 1572–1581.

[43] Choudhury, H.A., Goswami, P.P., Malani, R.S. and Moholkar, V.S., 2014. Ultrasonic biodiesel synthesis from crude Jatropha curcas oil with heterogeneous base catalyst: mechanistic insight and statistical optimization. Ultrasonics sonochemistry, 21(3), 1050–1064.

[44] Bhoi, R., Singh, D. and Mahajani, S., 2017. Investigation of mass transfer limitations in simultaneous esterification and transesterification of triglycerides using a heterogeneous catalyst. Reaction Chemistry & Engineering, 2(5), 740–753.

[45] Midathana, V.R. and Moholkar, V.S., 2009. Mechanistic studies in ultrasound–assisted adsorption for removal of aromatic pollutants. Industrial & Engineering Chemistry Research, 48(15), 7368–7377.

[46] Chakma, S. and Moholkar, V.S., 2011. Mechanistic features of ultrasonic desorption of aromatic pollutants. Chemical engineering journal, 175, 356–367.

Chapter 5

Ultrasound-Assisted Enzymatic Biodiesel Production Using Blended Feedstock of Non-Edible Oils: Kinetic and Thermodynamic Analysis

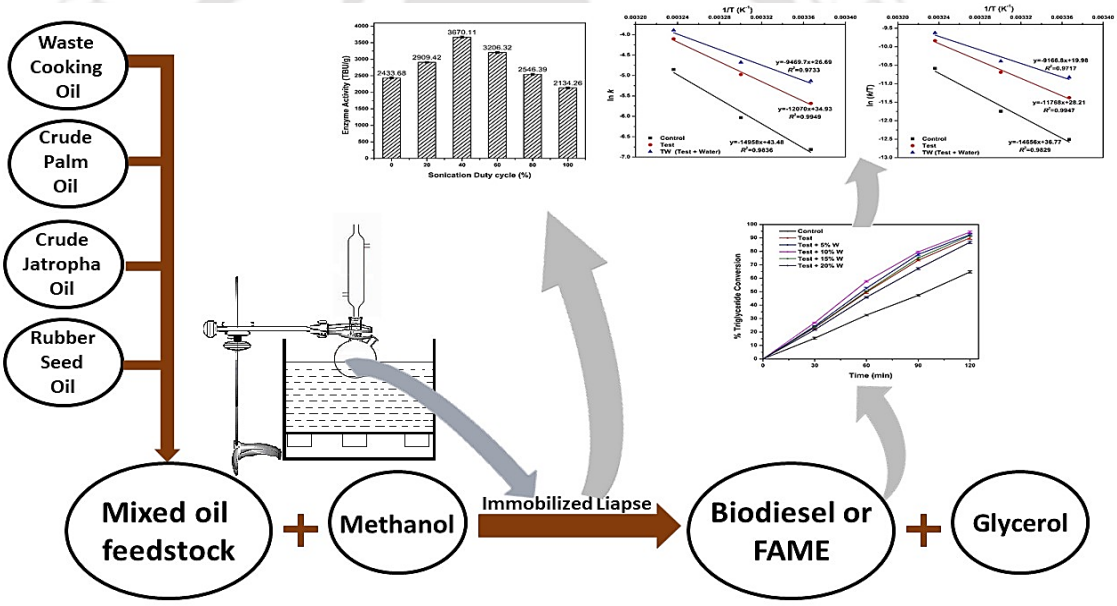

Chapter 5

Ultrasound–Assisted Enzymatic Biodiesel Production Using Blended Feedstock of Non–Edible Oils: Kinetic and Thermodynamic Analysis

5.1 Introduction

In preceding chapters ultrasound–assisted biodiesel production using mixed non–edible oil feedstock and heterogeneous acid or alkali/alkaline doped catalysts were investigated. Catalyst selection for biodiesel synthesis, whether alkaline or acidic – depending on type of feedstock, could be in either homogeneous or heterogeneous form. Major operational issue with application of homogeneous catalysts are: (i) corrosion of reaction vessels, (ii) required excess water for biodiesel purification, and (iii) impurity in by–product glycerol [1]. Substitution of homogeneous catalysts with heterogeneous ones has been investigated by numerous authors in past several years with publication of voluminous literature [1–4]. The heterogeneous catalyst offers solution to operational issues listed above, but suffers from major limitation of slow reaction kinetics due to 3–phase heterogeneity of the system. Possible means of enhancing kinetics of transesterification using heterogeneous catalyst are: use of high

reaction temperature or use of co–solvents that enhance miscibility between organic/aqueous phases or application of intense mixing of reaction mixture that reduces the mass transfer limitation [4–6].

An alternative to inorganic catalysts for biodiesel synthesis are the biocatalysts in the form of lipase enzyme [6]. The lipase–catalysed transesterification process has major merit of milder operating conditions and easier downstream processing without contamination of by–product glycerol [7–8]. However, lipase–catalysed transesterification process has its own limitations of high cost of enzyme, maintenance of uniform enzyme activity, operational stability and effective recyclability [9]. Use of immobilized lipase is a possible alternative, which can be recycled several times and has more stable activity as compared to the free enzyme [6,7,10]. Lipases from various sources immobilized on different supports has been applied by previous researchers for transesterification. Some of the sources and immobilization supports for lipases reported in previous literature include: *Candida Antarctica* / mesoporous silica [11], *Candida rugosa* / nanofibrous poly–membrane [12], *Thermomyces lanuginosus* / microporous polymer [13], *Thermomyces lanuginosus* / styrene divinylbenzene copolymer [14], *Burkholderia* / hydrophobic magnetic particles [15], *Candida Antarctica, Thermomyces lanuginosus* and *Rhizomucor miehei* / epoxy–functionalised silica [16,17], *Aspergillus niger* / micro–porous biosilica [18]. Comprehensive reviews on various supports for immobilization of lipase for transesterification have been published by Jegannathan et al. [6] and Zhao et al. [19].

In the present study, ultrasound–assisted transesterification of blend of non–edible oils with methanol and commercial lipase from *Thermomyces lanuginosus* immobilised on Immobed 150 as the biocatalyst has been studied. An attempt has been made to get physical insight into the effect of sonication on enzymatic

transesterification process with thermodynamic and kinetic analysis. Several researchers have reported that activity of lipase sharply declines when exposed to polar organic solvents such as methanol for longer duration [10,17,20]. An attempt has been made to reduce this adverse effect by the addition of small quantities of water. Earlier studies by Nelson et al. [21] reported that insufficient amount of water causes inactivation of enzyme as well as changes in its structural conformation. On the other hand, excess water promotes the hydrolysis reaction and significantly lowers the transesterification yield [22,23]. In view of these findings, an attempt was made to optimize the quantity of water addition to the reaction mixture in present study.

5.2 Material and methods

5.2.1 Materials and chemicals

Lipase from *Thermomyces lanuginosus* immobilized on Immobead 150 was procured from Sigma–Aldrich, India. Methanol (ACS grade, 99%) was procured from Merck, India. All other chemicals used in present study were ACS grade and procured from Himedia, Pvt. Ltd. India.

Four different non–edible oils (waste cooking oil, crude palm oil, rubber seed oil and jatropha oil) were blended and used as a feedstock from enzymatic transesterification reaction. The collection of oils (waste cooking oil, rubber seed oil and jatropha oil) were stated in chapter 2, section 2.2. Crude palm oil was procured from local market of Guwahati.

The blended non–edible oil feedstock was prepared by mixing the oils in following volumetric ratio: waste cooking oil – 30%; crude palm oil – 30%; rubber seed oil – 25% and jatropha oil – 15%. The blended feedstock had density 0.918 g/mL, viscosity (at 313 K) 27.68 mPa–s, acid value 11.68 mg KOH/g and saponification value

202.32 mg KOH/g. The average molecular weight was calculated as 882.82 g/mol using expression given below [24]

Average molecular weight = $56.1 \times 3 \times 1000/(SV - AV)$.

where, SV – saponification value and AV – acid value of the oil feedstock.

The commercial lipase immobilized on Immobead 150 was soaked in phosphate buffer (pH 7.5, 0.1 M) overnight and used for further experiments (activity assay and transesterification experiments).

5.2.2 Lipase activity assay

The activity of immobilised lipase was determined using 10% tributyrin assay as described by Rajshekar et al. [25]. 2 mL of tributyrin (AR Grade, Himedia Pvt. Ltd. India) was added to 18 mL phosphate buffer (pH 7.5, 0.1 M). Approximately, 200 mg of immobilized enzyme was added to reaction mixture and incubated for 5 min at 40°C. 20 mL methanol was added at the end of 5 min to stop the reaction. The solution was titrated against dilute alcoholic NaOH solution (0.1 M) using phenolphthalein as an indicator. The activity of immobilized enzyme (TBU/g) was defined as the amount of enzyme required to release 1 µmol titratable butyric acid per minute, under standard reaction conditions. The following equation was used to determine the enzyme activity:

$$\text{Enzyme activity (TBU/g)} = \frac{V \times M \times 1000}{W \times T}$$

where V – volume of dilute NaOH required for titration in mL; M – molarity of dilute NaOH solution; W – weight of enzyme loaded in g and T – time of reaction (min).

5.2.3 Experimental methodology for transesterification reaction

The lipase catalysed transesterification experiments were categorised in 3 parts, viz. (1) process optimization using Box–Behnken statistical design; (2) analysis of

effect of water addition on transesterification reaction and (3) kinetic and thermodynamic analysis of enzymatic transesterification process under various conditions. In first part the optimization of process parameters was carried out with statistical optimization design i.e. Box–Behnken design using Minitab 16 trial version software. The yield of enzymatic transesterification reaction was affected by various process parameters, viz. temperature, pH, presence of water content, oil to alcohol ratio, enzyme loading, etc. Thus, prior to main process parameter optimization using statistical experimental design effect of ultrasound duty cycles was analysed and optimized independently. It has been reported by various researchers that, the continuous exposure of enzyme to ultrasound irradiation results in its denaturing [26–28]. Thus before process optimization the duty cycles of ultrasound irradiation were optimized using 10% tributyrin assay as described above. The activity of lipase was tested at 20, 40, 60, 80 and 100% duty cycles. 20% duty cycle corresponds to 1 min sonication and 4 min stationary phase. Similarly, 100% duty cycle corresponds to whole 5 min sonication of reaction mixture at 40°C. The activity assay was repeated 3 times to reproduce the results. Based on the results of activity assay, the optimum duty cycles were employed in further process optimization experiments.

The Box–Behnken statistical experimental design comprising 3 process parameters (viz. Enzyme loading, alcohol to oil molar ratio and temperature) and 3 levels. The combinations of parameters in each experimental set of statistical design are listed in Table 5.1 (A) and (B). The reaction time and levels of independent parameters were selected based on the results of preliminary experiments. Each transesterification experiment was conducted for 2 h and 500 µL aliquots of reaction mixture were withdrawn every 30 min to determine the extent of triglyceride conversion. The effect of water addition on the yield of transesterification reaction were evaluated with

varying water addition of 5–20% (v/v methanol) at optimum experimental parameters obtained from statistical experimental design.

Table 5.1 (A): Box–Behnken experimental design range and level of independent variables

Variables	Symbol	Level of factors coded values (Actual values)		
Enzyme loading (wt% oil)	E	–1 (1)	0 (3)	+1 (5)
Molar ratio (Alcohol: Oil)	M	–1 (4:1)	0 (7:1)	+1 (10:1)
Temperature (K)	T	–1 (298)	0 (308)	+1 (318)

Table 5.1 (B): Experimental sets of Box–Behnken design with triglyceride conversion

Sr. No.	Enzyme Loading (% w/w)	Molar Ratio	Temperature (K)	Experimental % Conversion	Model Predicted % Conversion
1	3	10	298	30.17 ± 0.40	30.56
2	3	7	308	85.47 ± 1.97	86.01
3	3	4	318	29.78 ± 1.16	29.39
4	3	10	318	46.89 ± 0.54	46.06
5	5	10	308	64.58 ± 1.57	64.63
6	3	4	298	20.15 ± 0.33	20.98
7	5	4	308	50.89 ± 1.53	50.50
8	1	7	298	8.20 ± 0.23	7.42
9	3	7	308	86.70 ± 0.69	86.01
10	3	7	308	85.86 ± 0.95	86.01
11	1	10	308	35.62 ± 1.13	36.01
12	5	7	318	46.21 ± 1.26	46.99
13	1	7	318	10.78 ± 0.33	11.22
14	1	4	308	23.94 ± 0.62	23.89
15	5	7	298	27.32 ± 0.82	26.88

Experimental setup: All transesterification experiments were conducted in batch mode using an ultrasound bath (Elma Transonic, T–460, Germany) with a total working volume = 2 L; ultrasound frequency = 35 kHz; theoretical power = 35 W. These experiments were termed as test experiments. The ultrasound bath was filled 75% of its total volume with distilled water which act as a medium for transmission of ultrasound waves. Optimized duty cycle of ultrasound irradiation was used in all experiments. Transesterification reaction was carried out in two–necked 25 mL round bottom flask made up of borosilicate glass fitted with a double–coiled condenser to reflux methanol vapour. The transesterification reaction was carried out with total reaction volume of

15 mL. The temperature of reaction was controlled through a water circulating bath (Jeio Tech, Lab Companion, RW 0525G, Korea). The position of round bottom flask was kept cautiously constant throughout all experiments as pressure amplitude of ultrasound irradiation varies at different points in sonication bath [29]. The experiments were repeated twice to confirm the reproducibility of results.

Analytical method: Triglyceride conversion (overall) to biodiesel in transesterification reaction was determined by ^{1}H NMR (Nuclear Magnetic Resonance) spectroscopy (Bruker Advance III HD Ascend 600 MHz) with TMS (tetramethylsilane) as internal standard and $CDCl_3$ (Merck, India) as a solvent [30]. Using subsequent equation gross molar conversion of triglycerides to biodiesel was calculated [31,32]: $X = \left(2 \times A_{ME}\right) \times 100 \Big/ \left(3 \times A_{\alpha - CH_2}\right)$, where, A_{ME} – the strong singlet peak at 3.6 ppm which represents the integration value of methyl esters protons and $A_{\alpha - CH_2}$ – the multiplet peaks at 2.3 ppm which represents the integration value of methylene protons.

5.2.4 Reusability of lipase

The reusability of immobilised lipase was also evaluated. The immobilized lipase was separated by centrifuging the reaction mixture at 6000*g* at 298 K for 15 min at the end of transesterification reaction. The recovered immobilized lipase was washed 2 times with 5 mL n–hexane to remove the adsorbed impurities such as methanol, glycerol or triglyceride. The washed catalyst was freeze dried at 277 K and stored in phosphate buffer solution (pH 7.5, 0.1 M) at 277 K under refrigerated condition. The stored enzyme was analysed for its activity as described earlier and further used in the next cycle. The procedure was repeated till the enzyme activity reached below 50% of its initial activity.

5.2.5 Kinetic and thermodynamic analysis of transesterification reaction

Kinetic and thermodynamic analysis of transesterification reaction gives a mechanistic insight into physical mechanism of the process. To evaluate the physical insights of ultrasound effect on enzyme–catalysed transesterification reaction, the experiments were also performed with mechanical agitation and termed as control experiments. Ultrasound bath was replaced by mechanical agitation in control experiments. The experiments were carried out using magnetic stirrer (Tarson, Spinot, MC–02, India) at 400 rpm. The kinetic and thermodynamic analysis of control experiments helps in identifying the role of sonication in process intensification. At the same time, the effect of water addition on transesterification yield was also evaluated by kinetic and thermodynamic study. Thus, following categories of experiments were examined through kinetic and thermodynamic analyses.

1. Optimum process conditions with mechanical agitation – termed as control experiment.
2. Optimum process conditions with ultrasound – termed as test experiment.
3. Optimum process conditions along with optimum water content and ultrasound – termed as TW (Test + Water).

The triglyceride conversion profile with respect to time was determined by ^{1}H NMR analysis and fitted to pseudo–first order kinetic model. For determination of various kinetic and thermodynamic parameters, the experiments were performed at two different temperatures (at 297 and 303 K) other than optimum temperature and the kinetic rate constants (k) were determined for both test and control category.

Arrhenius equation expressed as: $k = A\exp\left(-E_a/RT\right)$ was used to determine the activation energy (E_a), where, R is universal gas constant and A is frequency factor. Eyring equation and Gibbs free energy relations (given below) were used for

determining the thermodynamic parameters viz. change in enthalpy (ΔH), entropy (ΔS) and Gibbs free energy (ΔG).

$$\ln\frac{k}{T} = -\frac{\Delta H}{R}\frac{1}{T} + \ln\frac{k_b}{h} + \frac{\Delta S}{R}$$

$$\Delta G = \Delta H - T\Delta S$$

where, k_b is Boltzmann constant and h is Plank's constant.

5.3 Results and discussion

5.3.1 Immobilized lipase activity assay and optimization of duty cycles

The activity of commercial immobilized lipase was analysed as per 10% tributyrin assay protocol. At the same time, the duty cycles of sonication were also optimized using activity assay. The results of enzyme activity at different duty cycles are shown in Fig. 5.1. The commercial enzyme has the activity of 2433.7 ± 24.2 TBU/g. With the application of ultrasound, the activity of enzyme increased up to 40% duty cycle and later decreased sharply.

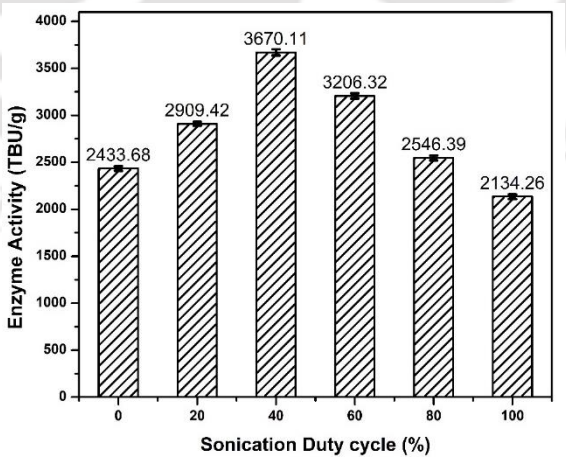

Figure 5.1: Optimization of sonication duty cycle through enzyme activity assay

The highest enzyme activity was found to be 3670.1 ± 32.8 TBU/g at 40% duty cycle. The results show that exposure of lipase to ultrasound irradiation make more

active enzyme–substrate contact but continuous exposure for long time can inactivate lipase. Similar trends in enzyme activities were also observed by Bhasarkar et al. [27] and Subhedar and Gogate [28], etc. They confirmed the structural changes in enzymes using Circular Dichroism (CD) analysis and reported that the exposure to ultrasound caused changes in α–helix, β–sheets, β–turns and random coils of enzyme molecule when compared with the native enzyme. The probable cause for varying change in enzyme activity at different duty cycles is the intensity of cavitation phenomenon. The transient collapse of gas/vapour bubbles during cavitation phenomenon results in release of high energy in the form of shock waves and local high temperature and pressure condition [27]. This causes unfolding of enzyme proteins and exposure of inner hydrophobic amino acid residues leading to higher enzyme activity. But, the continuous exposure to high intensity ultrasound can cause denaturation of the lipase or disruption of its configuration [28]. The activity of immobilized enzyme for extended time (30 min) was also evaluated as transesterification reaction was carried out for longer reaction times. The activity was evaluated at 10, 20 and 30 min time interval and listed in Table 5.2. The average activity of lipase was found to be 3656.7 ± 35.2 TBU/g. Based on these results, 40% duty cycle (2 min sonication and followed by 3 min stationary phase) was taken as optimum duty cycle for further ultrasound–assisted experiments.

Table 5.2: Enzyme activity assay with 40% sonication duty cycle at different time interval

Time	Enzyme Activity (TBU/g)
5	3670.1 ± 32.8
10	3655.4 ± 39.8
20	3656.9 ± 39.8
30	3644.6 ± 28.5

40% sonication duty cycle corresponds to 2 min sonication followed by 3 min stationary phase

5.3.2 Optimization of enzymatic transesterification process

After assessment of few preliminary experiments, the transesterification process using mixed non–edible oil feedstock was optimized using Box–Behnken statistical design. Table 5.1 (B) shows the experimental and model–predicted transesterification yield for 15 experimental sets. The values of experimental yields are the average of yields in two consecutive runs with standard deviation. The following equation was obtained by fitting the experimental results to quadratic model with coded values of process variables.

$$Y = 86.01 + 13.81E + 6.56M + 5.98T - 25.44E^2 - 16.82M^2 - 37.45T^2 + 0.50E \times M + 4.08T \times E + 1.77M \times T$$

where, Y is the yield of transesterification reaction.

The experimental results of transesterification yield matched closely with model predicted data as depicted in Table 1A, indicating the suitability of selected model and the range of process parameters. Regression coefficients, viz. R^2 = 0.9916; R^2 (predicted) = 0.9840; and R^2 (adjusted) = 0.9898, corroborates the above statement. ANOVA (Analysis of Variance) results of fitted model, which estimates the linear, square and interaction coefficients of quadratic model is provided in Table 5.3. The *F*–values of linear parameters are far higher as compared with the *F*–values of interaction coefficients, which effectively highlights the independent effects on response variables. The significance of process variable on transesterification yield was judged from *t*–stat and *p*–value. The *p*–value < 0.05 predicts the significance of the parameter or coefficient. The *p*–value of interaction coefficient “enzyme loading and molar ratio” was > 0.05 indicates the insignificant interaction as compared to other interaction coefficient “enzyme loading and temperature” and “molar ratio and temperature”. The absolute *t*–stat of linear parameters are much higher than interaction parameters, predicting the individual impact of these process variables on transesterification yield,

supporting the higher *F*–values of linear parameters. The *F*–value and *p*–value of Lack–of–Fit were 3.03 and 0.258, respectively, suggests that Lack–of–Fit is insignificant, when compared to pure error which also corroborates best fit of the model predicted data to experimental results. In other words, the selected model is significant.

Table 5.3: Statistical analysis of experimental results

(A) Estimated regression coefficients for triglyceride conversion

Term	Coefficients	SE coeff	*t*–stat	*p*–value
Constant (β)	86.01	0.5407	159.07	<0.001
Enzyme (E)	13.81	0.3311	41.70	<0.001
Molar ratio (M)	6.56	0.3311	19.82	<0.001
Temperature (T)	5.98	0.3311	18.05	<0.001
Enzyme × Enzyme (E^2)	–25.44	0.4874	–52.19	<0.001
Molar ratio × Molar ratio (M^2)	–16.82	0.4874	–34.50	<0.001
Temperature × Temperature (T^2)	–37.45	0.4874	–76.83	<0.001
Molar ratio × Enzyme (ME)	0.50	0.4683	1.07	0.132
Temperature × Enzyme (TE)	4.78	0.4683	8.71	<0.001
Temperature × Molar ratio (TM)	1.77	0.4683	3.79	0.013

(B) Analysis of variance (ANOVA) for transesterification reaction

Source	Degrees of freedom	Sq SS	F–value	*p*–value
Regression	9	9869.84	1250.34	<0.001
Linear	3	2155.54	819.22	<0.001
Square	3	7634.21	2501.37	<0.001
Interaction	3	80.08	30.43	0.001
Residual Error	5	4.39	–	–
Lack–of–Fit	3	3.60	3.03	0.258
Pure Error	2	0.79	–	–
Total	14	9874.22	–	–

R^2 = 99.96%; R^2 (pred) = 99.40%; R^2 (adj) = 99.88%

The estimated optimum set of parameters by quadratic model was: enzyme loading = 3.55% (w/w); molar ratio (alcohol/oil) = 7.64:1; temperature = 36°C. The validation experiment was carried out by using optimised set of parameters which resulted in triglyceride conversion of 90.1 ± 1.1%, which is close to the predicted triglyceride conversion of 88.9% by the model. The ^{1}H NMR spectrum of reaction mixture at the end of 2 h transesterification reaction is shown Fig. 5.2. Different characteristic peaks were identified from ^{1}H NMR spectra. A singlet peak at 3.6 ppm

represented the methyl ester, whereas the triplet peak was observed for α–carbonyl methylene protons at 2.3 ppm, as also reported earlier by Choudhury et al. [30]. Characteristic peak at 5.33 ppm confirms the presence of olefinic hydrogens in the biodiesel and also the different unsaturated and polyunsaturated carbons present in biodiesel as their peaks appeared between 2.0 to 2.8 ppm as reported earlier [30].

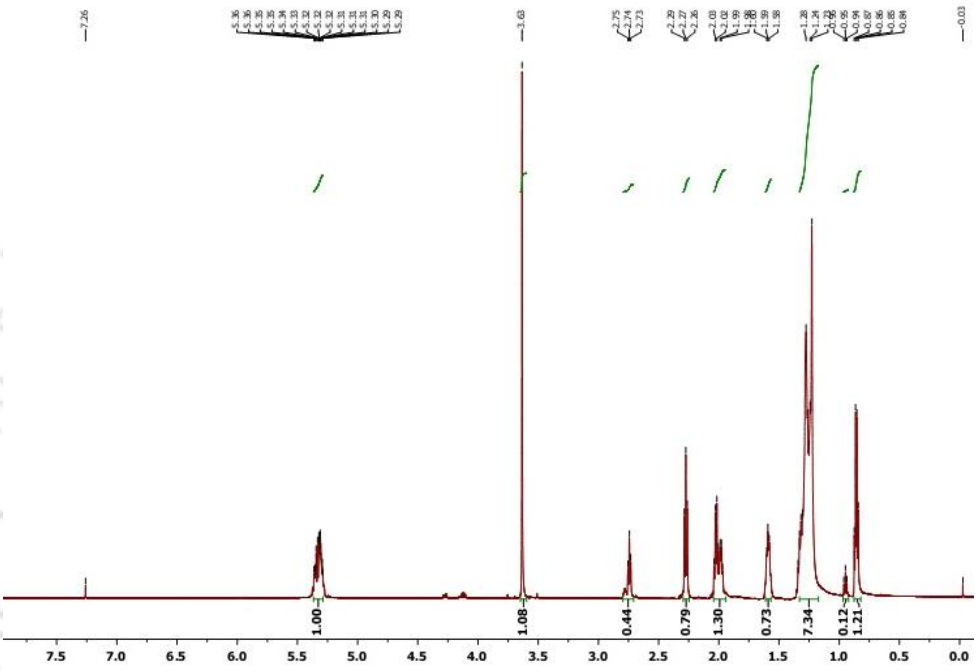

Figure 5.2: ^{1}H NMR of enzyme catalysed transesterification reaction at optimum condition at the end of 2 h reaction

The contour plots provided Fig. 5.3, depict the interaction between any two process variables with keeping the third variable at its centre point corresponding to maximum triglyceride conversion. The counter plot between temperature *vs* molar ratio (Fig. 5.3 (A)) and temperature *vs* enzyme loading (Fig. 5.3 (B)) shows that, with increase in temperature from 298 to 310 K the yield of transesterification reaction increases and further increase in temperature reduces the yield of transesterification reaction. Temperature of reaction is crucial parameter in case of lipase catalysed reactions, as the enzyme is highly sensitive to the temperature. The enzyme used in

present study has efficiently catalysed the reactions up to 313 K. Subhedar and Gogate [35] reported that temperature > 313 K, denatures the lipase, though it is in the immobilized state. On the other hand, the lower temperatures reduced the yield of transesterification reaction, as it cannot provide the required activation energy to initiate the reaction.

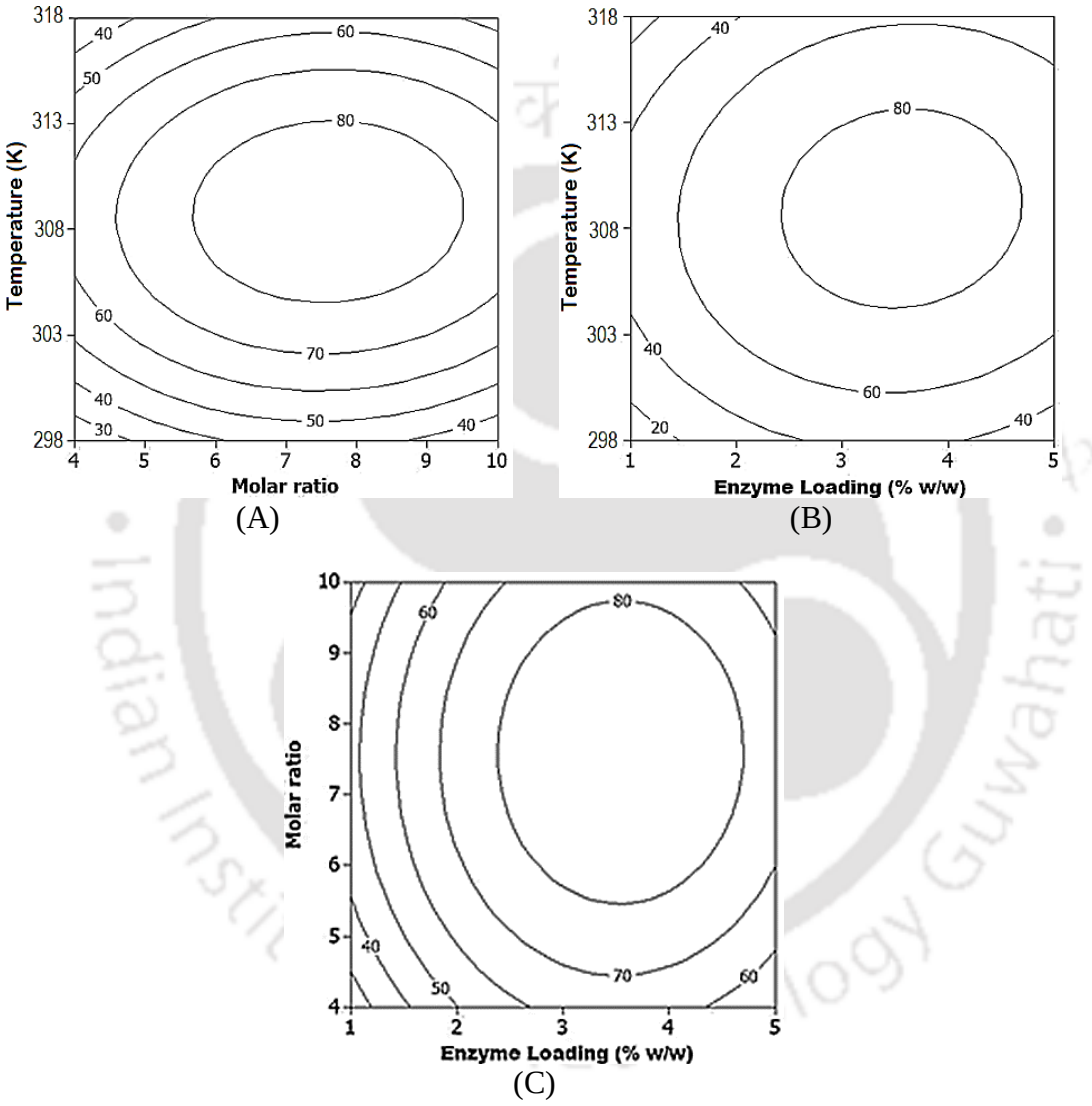

(A) (B)

(C)

Figure 5.3: Counter plots depicting interaction between the process parameters in transesterification process (A) molar ratio *vs* temperature; (B) enzyme loading *vs* temperature and (C) enzyme loading *vs* molar ratio

Similarly, the counter plots of enzyme loading vs temperature (Fig. 5.3(B)) and enzyme loading *vs* molar ratio (Fig. 5.3 (C)) shows that increase in enzyme loading

improves the transesterification yield. The maximum yield can be achieved with addition of 3 to 4%, w/w of enzyme. The lower enzyme loading resulted in low interaction between the substrate and enzyme molecule thus lowering the transesterification yield. The counter plots between temperature *vs* molar ratio (Fig. 5.3 (A)) and enzyme loading *vs* molar ratio (Fig. 5.3 (C)) predicts that increase in molar ratio from 4 to 8 increases transesterification yield and further increase in molar ratio lowers the transesterification yield. This may be due to the lower alcohol to oil molar ratio limits the extent of mixing with each other. The convections generated through sonication/ transient collapse of bubbles directly depends on the viscosity of the medium [33,34]. Very low convections from sonication will be generated in oil phase due to high viscosity of oil, ultimately resulting in lower transesterification yield, similar to the results observed by Choudhury et al. [30,35]. On the other hand, the higher alcohol to oil molar ratio also resulted in lower yield probably due to improper dispersion of oil phase in methanol that lowers the interfacial area for reaction, as reported by Kalva et al. [36]. Subhedar and Gogate [28] also reported that higher alcohol to oil molar ratio will denature the enzyme due to polar nature of methanol.

5.3.3 Effect of water addition on transesterification reaction

In all experiments, the immobilized lipase was soaked overnight in phosphate buffer (pH 7.5, 0.1 M) before experiment. Thus, some traces of water were carried into the reaction mixture with immobilized enzyme. However, effect of external addition of water to reaction mixture was examined. The optimum water content was evaluated by varying the water addition from 5 to 20 % (v/v, methanol) to transesterification reaction. Fig. 5.4 illustrates the results of water addition on transesterification reaction. The addition of 10% water to transesterification reaction increased the yield to 94.4 ± 0.8%

from 90.1 ± 1.1% with no water present. The increase in the yield can be attributed to activation of lipase through oil–water interface as reported by Xun et al. [37]. In many commercially immobilized lipases, the active catalytic site is covered within the protein structure through lid making it inactive. In presence of water the lid opens and exposes the active site to substrate molecule resulting in higher yield as reported by Babaki et al. [17].

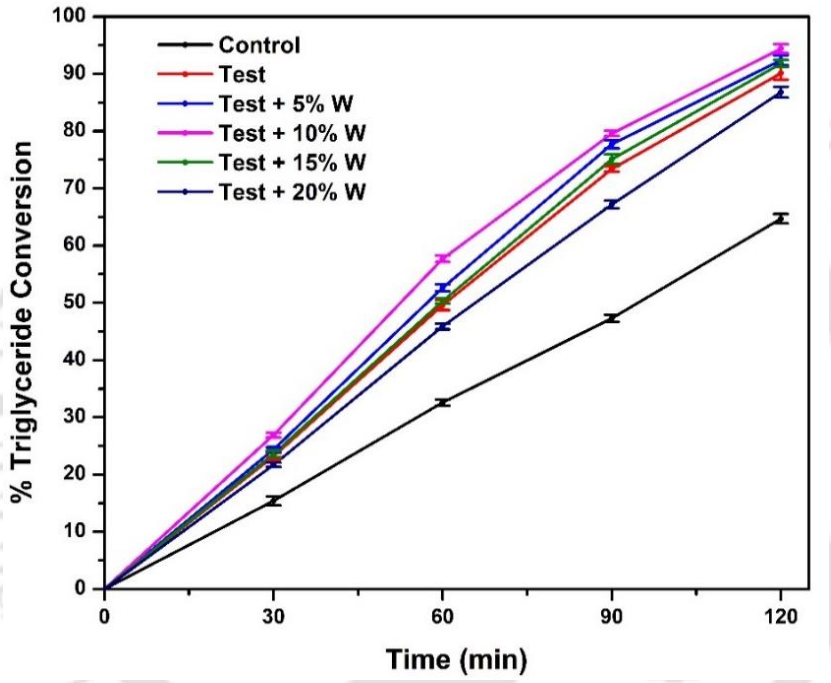

Figure 5.4: Triglyceride conversion for enzyme catalysed transesterification reaction under different categories

On the other hand, addition of 20% water reduced the transesterification yield to 86.8 ± 1%. Babaki et al. [17] also reported similar results with excess addition of water to transesterification reaction. The main cause for this reduction in transesterification yield was the favouring of the hydrolysis reaction and also excess water present creates the thick layer around the enzyme, thus increases the diffusion of oil through it resulting in enhanced mass transfer barrier. Rashid et al. [38] reported that the excess water content results in higher surface tension and thus leading to

aggregation of immobilized lipase. Thus, in present study 10% water was found to be optimum and it was used in further experiments for kinetic and thermodynamic analyses.

5.3.4 Kinetic and thermodynamic analyses of transesterification reaction

The kinetic and thermodynamic analysis of transesterification process was carried out in 3 categories, as described in section 3. The kinetic rate constants (*k*) were determined using pseudo–first order kinetic model and are listed in Table 5.4. The kinetic rate constants were used to determine the kinetic and thermodynamic parameters viz. activation energy (E_a) using Arrhenius equation; change in enthalpy (ΔH) and change in entropy (ΔS) using Eyring equation and change in Gibbs free energy (ΔG) using Gibbs free energy relation as stated in section 3. Graphical method was used to determine the E_a, ΔH and ΔS [39]. A plot between ln *k vs* 1/T was used to determine the activation energy, whereas the plot between ln *k*/T *vs* 1/T gives change in enthalpy and entropy of transesterification reaction as shown in Figs. 5.5 (A) and (B), respectively. The ΔG was calculated by using the obtained values of ΔH and ΔS at 309 K.

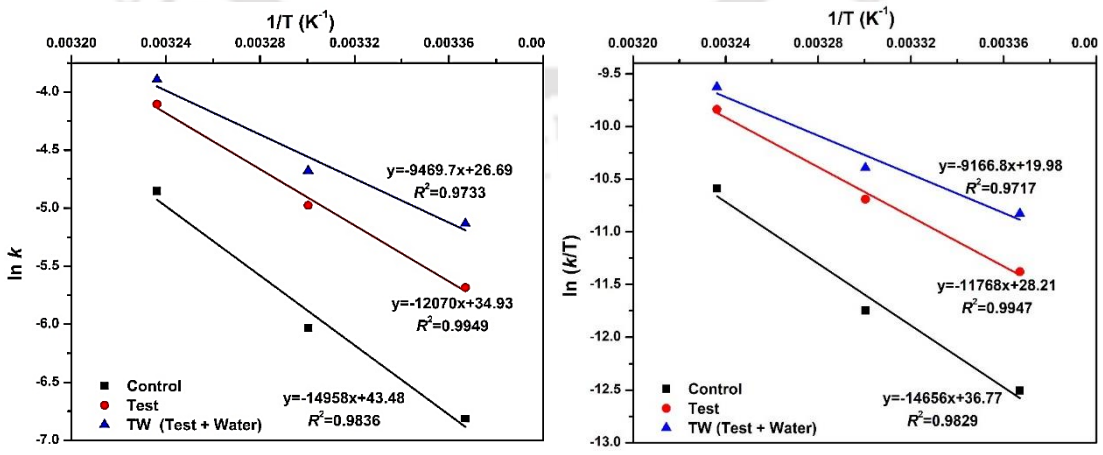

(A) (B)

Figure 5.5: (A) Arrhenius plot and (B) Eyring plot for enzyme catalysed transesterification reaction under different categories

Table 5.4: Kinetic rate constants of enzymatic transesterification process (min^{-1})

Category	309 K	303 K	297 K
Control	7.8×10^{-3}	2.4×10^{-3}	1.1×10^{-3}
Test	1.6×10^{-2}	6.9×10^{-3}	3.4×10^{-3}
TW (Test + Water)	2.0×10^{-2}	9.3×10^{-3}	5.9×10^{-3}

The values of all kinetic and thermodynamic parameters are listed in Table 5.5. The activation energy of mechanically agitated (control) system was found to be 124.4 kJ/mol, whereas for ultrasound assisted (Test) and 10% water in ultrasound assisted (TW) system were found to be 100.4 and 78.7 kJ/mol, respectively. The higher activation energy for control system as compared with test system shows the dominance of mass transfer limitation in the system. The application of sonication helps in mixing of oil and methanol phases (as fine emulsion) with each other through the micro–conventions generated from cavitation process. The ultrasound creates the fine emulsion of oil–methanol mixture and lowers interfacial tension as compared with mechanically agitated system. Further reduction in activation energy of TW (Test + Water) system can be correlated with the high activity of enzyme as the presence of water during transesterification reaction opens the lid and lowers the denaturing of enzyme in presence of polar solvents. Thus, application of ultrasound reduces the activation energy by 24 kJ/mol (i.e. 20%) as compared to mechanically agitated system. With addition of 10% water to reaction mixture, the activation energy further decreased by 21.62 kJ/mol (i.e. 21.5%) as compared to test condition.

Table 5.5: Kinetic and thermodynamic parameters of enzymatic transesterification process

Category	E_a (kJ/mol)	ΔH (kJ/mol)	ΔS (kJ/mol K)	ΔG (kJ/mol)
Control	124.36	121.85	0.11	88.43
Test	100.35	97.84	0.04	86.40
TW (Test + Water)	78.73	76.21	–0.03	85.92

The change in enthalpy, change in entropy and change in Gibbs free energy help in getting insight into the physical mechanism of the enzymatic transesterification reaction, which is governed by state of enzyme.

1. In present study, the ΔH values decreases from 121.85 kJ/mol (control condition) to 97.84 kJ/mol for test condition. ΔH further reduces to 76.21 kJ/mol with addition of water to reaction mixture. Reduction in ΔH with sonication and addition of water is a possible consequence of opening the lid of immobilised enzyme and other conformational changes in secondary structure of enzyme – which essentially lead to unfolding of proteins and exposure of the substrate–binding sites. This enhances formation of enzyme–substrate complex with concurrent lowering of activation energy for the overall reaction. Recently Bedade et al. [40] have also reported in their study decrease in ΔH value for enzyme catalysed reactions with immobilization of enzymes on magnetic nanoparticles. Bedade et al. [40] have shown that immobilization of the enzyme leads to conformational changes in enzyme structure and opening of the enzyme proteins.

2. The entropy change ΔS for control and test conditions was +ve, whereas for TW condition ΔS was –ve. Entropy change is essentially a measure of the "order" in the reaction system. Bedade et al. [40] have stated that entropy change is an indicator of the extent of variation in local distortion between ground state and transition state of enzyme molecules. In the context of present study, the trends in entropy change are essentially a manifestation of the changes in secondary structure of enzyme. Easier access to substrate binding sites due to unfolding of enzyme protein and removal of the lid makes the reaction system systematic and ordered with lesser requirement of energy to attain transition state. This is reflected in reduction in ΔS with sonication and even further reduction in ΔS with water addition in reaction mixture, as addition of water

enhances the intensity of transient cavitation in the reaction mixture [39].

3. ΔG values for control condition were marginally higher as compared to test and TW conditions. Bedade et al. [40] have correlated the ΔG values with unfolding of enzyme structure. Larger ΔG value indicates higher stability of enzyme and lower unfolding during the reaction. In control and test conditions, the ΔG values are smaller than ΔH values, due to the +ve ΔS contribution indicating more disordered reaction system. On the other hand, in TW conditions the ΔG values are larger than ΔH values, due to the –ve ΔS corresponding to unfolding of enzyme protein and more ordered reaction system.

5.3.5 Reusability of immobilized lipase

The immobilized lipase was separated from reaction mixture and reused as described in section 5.2.4. Prior to consecutive transesterification reactions with recycled lipase, the activity was assessed. The reusability study of enzyme was conducted in test and TW (test + water) category to evaluate the effect of water addition on activity of enzyme. The performance of recycled immobilized lipase in test and TW category is depicted in Figs. 5.6 (A) and (B) with the yardsticks of yields of successive transesterification reactions and the residual enzyme activity after each transesterification. The results showed that immobilized enzyme retains 37% of its initial activity in test category after 6 successive recycles. However, 50% of initial activity was retained by immobilized enzyme after 6 cycles in TW category. The results obtained in present study are comparable with the results reported by Subhedar and Gogate [28], where ~40% of initial activity was retained by enzyme after 6 cycles in presence of ultrasound. The reusability results of immobilized lipase in present study showed that 35% and 43% of triglyceride conversion (as analysed by NMR

spectroscopic analysis) can be achieved after 6 recycles in test and TW category, respectively. This result is much superior as compared to previous literature, e.g. Zhang et al. [41], where after 6 successive recycles of Lipozyme TLIM enzyme only 20% triglyceride conversion was achieved. The reduction in yield as well as in activity was probably due to the deactivation or irreversible denaturing of the enzyme during repeated cycles of separation and reuse.

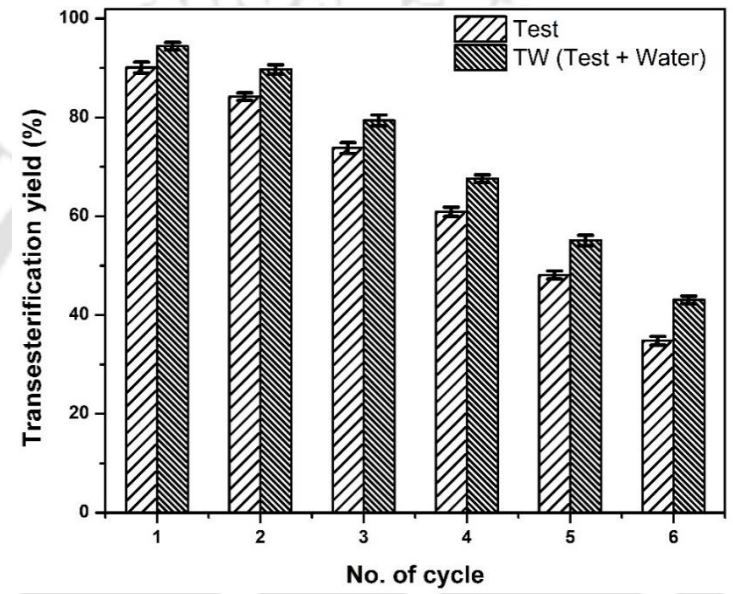

(A)

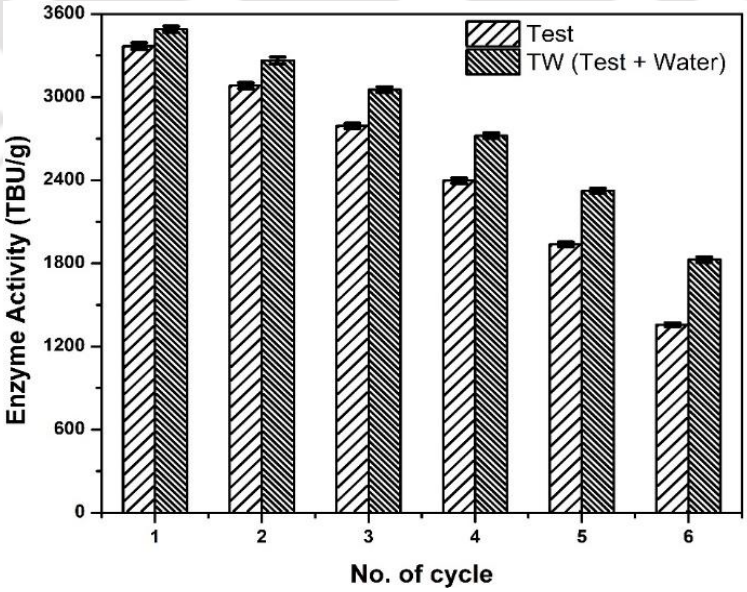

(B)

Figure 5.6: Performance of immobilized lipase during recycle and reuse (A) transesterification yield and (B) enzyme activity in consecutive cycles

The deactivation effect was relatively smaller in presence of water, which concurred with results of other authors [17,21,38], which essentially indicated that presence of certain (small) quantity of water enhances stability of conformational structure of enzyme and its activity.

5.4 Conclusion

The present study has investigated enzymatic transesterification of blend of non–edible oils with commercial immobilized lipase. The study has four components, viz. (1) process optimization using statistical method, (2) enhancement of catalytic action of enzyme through water addition, (3) kinetic and thermodynamic analysis of transesterification process under control (mechanical agitation), test (sonication) and TW (sonication + water addition) conditions, and (4) recycle/reuse of enzyme. Kinetic analysis of transesterification revealed that application of ultrasound and addition of water to reaction mixture lowers the activation energy. Thermodynamic analysis has revealed that both sonication and water addition reduces the enthalpy and entropy of transesterification. Furthermore, the addition of water makes entropy change of the process negative, indicating more ordered reaction. It is conjectured that these trends in kinetic and thermodynamic parameters are essentially manifestations of the conformational changes induced in the secondary structure of enzyme during sonication and water addition. Successive ultrasound–assisted transesterification reactions with recycled enzyme showed good retention of enzymatic activity up to 6 cycles. This effect further enhanced with water addition indicating higher stability of enzyme.

References

[1] Baskar, G. and Aiswarya, R., 2016. Trends in catalytic production of biodiesel from various feedstocks. Renewable and Sustainable Energy Reviews, 57, 496–504.

[2] Atadashi, I.M., Aroua, M.K., Aziz, A.A. and Sulaiman, N.M.N., 2013. The effects of catalysts in biodiesel production: A review. Journal of Industrial and Engineering Chemistry, 19(1), 14–26.

[3] Lam, M.K., Lee, K.T. and Mohamed, A.R., 2010. Homogeneous, heterogeneous and enzymatic catalysis for transesterification of high free fatty acid oil (waste cooking oil) to biodiesel: a review. Biotechnology Advances, 28(4), 500–518.

[4] Knothe, G. and Razon, L.F., 2017. Biodiesel fuels. Progress in Energy and Combustion Science, 58, 36–59.

[5] Melero, J.A., Iglesias, J. and Morales, G., 2009. Heterogeneous acid catalysts for biodiesel production: current status and future challenges. Green Chemistry, 11(9), 1285–1308.

[6] Jegannathan, K.R., Abang, S., Poncelet, D., Chan, E.S. and Ravindra, P., 2008. Production of biodiesel using immobilized lipase—a critical review. Critical Reviews in Biotechnology, 28(4), 253–264.

[7] Amini, Z., Ilham, Z., Ong, H.C., Mazaheri, H. and Chen, W.H., 2017. State of the art and prospective of lipase–catalyzed transesterification reaction for biodiesel production. Energy conversion and management, 141, 339–353.

[8] Tian, K., Tai, K., Chua, B.J.W. and Li, Z., 2017. Directed evolution of *Thermomyces lanuginosus* lipase to enhance methanol tolerance for efficient production of biodiesel from waste grease. Bioresource Technology, 245, 1491–1497.

[9] Bhangu, S.K., Gupta, S. and Ashokkumar, M., 2017. Ultrasonic enhancement of lipase–catalysed transesterification for biodiesel synthesis. Ultrasonics

Sonochemistry, 34, 305–309.

[10] Bajaj, A., Lohan, P., Jha, P.N. and Mehrotra, R., 2010. Biodiesel production through lipase catalyzed transesterification: an overview. Journal of Molecular Catalysis B: Enzymatic, 62(1), 9–14.

[11] Blanco, R.M., Terreros, P., Fernández–Pérez, M., Otero, C. and Dıaz–González, G., 2004. Functionalization of mesoporous silica for lipase immobilization: characterization of the support and the catalysts. Journal of Molecular Catalysis B: Enzymatic, 30(2), 83–93.

[12] Ye, P., Xu, Z.K., Wu, J., Innocent, C. and Seta, P., 2006. Nanofibrous poly (acrylonitrile–co–maleic acid) membranes functionalized with gelatin and chitosan for lipase immobilization. Biomaterials, 27(22), 4169–4176.

[13] Dizge, N., Aydiner, C., Imer, D.Y., Bayramoglu, M., Tanriseven, A. and Keskinler, B., 2009. Biodiesel production from sunflower, soybean, and waste cooking oils by transesterification using lipase immobilized onto a novel microporous polymer. Bioresource Technology, 100(6), 1983–1991.

[14] Aybastıer, Ö. and Demir, C., 2010. Optimization of immobilization conditions of *Thermomyces lanuginosus* lipase on styrene–divinylbenzene copolymer using response surface methodology. Journal of Molecular Catalysis B: Enzymatic, 63(3–4), 170–178.

[15] Liu, C.H., Huang, C.C., Wang, Y.W., Lee, D.J. and Chang, J.S., 2012. Biodiesel production by enzymatic transesterification catalyzed by *Burkholderia* lipase immobilized on hydrophobic magnetic particles. Applied Energy, 100, 41–46.

[16] Babaki, M., Yousefi, M., Habibi, Z., Brask, J. and Mohammadi, M., 2015. Preparation of highly reusable biocatalysts by immobilization of lipases on epoxy–functionalized silica for production of biodiesel from canola oil. Biochemical

Engineering Journal, 101, 23–31.

[17] Babaki, M., Yousefi, M., Habibi, Z., Mohammadi, M. and Brask, J., 2015. Effect of water, organic solvent and adsorbent contents on production of biodiesel fuel from canola oil catalyzed by various lipases immobilized on epoxy–functionalized silica as low cost biocatalyst. Journal of Molecular Catalysis B: Enzymatic, 120, 93–99.

[18] Bayramoglu, G., Akbulut, A., Ozalp, V.C. and Arica, M.Y., 2015. Immobilized lipase on micro–porous biosilica for enzymatic transesterification of algal oil. Chemical Engineering Research and Design, 95, 12–21.

[19] Zhao, X., Qi, F., Yuan, C., Du, W. and Liu, D., 2015. Lipase–catalyzed process for biodiesel production: enzyme immobilization, process simulation and optimization. Renewable and Sustainable Energy Reviews, 44, 182–197.

[20] Angajala, G., Pavan, P. and Subashini, R., 2016. Lipases: An overview of its current challenges and prospectives in the revolution of biocatalysis. Biocatalysis and Agricultural Biotechnology, 7, 257–270.

[21] Nelson, L.A., Foglia, T.A. and Marmer, W.N., 1996. Lipase-catalyzed production of biodiesel. Journal of the American Oil Chemists' Society, 73(9), 1191–1195.

[22] Puthli, M.S., Rathod, V.K. and Pandit, A.B., 2006. Enzymatic hydrolysis of castor oil: process intensification studies. Biochemical Engineering Journal, 31(1), 31–41.

[23] Lu, J., Chen, Y., Wang, F. and Tan, T., 2009. Effect of water on methanolysis of glycerol trioleate catalyzed by immobilized lipase *Candida sp.* 99–125 in organic solvent system. Journal of Molecular Catalysis B: Enzymatic, 56(2–3), 122–125.

[24] Deng, X., Fang, Z. and Liu, Y.H., 2010. Ultrasonic transesterification of

Jatropha curcas L. oil to biodiesel by a two–step process. Energy Conversion and Management, 51(12), 2802–2807.

[25] Rajasekar, V.W., Tambe, A. and Datla, A., 2013. Immobilization and characterization of recombinant Candida antarctica lipase B on poly (glycidyl methacrylate–ter–divinyl benzene–ter–ethylene dimethacrylate) beads, "DILBEADS™ TA". Biocatalysis and Biotransformation, 31(2), 79–88.

[26] Malani, R.S., Khanna, S. and Moholkar, V.S., 2013. Sonoenzymatic decolourization of an azo dye employing immobilized horse radish peroxidase (HRP): a mechanistic study. Journal of Hazardous Materials, 256, 90–97.

[27] Bhasarkar, J., Borah, A.J., Goswami, P. and Moholkar, V.S., 2015. Mechanistic analysis of ultrasound assisted enzymatic desulfurization of liquid fuels using horseradish peroxidase. Bioresource Technology, 196, 88–98.

[28] Subhedar, P.B. and Gogate, P.R., 2016. Ultrasound assisted intensification of biodiesel production using enzymatic interesterification. Ultrasonics Sonochemistry, 29, 67–75.

[29] Moholkar, V.S., Sable, S.P. and Pandit, A.B., 2000. Mapping the cavitation intensity in an ultrasonic bath using the acoustic emission. AIChE journal, 46(4), 684–694.

[30] Choudhury, H.A., Malani, R.S. and Moholkar, V.S., 2013. Acid catalyzed biodiesel synthesis from Jatropha oil: mechanistic aspects of ultrasonic intensification. Chemical Engineering Journal, 231, 262–272.

[31] Gelbard, G., Bres, O., Vargas, R.M., Vielfaure, F. and Schuchardt, U.F., 1995. ^{1}H nuclear magnetic resonance determination of the yield of the transesterification of rapeseed oil with methanol. Journal of the American Oil Chemists' Society, 72(10), 1239–1241.

[32] Knothe, G., 2001. Analytical methods used in the production and fuel quality assessment of biodiesel. Transactions of the ASAE, 44(2), 193–200.

[33] Ranjan, A., Singh, S., Malani, R.S. and Moholkar, V.S., 2016. Ultrasound–assisted bioalcohol synthesis: review and analysis. RSC Advances, 6(70), 65541–65562.

[34] Malani, R. S., Goyal, A. and Moholkar, V. S. Ultrasound–Assisted Biodiesel Synthesis: A Mechanistic Insight, in: Agrawal, A. K., Agarwal, R. A., Gupta, T. and Gurjar, B. R. (Eds.), Biofuels, Springer, Singapore, 2017, pp. 103–135.

[35] Choudhury, H.A., Goswami, P.P., Malani, R.S. and Moholkar, V.S., 2014. Ultrasonic biodiesel synthesis from crude *Jatropha curcas* oil with heterogeneous base catalyst: mechanistic insight and statistical optimization. Ultrasonics Sonochemistry, 21(3), 1050–1064.

[36] Kalva, A., Sivasankar, T. and Moholkar, V.S., 2008. Physical mechanism of ultrasound–assisted synthesis of biodiesel. Industrial & Engineering Chemistry Research, 48(1), 534–544.

[37] Xun, E.N., Lv, X.L., Kang, W., Wang, J.X., Zhang, H., Wang, L. and Wang, Z., 2012. Immobilization of Pseudomonas fluorescens lipase onto magnetic nanoparticles for resolution of 2–octanol. Applied biochemistry and biotechnology, 168(3), 697–707.

[38] Rashid, R., Zaharudin, N.A. and Idris, A., 2014. Enzymatic hydrolysis of used–frying oil using Candida rugosa lipase. Jurnal Teknologi (Sci Eng), 67, 101–107.

[39] Malani, R.S., Khanna, S., Chakma, S. and Moholkar, V.S., 2014. Mechanistic insight into sono–enzymatic degradation of organic pollutants with kinetic and thermodynamic analysis. Ultrasonics Sonochemistry, 21(4), 1400–1406.

[40] Bedade, D.K., Muley, A.B. and Singhal, R.S., 2019. Magnetic cross–linked enzyme aggregates of acrylamidase from *Cupriavidus oxalaticus* ICTDB921 for

biodegradation of acrylamide from industrial waste water. Bioresource Technolology, 272, 137–145.

[41] Zhang, D.H., Lv, Y.Q., Zhi, G.Y. and Yuwen, L.X., 2011. Kinetic biosynthesis of l–ascorbyl acetate by immobilized *Thermomyces lanuginosus* lipase (Lipozyme TLIM). Bioprocess and Biosystems Engineering, 34(9), 1163–1168.

CHAPTER 6

BIODIESEL PRODUCTION BY ULTRASONIC INTERESTERIFICATION OF NON-EDIBLE OIL BLENDS

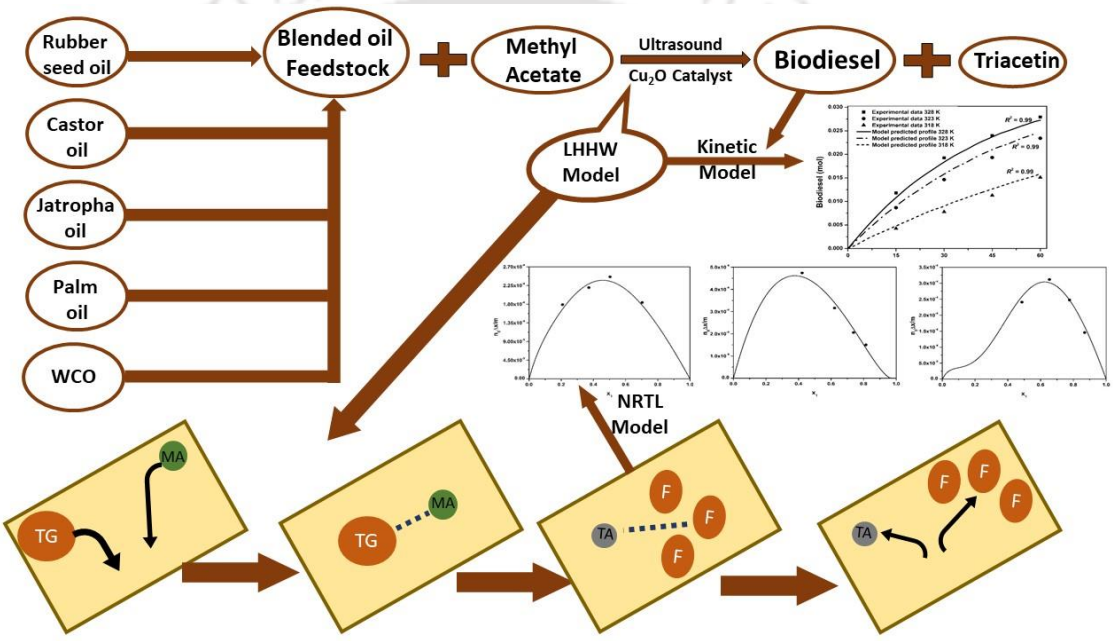

Chapter 6

Biodiesel Production by Ultrasonic Interesterification of Non–Edible Oil Blends

6.1 Introduction

In preceding chapters ultrasound–assisted biodiesel production using mixed non–edible oil feedstocks using heterogeneous catalysts were investigated. The transesterification of triglycerides with methanol yields by–product glycerol (approx. 10–15% w/w), which is contaminated with alkali catalyst and unreacted alcohol. The impurities or contaminations present in glycerol render it unsuitable for conventional applications in food, pharmaceutical and cosmetic industry. The contaminated glycerol, if sold in open market, also fetches very low price, and thus lowers the economy of large scale biodiesel production [1].

An alternate route for biodiesel production which does not involve formation of waste glycerol is interesterification. In this route, methanol is replaced by methyl acetate with triacetin as by–product [2,3]. Triacetin has higher commercial value than glycerol and used as food additive, plasticizer, solvent, excipient in pharmaceutical industry as well as anti–knocking agent in gasoline fuel and viscosity index improver in diesel fuel [4–6].

Conventionally, interesterification is carried out enzymatically with lipase as the catalyst [7,8]. However, this route is not attractive for commercial processes due to high cost of enzymes. Few researchers have investigated the interesterification process using inorganic catalyst either in homogeneous or heterogeneous form. Casas et al. [3,4] used solid sodium methoxide as catalyst for interesterification of sunflower oil, whereas Sustere et al. [1] used sodium methoxide solution for interesterification of rapeseed oil using various alkyl acetates. Maddikeri et al. [5,9] utilized KOH for interesterification of waste cooking oil with application of ultrasonic and hydrodynamic cavitation. Galia et al. [10] used tin octoate as catalyst for interesterification of rapeseed oil. Ribeiro et al. [11] used 4 different commercial heterogeneous catalysts, viz. niobium phosphate, niobium oxide, γ–alumina and zeolite HY for interesterification of macaw oil.

An added advantage of interesterification process is that the by–product triacetin can be re–blended with biodiesel. As per current biodiesel standard EN 14214, 10% blending of triacetin in biodiesel is allowed. Casas et al. [6] found that biodiesel/triacetin blends with as much as 20% w/w triacetin also meet the required standards of fuel properties.

In view of the potential of interesterification, the present study has made attempt to investigate mechanistic issues of the process. Another distinct features of this study are: (1) use of blend of non–edible oil as feedstock with cuprous oxide as heterogeneous base catalyst, and (2) employment of sonication (ultrasound irradiation) for intensification of the reaction. Initially, the reaction parameters were optimized using statistical methods. The kinetics of the reaction was investigated using a model based on Langmuir–Hinshelwood–Hougen–Watson (LHHW) reaction mechanism. The Non–random Two Liquid (NRTL) model was used to determine the relative adsorption equilibrium constant between reacting species. Fitting of experimental profiles of

reactant and product to kinetic model using Genetic Algorithm yields kinetic parameters, which provide mechanistic insight into the interesterification process. Comparative evaluation of kinetic parameters for interesterification with mechanical agitation and ultrasound irradiation has also given physical insight into the intensification of reaction induced by sonication.

6.2 Material and methods

6.2.1 Materials

Cu_2O (92% purity), methyl acetate (98% purity), sulphuric acid (98% conc.), methanol (99% purity) were procured from Himedia Pvt. Ltd., India. Four non–edible oils, viz. Palm, *Jatropha curcus*, Rubber, Castor, and waste cooking oil were collected from local sources. The collection of oils (waste cooking oil, Rubber, Castor and *Jatropha curcus*) were stated in chapter 2, section 2.2. Crude palm oil was procured from local market of Guwahati. Basic properties of these oils (density, viscosity, acid value (AV), saponification value (SV)) were determined and have been reported in Annexure B. Average molecular weights of oil samples were determined using following expression [12]:

Average molecular weight = $56.1\times3\times1000/(SV - AV)$.

where, SV – saponification value and AV – acid value of the oil feedstock.

Based on previous chapters the selected composition of blend of non–edible oils (% v/v) was as follows: Palm = 40%; Jatropha = 10%; Rubber = 20%; Castor = 10% and waste cooking oil = 20%. The blended feedstock had the acid value of 9.68 mg KOH/g; saponification value of 201.12 mg KOH/g with density and viscosity of 0.97 mg/mL and 30.48 mPa–s (at 313 K), respectively.

Prior to experiments, Cu_2O (with cubic morphology, size range of 0.2–2 µm) was dried in hot air oven at 393 K for 3 h, to remove the surface moisture. Dried Cu_2O powder was stored in a desiccator. Surface and structural properties of dried Cu_2O were determined using XRD and pore size and surface area analysis techniques and reported in detail in chapter 2, section 2.4.1. Briefly, the X–ray diffractogram of Cu_2O confirmed cubic FCC structure with different characteristic peaks at 30°, 37°, 43°, 61.5°, 74° and 77.5°, as compared with standard JCPDS 05–0667 file. BET surface area of dried Cu_2O was 2.94 m^2/g with average pore diameter of 15.05 nm.

6.2.2 Preliminary esterification experiments

The blended oil feedstock had acid value 9.68 mg KOH/g, which was significantly higher than typical limit (2 mg KOH/g) for direct transesterification using base catalyst. Thus, prior to main experiments, the acid value of oil blend was lowered by esterification using conc. H_2SO_4 and methanol. The esterification reaction was carried out at 338 K with following parameters: total reaction volume = 150 mL, acid concn. = 5% (w/w) H_2SO_4, methanol to oil molar ratio = 15:1, and mechanical agitation at 400 rpm, as reported in study of Choudhury et al. [13]. The final acid value of esterified oil blend was determined as 1.27 mg KOH/g, which was lower than the typical limit of 2 mg KOH/g. The viscosity of blended feedstock after esterification was found to be 16.87 mPa–s at 313 K. The esterified oil blend was further used for interesterification.

6.2.3 Interesterification experiments

Interesterification experiments were carried out in an ultrasound bath (Elma Transsonic, T–460, Germany, power: 35 W, frequency: 35 kHz, capacity: 2 L) and

termed as test experiments. The reaction mixture (total volume 20 mL) comprised of esterified blended oil, methyl acetate and Cu_2O as catalyst. The ultrasound bath was filled with distilled water that acted as medium for transmission of ultrasound waves. A 3–necked 50 mL round bottom flask (made up of borosilicate glass) fitted with a reflux coiled condenser was used for reaction. The temperature of water in the ultrasound bath was controlled using a circulating water bath (Jeio Tech, Lab Companion, RW 0525G, Korea).

Table 6.1 (A): Central Composite Design (CCD) statistical experimental design range and level of independent parameters

Variables	Symbol	Level of factors coded values (actual values)		
Catalyst loading (% w/w oil)	C	–1 (2)	0 (4)	+1 (6)
Alcohol: oil molar ratio	M	–1 (4:1)	0 (8:1)	+1 (12:1)
Temperature (K)	T	–1 (313)	0 (323)	+1 (333)

Table 6.1 (B): Experimental sets of CCD design with experimental and model predicted triglyceride conversion

Sr. No.	Catalyst Loading (% w/w)	Molar ratio	Temperature (K)	% Triglyceride conversion (Experimental)	% Triglyceride conversion (Model predicted)
1	2	8	323	57.1 ± 0.42	56.77
2	2	4	333	42.3 ± 0.57	42.37
3	4	8	323	85.6 ± 0.71	85.30
4	4	8	323	84.9 ± 0.85	85.30
5	4	8	333	82.9 ± 0.57	82.91
6	4	8	323	85.1 ± 0.71	85.30
7	4	8	323	85.4 ± 0.71	85.30
8	6	8	323	82.1 ± 0.57	82.29
9	4	4	323	73.6 ± 0.99	73.31
10	2	4	313	17.1 ± 0.28	17.31
11	4	8	313	48.3 ± 0.87	48.15
12	6	4	333	70.9 ± 0.42	70.94
13	4	8	323	85.2 ± 0.56	85.30
14	2	12	333	27.1 ± 0.28	27.17
15	4	12	323	70.6 ± 0.42	70.75
16	6	12	313	30.6 ± 0.57	30.57
17	6	12	333	75.2 ± 0.70	75.03
18	2	12	313	08.1 ± 0.28	08.11
19	4	8	323	85.3 ± 0.56	85.30
20	6	4	313	20.5 ± 0.56	20.48

Statistical optimization of interesterification parameters: Central composite statistical design (CCD) was used to optimize the process parameters of interesterification process. The CCD design consisted of 3 factors (Catalyst loading, Molar ratio of methyl acetate to oil and Temperature) and at 3 levels which resulted in 20 experimental sets through permutation–combination of operating parameters. The range and levels of the independent parameters in each experimental set formulated using Minitab 16 trial version software are shown in Table 6.1 (A) and (B). The conversion of triglyceride in each experimental set was monitored using ^{1}H NMR (Nuclear magnetic resonance) spectroscopic analysis.

Control experiments: For accounting of enhancement of interesterification by ultrasound, control experiments were conducted with mechanical agitation of reaction mixture at 400 rpm (Tarson–Spinot, MC–02, India). Other reaction parameters were same as that for experiments conducted with ultrasound.

All the experiments were carried out in duplicate to ascertain the reproducibility.

6.2.4 Kinetic analysis of interesterification reaction

Langmuir–Hinshelwood–Hougen–Watson (LHHW) kinetic model was used to correlate the experimental data. The value of rate constant (k) was determined by LHHW kinetic model. To determine the activation energy (E_a), experiments were performed at 318 K and 323 K, in addition to the optimum temperature of 328 K as per statistical optimization. The activation energy of interesterification reaction was determined using Arrhenius equation: $k = A\exp\left(-E_a/RT\right)$, where, R is universal gas constant and A is frequency factor.

6.2.5 Adsorption of reactants on catalyst surface

The key steps involved in LHHW kinetic model are: (i) both reactants absorb on the active sites of catalyst surface, and (ii) the reaction occurs with product formation in adsorbed form. Thus, for application of LHHW model, determination of adsorption equilibrium constant on the catalyst surface is necessary. To determine the equilibrium constants of reactant and product species over the catalyst surface, the experiments were conducted by selecting a non–reactive pair as reported by Tsai et al. [14,15]. In present context, the principal reactant was a blend of non–edible oils and principal product was fatty acid methyl esters (FAME or biodiesel). Both reactant and product comprised of both saturated and unsaturated organic molecules containing 12 to 22 carbon atoms (C_{12} to C_{22}). In such situation, it is difficult to define a single adsorption equilibrium constant representing entire reaction mixture. As an approximate solution to this issue, refined Canola oil (procured from local market) was selected as reference reactant, and FAME or biodiesel obtained from this oil as reference product (details provided in Annexure D). The rationale underlying use of refined canola oil as reference material was its composition. Refined Canola oil contains >95% C_{18} chains with major fraction (~ 65%) of $C_{18:1}$ (triolein) [16]. Thus, for determining adsorption constants of oil and biodiesel on Cu_2O surface, only the changes in mole fractions of triolein and methyl oleate (triolein methyl ester) in reaction mixture were considered.

Adsorption experiments were carried out in a 20 mL vial made up of borosilicate glass (Merck, India). The optimum catalyst loading (as deduced by statistical model) was 0.6 g catalyst for 20 mL binary mixture. Thus, in each adsorption experiment, 0.6 g catalyst was added with different concentrations of non–reactive binary mixture. The following binary reactant systems representing the interesterification reaction mixture were considered: (1) methyl acetate + triacetin; (2) methyl acetate + methyl oleate; and

(3) methyl oleate + triolein. In these pairs, triolein represented the canola oil, while methyl oleate represented the FAME (or biodiesel) formed from canola oil. The vapour space in vial was kept minimum to minimize the effect of vaporization of any component of binary mixture. The glass vial was sealed with paraffin film and shaked vigorously. Later, it was placed in a water bath for 8 h at 328 K (optimum reaction temperature) to attain equilibrium. Finally, an aliquot (500 µL) of binary mixture was drawn from the vial and was analysed after filtration for residual concentrations of the reactants using HPLC (high performance liquid chromatography).

Kipling et al. [17] derived an expression for overall material balance of isothermal non–reactive binary system as follows:

$$\frac{n_0 \Delta x}{m} = n_1^S x_2 - n_2^S x_1 \qquad (1)$$

where, n_0 – total initial moles present in liquid phase; Δx – change in mole fraction of liquid phase; n_i^S – number of moles of i^{th} component adsorbed on per unit mass of adsorbent; x_i – mole fraction of i^{th} component in binary system. Song et al. [18] modified the above mass balance equation and developed a material balance equation in terms of mole fraction x_i, activity $a_i = x_i \gamma_i$ (γ_i – activity coefficient of i^{th} component in binary system), adsorption equilibrium constant for binary system $K_{1,2}$ and total number of moles adsorbed per unit mass of adsorbent n^S as follows:

$$\frac{n_0 \Delta x}{m} = \frac{n^S \left(K_{1,2} a_1 x_2 - a_2 x_1 \right)}{K_{1,2} a_1 + a_2} \qquad (2)$$

Eqs. 1 and 2 were used to determine adsorption equilibrium constants ($K_{1,2}$) of the three binary systems, as described in greater details subsequently.

***Analytical method: ^{1}H NMR analysis*:** The gross conversion of triglycerides in oil blend was determined by ^{1}H NMR (Nuclear Magnetic Resonance) spectroscopy

(Bruker Advance III HD Ascend 600 MHz) using $CDCl_3$ (Merck, India) as a solvent with TMS (tetramethylsilane) as internal standard [13,19]. Following equation was used to calculate the gross molar conversion of triglycerides to biodiesel [20,21]: $X = \left(2 \times A_{ME}\right) \times 100 \Big/ \left(3 \times A_{\alpha - CH_2}\right)$, where, A_{ME} – the singlet peak at 3.6 ppm which represents the methyl esters protons and $A_{\alpha - CH_2}$ – the multiplet peaks at 2.3 ppm which represents the methylene protons.

***HPLC analysis*:** Triolein and methyl oleate standards were procured from Sigma–Aldrich, USA. Acetonitrile and acetone (purity 99.9%, HPLC grade) were procured from Merck, India. The calibration plots for methyl acetate, triolein, triacetin and methyl oleate were prepared using HPLC (Agilent Technologies, Model: 1220, Infinity LC) equipped with Agilent Eclipse XDB C–18 column (dimensions: 3 mm × 150 mm, 5–micron) and RI detector (Refractive Index, Agilent Technologies, Model: 1260, Infinity). Samples were analysed using mobile phase of acetonitrile: acetone (70:30) with flow rate of 1 mL/min. Sample was prepared by dissolving 1 mL of binary mixture in 10 mL of mobile phase and further diluted in 1:2 ratios (500 µL of diluted sample in 500 µL of mobile phase) and analysed in HPLC after filtration through 0.22–micron syringe filter.

6.3 Langmuir–Hinshelwood–Hougen–Watson (LHHW) kinetic model for interesterification reaction

Reactions with heterogeneous catalyst involve adsorption of one or more reactants on the active sites of the catalyst surface. Subsequently, reaction occurs between either two adsorbed species, or one species in adsorbed form and other in free form in bulk medium. The resulting product is in adsorbed form, which is then desorbed

from catalyst surface into the bulk medium, which makes the active catalyst site vacant for adsorption of next reactant molecules. As noted earlier, Langmuir–Hinshelwood–Hougen–Watson (LHHW) mechanism based kinetic model has been used in present study. The interesterification process involves three stepwise elementary conversions: (1) first triglycerides to diglycerides, (2) diglycerides to monoglycerides, and (3) monoglycerides to glycerol. In present study, the kinetic expressions have been developed on the basis of overall reaction of triglyceride to esters – as the intermediates are highly unstable and determination of their adsorption coefficients and time profiles of concentration is highly error–prone. Thus, the steps of interesterification reaction based on LHHW model involving equilibrium constants are as follows:

Step 1: Adsorption of reactants

$$* + MA \rightleftarrows MA^* \qquad K_{MA} = \frac{[MA^*]}{[MA][*]_f} \qquad (3)$$

$$* + T \rightleftarrows T^* \qquad K_T = \frac{[T^*]}{[T][*]_f} \qquad (4)$$

Step 2: Surface reaction

$$3MA^* + T^* \rightleftarrows 3F^* + TA^* \qquad K_{ov} = \frac{k_1}{k_1'} \qquad (5)$$

Step 3: Desorption of products

$$F^* \rightleftarrows F + * \qquad K_F = \frac{[F^*]}{[F][*]_f} \qquad (6)$$

$$TA^* \rightleftarrows TA + * \qquad K_{TA} = \frac{[TA^*]}{[TA][*]_f} \qquad (7)$$

Different notations are: MA – methyl acetate; T – triglyceride; F – fatty acid methyl ester or biodiesel; TA – triacetin, k_1 – forward reaction rate constant, k_1' – backward

reaction rate constant, K – equilibrium constant, $*$ – free active site on catalyst surface.

Rate expression for reaction between adsorbed species on catalyst surface is written as:

$$-r_T = k_1\left[MA^*\right]\left[T^*\right] - k_1^{'}\left[F^*\right]\left[TA^*\right] \tag{8}$$

$$-r_T = k_1\left\{\left[MA^*\right]\left[T^*\right] - \frac{1}{K_{ov}}\left[F^*\right]\left[TA^*\right]\right\} \tag{9}$$

Adsorbed species concentrations can be converted to bulk concentration using equilibrium correlations at equilibrium condition

$$-r_T = k_1\left\{K_{MA}K_T\left[MA\right]\left[T\right] - \frac{K_F K_{TA}}{K_{ov}}\left[F\right]\left[TA\right]\right\}\left[*\right]_f^2 \tag{10}$$

The value of $\left[*\right]_f$ can be find out using site balance of active sites:

$$\left[*\right]_f + \left[*\right]_o = 1 \tag{11}$$

$$\left[*\right]_f + \left[MA^*\right] + \left[T^*\right] + \left[F^*\right] + \left[TA^*\right] = 1 \tag{12}$$

At steady state condition, the rate of formation of adsorbed species is same as their rate of consumption, thus converting the concentration of adsorbed species to bulk concentration

$$\left[*\right]_f\left\{1 + K_{MA}\left[MA\right] + K_T\left[T\right] + K_F\left[F\right] + K_{TA}\left[TA\right]\right\} = 1 \tag{13}$$

Thus,

$$\left[*\right]_f = \frac{1}{1 + K_{MA}\left[MA\right] + K_T\left[T\right] + K_F\left[F\right] + K_{TA}\left[TA\right]} \tag{14}$$

Therefore,

$$-r_T = \frac{k_1\left\{K_{MA}K_T\left[MA\right]\left[T\right] - \frac{K_F K_{TA}}{K_{ov}}\left[F\right]\left[TA\right]\right\}}{\left\{1 + K_{MA}\left[MA\right] + K_T\left[T\right] + K_F\left[F\right] + K_{TA}\left[TA\right]\right\}^2} \tag{15}$$

^{1}H NMR analysis of aliquots drawn from reaction mixture gives time profiles of triglyceride conversion. The time profiles of methyl acetate, biodiesel or FAME and triacetin were calculated from reaction (eq. 5) using stoichiometry. The eq. 15 has six unknown entities, viz. k_1, K_{MA}, K_T, K_F, K_{TA} and K_{ov}. The values adsorption equilibrium constants, viz. K_{MA}, K_T, K_F and K_{TA}, were determined experimentally as explained in previous section. Eq. 15 after substitution of numerical values of adsorption equilibrium constants was solved in MATLAB R2016b using Runge–Kutta 4th order method on MATLAB (ODE solver) as IVP (initial value problem) coupled with Genetic Algorithm (GA) solver. In this approach, the numerical values of kinetic constants are selected randomly by GA solver (within specified bound limits) to generate simulated (or numerical) profile of triglyceride. The numerical profile is then compared with experimental profile of triglyceride conversion, and root mean square error between experimental and generated profile is calculated. The objective function (Obj) is defined as[16]: $Obj = \min\left(\sum_{i=1}^{n} er_i\right)$, where, n is the number of experimental data points for concentrations of triglycerides. The error (er) is defined as: $er_i = \left[\left(T_i^{\exp}\right)^2 - \left(T_i^{\text{model}}\right)^2\right]^{1/2}$ The final numerical solution from ODE solver was selected for which the objective function is minimum.

6.4 Results and discussion

6.4.1 Statistical optimization of interesterification parameters

The process optimization for interesterification reaction was carried out in presence of ultrasound using CCD design. The experimental set and corresponding conversion at the end of 1 h reaction is listed in Table 6.1 (B). The experimental conversion results depicted in Table 6.1 (B) are the average of two consecutive

experimental runs. The experimental results were fitted to quadratic model using coded values of process parameters yields the following reaction:

$$Y = 85.30 + 12.76C - 1.28M - 17.38T - 15.79C^2 - 13.27M^2 - 19.77T^2 + 4.83M \times C + 6.35T \times C - 1.50T \times M$$

Table 6.1 (B) shows a close match between experimental and model–predicted values of triglyceride conversion suggesting the selected model fits satisfactory to the experimental results. The regression coefficient values, viz. R^2 = 0.9930; R^2 (predicted) = 0.99.48; R^2 (adjusted) = 0.9889 also corroborated the same result.

Table 6.2: Statistical analysis of experimental results

(A) Estimated regression coefficients for % triglyceride conversion

Term	Coefficients	SE coeff	*t*–stat	*p*–value
Constant (β)	85.30	0.09	960.66	0
Catalyst (C)	12.76	0.08	156.29	0
Molar ratio (M)	–1.28	0.08	–15.67	0.001
Temperature (T)	–17.38	0.08	212.79	0
Catalyst × Catalyst (C^2)	–15.79	0.16	–101.24	0
Molar ratio × Molar ratio (M^2)	–13.27	0.16	–85.19	0
Temperature × Temperature (T^2)	–19.77	0.16	–126.92	0
Molar ratio × Catalyst (MC)	4.83	0.09	52.84	0
Temperature × Catalyst (TC)	6.35	0.09	69.54	0
Temperature × Molar ratio (TM)	–1.50	0.09	–16.43	0

R^2 = 99.30%; R^2 (pred) = 99.48%; R^2 (adj) = 98.89%

(B) Analysis of variance (ANOVA) for interesterification reaction

Source	Degrees of freedom	Sq SS	F–value	*p*–value
Regression	9	13968.6	2326.62	0
Linear	3	4665.2	2331.12	0
Square	3	8776.6	4385.49	0
Interaction	3	526.8	263.25	0
Residual Error	10	0.7	—	—
Lack–of–Fit	5	0.4	1.26	0.403
Pure Error	5	0.3	—	—
Regression	19	13969.3	—	—

The values of different coefficients of quadratic model such as linear, square and interaction, along with corresponding *p*– and *t*–values are listed in Table 6.2 (A). Table 6.2 (B) lists the ANOVA (analysis of variance) of the selected CCD model. The

t–stat value and *p*–value signifies the coefficient as well as corresponding parameter of the model. The parameter or coefficients having *p*–value < 0.05, were considered to be significant having their direct impact on the yield of interesterification reaction. Finally, the *p*–value and *F*–value of Lack–of–fit were found to be 0.403 and 1.26, respectively, suggesting that Lack–of–Fit was insignificant as compared to the pure error or in other words the model was significant.

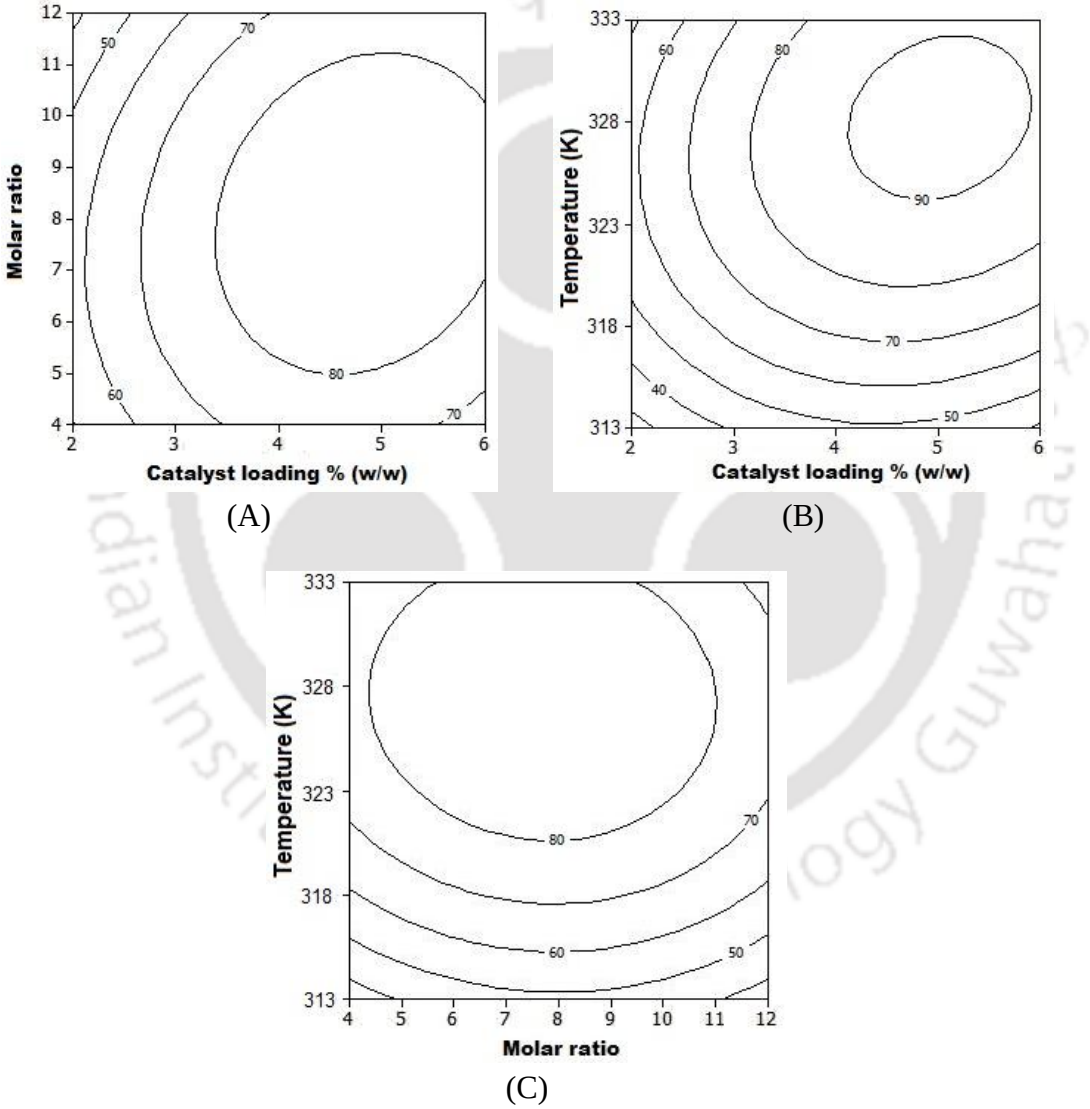

(A) (B)

(C)

Figure 6.1: Contour plots depicting interaction between the process parameters in interesterification process (a) molar ratio *vs* catalyst loading %(w/w); (b) Temperature (K) *vs* catalyst loading %(w/w) and (c) Temperature (K) *vs* molar ratio

The contour plots shown in Fig. 6.1, depicts the interaction between any two process parameters holding third variable at its centre point. The innermost contours in contour plots predicts the maximum triglyceride conversion.

The quadratic model was used to obtain the set of values of parameters which gave the optimum triglyceride conversion of 94.08% are as follows: catalyst loading = 5.03% (w/w); molar ratio = 8.04; temperature = 328.2 K. The validation experiment was performed using the predicted optimum conditions by the model resulted in 94.85 ± 0.83% triglyceride conversion into biodiesel, which validated the predicted statistical design. Fig. 6.2 shows the representative ^{1}H NMR spectrum which was used to calculate the triglyceride conversion, at the end of 1 h interesterification reaction carried out at optimum conditions.

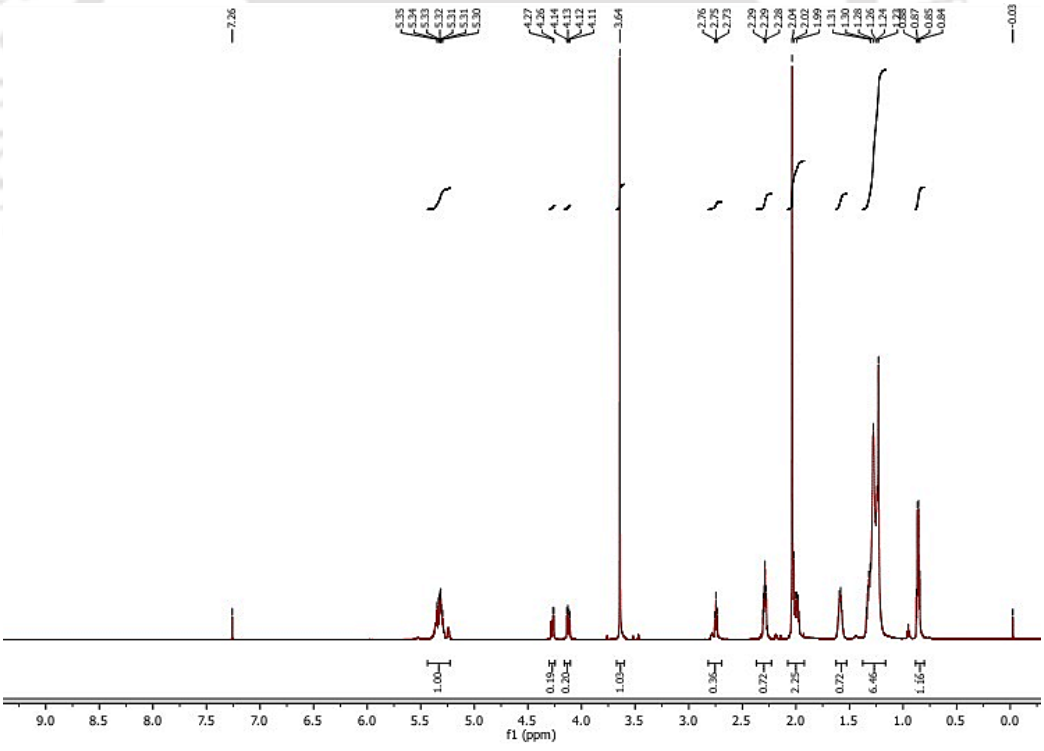

Figure 6.2: ^{1}H NMR spectrum of interesterification reaction with mixed non–edible oil and methyl acetate at optimised conditions

6.4.2 Results of adsorption experiments on catalyst surface

The results of adsorption of three pairs of non–reactive species were analysed using method of Song et al. [18]. The activity coefficients of three binary systems (methyl acetate – triacetin; methyl acetate – methyl oleate and methyl oleate – triolien) were calculated using NRTL (Non–random Two Liquid) model. The binary parameters necessary for calculating activity coefficients are taken from the databank of ASPEN plus (version 8.0) and are listed in Table 6.3. The relative adsorption equilibrium coefficients of methyl acetate, triolein, triacetin and methyl oleate were determined from three binary systems of methyl acetate/ triacetin; methyl acetate/ methyl oleate and methyl oleate/ triolien. Fig. 6.3 (A)–(C) represents the mass balance of binary system and model predicted adsorption data calculated from eq. 2.

Table 6.3: Binary parameters of NRTL[#] model for mixtures containing methyl acetate (1), triolein (2), triacetin (3) and methyl oleate (4), obtained from ASPEN plus 8.0

(i–j)	a_{ij}	a_{ji}	b_{ij} **(K)**	b_{ji} **(K)**	α_{ij}
(1–2)	–	–	–100.82	–156.61	0.3
(1–3)	–	–	–516.27	778.93	0.3
(1–4)	–	–	791.33	–346.49	0.3
(2–3)	–	–	410.24	2718.32	0.3
(2–4)	–	–	1019.27	–614.87	0.3
(3–4)	–	–	966.19	440.94	0.3

[#] NRTL model expression: $\ln\gamma_i = \dfrac{\sum_{j=1}^{m}\tau_{ji}G_{ji}x_j}{\sum_{l=1}^{m}G_{li}x_l} + \sum_{j=1}^{m}\dfrac{x_jG_{ij}}{\sum_{l=1}^{m}G_{lj}x_l}\left(\tau_{ij} - \dfrac{\sum_{r=1}^{m}x_r\tau_{ri}G_{ri}}{\sum_{l=1}^{m}G_{lj}x_l}\right)$

where $G_{ji} = \exp\left(-\alpha_{ji}\tau_{ji}\right)$ and $\tau_{ji} = a_{ij} + b_{ij}/T$

Table 6.4 represents the values of parameters $K_{1,2}$ and n^S obtained through fitting the results of isothermal adsorption experiments to mass balance (eq. 2). Results in Table 6.4 reveal that extent of adsorption of the four non–reactive species is in the order: methyl acetate > methyl oleate > triacetin > triolein.

Table 6.4: Data obtained from adsorption experiments

Mixture (1) + (2)	n^S (mol/g)	$K_{1,2}$	Cumulative error[$] (%)
Methyl Acetate (1) +Triacetin (2)	0.008	3.75	4.91
Methyl Acetate (1) +Methyl Oleate (2)	0.002	2.14	4.38
Methyl Oleate (1) + Triolein (2)	0.002	1.84	2.01

[$] Cumulative error $= \frac{100}{N} \times \sum_{i=1}^{N} \left\{ \left| [n_0 \Delta x / m]_i^{\exp} - [n_0 \Delta x / m]_i^{cal} \right| \Big/ [n_0 \Delta x / m]_i^{\exp} \right\}$

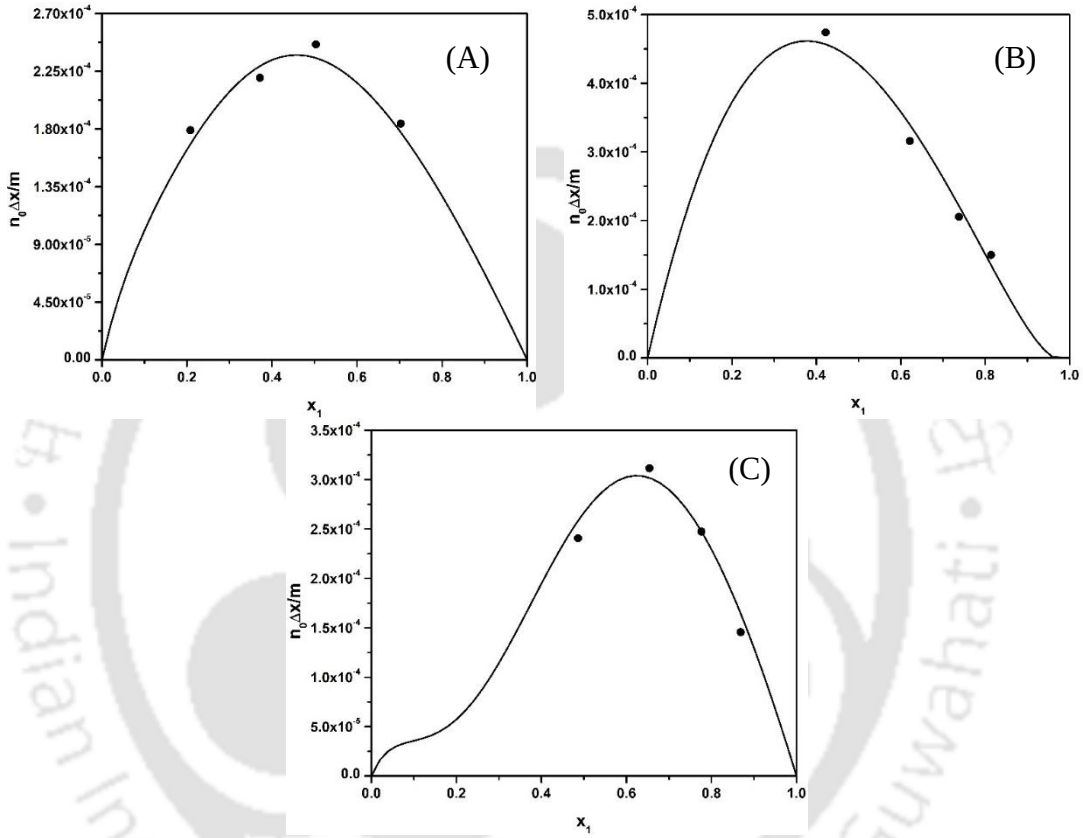

Figure 6.3: Results of adsorption experiments for three binary systems. (A) methyl acetate (1) + triacetin (2); (B) methyl acetate (1) + methyl oleate (2); and (C) methyl oleate (1) + triolein (2).

Equilibrium constants K_T, K_F and K_{TA} were expressed in the form of ratio with respect to K_{MA} as: $K_F = 0.47\ K_{MA}$; $K_{TA} = 0.27\ K_{MA}$ and $K_T = 0.25\ K_{MA}$. Substituting these values in eq. 15, results in following kinetic expression with only three unknowns k_1, K_{MA} and K_{ov}.

$$-r_T = \frac{k_1 \left\{ K_{MA} \times 0.25 K_{MA} [MA][T] - \frac{0.47 K_{MA} \times 0.27 K_{MA}}{K_{ov}} [F][TA] \right\}}{\left\{ 1 + K_{MA}[MA] + 0.25 K_{MA}[T] + 0.47 K_{MA}[F] + 0.27 K_{MA}[TA] \right\}^2} \qquad (16)$$

On simplifying the above equation, the final form of equation is

$$-r_T = \frac{k_1 K_{MA}^2 \left\{ 0.25[MA][T] - \frac{0.1269}{K_{ov}}[F][TA] \right\}}{\left\{ 1 + K_{MA}[MA] + 0.25K_{MA}[T] + 0.47K_{MA}[F] + 0.27K_{MA}[TA] \right\}^2} \qquad (17)$$

Eq. 17 was used to solve in MATLAB and to determine the rate constants as stated in previous section.

6.4.3 Kinetic analysis of interesterification reaction

The kinetic analysis of interesterification reaction was carried out at optimised conditions predicted by statistical design in test (with ultrasound) and control (with mechanical agitation) categories by fitting the experimental profiles of triglyceride conversion to eq. 17.

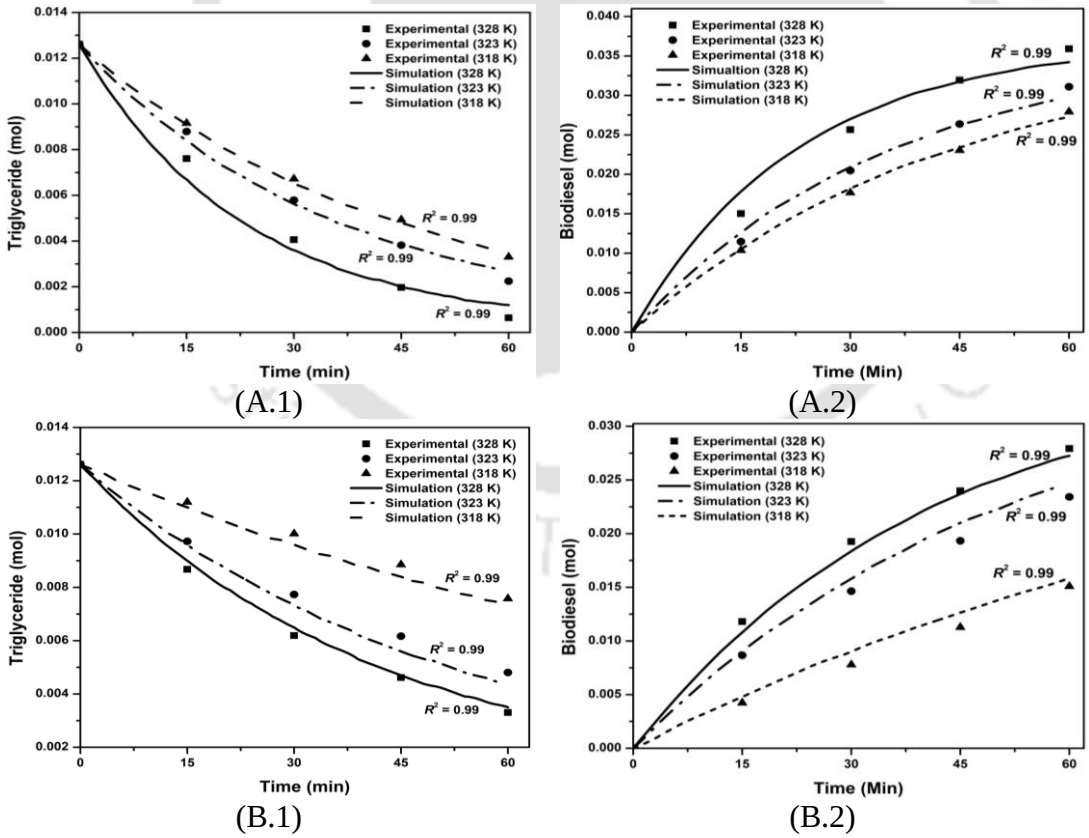

Figure 6.4: Experimental and simulated profiles of triglyceride (1) and biodiesel (2) in interesterification. (A) test (ultrasound–assisted) experiments; (B) control (mechanical agitation) experiments

To determine the activation energy (E_a), as stated earlier, the experiments were also conducted at 318 K and 323 K and the rate expression (eq. 17) was also solved for these process conditions. Fig. 6.4 represents experimental and simulated profiles of triglyceride and biodiesel for both test and control experiments different temperatures. As seen in Fig. 6.4, the close match of the experimental and simulated profiles of reactants and products in interesterification under control and test conditions (as indicated by regression coefficient $R^2 \sim 0.99$) signifies the validation of LHHW kinetic model.

Table 6.5: Kinetic rate constant and equilibrium constant for interesterification reaction

Temperature (K)	k_1 (min^{-1})	K_{MA}	K_{ov}	Error (Obj function)	E_a (kJ/mol)
Test (with sonication) category					
328	4.26×10^{-2}	18.11	38.17	2.53×10^{-3}	
323	2.56×10^{-2}	20.16	33.18	2.19×10^{-3}	66.97
318	1.96×10^{-2}	21.86	29.63	1.96×10^{-3}	
Control (with mechanical agitation) category					
328	2.08×10^{-2}	20.85	33.99	2.36×10^{-3}	
323	1.51×10^{-2}	24.17	30.32	2.04×10^{-3}	89.04
318	7.46×10^{-3}	25.59	28.88	1.89×10^{-3}	

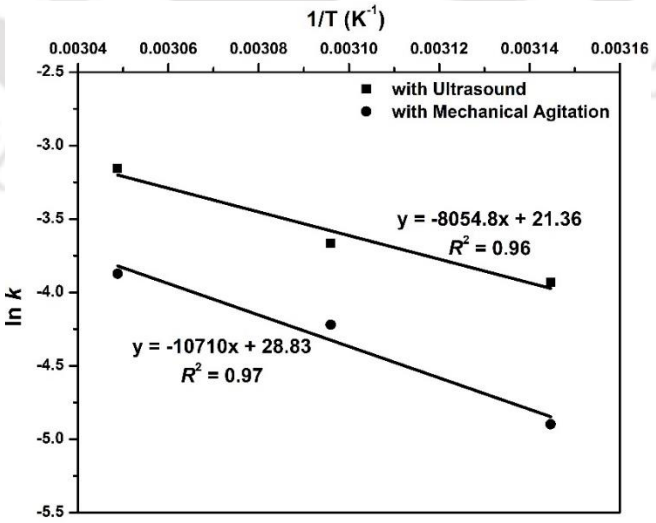

Figure 6.5: Arrhenius plot of interesterification reaction under control (mechanical agitation) and test (ultrasound assisted) categories

The values of the model parameters obtained by fitting of experimental and simulated profiles, viz. K_{MA}, K_{ov} and k_1, in both test and control experiments are listed in Table 6.5. Fig. 6.5 depicts the Arrhenius plot (ln k vs. 1/T) for control and test experiments. The kinetic analysis of interesterification reaction through LHHW model revealed several trends and the major findings of analysis with plausible explanations are as follows:

1. The values of kinetic rate constants (k_1) increase with temperature for both test and control experiments, as seen from Table 6.5. This is essentially a manifestation of enhanced mass transfer (liquid–solid) between the reaction mixture and Cu_2O catalyst resulting in higher triglyceride conversion. Furthermore, the overall kinetic rate constant (k_1) for test experiments employing sonication was higher (two–fold rise) than control experiments employing mechanical agitation at all three reaction temperatures. This essentially can be attributed to strong micro–turbulence generated due to sonication, which uniformly distributes Cu_2O particles in reaction mixture and also eliminates the mass transfer barriers [22,23]. The shock waves generated by transient cavitation bubbles help in faster desorption of the product from catalyst active sites which enhances their accessibility for reactants [23,24].
2. Table 6.5 showed that the adsorption equilibrium constant (K_{MA}) decreases with increase in temperature, i.e. as reaction temperature increases the extent of adsorption decreases. Basically adsorption is favoured at lower temperatures and desorption is favoured at higher temperatures. Thus, increase in reaction temperature decreases the value of K_{MA}. This decrease in adsorption of reactant and product was further augmented with application of ultrasound as compared with mechanical agitation as seen from Table 6.5. This was probably due to the

shock waves generated during the transient collapse of bubbles [23, 25]. Random motion of the catalyst particles in these shock waves can cause desorption of the adsorbed molecules as also demonstrated by Midathana and Moholkar [26] and Chakma and Moholkar [27].

3. The equilibrium rate constant (K_{ov}) increased with increase in temperature as noted from Table 6.5. This means that the rate of backward reaction decreased relatively with increase in temperature and equilibrium shifted towards forward direction of this reversible reaction. The value of K_{ov} was further boosted with application of ultrasound as compared to mechanical agitation. The possible reason for enhancement of K_{ov} values with application of ultrasound could be higher desorption of product molecules in test experiments (induced by shock waves generated by transient bubbles) as compared to control experiments. This phenomenon essentially leaves less opportunity for the adsorbed product molecules to undergo backward reaction. Net manifestation of these phenomena is relatively reduced rate of backward reaction and larger K_{ov} values with higher reaction yield.
4. Application of sonication to interesterification reaction resulted in marked reduction of activation energy – as indicated by activation energy of 89.04 kJ/mol in control experiments that reduces to 66.97 kJ/mol in test experiments. Maddikeri et al. [5] have reported activation energy of 58.17 kJ/mol for ultrasound–assisted interesterification of waste cooking oil with homogeneous base (KOH) catalyst. In present study, the activation energy in test experiments was slightly higher than that reported by Maddikeri et al. [5]. This result is attributed to use of heterogeneous catalyst in present study, which increases the mass transfer barriers in the reaction system.

6.5 Conclusion

This study has attempted to investigate mechanistic features of interesterification of blend of non–edible oils with heterogeneous Cu_2O catalyst, and the intensification of this reaction with application of sonication. The approach adopted in this study essentially involves correlation of experimental results with a kinetic model using Genetic Algorithm. Langmuir–Hinshelwood–Hougen–Watson (LHHW) mechanism based kinetic model has been used in present study that involves adsorption of both reactants on the catalyst. Equilibrium adsorption constants for different species in reaction mixture were determined using the NRTL model. This analysis showed that adsorption constants of reacting species followed the order: methyl acetate > methyl oleate > triacetin > triolein. Fitting of experimental profiles of triglyceride and biodiesel (FAME) to the kinetic model revealed two–fold rise in overall rate constant interesterification (from 2.08×10^{-2} to 4.26×10^{-2} min^{-1}) with application of ultrasound. Moreover, increase in reaction temperature with simultaneous application of ultrasound lowered the rate of backward reaction, which is attributed to faster desorption of product molecules due to the shock waves generated by transient cavitation bubbles. Arrhenius analysis of reaction kinetics also revealed significant reduction in the activation energy of interesterification, which is also attributed to strong microturbulence generated by sonication that reduces the mass transfer barriers in the reaction mixture.

References

[1] Sustere, Z., Murnieks, R. and Kampars, V., 2016. Chemical interesterification of rapeseed oil with methyl, ethyl, propyl and isopropyl acetates and fuel properties of obtained mixtures. Fuel Processing Technology, 149, 320–325.

[2] Petrauskaite, V., De Greyt, W., Kellens, M. and Huyghebaert, A., 1998. Physical and chemical properties of trans-free fats produced by chemical interesterification of vegetable oil blends. Journal of the American Oil Chemists' Society, 75(4), 489–493.

[3] Casas, A., Ramos, M.J. and Pérez, Á., 2011. Kinetics of chemical interesterification of sunflower oil with methyl acetate for biodiesel and triacetin production. Chemical Engineering Journal, 171(3), 1324–1332.

[4] Casas, A., Ramos, M.J. and Pérez, Á., 2011. New trends in biodiesel production: Chemical interesterification of sunflower oil with methyl acetate. Biomass and Bioenergy, 35(5), 1702–1709.

[5] Maddikeri, G.L., Pandit, A.B. and Gogate, P.R., 2013. Ultrasound assisted interesterification of waste cooking oil and methyl acetate for biodiesel and triacetin production. Fuel Processing Technology, 116, 241–249.

[6] Casas, A., Ruiz, J.R., Ramos, M.J. and Pérez, A., 2010. Effects of triacetin on biodiesel quality. Energy & Fuels, 24(8), 4481–4489.

[7] Nelson, L.A., Foglia, T.A. and Marmer, W.N., 1996. Lipase-catalyzed production of biodiesel. Journal of the American Oil Chemists' Society, 73(9), 1191–1195.

[8] Xu, Y., Du, W. and Liu, D., 2005. Study on the kinetics of enzymatic interesterification of triglycerides for biodiesel production with methyl acetate as the acyl acceptor. Journal of Molecular Catalysis B: Enzymatic, 32(5–6), 241–245.

[9] Maddikeri, G.L., Gogate, P.R. and Pandit, A.B., 2014. Intensified synthesis of biodiesel using hydrodynamic cavitation reactors based on the interesterification of waste cooking oil. Fuel, 137, 285–292.

[10] Galia, A., Centineo, A., Saracco, G., Schiavo, B. and Scialdone, O., 2014. Interesterification of rapeseed oil catalyzed by tin octoate. Biomass and Bioenergy, 67, 193–200.

[11] dos Santos Ribeiro, J., Celante, D., Simoes, S.S., Bassaco, M.M., da Silva, C. and de Castilhos, F., 2017. Efficiency of heterogeneous catalysts in interesterification reaction from macaw oil (Acrocomia aculeata) and methyl acetate. Fuel, 200, 499–505.

[12] Deng, X., Fang, Z. and Liu, Y.H., 2010. Ultrasonic transesterification of Jatropha curcas L. oil to biodiesel by a two–step process. Energy Conversion and Management, 51(12), 2802–2807.

[13] Choudhury, H.A., Malani, R.S. and Moholkar, V.S., 2013. Acid catalyzed biodiesel synthesis from Jatropha oil: mechanistic aspects of ultrasonic intensification. Chemical Engineering Journal, 231, 262–272.

[14] Tsai, Y.T., Lin, H.M. and Lee, M.J., 2010. Kinetics of catalytic esterification of propionic acid with methanol over Amberlyst 36. Industrial & Engineering Chemistry Research, 50(3), 1171–1176.

[15] Tsai, Y.T., Lin, H.M. and Lee, M.J., 2011. Kinetics behavior of esterification of acetic acid with methanol over Amberlyst 36. Chemical Engineering Journal, 171(3), 1367–1372.

[16] Lee, S.B., Han, K.H., Lee, J.D. and Hong, I.K., 2010. Optimum process and energy density analysis of canola oil biodiesel synthesis. Journal of Industrial and Engineering Chemistry, 16(6), 1006–1010.

[17] Kipling, J.J., 2017. Adsorption from Solutions of Non–electrolytes. Academic

Press.

[18] Song, W., Venimadhavan, G., Manning, J.M., Malone, M.F. and Doherty, M.F., 1998. Measurement of residue curve maps and heterogeneous kinetics in methyl acetate synthesis. Industrial & Engineering Chemistry Research, 37(5), 1917–1928.

[19] Choudhury, H.A., Goswami, P.P., Malani, R.S. and Moholkar, V.S., 2014. Ultrasonic biodiesel synthesis from crude Jatropha curcas oil with heterogeneous base catalyst: mechanistic insight and statistical optimization. Ultrasonics Sonochemistry, 21(3), 1050–1064.

[20] Gelbard, G., Bres, O., Vargas, R.M., Vielfaure, F. and Schuchardt, U.F., 1995. ^{1}H nuclear magnetic resonance determination of the yield of the transesterification of rapeseed oil with methanol. Journal of the American Oil Chemists' Society, 72(10), 1239–1241.

[21] Knothe, G., 2001. Analytical methods used in the production and fuel quality assessment of biodiesel. Transactions of the ASAE, 44(2), 193–200.

[22] Moholkar, V.S., Sable, S.P. and Pandit, A.B., 2000. Mapping the cavitation intensity in an ultrasonic bath using the acoustic emission. AIChE Journal, 46(4), 684–694.

[23] Malani RS, Goyal A, Moholkar VS. Ultrasound–Assisted Biodiesel Synthesis: A Mechanistic Insight. In Agarwal AK, Agarwal RA, Gupta T, Gurjar BR. Biofuels. Springer, Singapore. 2017:103–135.

[24] Shah, Y.T., Pandit, A.B., Moholkar, V.S., 1999. Cavitation Reaction Engineering, Plenum Press, New York.

[25] Choudhury, H.A., Srivastava, P. and Moholkar, V.S., 2014. Single-step ultrasonic synthesis of biodiesel from crude Jatropha curcas oil. AIChE Journal, 60(5), 1572–1581.

[26] Midathana, V.R. and Moholkar, V.S., 2009. Mechanistic studies in ultrasound–assisted adsorption for removal of aromatic pollutants. Industrial & Engineering Chemistry Research, 48(15), 7368–7377.

[27] Chakma, S. and Moholkar, V.S., 2011. Mechanistic features of ultrasonic desorption of aromatic pollutants. Chemical Engineering Journal, 175, 356–367.

CHAPTER 7

OVERVIEW AND SCOPE FOR FUTURE WORK

Chapter 7

Overview and Scope for Future Work

7.1 Overview

Last few decades, remarkable growth of biofuels was observed worldwide, due to fluctuating crude oil prices, incremental increase in energy demand and environmental pollution. Moreover, rising issue of global warming and greenhouse gases, has been an important driving factor for use of biofuel especially in transportation sector. To counter these issues strong policies have been implemented worldwide. Many countries including India have made strong framework for blending of biofuel with conventional fuel. To achieve these targets, Government of India has proposed and implemented many schemes which promote production and use of biofuel. Despite these incentives, implementation of 20% blends of ethanol-gasoline and biodiesel-diesel by 2022 looks difficult in India [1].

Global biofuel production has grown remarkably from 27.9 Mtoe in 2006 to 82.3 Mtoe in 2016 with an average 14% annual growth rate. As a result of these efforts,

the biofuels today provide around 5% of total road transport fuel globally [2]. However, this is far lesser than the actual potential of biofuel.

Thus, the present thesis work was undertaken with an aim of developing a new methodology and alternative feedstock (blend of non-edible oils) for biodiesel synthesis that boosts both viability and profitability of the process. Moreover, the thesis has also made attempts for developing new methodologies of intensification of the kinetics of biodiesel production with relatively new technique of sonication. The major findings of present thesis addressing different facets of the ultrasound-assisted biodiesel synthesis are summarised below. These results, when viewed at a glance, give a coherent and interesting picture of the potential of ultrasound-assisted biodiesel production processes.

- Chapter 1 gives the general introduction of the thesis theme and the literature review on various aspects of biodiesel synthesis with ultrasound. In this chapter, a picture of energy sector scenario (especially, in terms of CO_2 enhancement, oil production and biofuel production) worldwide as well as India's viewpoint is discussed with several statistical data. In this chapter, the efforts on renewable energy in India and India's biofuels policy were also discussed. With this motivation the aim and scope of present thesis was described. At the same time, in view of the theme of the thesis, the literature on biodiesel synthesis with heterogeneous catalyst (alkali, acid and enzymatic routes) using ultrasound-assisted techniques has also been reviewed. Also a general introduction to basic principles of ultrasound and cavitation is provided for convenience of readers who are new in this area.
- Chapter 2 presents studies in mechanistic analysis of ultrasound–assisted biodiesel synthesis with Cu_2O catalyst and mixed oil feedstock using continuous (packed bed) and batch (slurry) reactors. The optimum conditions for transesterification

have been determined using statistical experimental design in packed bed catalytic reactor. The kinetic constants of different steps of transesterification process have been determined using kinetic model based on Eley–Rideal mechanism coupled to time profiles of reactants and products of transesterification in batch slurry reactors. The batch experiments have been performed at optimum conditions predicted by statistical experimental design: alcohol/oil molar ratio = 10.6, temperature = 335.5 K, catalyst concentration = 7.25 wt% oil. Sonication enhanced the kinetics of reaction steps of transesterification process, but its effect on methanol adsorption on Cu_2O catalyst was adverse. The activation energy of overall transesterification process was 90.14 kJ/mol; while, the sum total of activation energies of the three reaction steps of triglyceride conversion was 40.98 kJ/mol. These results essentially point to strong mass transfer influence on Cu_2O–catalyzed transesterification process, even in presence of sonication.

- Chapter 3 has presented the physical insight into ultrasound–assisted biodiesel production using heterogeneous base catalyst and mixed non–edible oils. In this chapter, the ultrasound–assisted biodiesel production from mixed feedstock of non–edible oils in presence of KI impregnated ZnO catalyst in batch reactor was investigated. The production was optimized by using two approaches (1) feedstock optimization and (2) process parameters optimization. The maximum triglyceride conversion of 92.35 ± 1.08% was achieved at optimized conditions of catalyst loading = 7 % (w/w); alcohol/oil molar ratio = 11.68:1 and reaction temperature = 332 K. Transesterification process with mechanical agitation was used as base case for identification of role of sonication in the process. The transesterification process was analysed for kinetic behaviour using pseudo first order kinetics and Eley–Rideal mechanism based model. Overall activation energy of transesterification process for

mechanically agitated and ultrasound–assisted systems was calculated as 135.4 and 123.65 kJ/mol, respectively. However, the sum of activation energies of three reaction steps of Eley–Rideal mechanism (64.69 kJ/mol and 46.63 kJ/mol, for mechanically agitated and ultrasound–assisted system, respectively) was much lower. This discrepancy is attributed to mass transfer limitations in the system, even in presence of sonication.

- Chapter 4 reports ultrasound intensified biodiesel production from mixed non–edible oil feedstock using heterogeneous acid catalyst supported on rubber de–oiled cake. This chapter investigates synthesis of waste–derived heterogeneous acid catalyst from rubber de–oiled cake using sulfuric and chloro–sulfonic acid. The synthesized catalyst was characterized using XRD, XPS, FE–SEM, EDX, BET and acid density titration. Maximum biodiesel yields of 91.2 ± 1.1% and 93.7 ± 1.3% were obtained at molar ratio = 12.8:1; catalyst loading = 8.18% (w/w) and temperature = 336 K in single–step process (duration 3 h) and two–step process (duration 1 h), respectively. Two–step process resulted in lower activation energy of 55.98 kJ/mol, as compared to 69.62 kJ/mol in single–step process. Predominant role of ultrasound in process intensification was observed in two–step process, where sum of activation energies (27.47 kJ/mol) of three individual reaction steps was lower as compared to mechanically agitated system (49.07 kJ/mol). The catalyst retained activity till 3 cycles of re–use.
- In Chapter 5, the studies on ultrasound–assisted biodiesel synthesis using blended feedstock of non–edible oils and commercial immobilized lipase from *Thermomyces lanuginosus*. Optimization of transesterification process with sonication using Box-Behnken statistical design resulted in 90% conversion at alcohol/oil molar ratio = 7.64:1, enzyme loading = 3.55% (w/w) and temperature = 36^{o}C. 10% v/v water addition to reaction mixture boosted biodiesel yield from 90% to 94%. Activation

energy of transesterification reduced from 124.4 kJ/mol (under mechanical agitation) to 100.4 kJ/mol with application of sonication. 10% v/v addition of water to reaction mixture further reduced activation energy to 78.7 kJ/mol. Finally, the recycled enzyme showed good retention of activity up to 6 cycles in presence of ultrasound, which further enhanced with water addition to reaction mixture.

- Chapter 6 reports investigations in Biodiesel production by ultrasonic interesterification of non–edible oil blends. Interesterification of triglycerides (with methyl acetate) has been investigated as an alternative to transesterification (with methanol) for synthesis of biodiesel. An attempt is made to identify mechanistic features of ultrasound-assisted interesterification of blend of non–edible oils with solid Cu_2O catalyst with approach of analysing experimental results vis-à-vis a kinetic model coupled with Genetic Algorithm. The kinetic model is based on Langmuir–Hinshelwood–Hougen–Watson (LHHW) mechanism. Equilibrium adsorption constants for different species were determined using NRTL model. Sonication of solid-liquid heterogeneous reaction mixture caused ~ 2-fold enhancement (from 2.08×10^{-2} to 4.26×10^{-2} min^{-1}) in interesterification kinetics with lowering of activation energy (from 89.04 kJ/mol in control experiments to 66.97 kJ/mol in test experiments). Rise in reaction temperature with simultaneous sonication causes reduction in adsorption constant of various species with rise in overall equilibrium constant. This result was attributed to microturbulence generated by sonication that enhanced mass transfer. Shock waves generated by transient cavitation bubbles induce desorption of product species that lowered the rate of backward reaction.

The comparative analysis of all the process carried out in present thesis is tabulated in Table 7.1, which highlights the major findings at a glance.

Table 7.1: Comparative analysis of studies in present thesis

Chapter	Feedstock Oil Composition (volume)	Catalyst	Optimum operating conditions	%Conversion	Reusability of Catalyst	E_a (kJ/mol)
2	Jatropha (15%), castor (25%), rubber seed (20%), cotton seed (25%), waste cooking (15%)	Cu_2O	Molar ratio = 10.62:1; Temperature = 335.5 K; Ultrasound = 35 kHz, 35 W; For packed bed reactor: Catalyst packing height = 35.61 mm and residence time = 33.5 min; For batch reactor: Catalyst loading = 7.25 wt%	89.95 ± 0.78% (packed bed) and 98.3± 0.52% (batch reactor in 1 h duration)	Not Tested	90.14 in batch process
3	Jatropha (5%), castor (5%), rubber seed (50%), palm (20%), waste cooking (20%)	KI/ZnO	Molar ratio = 11.68:1; Temperature = 332 K; Ultrasound = 35 kHz, 35 W; Catalyst loading = 7 wt%,	92.35 ± 1.08% at the end of 1 h	Catalyst retained ~ 50% of its initial activity after 5 cycles	123.65 and 135.40 for test and control conditions
4	Jatropha (15%), castor (10%), rubber seed (30%), palm (20%), waste cooking (25%)	Chloro-sulfonated carbon	Molar ratio = 12.8:1; Temperature = 336 K; Ultrasound = 35 kHz, 35 W; Catalyst loading = 8.18 wt%,	91.2 ± 1.1% in single–step (3 h) and 93.7 ± 1.3% in two–step (1 h).	Catalyst loses ~ 40% and ~ 10% activity in single and two step process after 3 cycles, respectively.	69.62 and 55.98 for single and two step test conditions
5	Jatropha (15%), rubber seed (25%), palm (30%), waste cooking (30%)	Immobilized lipase on immobead 150	Molar ratio = 7.64:1; Temperature = 309 K; Ultrasound = 35 kHz, 35 W; Duty cycle = 40%; Enzyme loading = 3.55 wt%, water addition = 10% (v/v of alcohol)	90.1 ± 1.1% (without water) and 94.4 ± 0.8% (with 10% water addition) duration 2 h	Retains ~50% of initial activity after 6 cycles in TW category	100.35 and 78.73 for test and TW (test + Water) conditions
6	Jatropha (10%), castor (10%), rubber seed (20%), palm (40%), waste cooking (20%)	Cu_2O	Molar ratio = 8.04:1; Temperature = 328 K; Ultrasound = 35 kHz, 35 W; Catalyst loading = 5.03 wt%,	94.85 ± 0.83% duration 1 h	Not Tested	89.04 and 66.97 for control and test conditions

Test – Ultrasound-assisted system, Control – Mechanically agitated system at 400 rpm

On a whole, this thesis has attempted to investigate diverse facets of ultrasound-assisted process for biodiesel production from blended non-edible oil feedstock from both fundamental and practical viewpoints. The problems associated with conventional heterogeneously catalysed transesterification were overcome with application of ultrasound, which enhances the mass transfer between the phases.

The interesterification process is an alternate route for biodiesel production and has a great potential in terms of economic viability. The by-product of the process i.e. triacetin has higher commercial value than glycerol and used as food additive, plasticizer, solvent, excipient in pharmaceutical industry as well as anti–knocking agent in gasoline fuel and viscosity index improver in diesel fuel [3,4].

The outcome of present thesis also opens new avenues and opportunities for undertaking future research in this area. Some suggestions in this regard are given below:

7.2 Scope for Future Work

The work presented in this thesis can be extended in many ways which can have focus on further optimization with ultrasound parameters like frequency and intensity or development and use of better solid catalysts or biodiesel synthesis. It is also worth carrying out some of the optimized ultrasonic biodiesel synthesis processes in this work at higher scale. Some suggestions for the future work are as follows:

1. Optimization of ultrasound power and frequency for ultrasound-assisted biodiesel production system, as it directly affects the operating cost of the process and comparison of energy input with the conventional mechanical agitation

2. One can study the mixing number of oil-alcohol in mechanically agitated system and ultrasound-assisted system and improve the mixing number with

optimization of ultrasound power, frequency and location of transducers.

3. Establishing a proper bench scale unit and extending the present experimental work on a larger scale for commercial production of biodiesel.

4. Multi–transducer (source of ultrasound) reactors are necessary while operating at larger scale. Thus, optimization of reactor geometry of pilot scale unit is also necessary.

5. One can study the simultaneous extraction of oil from seed, esterification and trans-esterification with ultrasound.

6. One can use the co-solvent approach to lower mass transfer limitation in the heterogeneously catalysed transesterification/interesterification process.

References

[1] A report on "Energy Statics" from "Central Statistics Office Ministry of Statistics and Programme Implementation, Government of India" available online at http:// www.mospi.nic.in/sites/default/files/publication_reports/ Energy_Statistics_2017r.pdf.pdf (Access on 21st July 2018)

[2] A report on "Statistical Review of World Energy June 2017" from "BP Statistical Review" available online at https://www.bp.com /content/dam/bp/en/corporate/pdf/energy–economics/statistical–review–2017/ bp–statistical–review–of–world–energy–2017–full–report.pdf (Access on 25th June 2018).

[3] Casas, A., Ruiz, J.R., Ramos, M.J. and Pérez, A., 2010. Effects of triacetin on biodiesel quality. Energy & Fuels, 24(8), 4481-4489.

[4] Casas, A., Ramos, M.J. and Pérez, Á., 2011. Kinetics of chemical interesterification of sunflower oil with methyl acetate for biodiesel and triacetin production. Chemical Engineering Journal, 171(3), 1324-1332.

भारतीय प्रौद्योगिकी संस्थान गुवाहाटी
Indian Institute of Technology Guwahati

Annexure A

Determination of Acid Value: Initially alcoholic KOH solution of 0.1N was prepared & standardize against 0.1N oxalic acid. Then 5g of sample and 25 mL of neutral alcohol were added into 250 mL flat bottom flask & the mixture was heated to boiling on hot plate magnetic stirrer with constant stirring so that the complete extraction of acid will takes place by alcohol. ~1mL of phenolphthalein indicator was added and the mixture was cooled to 45-50^{o}C and titrate against alc. KOH solution to the end point (pink colour), which should persist at least for 30 seconds. Following equation was used to determine the acid value: $AV = \frac{56.1 \times N \times V}{W}$; where, AV = Total acidity in mg KOH/g of sample; V = Volume of KOH solution(mL); N = Normality of KOH solution; W = Weight of sample taken.

Determination of Saponification Value (ASTM-D5558 – 95): Initially 0.5 N of HCl solution was prepared and standardized by using 0.5N NaOH solution. To a flat bottom flask accurately weighed oil sample of 5g was taken and mixed with 50 mL of alcoholic KOH. The mixture was refluxed for 1 h for complete saponification. After the completion of saponification, titration of the solution was done with 0.5N HCl, using 0.5 mL of phenolphthalein indicator. A blank determination (without oil sample) was done simultaneously using the same quantity of reagents and the following equation was used to calculate the saponification value: $SV = \frac{(B-S) \times N \times 56.1}{W}$; where, SV = Saponification value of oil in mg KOH/ g of sample; B = volume of titrant (mL) for blank; S = volume of titrant (mL)for sample; N = normality of HCl; 56.1 = MW of KOH; W = weight of sample oil in g.

Annexure B

Table: Properties of oil samples

(A) Crude/ Raw oils

Properties	Castor oil	Jatropha oil	Rubber seed oil	Waste cooking oil	Cotton seed oil	Palm oil
Density (g/mL)	0.986	0.928	0.919	0.989	0.91	0.951
Viscosity at 40^{o}C (mPa-s)	43.9	21.3	24.9	27.4	36.1	33.0
Acid value (mg KOH/g)	1.73	21.18	20.55	4.35	1.68	5.95
Saponification value (mg KOH/g)	177.6	201.3	217.3	198.1	183.8	198.6
Average Molecular weight (g/mol)	956.9	934.3	855.4	868.8	923.9	873.8

(B) After esterification

Properties	Castor oil	Jatropha oil	Rubber seed oil	Waste cooking oil	Cotton seed oil	Palm oil
Viscosity at 40^{o}C (mPa-s)	24.5	12.5	14.6	14.3	22.9	18.6
Acid value (mg KOH/g)	0.36	2.33	2.06	0.71	0.28	0.95
Reduction in acid value (%)	80.0	89.0	90.0	83.7	83.3	84.0

Annexure C

Calculation of catalyst to oil feed ratio (from packed bed to batch reaction)

Weight of fresh glass beads (15 mm packing height)	7.20 g
Weight of glass beads with catalyst thin film (15 mm packing height)	9.32 g
Catalyst weight for film coating (15 mm packing height)	2.12 g
Catalyst weight for film coating (35.61mm packing height)	5.04 g
Methanol/oil mixture volume for hold-up (packed bed reactor)	100 mL
Catalyst to feed ratio	0.0504 g/mL
Methanol/oil mixture volume for batch process	15 mL
Catalyst weight for batch process	0.756 g
Corresponding catalyst weight % (oil)	7.25%

Annexure D

Biodiesel synthesis from refined canola oil

Material: Commercial edible grade Canola oil was procured from local market of Guwahati. Methanol (99%, ACS grade) was procured from Merck, India. Methanol was distilled to get anhydrous methanol.

Method: Biodiesel from Canola oil was synthesised by using the optimum conditions reported in Chapter 2, Section 2.4.3. Briefly, the transesterification reaction mixture comprised of 69.15 mL oil, 30.85 mL methanol and 5 g Cu_2O dried powder. This corresponded to alcohol/oil molar ratio of 10.6:1 with catalyst concentration of 7.25% (w/w). The reaction was carried out in presence of ultrasound bath (Elma Transsonic T–460 type, Germany, capacity: 2 L, frequency: 35 kHz, power: 35 W) and 336 K in a two-neck round bottom flask fitted with a reflux condenser. The temperature of water in the ultrasound bath was maintained at desired level using an immersed heating element coupled with temperature indicator and controller. After the reaction, the reaction mixture was centrifuged to separate the catalyst and glycerol from biodiesel at 6000*g* for 15 min at 298 K. The separated biodiesel layer was given hot water wash to remove traces of alcohol. The traces of water left out in the biodiesel layer were removed using prior dried activated silica (230–400 mesh, Merck, India). The final biodiesel was filtered using Whatmann 40 filter paper to remove the silica particles and stored in air-tight container. The biodiesel synthesized was characterized using ^{1}H NMR for calculation of triglyceride conversion.

Analysis: The following equation has been used for calculating gross molar conversion of triglycerides in oil [1,2]: $X = \left(2 \times A_{ME}\right) \times 100 \Big/ \left(3 \times A_{\alpha - CH_2}\right)$, where, A_{ME} = integration

value of the protons of the methyl esters (the strong singlet peak at 3.6 ppm), $A_{\alpha-CH2}$ = integration value of the methylene protons at 2.3 ppm.

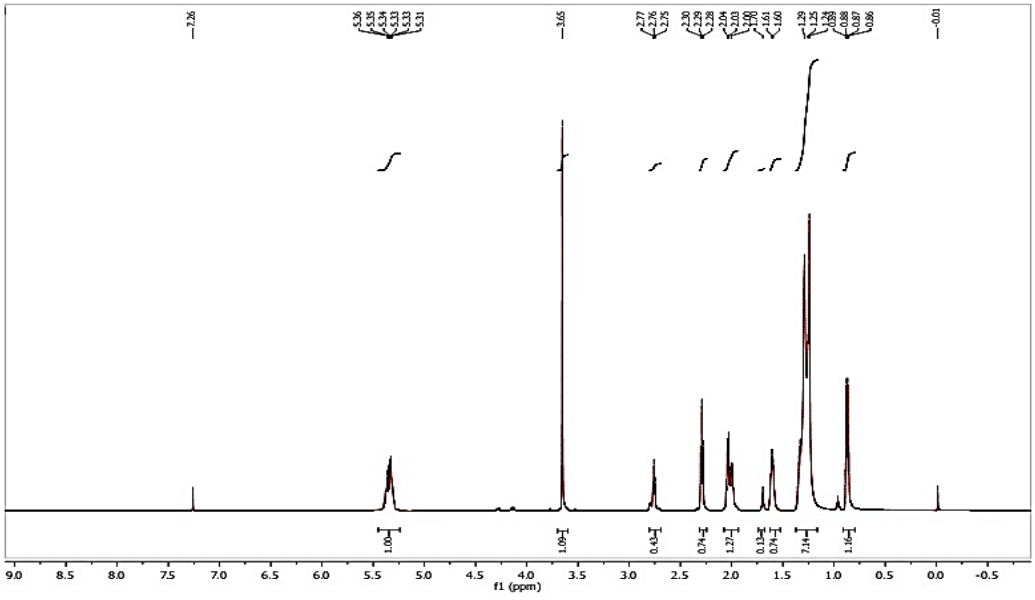

Figure: ^{1}H NMR spectrum of Canola oil transesterification reaction

Result: The ^{1}H NMR analysis of transesterification reaction (spectrum is given above) confirms the 98.19% conversion of triglycerides from canola oil to biodiesel.

References

1 Gelbard G, Bres O, Vargas RM, Vielfaure F, Schuchardt UF. ^{1}H nuclear magnetic resonance determination of the yield of the transesterification of rapeseed oil with methanol. *J Am Oil Chem Soc.* 1995; 72(10):1239–1241.

2 Knothe G. Analytical methods used in the production and fuel quality assessment of biodiesel. *T ASAE.* 2001; 44(2):193–200.

Annexure E

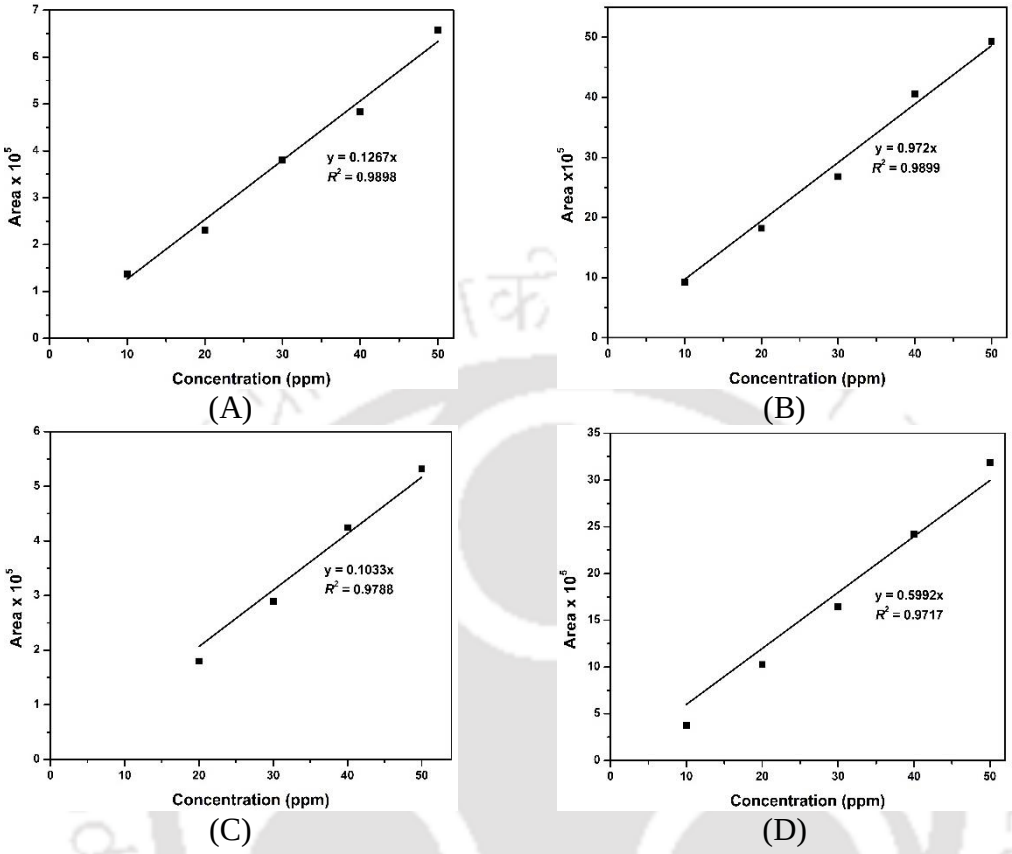

Figure: HPLC calibration plots of standards (A) methyl acetate; (B) triolein; (C) triacetin and (D) methyl oleate

ACKNOWLEDGEMENTS

I owe my deepest gratitude to all those who made this thesis possible. The first and foremost appreciation goes to my supervisors **Prof. Vijayanand S. Moholkar** and **Prof. Arun Goyal** for their valuable guidance throughout the research work. I thank them for their encouragement, guidance, support and most importantly their time from the initial to the final level, which enabled me to develop a better understanding of the subject leading to the present thesis.

I would like to acknowledge my sincere gratitude to my doctoral committee members, **Prof. Pallab Gosh**, **Prof. Niranjan Sahoo**, **Prof. Debashish Das** and **Dr. Pankaj Tiwari** for their insightful advices and suggestions throughput the research.

My sincere thanks to faculty member of Center for Energy and also to the faculty members associated with Center for Energy, for their constant inspiration and valuable suggestions. The kind and constant help of the staff members of the Center for Energy is also duly acknowledged. I also acknowledged the constant support from staff members of Department of Chemical Engineering as well as Central Instruments Facility. I am also thankful to the Indian Institute of Technology Guwahati for providing me with the infrastructure and facilities for advanced research.

I am thankful to my seniors Dr. Amrita Ranjan, Dr. Swati Khanna, Dr. Hanif Choudhury, Dr. Sankar Chakma, Dr. Jaykumar Bhasarkar, Dr. Pritam Kumar Dikshit and Dr. Debarshi Mallick for their valuable guidance. I extend my thanks to my colleagues and lab members Sushobhan, Mariganka, Bhaskar, Philip, Niharika, Kajal, Udangshree, Aaradhana, Karan, Pushpita, Rishiraj and others for their constant help

and enthusiastic company. I also extend thanks to my friends Dr. Rahul Saha, Sanjeev Mishra, Sounak Bera, and others friends from Centre for Energy and other departments of IIT Guwahati for their support and encouragement.

Finally, I would like to express my heartfelt thanks to my wife Mrs. Pallavi for all the sacrifices she made for my better future and her support, love, immense care and encouragement. I also extent my indebted thanks to my parents Mrs. Pushpa Malani and Mr. Satyanarayanji Malani, and my sister Mrs. (Dr.) Shubhangi Sarda for their support, endless love and blessings.

At last but not the least, I would like to thank the God Almighty.

Ritesh S. Malani

April, 2019
Guwahati

RESEARCH OUTPUT

Research papers

1. **Malani, R.S.**, Patil, S., Roy, K., Chakma, S., Goyal, A. and Moholkar, V.S. 2017. Mechanistic analysis of ultrasound-assisted biodiesel synthesis with Cu_2O catalyst and mixed oil feedstock using continuous (packed bed) and batch (slurry) reactors. Chemical Engineering Science, 170, 743-755.

2. **Malani, R.S.**, Sardar, H., Malviya, Y., Goyal, A. and Moholkar, V.S. 2018. Ultrasound intensified biodiesel production from mixed non–edible oil feedstock using heterogeneous acid catalyst supported on rubber de–oiled cake. Industrial and Engineering Chemistry Research, 57(44), 14926–14938.

3. **Malani, R.S.**, Shinde, V., Ayachit, S., Goyal, A. and Moholkar, V.S. 2018. Ultrasound–assisted biodiesel production using heterogeneous base catalyst and mixed non–edible oils. Ultrasonics Sonochemistry (doi: 10.1016/j.ultsonch. 2018.11.021).

4. **Malani, R.S.**, Umriwad, S., Kumar, K., Goyal, A. and Moholkar, V.S. 2019. Ultrasound–assisted enzymatic biodiesel production using blended feedstock of non–edible oils: Kinetic analysis. Energy Conversion and Management, 188, pp. 142-150.

5. **Malani, R.S.**, Pradhan, S., Goyal, A. and Moholkar, V.S. Biodiesel production by ultrasonic interesterification of non–edible oil blends. (Under Review)

Book chapters

1. **Malani, R.S.**, Goyal, A. and Moholkar, V.S., 2017. *Ultrasound-Assisted Biodiesel Synthesis: A Mechanistic Insight*, in: Agrawal, A.K., Agarwal, R.A., Gupta, T., Gurjar, B.R. (Eds.), Biofuels, Springer, Singapore, pp. 103–135.

2. **Malani, R.S.**, Singh, S., Goyal, A. and Moholkar, V.S., 2018. *Ultrasound-Assisted Biodiesel Production Using KI-Impregnated Zinc Oxide (ZnO) as Heterogeneous Catalyst: A Mechanistic Approach*. In Conference Proceedings of the Second International Conference on Recent Advances in Bioenergy Research (ICRABR-2016), Springer, Singapore, pp. 67-81.

Conferences attended

1. **Ritesh S. Malani**, Sohan Singh, Arun Goyal and Vijayanand S. Moholkar (2016) Ultrasound–assisted biodiesel production using KI–impregnated zinc oxide (ZnO) as heterogeneous catalyst: a mechanistic approach. 2nd International Conference on 'Recent Advances in Bio-energy Research' (ICRABR-2016). 25–27th February 2016, Sardar Swaran Singh National Institute of Renewable Energy, (SSS NIBE), Kapurthala, Punjab, India. (Oral presentation)

2. **Ritesh S. Malani**, Sushobhan Pradhan, Arun Goyal and Vijayanand S. Moholkar (2016) Ultrasound–assisted interesterification of waste cooking oil with heterogeneous catalyst. Large Scale Multi-disciplinary Systems of National Significance (LAMSYS–2016). 24–25th June 2016, Satish Dhawan Space Centre (SDSC) SHAR–Indian Space Research Organization (ISRO), Sriharikota, Andhra Pradesh, India. (Oral presentation. Received best paper award)

3. **Ritesh S. Malani**, Yash Malviya, Arun Goyal and Vijayanand S. Moholkar (2017) Ultrasound-assisted biodiesel production from mixed oil feedstock using non-conventional heterogeneous acid catalyst: a mechanistic investigation. 7th Asia-Pacific Congress on Catalysis (APCAT-7). 17-21st January 2017, Hotel Lalit, Mumbai, Maharashtra, India. (Poster presentation)

4. **Ritesh S. Malani**, Arun Goyal and Vijayanand S. Moholkar (2017) Mechanistic investigations in ultrasound-assisted biodiesel synthesis from mixed-oil feedstock and heterogeneous base catalyst. 3rd Asia-Oceania Sonochemical Society Conference (AOSS-3). 14-16th September 2017, SRM Research Institute, SRM University, Kattankulathur, Chennai, Tamil Nadu, India. (Poster presentation)